

ISSN 1854-6250

APEM
journal

Advances in Production Engineering & Management

Volume 17 | Number 2 | June 2022




University of Maribor

Published by CPE
apem-journal.org

Advances in Production Engineering & Management

Identification Statement

	ISSN 1854-6250 Abbreviated key title: Adv produc engineer manag Start year: 2006 ISSN 1855-6531 (on-line)
	Published quarterly by Chair of Production Engineering (CPE), University of Maribor Smetanova ulica 17, SI – 2000 Maribor, Slovenia, European Union (EU) Phone: 00386 2 2207522, Fax: 00386 2 2207990 Language of text: English APEM homepage: apem-journal.org University homepage: www.um.si

APEM Editorial

Editor-in-Chief

Miran Brezocnik

editor@apem-journal.org, info@apem-journal.org
University of Maribor, Faculty of Mechanical Engineering Smetanova ulica 17, SI – 2000 Maribor, Slovenia, EU

Desk Editor

Martina Meh

desk1@apem-journal.org

Janez Gotlih

desk2@apem-journal.org

Website Technical Editor

Lucija Brezocnik

desk3@apem-journal.org

Editorial Board Members

Eberhard Abele, Technical University of Darmstadt, Germany
Bojan Acko, University of Maribor, Slovenia
Joze Balic, University of Maribor, Slovenia
Agostino Bruzzone, University of Genoa, Italy
Borut Buchmeister, University of Maribor, Slovenia
Ludwig Cardon, Ghent University, Belgium
Nirupam Chakraborti, Indian Institute of Technology, Kharagpur, India
Edward Chlebus, Wroclaw University of Technology, Poland
Igor Drstvensek, University of Maribor, Slovenia
Illes Dudas, University of Miskolc, Hungary
Mirko Ficko, University of Maribor, Slovenia
Vlatka Hlupic, University of Westminster, UK
David Hui, University of New Orleans, USA
Pramod K. Jain, Indian Institute of Technology Roorkee, India
Isak Karabegović, University of Bihać, Bosnia and Herzegovina

Janez Kopac, University of Ljubljana, Slovenia
Qingliang Meng, Jiangsu University of Science and Technology, China
Lanndon A. Ocampo, Cebu Technological University, Philippines
Iztok Palcic, University of Maribor, Slovenia
Krsto Pandza, University of Leeds, UK
Andrej Polajnar, University of Maribor, Slovenia
Antonio Pouzada, University of Minho, Portugal
R. Venkata Rao, Sardar Vallabhbhai National Inst. of Technology, India
Rajiv Kumar Sharma, National Institute of Technology, India
Katica Simunovic, J. J. Strossmayer University of Osijek, Croatia
Daizhong Su, Nottingham Trent University, UK
Soemon Takakuwa, Nagoya University, Japan
Nikos Tsourveloudis, Technical University of Crete, Greece
Tomo Udiljak, University of Zagreb, Croatia
Ivica Veza, University of Split, Croatia



Subsidizer: The journal is subsidized by Slovenian Research Agency



Creative Commons Licence (CC): Content from published paper in the APEM journal may be used under the terms of the Creative Commons Attribution 4.0 International Licence (CC BY 4.0). Any further distribution of this work must maintain attribution to the author(s) and the title of the work, journal citation and DOI.

Statements and opinions expressed in the articles and communications are those of the individual contributors and not necessarily those of the editors or the publisher. No responsibility is accepted for the accuracy of information contained in the text, illustrations or advertisements. Chair of Production Engineering assumes no responsibility or liability for any damage or injury to persons or property arising from the use of any materials, instructions, methods or ideas contained herein.

Published by CPE, University of Maribor.

Advances in Production Engineering & Management is indexed and abstracted in the **WEB OF SCIENCE** (maintained by **Clarivate Analytics**): **Science Citation Index Expanded**, **Journal Citation Reports** – Science Edition, **Current Contents** – Engineering, Computing and Technology • **Scopus** (maintained by **Elsevier**) • **Inspec** • **EBSCO**: Academic Search Alumni Edition, Academic Search Complete, Academic Search Elite, Academic Search Premier, Engineering Source, Sales & Marketing Source, TOC Premier • **ProQuest**: CSA Engineering Research Database – Cambridge Scientific Abstracts, Materials Business File, Materials Research Database, Mechanical & Transportation Engineering Abstracts, ProQuest SciTech Collection • **TEMA (DOMA)** • The journal is listed in **Ulrich's** Periodicals Directory and **Cabell's** Directory



University of Maribor
Chair of Production Engineering (CPE)

Advances in Production Engineering & Management

Volume 17 | Number 2 | June 2022 | pp 137–258

Contents

Scope and topics	140
A method for prediction of S-N curve of spot-welded joints based on numerical simulation	141
Yang, L.; Yang, B.; Yang, G.W.; Xiao, S.N.; Zhu, T.; Wang, F.	
Sustainability and digitalisation: Using Means-End Chain Theory to determine the key elements of the digital maturity model for research and development organisations with the aspect of sustainability	152
Kupilas, K.J.; Rodríguez Montequín, V.; Díaz Piloñeta, M.; Alonso Álvarez, C.	
Supply chain coordination based on the probability optimization of target profit	169
Jian, M.; Liu, T.; Hayrutdinov, S.; Fu, H.	
A bi-objective optimization of airport ferry vehicle scheduling based on heuristic algorithm: A real data case study	183
Han, X.; Zhao, P.X.; Kong, D.X.	
Ultrasonic abrasive polishing of additive manufactured parts: An experimental study on the effects of process parameters on polishing performance	193
Liu, X.; Wang, J.; Zhu, J.; Liew, P.J.; Li, C.; Huang, C.	
Machinability analysis and multi-response optimization using NGSA-II algorithm for particle reinforced aluminum based metal matrix composites	205
Umer, U.; Mohammed, M.K.; Abidi, M.H.; Alkhalefah, H.; Kishawy, H.A.	
Supply chain coordination contract design: The case of farmer with capital constraints and behavioral preferences	219
Wang, Y.L.; Yin, X.M.; Zheng, X.Y.; Cai, J.R.; Fang, X.	
Numerical study of racking resistance of timber-made double-skin façade elements	231
Kozem Šilih, E.; Premrov, M.	
A Plant Simulation approach for optimal resource utilization: A case study in the tire manufacturing industry	243
Butrat, A.; Supsomboon, S.	
Calendar of events	256
Notes for contributors	257

Journal homepage: apem-journal.org

ISSN 1854-6250 (print)

ISSN 1855-6531 (on-line)

Published by CPE, University of Maribor.

Scope and topics

Advances in Production Engineering & Management (APEM journal) is an interdisciplinary refereed international academic journal published quarterly by the *Chair of Production Engineering* at the *University of Maribor*. The main goal of the *APEM journal* is to present original, high quality, theoretical and application-oriented research developments in all areas of production engineering and production management to a broad audience of academics and practitioners. In order to bridge the gap between theory and practice, applications based on advanced theory and case studies are particularly welcome. For theoretical papers, their originality and research contributions are the main factors in the evaluation process. General approaches, formalisms, algorithms or techniques should be illustrated with significant applications that demonstrate their applicability to real-world problems. Although the *APEM journal* main goal is to publish original research papers, review articles and professional papers are occasionally published.

Fields of interest include, but are not limited to:

Additive Manufacturing Processes	Machine Learning in Production
Advanced Production Technologies	Machine-to-Machine Economy
Artificial Intelligence in Production	Machine Tools
Assembly Systems	Machining Systems
Automation	Manufacturing Systems
Big Data in Production	Materials Science, Multidisciplinary
Block Chain in Manufacturing	Mechanical Engineering
Computer-Integrated Manufacturing	Mechatronics
Cutting and Forming Processes	Metrology in Production
Decision Support Systems	Modelling and Simulation
Deep Learning in Manufacturing	Numerical Techniques
Discrete Systems and Methodology	Operations Research
e-Manufacturing	Operations Planning, Scheduling and Control
Evolutionary Computation in Production	Optimisation Techniques
Fuzzy Systems	Project Management
Human Factor Engineering, Ergonomics	Quality Management
Industrial Engineering	Risk and Uncertainty
Industrial Processes	Self-Organizing Systems
Industrial Robotics	Smart Manufacturing
Intelligent Manufacturing Systems	Statistical Methods
Joining Processes	Supply Chain Management
Knowledge Management	Virtual Reality in Production
Logistics in Production	

A method for prediction of $S-N$ curve of spot-welded joints based on numerical simulation

Yang, L.^a, Yang, B.^a, Yang, G.W.^{a,*}, Xiao, S.N.^a, Zhu, T.^a, Wang, F.^a

^aState Key Laboratory of Traction Power, Southwest Jiaotong University, Chengdu, P.R. China

ABSTRACT

Currently, $\Delta F-N$ curves are often used to predict the fatigue lives of spot-welded joints, but the method for obtaining these $\Delta F-N$ curves is time-consuming, laborious, and non-universal. Tensile-shear fatigue tests were performed to obtain the fatigue lives and the corresponding normalized $S-N$ curves of spot-welded joints. Subsequently, the force acting at the spot-welded joints was obtained by extracting the force and moment of the beam element in the shell-element-based finite element model, and the equivalent structural stress at the spot-welded joint was obtained based on the equivalent structural stress method. Finally, the $S-N$ curves of the spot-welded joints were fitted using the least-squares method. A comparison of the $S-N$ curves of the spot-welded joints with those of different materials revealed that the material type had a significant influence on the $S-N$ curve. To avoid this influence, a method for predicting the $S-N$ curve of the spot-welded joints was proposed based on the relationship between the ratio of the tensile strength and that of the fatigue limit of each material. This research provides guidance for predicting the fatigue life of spot-welded joints in engineering applications.

ARTICLE INFO

Keywords:

Spot-welded joints;
Simulation;
Numerical simulation;
Finite element methods (FEM);
 $S-N$ curve;
Prediction method;
Equivalent structural stress

*Corresponding author:

gwyang@home.swjtu.edu.cn
(Yang, G.W.)

Article history:

Received 4 April 2022
Revised 16 August 2022
Accepted 20 August 2022



Content from this work may be used under the terms of the Creative Commons Attribution 4.0 International License (CC BY 4.0). Any further distribution of this work must maintain attribution to the author(s) and the title of the work, journal citation and DOI.

1. Introduction

Spot-welded structures are widely used in modern industrial production owing to their advantages of light weight, stable performance, and high automated production efficiency. This is an important connection mode in the mechanical manufacturing process [1]. Spot welding is mainly used in the fields of automobile manufacturing, rail-vehicle manufacturing, aerospace, and ship building, especially in automobile bodies and stainless-steel bodies of rail vehicles. According to statistics, a stainless-steel body of rail vehicles usually has up to 50000 spot-welded joints, and an automotive body has approximately 4000-6000 spot-welded joints [2].

As the spot-welding nugget is located between two relatively close plates and fatigue cracks often appear on the inner side of the plate, it becomes difficult to monitor the crack length and depth and perform non-destructive inspection [3-6]. Spot-welding fatigue-assessment methods mainly include the load-life, nominal stress, hot-spot stress, local, notch stress, fracture mechanics, and equivalent structural stress methods. At present, the load-life method specified in the standards ISO 14324-2003 [7], NF A89-571-2004 [8], JIS Z3138-1989 [9], KS B 0528-2001 [10], and GB/T 15111-1994 [11] are still used to predict the fatigue life of spot-welded joints. Howev-

er, the $\Delta F-N$ (load-amplitude-life) curves corresponding to different types of spot-welded joints in these standards are limited, and it is impossible to establish $\Delta F-N$ curves for individual spot-welding structures; furthermore, the load-life method is an approximate estimation method [12]. Therefore, the limitations of the load-life method are evident. In addition, other spot-welding fatigue assessment methods have limitations, such as high sensitivity to finite element meshes and a small application range, while the equivalent structural stress method has been widely used owing to its insensitivity to meshes.

Current spot-welding fatigue-life prediction methods based on equivalent structural stress include the Radaj [13], Rupp [14], Sheppard [15], Kang [16], and Dong methods [17]. In the early stages of fatigue research of spot-welded joints, Radaj [13] derived the formula for the maximum equivalent structural stress at the edge of a weld nugget. Based on the Roark stress-strain formula, Rupp [14] predicted the fatigue lives of spot-welded joints using the structural stress and verified the accuracy of the structural stress via tests. Sheppard [15] calculated the equivalent structural stress using the spot-welding finite element model and evaluated the fatigue lives of spot-welded joints according to the relationship between the structural stress and fatigue life. Kang [16] substituted the stress components in the von Mises equation with the local structural stresses in the vicinity of the spot weld and used the forces and moments that were determined via finite element analysis to calculate the structural stresses at the edges of the weld nugget in each sheet. Through a finite element simulation, Dong [17] transformed the nodal forces and moments at the edge of the spot-welding nugget into the linear membrane stress and bending stress and proposed a structural-stress calculation method that was insensitive to meshes. Subsequently, Yan [18] combined the Dong and Rupp methods and proposed a new fatigue characteristic parameter and simplified structural stress of the spot welding. Subsequently, the author determined the correlations of the spot-welding fatigue characteristic parameters of the Rupp, Kang, Dong, and Sheppard structure stresses on the fatigue performance of single and double spot welding [19]. Wu [20] used the classical, nonlinear generalized reduced-gradient algorithm to propose a process for optimizing the empirical parameter terms in the Rupp structural stress formula. The optimized Rupp structural-stress formula can effectively correlate the fatigue lives of spot-welded joints of various geometric sizes.

The aforementioned studies have made significant contributions to the fatigue-life evaluation method, equivalent-structural-stress calculation method, finite element simulation method, fatigue characteristic parameters, and fatigue influence parameters of spot welding. However, there is insufficient research on the normalized-spot-welding $S-N$ curve and the method for predicting the $S-N$ curve.

Different from the above studies, in this study, the quasi-static failure loads of spot-welded joints of different materials were obtained by carrying out quasi-static tensile tests. Based on the quasi-static failure loads, the load levels of tensile-shear fatigue tests were determined, and the fatigue lives of the spot-welded joints were obtained via tensile-shear fatigue tests. The equivalent structural stresses of the spot-welded joints were obtained based on the Rupp equivalent structural stress method, and the $S-N$ curves of the spot-welded joints were fitted based on the least-squares method. Finally, based on the influence of the material on the $S-N$ curve, a method for predicting the $S-N$ curve of spot-welded joints was proposed, which provides a useful reference for engineering applications.

2. Materials, methods, and experimental testing

In this study, tensile-shear fatigue tests were performed on spot-welded specimens to study the fatigue lives of spot-welded joints. Because the process of welding the stainless-steel body of rail vehicles often comprises the use of spot-welded joints, the SUS301L stainless steel commonly used in the stainless-steel body was selected as the specimen material. To avoid eccentricity in the fatigue test process of the plate welding specimens of various thicknesses, the upper and lower auxiliary plates were welded onto the plate to ensure that the spot-welded joint was stressed uniformly. The parameters of the spot-welded specimens are listed in Table 1, and the structural diagram is presented in Fig. 1.

Table 1 Parameters of spot-welded specimens

Type	Upper plate		Lower plate		Yield strength (MPa)	Tensile strength (MPa)	Weld nugget diameter (mm)	Load ratio
	Material	Thickness (mm)	Material	Thickness (mm)				
A ₁	SUS301L_1/8H	1.5	SUS301L_1/8H	2	380	690	6	0.1
A ₂	SUS301L_1/8H	2	SUS301L_1/8H	2	380	690	7	0.1
B	SUS301L_1/16H	1.5	SUS301L_1/16H	3	450	790	6	0.1
C	SUS301L_1/4H	2	SUS301L_1/4H	2	515	860	7	0.1

Note: Type-A₁ and Type-A₂ comprise the same material, and only their sizes are different. Type-A is the name used to indicate Type-A₁ and Type-A₂.

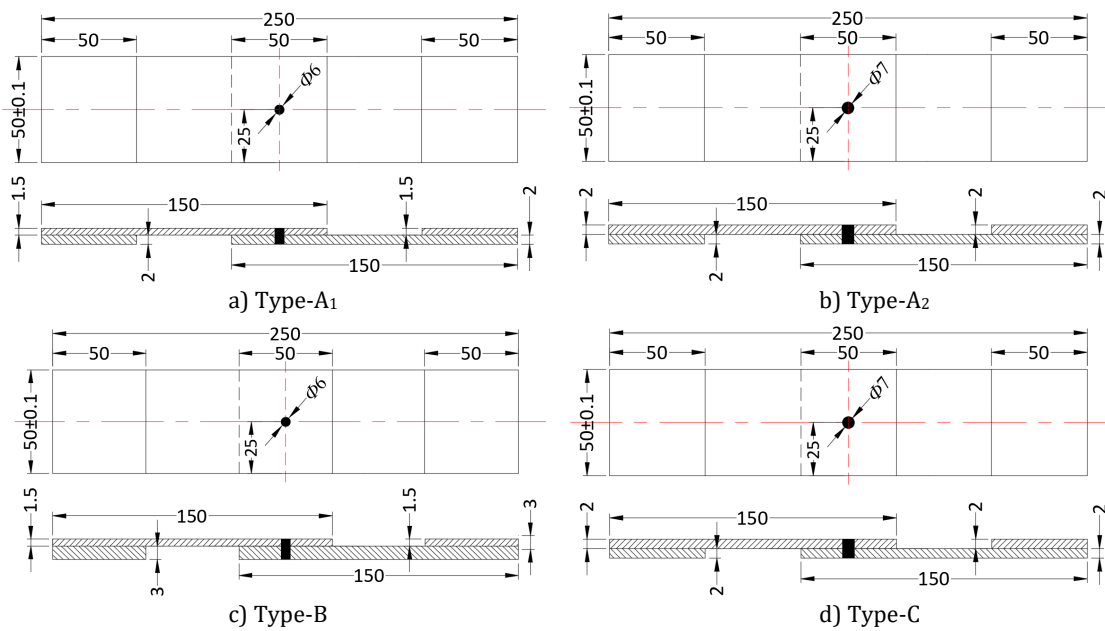


Fig. 1 The structural diagram of spot-welded specimens

Table 2 Quasi-static tensile test results of spot-welded specimens

Specimen serial number	Failure load F (kN)			
	Type-A ₁	Type-A ₂	Type-B	Type-C
1	20.66	23.42	26.24	40.53
2	21.01	22.98	26.77	41.61
3	20.50	23.57	26.84	42.01
4	23.31	23.29	26.93	41.98
5	22.26	22.75	26.72	41.74
Average failure load \bar{F}	21.548	23.202	26.70	41.574

First, the specimens presented in Fig. 1 were installed on a hydraulic universal testing machine (WE-30) for the quasi-static tensile test to determine the failure load of the spot-welded specimens. The test results are listed in Table 2.

Based on the average failure load \bar{F} in Table 2, the tensile-shear fatigue tests were then performed under four sets of load levels (multiples of \bar{F}) on a PLG-20C high-frequency tension-and-compression fatigue-testing machine for each spot-welded specimen. The group and the ladder test methods were used, the load form was an equal-amplitude sinusoidal curve, and the load ratio was 0.1 (F_{min}/F_{max}). The loading frequency gradually decreased with the crack propagation in the specimens, and the frequency range was 50-1000 Hz. While considering the fatigue fracture of the spot-welded specimens as the failure criterion, the fatigue lives of the spot-welded specimens were obtained, as shown in Table 3.

Table 3 Tensile-shear fatigue test loads and fatigue lives of spot-welded specimens

Type-A ₁		Type-A ₂		Type-B		Type-C	
F_{max} (kN)	N (cycle)	F_{max} (kN)	N (cycle)	F_{max} (kN)	N (cycle)	F_{max} (kN)	N (cycle)
3.2322 kN (15 % \bar{F})	340800	4.6404 kN (20 % \bar{F})	186700	4.005 kN (15 % \bar{F})	358500	4.1574 kN (10 % \bar{F})	373750
	495300		202600		400600		406659
	671700		209000		418209		419313
	997900		307843		433200		426488
	1085900		522400		537000		497444
4.3096 kN (20 % \bar{F})	150900	6.9606 kN (30 % \bar{F})	36500	6.675 kN (25 % \bar{F})	92100	8.3148 kN (20 % \bar{F})	58208
	199600		38300		97100		59175
	205700		42900		105700		81142
	218300		53500		120500		152638
	356100		55300		134700		162663
5.387 kN (25 % \bar{F})	35100	9.2808 kN (40 % \bar{F})	15300	9.345 kN (35 % \bar{F})	32100	12.4722 kN (30 % \bar{F})	14028
	62800		16700		36600		14133
	85500		22200		40500		14439
	91300		22300		57200		15123
	93300		25300		58800		15476
6.4644 kN (30 % \bar{F})	22300	11.6010 kN (50 % \bar{F})	4700	12.015 kN (45 % \bar{F})	14200	16.6296 kN (40 % \bar{F})	4986
	28300		7600		16100		5118
	37800		8400		22400		5366
	46900		9000		23100		5439
	50700		10600		28000		5817

The $\Delta F-N$ curves of the spot-welded specimens were obtained according to the test loads and tensile-shear fatigue lives of the specimens, as shown in Fig. 2. It can be observed that the overall dispersion of the data points was relatively high, and the correlations between the $\Delta F-N$ curves for each material were weak. It was found that the correlation between the load amplitude ΔF and fatigue life N of the spot-welded joint was weak, and the $\Delta F-N$ curves fitted appropriately only for the spot-welded joints of the same material. When predicting the fatigue lives of the spot-welded joints of different materials, fatigue tests were performed for each structure. This is time-consuming and laborious. Furthermore, the selection process also becomes cumbersome when too many curves are considered. Therefore, it is of greater engineering significance to plot the normalized $S-N$ curves of spot-welded joints suitable for different steels and different weld sizes.

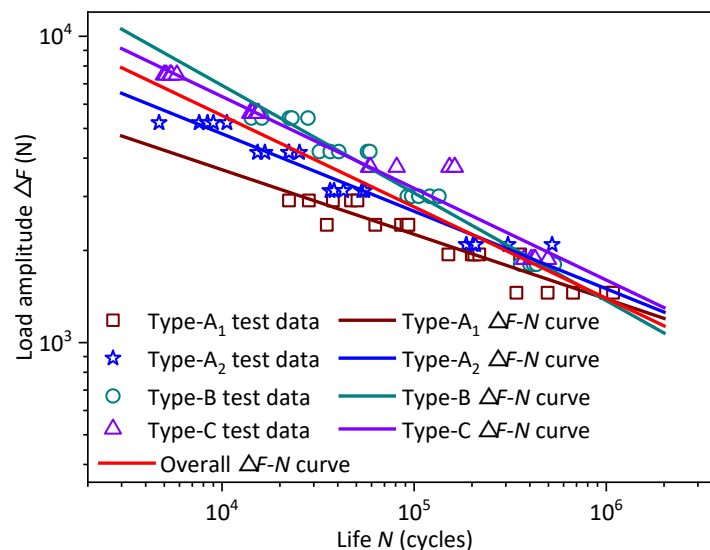


Fig. 2 $\Delta F-N$ curves

3. Structural-stress calculation method

3.1 Structural-stress calculation model

To fit the $S-N$ curve, it was necessary to obtain the structural stress (S) of the spot-welded joints. The spot-welding equivalent structural stress proposed by Rupp based on Roark's stress-strain formula is widely used in the fatigue-strength evaluation of spot-welded joints; its equivalent structural stress calculation model is presented in Fig. 3.

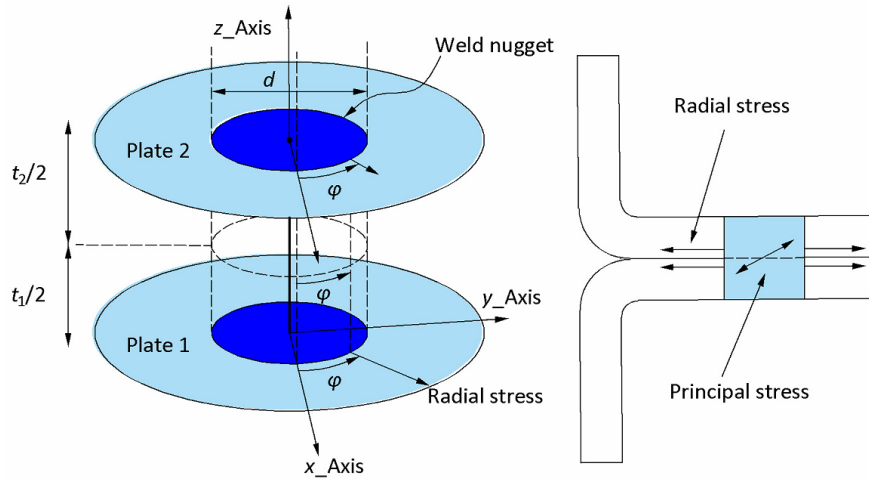


Fig. 3 Method for calculating equivalent-structural-stress of spot-welded joints

The plate thickness of the spot-welded joint in this study satisfied the relation $d > 3.5\sqrt{t}$ (d is the diameter of the weld nugget, t is the thickness of sheet). According to the structural-stress calculation model, the equivalent structural stress of a spot-welded joint was obtained, as shown in Eqs. 1 to 7, respectively [14].

$$\sigma_{v1} = -\sigma_{\max}(F_{x1})\cos\varphi - \sigma_{\max}(F_{y1})\sin\varphi + \sigma_{\max}(F_{z1}) + \sigma_{\max}(M_{x1})\sin\varphi - \sigma_{\max}(M_{y1})\cos\varphi \quad (1)$$

where

$$\sigma_{\max}(F_{x1}) = \frac{F_{x1}}{\pi dt_1} \quad (2)$$

$$\sigma_{\max}(F_{y1}) = \frac{F_{y1}}{\pi dt_1} \quad (3)$$

$$\sigma_{\max}(M_{x1}) = K_1 \left(\frac{1.872M_{x1}}{dt_1^2} \right) \quad (4)$$

$$\sigma_{\max}(M_{y1}) = K_1 \left(\frac{1.872M_{y1}}{dt_1^2} \right) \quad (5)$$

where t_1 is the thickness of sheet 1, $K_1 = 0.6\sqrt{t_1}$ is an empirical correction factor, and φ is the radial stress angle.

When the axial force on the weld nugget is a tensile force, it results in fatigue failure, and the influence of the axial force should be considered, that is, when $F_{z1} > 0$:

$$\sigma(F_{z1}) = K_1 \left(\frac{1.774F_{z1}}{t_1^2} \right) \quad (6)$$

When the axial force on the weld nugget is the result of a pressure, fatigue does not occur. At this time, the effect of the axial force is ignored, that is, when $F_{z1} \leq 0$:

$$\sigma(F_{z1}) = 0 \quad (7)$$

3.2 Equivalent structural stress calculation

To obtain the force and moment at the spot welding, a finite element model of the spot-welded joint was established in the software HyperMesh, wherein the base metal was simulated as the shell element and the weld nugget was simulated as the CBAR element. The weld nugget center nodes of the upper-plate and lower-plate nuggets were connected using a CBAR element. The mesh size of the model was 2 mm, and the load and boundary conditions were consistent with

those of the test. One end of the specimen was fully constrained, the other end was connected to the rbe2 rigid elements, and the specimen was unconstrained in the direction of the load. The time of finite element model simulation was 38 s, and the required storage space was 8.04 MB. The spot-welded shell-element-based finite element model is presented in Fig. 4. This finite element model can accurately simulate the actual stress of the spot welding and easily obtain the stress of the spot-welded structure [2, 19, 21].

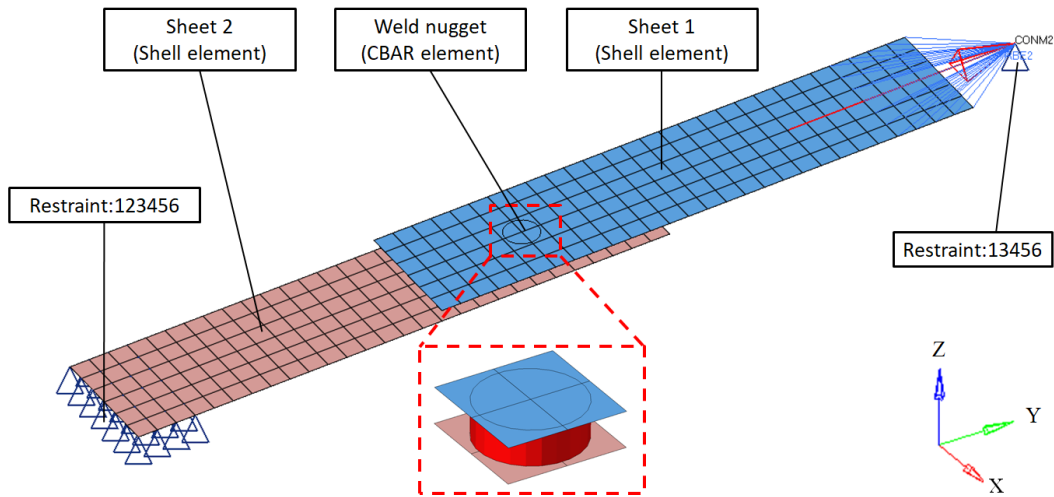


Fig. 4 Spot-welded shell-element-based finite element model

In the finite element simulation, first, the maximum and minimum loading forces F_{max} and F_{min} , respectively, of the different types of spot-welded specimens were applied to the finite element models. Then, the software NASTRAN was used to calculate the force and moment of the beam element nodes of the finite element models. Finally, the force and moment of the beam element nodes were introduced into Eqs. 1 to 7 to obtain the equivalent structural stresses of the spot-welded joints under tensile-shear loads. The calculation process is presented in Fig. 5 (A and B indicate the nodes at each end of the beam element).

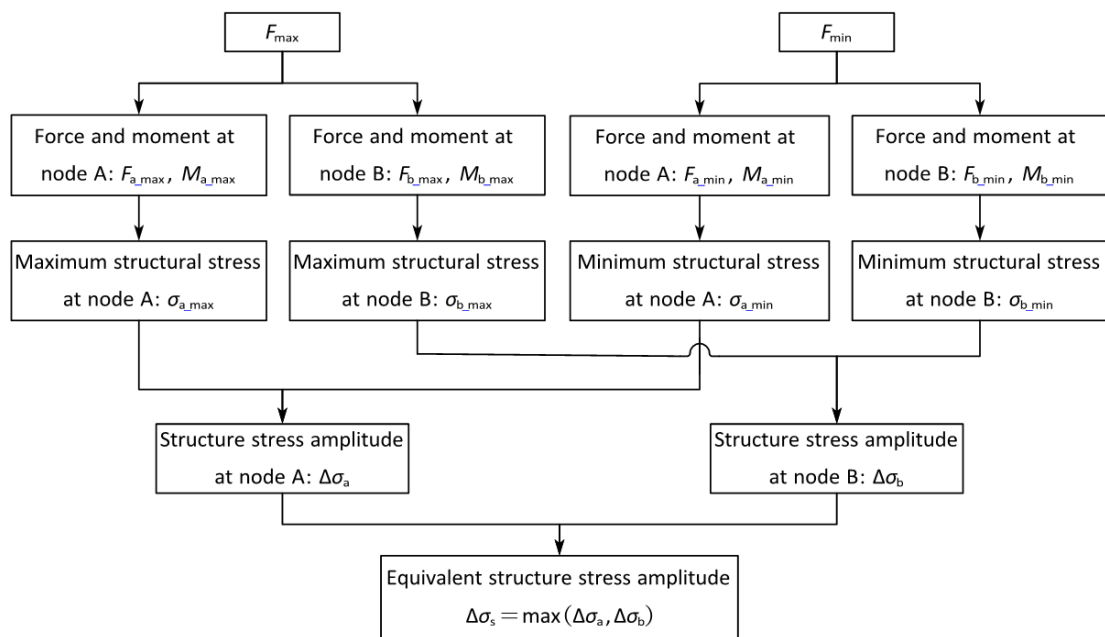


Fig. 5 Equivalent structural stress calculation process [22]

On considering the Type-B specimen, with $F_{max} = 6.675$ kN, as an example, according to the calculation process shown in Fig. 5, the force and moment of the beam-element nodes in the model and the equivalent-structural-stress amplitude of the spot-welded joint were obtained, as shown in Table 4.

Table 4 Force and moment of beam element nodes in the model and the equivalent-structural-stress amplitude of spot-welded joint

Nodes	Force and moment	$F_{max} = 6675$ N	$F_{min} = 667.5$ N	$\sigma_{a_max}, \sigma_{b_max}$ (MPa)	$\sigma_{a_min}, \sigma_{b_min}$ (MPa)	$\Delta\sigma_a, \Delta\sigma_b$ (MPa)	$\Delta\sigma_s$ (MPa)
Node A	M1 (N·mm)	-11490	-1149				
	M2 (N·mm)	-2.929e-10	-2.884e-11				
	Shear1 (N)	-6675	-667.5	549.184	54.918	494.266	
	Shear2 (N)	-4.897e-11	-4.608e-12				
	Axial (N)	85.4	8.54				
	Torque (N·mm)	9.185e-15	8.526e-16				580.166
Node B	M1 (N·mm)	3532	353.2				
	M2 (N·mm)	-1.827e-10	-1.847e-11				
	Shear1 (N)	-6675	-667.5	644.629	64.463	580.166	
	Shear2 (N)	-4.897e-11	-4.608e-12				
	Axial (N)	85.4	8.54				
	Torque (N·mm)	9.185e-15	8.526e-16				

4. S-N Curve and prediction method

4.1 Fitting S-N curve

The test data were fitted in a double-logarithmic coordinate system using the least-squares method by plotting the equivalent-structural-stress amplitude $\Delta\sigma_s$ along the ordinate and the fatigue life N along the abscissa, and the S-N curves of the spot-welded joints of the same material and of different materials were obtained as shown in Fig. 6.

In the processing of the fatigue test data, five times the lifespan (hereinafter referred to as “5×lifespan”) is typically used to evaluate the S-N curve. If the data points are within the 5×lifespan, the S-N curve is considered to have a high correlation [2, 20, 22, 23]. It can be observed from Fig. 6 that all the spot-welding data points of the same material were within the 5×lifespan, the data points were relatively compact, and the squared correlation coefficient (R^2) of the S-N curves were greater than 0.8769; however, the spot-welding data points in the case of different materials were more dispersive, and R^2 was only 0.8667 in the S-N curve. Thus, the S-N curve of the spot welding of the same material had a higher correlation and a better fitting effect. The dispersion of the spot-welding data points for different materials resulted in a weak correlation of the overall S-N curve with R^2 of only 0.8742. It can be observed that the material had a significant influence on the S-N curve; therefore, the influence of the material cannot be ignored in the fatigue analysis of the spot-welded joints. It is necessary to distinguish the materials of spot-welded joints for the fatigue evaluation.

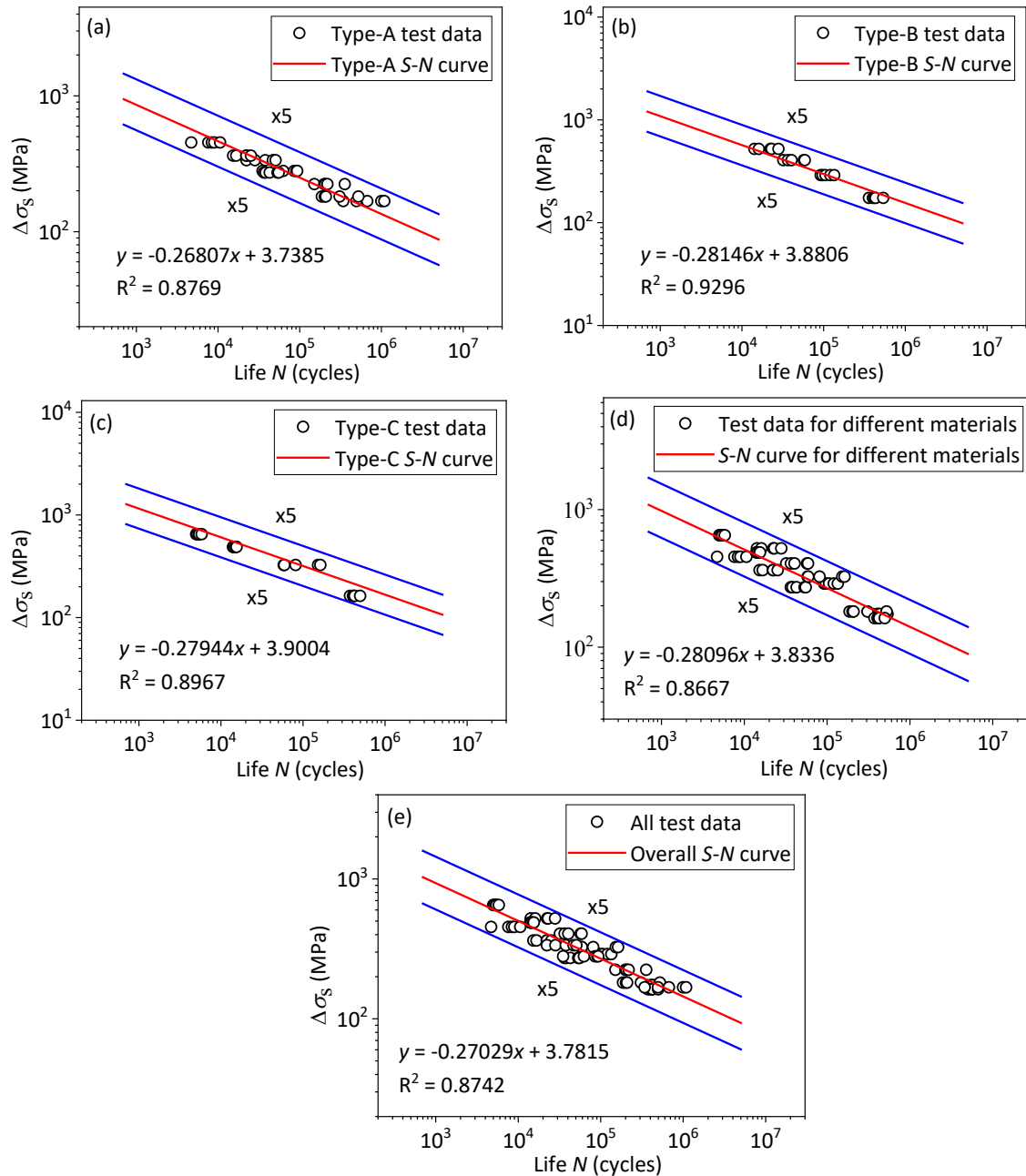


Fig. 6 S-N curves of spot-welded joints

4.2 S-N curve prediction method

The standard-power-function expression of the S-N curve is shown in Eq. 8, and all the spot-welding test fatigue lives N can be equivalent to the fatigue life N_e when the fatigue limit is $5e6$ cycles as shown in Eq. 8 [24] and the equivalent equation is given by Eq. 9.

$$S^m N = C \tag{8}$$

where m and C are parameters related to the material properties, specimen form, stress ratio, and loading mode, respectively.

$$N_e = N \left(\frac{S}{S_e}\right)^m \tag{9}$$

where S_e is the stress amplitude corresponding to the S-N curve of the spot welding when N is $5e6$ cycles.

The equivalent S-N curves are presented in Fig. 7, and it can be observed that the S-N curves of the spot-welded joints of all the materials after equivalence are almost parallel. The slopes and relative deviations of the S-N curves of the spot-welded joints are listed in Table 5. It can be

observed that the relative deviations of all the slopes are within 5 %. Within the acceptable error range, the S-N curves of the spot-welded joints of various materials were considered to be parallel. This indicates that the ratio of fatigue limit or that of the fatigue strength under different cycles of spot welding is a constant value, and the spot-welding S-N curve of one material can be derived from that of another material.

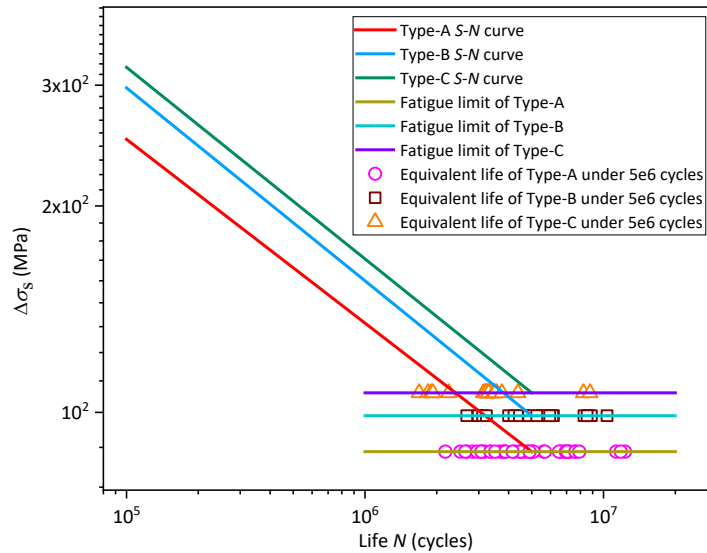


Fig. 7 The equivalent S-N curves of spot-welded joints

Because the fatigue limit of the material has a good correlation with the tensile strength [25], the tensile strength of the spot-welded joint material was compared with the fatigue limit, and the results are shown in Table 6. It can be observed that the ratio of the tensile strength of each material is very close to that of the fatigue limit, and the ratio deviation is within 3 %. This shows that the spot-welding S-N curve of other materials can be derived from the known spot-welding S-N curve of one material according to the ratio relationship of the tensile strength.

Table 5 Slopes and relative deviations of S-N curves of spot-welded joints

Item	Spot welding type			Slope relative deviation (%)		
	Type-A	Type-B	Type-C	Type-A versus Type-B	Type-A versus Type-C	Type-B versus Type-C
Slope of S-N curve	-0.26807	-0.28146	-0.27944	4.995	4.241	0.718

Table 6 Relationship between tensile strength of spot-welded joint material and S-N curve

Item	Type-A	Type-B	Type-C	Ratio of Type-A to Type-B	Ratio of Type-A to Type-C	Ratio of Type-B to Type-C
Tensile strength, MPa	690	790	860	0.873	0.802	0.919
Fatigue limit, MPa	87.641	98.880	106.768	0.886	0.821	0.926
Deviation (%)	/	/	/	1.458	2.258	0.812

According to the ratio relationship of the tensile strength of spot-welding materials, the spot-welding S-N curve of other materials was derived from the known spot-welding S-N curve of one material, as shown in Table 7. It can be observed that the derived fatigue limit of the spot welding was very close to the fatigue limit fitted according to the test data, and the corresponding error was within 3 %. Therefore, according to the ratio relationship of the tensile strength of the spot-welding materials, the spot-welding S-N curve of other materials can be predicted relatively accurately from the known spot-welding S-N curve of one material. In engineering applications, it is not necessary to perform tests on spot-welded joints of each material individually. Using the S-N-curve prediction method, the predicted S-N curves of other materials can be obtained, which is timesaving, labor-saving, and more universal and provides references for the design of spot-welding structures and life predictions in engineering applications.

Table 7 Spot welding $S-N$ curves were derived according to the ratio relationship of the tensile strength of spot-welding materials

Item	Type-B derives Type-A	Type-C derives Type-A	Type-A derives Type-B	Type-C derives Type-B	Type-A derives Type-C	Type-B derives Type-C
Derived $S-N$ curves	$y = -0.28146x + 3.8218$	$y = -0.27944x + 3.8048$	$y = -0.26807x + 3.7973$	$y = -0.27944x + 3.8635$	$y = -0.26807x + 3.8341$	$y = -0.28146x + 3.9175$
Derived fatigue limit (MPa)	86.363	85.662	100.343	98.077	109.234	107.641
Fitted fatigue limit (MPa)	87.641	87.641	98.880	98.80	106.768	106.768
Error (%)	-1.458	-2.258	1.479	-0.812	2.310	0.818

5. Results and discussion

In this study, through fatigue tests and finite element simulations of spot-welded joints, the normalized $S-N$ curve of spot-welded joints was studied based on the structural stress method, and a method for predicting the $S-N$ curve was proposed. The following conclusions were drawn.

The correlation of the $\Delta F-N$ curves of the spot-welded joints was weak, and the materials had a significant influence on the curves. When predicting the fatigue life of the spot-welded joints with different materials, fatigue tests had to be performed for each structure; therefore, the $\Delta F-N$ curves were non-universal.

The stress of the spot-welded joint can be easily obtained by extracting the force and moment of the beam-element nodes in the spot-welded shell-element model. Using the equivalent-structural-stress calculation model, the equivalent structural stress of the spot-welded joint can be accurately obtained.

The correlation of the $S-N$ curves of the spot-welded joints of the same material was satisfactory, and the correlation of the $S-N$ curves of different materials was weak. Therefore, the material has a significant influence on the $S-N$ curves, and the influence of materials cannot be ignored in the fatigue analysis of spot-welded joints.

To avoid the influence of materials on the $S-N$ curves of spot-welded joints, a method for predicting the $S-N$ curve was proposed based on the relationship between the ratio of the tensile strength and that of the fatigue limit of each material, which provides references for the design of spot-welding structures and life prediction in engineering applications.

Owing to the limitations of the test conditions and the amount of available test data, some data were dispersive and did not provide accurate solutions; therefore, supplementary tests should be conducted to improve the accuracy of the results. In the future, the influence of residual stress on the fatigue life and fatigue characteristics of spot-welded joints under tensile loads can be further investigated.

Acknowledgement

The authors are grateful for the financial support provided by the the National Natural Science Foundation of China (grant number 52175123) and the Independent Subject of State Key Laboratory of Traction Power (grant number 2022TPL_T03).

References

- [1] Yang, L., Yang, B., Yang, G.W., Xiao, S.N., Zhu, T., Wang, F. (2020). $S-N$ curve and quantitative relationship of single-spot and multi-spot weldings, *International Journal of Simulation Modelling*, Vol. 19, No. 3, 482-493, doi: [10.2507/IJSIMM19-3-C011](https://doi.org/10.2507/IJSIMM19-3-C011).
- [2] Wang, F. (2018). *Research on equivalent stress method of spot welding and ring welding*, Master Thesis, Southwest Jiaotong University, Chengdu, China.
- [3] Ismail, M.I.S., Afieq, W.M. (2016). Thermal analysis on a weld joint of aluminium alloy in gas metal arc welding, *Advances in Production Engineering & Management*, Vol. 11, No. 1, 29-37, doi: [10.14743/apem2016.1.207](https://doi.org/10.14743/apem2016.1.207).
- [4] Talabi, S.I., Owolabi, O.B., Adebisi, J.A., Yahaya, T. (2014). Effect of welding variables on mechanical properties of low carbon steel welded joint, *Advances in Production Engineering & Management*, Vol. 9, No. 4, 181-186, doi: [10.14743/apem2014.4.186](https://doi.org/10.14743/apem2014.4.186).

- [5] Dunder, D., Samardzic, I., Simunovic, G., Konjatic, P. (2020). Steel weldability investigation by single and double-pass weld thermal cycle simulation, *International Journal of Simulation Modelling*, Vol. 19, No. 2, 209-218, doi: [10.2507/IJSIMM19-2-510](https://doi.org/10.2507/IJSIMM19-2-510).
- [6] Edwin Raja Dhas, J. Kumanan, S. (2013). Modeling and prediction of HAZ using finite element and neural network modeling, *Advances in Production Engineering & Management*, Vol. 8, No. 1, 13-24, doi: [10.14743/apem2013.1.149](https://doi.org/10.14743/apem2013.1.149).
- [7] ISO 14324-2003. Resistance spot welding – Destructive tests of welds – Method for the fatigue testing of spot welded joints, from <https://www.iso.org/standard/24088.html>, accessed January 6, 2022.
- [8] NF A89-571-2004. Resistance spot welding – Destructive tests of welds – Method for the fatigue testing of spot welded joints, from <https://www.antpedia.com/standard/573005.html>, accessed January 5, 2022.
- [9] JIS Z3138-1989. Method of fatigue testing for spot welded joint, from <https://www.docin.com/p-323321200.html>, accessed January 5, 2022.
- [10] KS B 0528-2001. Resistance spot welding-Destructive tests of welds – Methods for the fatigue testing of spot welded joints, from <https://www.antpedia.com/standard/7006344-1.html>, accessed January 4, 2022.
- [11] GB/T 15111-1994. Test method for shear tensile fatigue of spot welded joints, from <http://www.doc88.com/p-1478459027386.html>, accessed January 3, 2022.
- [12] Wang, R.J., Shang, D.G., Shen, T., Yan, C.L. (2006). A review on fatigue life prediction approaches for spot-welded joint, *Mechanics in Engineering*, Vol. 28, No. 3, 9-14, doi: [10.3969/j.issn.1000-0879.2006.03.002](https://doi.org/10.3969/j.issn.1000-0879.2006.03.002).
- [13] Radaj, D., Zhang, S. (1991). Stress intensity factors for spot welds between plates of unequal thickness, *Engineering Fracture Mechanics*, Vol. 39, No. 2, 391-413, doi: [10.1016/0013-7944\(91\)90053-4](https://doi.org/10.1016/0013-7944(91)90053-4).
- [14] Rupp, A., Störzel, K., Grubisic, V. (1995). Computer aided dimensioning of spot-welded automotive structures, *SAE Technical Paper 950711*, doi: [10.4271/950711](https://doi.org/10.4271/950711).
- [15] Sheppard, S.D. (1993). Estimation of fatigue propagation life in resistance spot welds, *Advances in Fatigue Predictive Techniques*, ASTM STP 1211, Vol. 2, 169-185, doi: [10.1520/STP15085S](https://doi.org/10.1520/STP15085S).
- [16] Kang, H.T. (2007). Fatigue prediction of spot welded joints using equivalent structural stress, *Materials & Design*, Vol. 28, No. 3, 837-843, doi: [10.1016/j.matdes.2005.11.001](https://doi.org/10.1016/j.matdes.2005.11.001).
- [17] Dong, P. (2001). A structural stress definition and numerical implementation for fatigue analysis of welded joints, *International Journal of Fatigue*, Vol. 23, No. 10, 865-876, doi: [10.1016/S0142-1123\(01\)00055-X](https://doi.org/10.1016/S0142-1123(01)00055-X).
- [18] Yan, K. (2015). *Fatigue strength analysis of tensile-shear spot weld specimen based on structural stress*, Kunming University of Science and Technology, Kunming, China.
- [19] Yang, L., Yang, B., Yang, G., Xiao, S., Zhu, T. (2020). Overview of fatigue research of spot welded joints, *Journal of Mechanical Engineering*, Vol. 56, No. 14, 26-43, doi: [10.3901/JME.2020.14.026](https://doi.org/10.3901/JME.2020.14.026).
- [20] Wu, X. (2016). *Study on fatigue testing and life prediction method of spot welded joints of steel*, Chongqing University, Chongqing, China.
- [21] Yang, L., Yang, B., Yang, G., Xiao, S., Zhu, T., Wang, F. (2020). Analysis on fatigue characteristics of spot welded joints of stainless steel car body, *Transactions of the China Welding Institution*, Vol. 41, No. 7, 18-24, doi: [10.12073/j.hjxb.20191204005](https://doi.org/10.12073/j.hjxb.20191204005).
- [22] Yang, G., Che, C., Yang, B., Zhu, T., Wang, F., Wang, J. (2019). Optimization research on S-N curve of ring welding structure based on structural stress method, *Fatigue & Fracture of Engineering Materials & Structures*, Vol. 42, No. 10, 2207-2219, doi: [10.1111/ffe.13023](https://doi.org/10.1111/ffe.13023).
- [23] Kang, H.-T., Wu, X., Khosrovaneh, A., Li, Z. (2017). Data processing procedure for fatigue life prediction of spot-welded joints using a structural stress method, In: Harlow, G., McKeighan, P., Nikbin, K., Wei, Z. (eds.), *Fatigue and Fracture Test Planning, Test Data Acquisitions and Analysis*, Vol. 1598, 198-211, doi: [10.1520/STP159820160054](https://doi.org/10.1520/STP159820160054).
- [24] BS EN 1999-1-3:2007. Eurocode 9: Design of aluminium structures-Part 1-3: Structures susceptible to fatigue, from <http://www.doc88.com/p-1106362384048.html>, accessed January 4, 2022.
- [25] Luo, S., Liu, M., Zheng, X. (2020). Characteristics and life expression of fatigue fracture of G105 and S135 drill pipe steels for API grade, *Engineering Failure Analysis*, Vol. 116, Article No. 104705, doi: [10.1016/j.engfailanal.2020.104705](https://doi.org/10.1016/j.engfailanal.2020.104705).

Sustainability and digitalisation: Using Means-End Chain Theory to determine the key elements of the digital maturity model for research and development organisations with the aspect of sustainability

Kupilas, K.J.^a, Rodríguez Montequín, V.^{a,*}, Díaz Piloñeta, M.^a, Alonso Álvarez, C.^a

^aUniversity of Oviedo, Oviedo, Project Engineering Area, Spain

ABSTRACT

Organisations are under pressure to digitally transform and become more sustainable. Thus, the convergence of digitalisation and sustainability is inevitable. There are several Digital Maturity models that help companies to develop their digital roadmaps, however, none of them have been developed for Research and Development (R&D) organisations. Additionally, none of these models include the dimension of sustainability. In this paper the authors used the Means-End Chain method to determine which are the key dimensions of the digital maturity model tailored for R&D, as well as to investigate the link between digital transformation and sustainability. The results show that although technologies are important, they cannot successfully transform the organisation on their own. They must be supported by people and culture change. The results also highlighted that sustainability is high on the agenda and cannot be ignored when progressing towards the higher level of Digital Maturity. The findings may serve as a reference for any organisation that is building or revising its digitalisation or sustainability strategies. It highlights the important dimensions that should be considered and prioritised when preparing the transformation roadmap. These dimensions are tailored for R&D but can be a good indication for any other type of organisation.

ARTICLE INFO

Keywords:

Sustainability;
Digitalisation;
Digital transformation;
Means-End Chain Theory (MEC);
Research and development (R&D)

*Corresponding author:

montequi@uniovi.es
(Rodríguez Montequín, V.)

Article history:

Received 8 March 2022
Revised 15 August 2022
Accepted 18 August 2022



Content from this work may be used under the terms of the Creative Commons Attribution 4.0 International Licence (CC BY 4.0). Any further distribution of this work must maintain attribution to the author(s) and the title of the work, journal citation and DOI.

1. Introduction

To remain competitive in today's market and to assure long-term survival, organisations must continuously develop innovative, high-quality products and services and renew their way of operating [1]. Therefore, they are under tremendous pressure to transform. It is the case for organisations from both developed and transitioning countries [2]. The majority of them are taking advantage of new technologies, pursuing their “digital transformations” [3–5]. At the same time, companies must reduce their carbon footprint and become more sustainable overall [6, 7]. These two strategies are interconnected and some of these connections have been demonstrated in [8], where the authors argue that they are positively related. It can be stated that a given company that transforms itself becomes more efficient and thus automatically more sustainable. On the other hand, new technologies offer resources that can be applied to accelerate sustainability [7, 9].

Additionally, recent events (mainly the global pandemic that started in early 2020) highlighted the growing need for organisations to become more digitally mature. This is supported by the emerging research including the study of Fletcher and Griffiths [10] suggesting that VUCA environments (VUCA stands for Volatility, Uncertainty, Complexity and Ambiguity) strengthen the need for digital transformation. After analysing the effects of global pandemic, they even suggest, that digital is no longer an option but became a necessity. Such events affect more severely less digitally mature organisations. Another research by Vandana and Ashutosh [11] supports this observation.

The task of continuous reinvention of a given organisation in many cases is performed by Research and Development departments (R&D). As leaders of such creativity and innovation, R&D organisations are at the forefront of progress. They contribute towards new technologies, products, and manufacturing processes more than any other entity. It is their mission to apply innovation to make new processes more efficient, products more attractive and cheaper, and overall to help to become more efficient, generate less waste and reduce the impact on the environment, business, and society [12].

A good way to progress on such a transformational journey is to apply a concept of digital maturity. Assessing the state of digital maturity and deciding how to proceed to a higher maturity level can help to create transformation programs using a systematic approach and eliminate blind spots. Digital maturity models are used for prescriptive, descriptive and comparative purposes [13, 14]. Many of them have been developed by organisations to assess their processes, identify improvement areas and use them to drive the way they operate [15]. Maturity assessments can be applied to an entire organisation or part of it, and can also be specifically developed and applied to certain aspects of any business process. The usual way of employing a maturity model is to use it to assess an organisation's current maturity and then prepare a strategy for the future to achieve a higher level.

Although there are several publications about digital maturity within the existing literature, the authors noticed that there is a gap when it comes to digital maturity tailored to the needs of R&D organisations, and they hope that this publication can contribute towards closing this gap. It attempts to describe which digital maturity dimensions should be considered to fit into R&D specifics. It also tries to explore the relation between digital transformation and sustainability.

The authors' understanding of sustainability is based on the "Brundtland Report", which was published in 1987 by the World Commission on Environment and Development (WCED) [16]. In this report sustainability or sustainable development is described as "development that meets the needs of the present without compromising the ability of future generations to meet their own needs". It is based on three pillars: social, economic and environmental sustainability [17]. Currently, both sustainability and digitalisation strategies are at the top of most companies' agenda. Even if this is the case, in many organisations both strategies are operating in parallel, being executed by separate departments with people with different skillsets. Recently, however, there is emerging scientific evidence that digitalisation and sustainability are interconnected [8, 18]. There is an emerging opportunity to join efforts to accelerate sustainability goals by using digital technologies. It is worth noticing the work of Gupta et al., who presented the Digitalisation–Sustainability Matrix, where they researched how technologies impact Sustainable Development Goals (SDGs) [19].

The authors firmly believe that there is no responsible digitalisation without considering the dimension of sustainability. A digitally transformed company becomes more efficient, generates less waste and uses fewer resources, which makes it more sustainable.

The first research goal of this study was to determine the key elements of a digital maturity model tailored for such an R&D organisation. The focus was on the model's key dimensions (often also referred to as "goals" or "values"). The second goal was to conduct a preliminary study on the sustainability dimension as part of the digital maturity model, considering the fact that digital technologies have a big potential to accelerate sustainability [20]. The objectives were achieved by applying a 2-step approach. Firstly, the authors prepared an initial set of dimensions based on the literature review of the existing digital maturity models. Secondly, by using the Means-End Chain (MEC) method, they refined this initial set and suggested a usable com-

promise which can be used for an R&D digital maturity model. Information for the MEC was taken from the outputs from interviews conducted with experts from both inside and outside R&D.

This paper starts with the literature review and the description of methods used. These are then followed by empirical data analysis, discussion of results and conclusions, with suggestions for further potential research areas.

2. Literature review

The authors conducted the literature review according to the guidelines proposed by Kitchenham at Keele University [21]. They searched Google Scholar, SCOPUS, EBSCO and ProQuest for the terms “Digital AND Maturity AND Literature AND Review”. The initial result showed 292,000 entries in Google Scholar, 168 in SCOPUS, 834 in ProQuest and 32 in EBSCO. To limit the results to the most relevant ones, the authors applied several filters. As the various repositories were constructed in different ways, it was impossible to apply the same filters on all of them in the same way so, in order to ensure that the review was comprehensive, the authors applied filters where it was possible without changing the number of results in the repositories where such filters did not exist. For example, ProQuest offered the filter called “literature reviews” which reduced the number of papers initially found from 834 to 151, however, such filter did not exist in Google Scholar, SCOPUS and EBSCO. The next level of filters applied was the language (English), which reduced the number of results in SCOPUS from 168 to 164. An additional filter applied was to include results that were “peer reviewed”, which reduced the number of results in ProQuest to 149 and EBSCO to 27. The last filter applied was to look for results in the paper title and this reduced the number of results to 259 (Google Scholar 8, SCOPUS 3, ProQuest 149, EBSCO 99). The authors analysed these 259 results, eliminated overlaps across repositories and selected 8 publications which were relevant in the first stage of the research. These publications were used to find the existing most relevant digital maturity models, determine if there are gaps related to specifics of Research and Development organisations and which potential dimensions of the existing models could be adapted and used for building a model that is better tailored to R&D specifics. Table 1 lists the literature selected by the authors.

The nine models shown in Table 2 represent the results of the authors’ analysis of the models developed by both academics and practitioners. More models were found but either their research was not completed or there were not enough details about the model, making it too open to individual interpretation and thus too difficult to use, making the result unpredictable.

Table 1 Literature review output – selected publications

Publication name	Authors	Year published
Multi-Attribute Assessment of Digital Maturity of SMEs [22]	Kljajić Borštnar, M., Pucihar, A.	2021
Digital Maturity Models: a systematic literature review [23]	Ochoa-Urrego, R.-L., Peña-Reyes, J.-I.	2021
Industry 4.0 Roadmap: Implementation for Small and Medium-Sized Enterprises [24]	Cotrino, A., Sebastián, M.A., González-Gaya, C.	2020
Towards a Comprehensive Exploration and Mapping of Maturity Models in Digital Business: A Systematic Literature Review [25]	Gandhi, A., Sucahyo, Y.G	2020
Digital Transformation Maturity: A Systematic Review of Literature [26]	Teichert, R.	2019
Digital Maturity Models for Small and Medium-sized Enterprises: A Systematic Literature Review [27]	Williams, C., Schallmo, D., Lang, K., Boardman, L.	2019
An Industry 4.0 maturity model proposal [28]	Santos, R.C., Martinho, J.L.	2019
Development of an Assessment Model for Industry 4.0: Industry 4.0-MM [29]	Gökalp, E., Şener, U., Eren, P.	2017

Table 2 Literature review output – Digital Maturity Models

Model/Research name	Research context	Maturity levels	Dimensions
IMPULS Industry 4.0 Readiness [30]	Industry 4.0 readiness	6 maturity levels (Outsiders, Beginner, Intermediate, Experienced, Expert, Top performers)	6 dimensions (Strategy & Organisation, Smart Factory, Smart Operations, Smart Products, Data-driven Services, Employees)
Industry 4.0 / Digital Operations Self-Assessment [31]	Digital readiness for Industry 4.0	3 maturity levels (Vertical Integrator, Horizontal Collaborator, Digital Champion)	6 dimensions (Business Models, Product & Service, Portfolio Market & Customer Access, Value Chains & Processes, IT Architecture, Compliance, Legal, Risk, Security & Tax, Organisation & Culture)
SIMMI 4.0 [32]	Industry 4.0 maturity	5 maturity stages (Basic Digitisation, Cross-departmental Digitisation, Horizontal and Vertical Digitisation, Full Digitisation, Optimised Full Digitisation)	3 dimensions (Vertical Integration, Horizontal Integration, Cross-sectional Technology Criteria)
Acatech Industry 4.0 Maturity Index [33]	Industry 4.0 maturity	6 maturity stages (Computerisation, Connectivity, Visibility, Transparency, Predictive Capacity, Adaptability)	4 structural areas (Resources, Organisational Structure, Information Systems, Culture)
DREAMY (Digital REadiness Assessment MaturitY model) [34]	Digital readiness for Industry 4.0	5 maturity stages (Initial, Managed, Defined, Integrated and Interoperable, Digital-Oriented)	5 structural areas (Design and Engineering, Production Management, Quality Management, Maintenance Management, Logistics Management)
A maturity model for Industry 4.0 Readiness [35]	Industry 4.0 maturity	Likert scale maturity levels (from rating 1= “not important” to rating 4 = “very important”)	9 dimensions (Strategy, Leadership, Customers, Products, Operations, Culture, People, Governance, Technology)
360 Digital Maturity Assessment [36]	Digital readiness for Industry 4.0	6 maturity stages (None, Basic, Transparent, Aware, Autonomous, Integrated)	5 digital dimensions (Governance, Technology, Connectivity, Value Creation, Competence)
HADA http://hada.industriaconnect.ada40.gob.es/	Model developed by Spanish Government	6 maturity stages assigned by point system 0-1000 based on survey results (Static, Aware, Competent, Dynamic, Reference, Leader)	5 dimensions (Strategy and business model, Processes, Organisation and people, Infrastructures, Products and services)
Multi-Attribute Assessment of Digital Maturity [22]	Digital Maturity of SMEs	4 maturity stages (Lagging behind, Initial, Advanced, Digital winner)	2 dimensions (Digital capability, Organisational capability)

The authors found the literature review very insightful. It showed that the topic of digital maturity is increasingly on the agendas of researchers and practitioners. It was also interesting that there is a big overlap between digital maturity and Industry 4.0 readiness, and in many cases these terms were used as synonyms. They concluded, however, that while Industry 4.0 readiness

was mainly targeting industrial applications, digital maturity can be used across a wider set of organisations, including public services or non-profit. The review also showed that relevant research and adoption accelerated over the last 10 years, demonstrating the growing need for frameworks that would help organisations build their roadmaps and strategies in a structured and unbiased way.

The further explanation of how authors used the outcomes from this literature review and arrived at the initial set of dimensions is described in more detail in chapter 3: “Research design”. It is also worth noticing that none of the existing maturity models described in the literature contains the sustainability dimension, which prompted the authors to include it in their proposed set of dimensions and then discuss further with experts whether it should or should not be considered.

3. Research design

3.1 General design

To address the research questions, the work was organised into two main phases as shown in Fig. 1. In Phase 1, the authors wanted to find and analyse the research already available. This served two goals. Firstly, the authors wanted to validate if there is a gap in the existing literature in relation to R&D organisations to ensure the scientific value and contribution of their work. The second goal was to derive the initial set of dimensions to be validated in Phase 2. In this phase the authors conducted interviews with experts and applied the Means-End Chain method to arrive at the final set of dimensions addressing the needs of research and development.

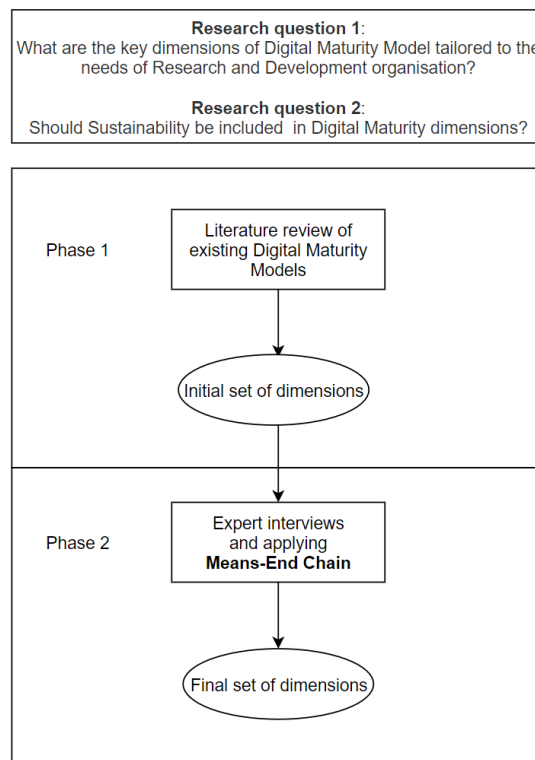


Fig. 1 The structure of the research

To prepare the initial set of dimensions, the authors summarised and grouped the output from the literature review (dimension elements from Table 2) into three categories, namely, “External factors”, “Internal factors” and “Organisation” as shown in Table 3.

From “External factors”, the authors suggested the following “Products” and “Services” as initial dimensions. From “Internal factors”, the most prevailing to be added to the initial list were “Operations” and “Facilities”, and from the “Organisation” side the authors suggested using “People” and “Strategy”. Additionally, the authors added the “Sustainability” dimension to test its

viability as part of the digital maturity model of an R&D organisation. The rest of the elements in Table 2 did not need to form separate dimensions. For example, “Business Models” can be classified as part of “Operations” similarly to “Compliance, Legal, Risk, Security and Tax”. “IT architecture” can be part of “Facilities” and does not require a separate dimension to be formed. The authors believed that the initial proposed set of dimensions catered well for all the elements identified during the literature review.

To verify this initial list of dimensions and to refine the findings, the authors applied the Means-End Chain (MEC) method. This method is widely known and used in marketing, but has not previously been used to compile and verify the elements of digital maturity. However, it was used in several studies outside of marketing that inspired the authors to apply it in their research. For example, in project management, in 2010 Verburg et al. used MEC to determine critical success factors for project managers in virtual work settings [37]. Later, in 2018, Chen et al. used MEC for innovation research program performance evaluation [38].

Table 3 Initial grouping of the dimensions

Model/Research name	External factors	Internal factors	Organisation
IMPULS	Smart products Data-driven services	Smart factory Smart operations	Employees Strategy and organisation
Industry 4.0 / Digital Operations Self-Assessment	Market & customer access	Business models Product & service portfolio Compliance, legal, risk, security & tax IT architecture Value chains & processes	Organisation & culture
SIMMI 4.0		Vertical integration Horizontal integration Digital product development Cross-sectional technology criteria	
Acatech Industry 4.0 Maturity Index		Resources Information systems	Resources Information systems
DREAMY (Digital REadiness Assessment Maturity model)		Process monitoring and control Technology	Organisation
A maturity model for Industry 4.0 Readiness	Customers product	Operations Technology	Strategy Leadership Culture People Governance
360 Digital Maturity Assessment		Technology Connectivity Value creation	Governance Competence
HADA	Products and services	Infrastructure Strategy and business model Processes	Strategy and business model Organisation and people
Multi-Attribute Assessment of Digital Maturity		Digital capability	Organisational capability

3.2 Means-End Chain

The Means-End Chain (MEC) method is based on the attributes–benefits–values/goals sequence that forms a means-end chain. It was used initially by Gutman to understand the perceptions and motivations of consumers when they make their purchasing choices [39]. In that sense, it connects product or service attributes to the consequences produced by these and the latter to values. The MEC method is based on the sequence or hierarchy shown in Fig. 2 [40]. The links are identified by means of interviews conducted with the focus group individuals (customers, experts, etc.). The laddering interviewing technique is used for the elicitation. Laddering involves a

tailored reviewing format using a series of directed probes, typified by the “Why is it important to you that...” question [41]. The answers are explored further, and a ladder of constructs is created. The soft laddering method [42] is the recommended technique with a relatively small sample size (<50) and research of an exploratory nature [43].

In the case of this research, the values are the dimensions of the digital maturity model that are selected by experts for their attributes as well as their benefits. The links between products, values and attributes were identified through interviews conducted with subject matter experts following the laddering technique [41]. These interviews were conducted by asking about the attributes, why they are important (what benefits would be realised) and what values/goals they would serve. For example, if the goal is to have “Smart operations and research” in place, then products can be developed faster (benefit). To achieve this benefit, there is a need to “digitise information” (attribute) or have “digital platforms in place” (another attribute).

Once the interviews were finished, the Implication Matrix (IM) and Hierarchical Value Map (HVM) were created by LadderUX software to analyse the results. The Implication Matrix is a tabular representation of the interview outcomes, while the Hierarchical Value Map (HVM) visually links attributes, benefits and goals. Examples of the HVMs created during this research can be found in the “Discussion” section (Figs. 3-6).

To determine the order of importance for all the attributes, benefits and dimensions, the authors calculated their centrality as described in the following section.

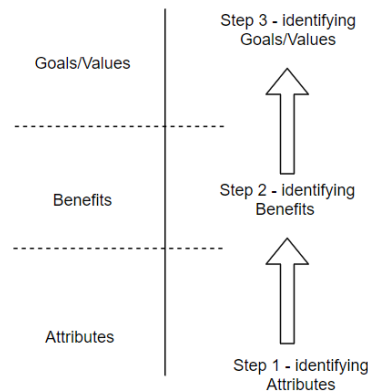


Fig. 2 The sequence flow of the Means-End Chain method

3.3 Calculating centrality

Centrality is defined as the ratio of in-degrees plus out-degrees of a particular element over the sum of all cell-entries in the implication matrix [44]. It highlights those mentioned by most of the experts. The equations below represent the Implication Matrix (IM) and illustrate how the centrality is calculated. The columns of the IM are represented by index i – from 1 to the n^{th} element, the rows by index j – from 1 to the n^{th} element. Column S includes the sum of “out” elements in the row and column T includes the sum of “out” elements from both relevant rows and columns (the figure in column S). Column C displays the calculated centrality.

$$IM = \begin{bmatrix} a_{11} & a_{12} & \cdots & a_{1i} & \cdots & a_{1n} \\ a_{21} & a_{22} & \cdots & a_{2i} & \cdots & a_{2n} \\ \vdots & \vdots & \ddots & \vdots & \cdots & \vdots \\ a_{j1} & a_{j2} & \cdots & a_{ji} & \cdots & a_{jn} \\ \vdots & \vdots & \cdots & \vdots & \cdots & \vdots \\ a_{n1} & a_{n2} & \cdots & a_{ni} & \cdots & a_{nn} \end{bmatrix} \quad (1)$$

Calculation of the values of the elements is shown below:

$$S_j = \sum_{j=1}^n a_{ji} \quad (2)$$

$$T_j = S_j + \sum_{i=1}^n a_{ji} \quad (3)$$

$$\sum T = \sum_{j=1}^n T_j \quad (4)$$

Finally, the centrality of each element is calculated as:

$$C_j = \frac{T_j}{\sum T} \quad (5)$$

4. Empirical data analysis

The process of interviewing started on 26 May 2020 and lasted until 2 February 2021. Considering the situation with the global pandemic (COVID-19) and the physical location of the experts, the authors conducted interviews using Microsoft Teams. All of them were recorded and stored in Microsoft Stream. At this stage, 32 senior experts (28 men and 4 women) from various functions and companies were interviewed, of whom two experienced technical difficulties and were not included further in the study. These experts are connected to digital transformation either within their own organisation or participating in the digital transformation of several organisations as a partner or consultant. They reside in both the Americas and Europe and work in companies of various sizes, from a single consultant to multinational corporations with over 200 000 employees. It was very important to ensure a wide representation of experts and not to limit the research to specific segments or industries. These segments and industries included tech start-ups, telecommunication, recruitment, research and development, fast-moving consumer goods (FMCG), manufacturing, management consulting, technology companies and academia. The authors wanted to collect both R&D views as well as external views to eliminate blind spots and biases. The interviewees resided in the following countries: Canada (1), Denmark (1), France (3), Luxembourg (2), Netherlands (2), Spain (2), UK (15) and USA (6). Authors' criteria for selection were not specifically related to the countries but to the area of expertise of the interviewee and to the type of their organization. Authors wanted to get the view from both inside or outside the R&D, from small and big organisations and they believe that it has been achieved.

When it comes to the question about the number of interviews to conduct in order to obtain meaningful results, the authors used the study conducted by Guest et al. [45]. In this publication they discuss the data saturation and variability in extracting information from interviews to determine how many interviews are enough to get meaningful results. In their experiment they concluded that to achieve meaningful themes and useful interpretation it takes as little as 6 to 12 interviews for this kind of study. They caution, however, that in some cases 12 interviews may not be enough. For example, if the "selected group is heterogeneous, the data quality is poor, and the domain of inquiry is diffuse and/or vague. Likewise, you will need larger samples if your goal is to assess variation between distinct groups or correlation among variables". With that in mind, considering that the population selected for this research is relatively homogeneous (each of the interviewees has certain expertise in the field of digital transformation) and to accommodate a certain margin to eliminate insufficient data, the authors decided to conduct 30 interviews. Patterns were noticed after 12 of them, when the goals, attributes, and benefits started to repeat themselves (although some of them were named differently like "Employees" versus "People", the meaning was the same).

With the initial set of goals (dimensions), the in-depth interviews were conducted by asking the following questions: "Which attributes would need to be in place to become digitally mature?" and "Why are these attributes important?". The purpose of the first question was to identify the attributes, the purpose of the second was to identify benefits and goals/values. After each interview, the values (goals) were noted down together with their links to the benefits, as well as the attributes that were mentioned by the experts. These links were entered into the LadderUX software [46], which generated the Implication Matrix (with calculated centralities) as well as the Hierarchical Value Map showing graphically these connections. After several interviews the set of values evolved to "Smart operations and research" (to include the scientific aspect as well as the organisational), "Smart facilities", "Smart products and services", "People", "Strategy and organisation" and "Sustainability", which was consistent throughout the majority

of the interviews. It also became evident that there is a need to standardise responses as much as possible to avoid overlap (for example, some experts referred to a dimension called “Employees”, some to “People” and some to “People and Culture”). To represent the degree of the central role of each element [47], the authors calculated the centrality. Centrality can be interpreted as a key element that determines the importance of the goals, benefits and attributes. Once calculated, the elements in each group were arranged from the largest to the smallest value of their centrality.

Overall, the authors collected 111 elements that were grouped into 7 Goals (Dimensions), 47 Benefits and 57 Attributes. After calculating each element’s centrality, they were sorted by it. The tables below show each of the elements from the largest to the smallest value of centrality. The Goals are shown in Table 4 and Benefits and Attributes in Table 5.

Table 4 List of the Goals

	Goal	Centrality
G1	Smart operations and research	0.076
G2	People	0.057
G3	Sustainability	0.051
G4	Strategy and organisation	0.024
G5	Smart facilities	0.02
G6	Smart products and services	0.013
G7	Smart innovation	0

Table 5 Summary of Benefits and Attributes

Benefit	Centrality	Attribute	Centrality
B1 Faster product development	0.051	A1 Data management	0.052
B2 Increased efficiency of operations	0.051	A2 Education of people	0.035
B3 Innovative workforce	0.047	A3 Analytics tools	0.013
B4 Faster process development	0.046	A4 Knowledge creation and management platform	0.013
B5 Faster response to market dynamics	0.037	A5 Smart platforms	0.009
B6 Skilled workforce	0.032	A6 Communication	0.009
B7 New revenues	0.019	A7 Collaboration tools	0.007
B8 More value for customers	0.019	A8 Digitalise the equipment	0.006
B9 Profitability	0.013	A9 Sharing scientific information	0.006
B10 Understand carbon footprint	0.012	A10 Sharing experimental information	0.006
B11 Increased competitiveness	0.011	A11 Digital twins/simulations	0.005
B12 Understand the strategy	0.009	A12 Access to right talent	0.005
B13 Outcome-based pricing	0.008	A13 Sustainability score dashboard	0.005
B14 Driving reputation	0.008	A14 Efficiency dashboards	0.004
B15 Increased customer satisfaction	0.006	A15 Continuous improvement for process and culture	0.004
B16 Lower energy consumption	0.006	A16 Digitise information	0.003
B17 Lower emissions	0.006	A17 Product tracking technology	0.003
B18 Less waste	0.006	A18 Change management process	0.003
B19 Operational flexibility	0.006	A19 Enabling experimentation	0.003
B20 Improved health and safety	0.006	A20 Efficient and secure IT	0.003
B21 Educated workforce	0.006	A21 Sharing data with suppliers and customers	0.003
B22 Lower carbon footprint	0.006	A22 Shared environmental data	0.003
B23 Reduced time to market	0.004	A23 Shared customer data	0.002
B24 People understand emerging technologies	0.004	A24 Predictive maintenance	0.002
B25 Limit the negative consequences of operations	0.004	A25 Smart horizontal and vertical integration	0.002
B26 Effective usage of available data	0.004	A26 Capturing value creation	0.002
B27 New customers	0.004	A27 Meaningful data exchange	0.002
B28 Market adaptability	0.004	A28 Sourcing green energy	0.002
B29 Increased employee satisfaction	0.004	A29 Sustainability assessment process	0.002
B30 Making right decisions	0.004	A30 Innovation performance reviews	0.002
B31 Longer asset lifecycle	0.004	A31 Innovation workshops	0.002
B32 Product life cycle control	0.004	A32 Innovation strategy	0.002
B33 Right pricing	0.004	A33 Technology-based intelligence	0.002
B34 Improved quality of products and services	0.004	A34 Innovation governance	0.002
B35 Faster pace to sustainability	0.004	A35 Process automation	0.002
B36 Articulate and share organisational goals	0.002	A36 Usage of standards	0.002
B37 Proactiveness	0.002	A37 Automatic commissioning of the equipment	0.001
B38 Enhanced product life	0.002	A38 Collaboration with academia	0.001

Table 5 (Continuation)

Benefit	Centrality	Attribute	Centrality
B39 Data-driven decision-making	0.002	A39 Measuring environmental impact	0.001
B40 Ability to measure impact	0.002	A40 Leadership fit	0.001
B41 Efficient resource usage	0.002	A41 Distributed team	0.001
B42 Supply chain transparency	0.002	A42 Agile strategy	0.001
B43 Positive impact on supply chain	0.002	A43 Carbon offsetting activities	0.001
B44 Attract investors	0.002	A44 Rotating people across organisation	0.001
B45 Common IT platforms	0.001	A45 Coaching/mentoring process	0.001
B46 Knowledge created and shared	0	A46 Circular economy principles	0.001
B47 Optimised use of budget	0	A47 Supply chain carbon footprint	0.001
		A48 Drone technology	0.001
		A49 Image recognition	0.001
		A50 Digital hiring tools	0.001
		A51 Governance	0.001
		A52 ISO 14001	0.001
		A53 Digitalise partnerships	0
		A54 LIMS system in place	0
		A55 Production data tracking and linking with product	0
		A56 Leverage external partners	0
		A57 Budget	0

The Hierarchical Value Map (HVM) generated by Ladderux.org [29] consisted of 242 ladders with a total of 708 links. 475 of these links were direct and 233 were indirect. The number of elements and links made the visualisation of the entire HVM difficult for the purpose of this publication. To make the ladder examples presentable, the authors carried out a separate analysis for the top three dimensions and show them in more detail in chapter 5 “Discussion”.

5. Discussion

After the round of interviews, the authors arrived at 6 dimensions. These dimensions are: “Smart operations and research”, “People”, “Sustainability”, “Strategy and organisation”, “Smart facilities” and “Smart products and services”. Due to the fact that the centrality of the “Smart innovation” dimension was 0, it was removed from the final list (see Table 4).

Out of 47 collected benefits, the 5 most prevailing ones by centrality were “Faster product development”, “Increased efficiency of operations”, “Innovative workforce”, “Faster process development” and “Faster response to market dynamics”. Four of these are related to efficiency and the speed of the response to the market, but it is worth noticing that the third most central element was related to people and innovation. It could be said that an innovative workforce benefits from the technology and education, which in return helps to achieve the goals of the organisation.

The 57 collected attributes are a mixture of technologies, tools, platforms (e.g. “Data management”, “Collaboration tools”, “Digital twins/simulations” etc.) and processes (e.g. “Collaboration with academia”, “Sustainability assessment process”, “Usage of standards”, etc.) The top ones by centrality are “Data management”, “Education of people”, “Analytics tools”, “Knowledge creation and management platform” and “Sustainable operations”. It is understandable that the “Data management” had the highest centrality score. This is required as a foundation for any operations to become “data-driven”. It was very interesting to see that the “Education of people” was placed in second position, which confirms that digitalisation is not purely dependent on technologies. On the contrary, the right education of people will be a critical attribute driving the culture shift required to move to the higher level of digital maturity. “Analytics tools” were placed in third position, which underlines the need for tools to act on the collected data. The explosion of various analytics tools offerings on the market confirms the importance of this attribute. Next in line, “Knowledge creation and management platform” seems an important attribute especially for R&D organisations where scientists create and share both scientific and organisational knowledge. As a side observation from the interviews, the authors noted that in many organisations the knowledge is scattered in various repositories, creating a challenge for people to find the right information. What is more, often there is not a single digital tool which would connect these separate pockets of knowledge. This was more visible in large organisa-

tions with various legacy knowledge repositories. However, the majority of them stated that deploying a digital tool that will connect various repositories and help to extract value from them was one of their priorities in order to speed up future development and accelerate research.

To further focus on the first three dimensions, the authors separated them from the other elements in the LadderUX tool [46]. Fig. 3 shows the dimension “Smart operations and research”, focusing on the benefit B1 – “Faster product development”.

The authors observed that “Data management” and “Analytics tools” were the first attributes contributing towards “Faster product development”. However, it is worth mentioning the “Knowledge creation and management platform” - although it is a technical tool, it fosters collaboration and teamwork as people will use it to document their work and to learn from what was already done in the past on any given topic or project.

A very similar pattern could be observed for “Faster process development”. This is due to the fact that, usually, to produce any given product faster, the production or manufacturing process needs to be more efficient.

Interestingly, taking a closer look at the three further benefits with the largest centrality, it can be concluded that their key attributes are the same as those previously described and illustrated in Figs 5 and 6. These benefits are “Increased efficiency of operations”, “Faster response to market dynamics” and “Faster pace to sustainability” (see Fig. 4). The important thing to notice in this ladder is the link between digital transformation and sustainability. It shows that, by achieving the goal of “Smart operations and research”, the organisation will not only become more efficient and faster in terms of product development and manufacturing. It clearly also accelerates the path to sustainability and proves that, by moving up on the digital maturity curve, companies become more sustainable.

Fig. 5 shows the simplified HVM for the “People” dimension. The simplification eliminated elements with fewer than 5 connections.

For this dimension the emphasis should be put on the education attribute. Arming people with the right skillset future-proofs the existence of the organisation. Education also makes people more aware of the context of digitalisation and its purpose, which makes it easier to accept change. Additionally, education, training and overall career development have a big influence on employee satisfaction and a significant impact on their performance, driving the performance of the organisation [48].

To visualise the sustainability, the authors disabled all other dimensions in the laddering tool and then set cut-off values for connections equal to or less than 2 for the attributes and benefits, ending up with the ladder shown in Fig. 6.

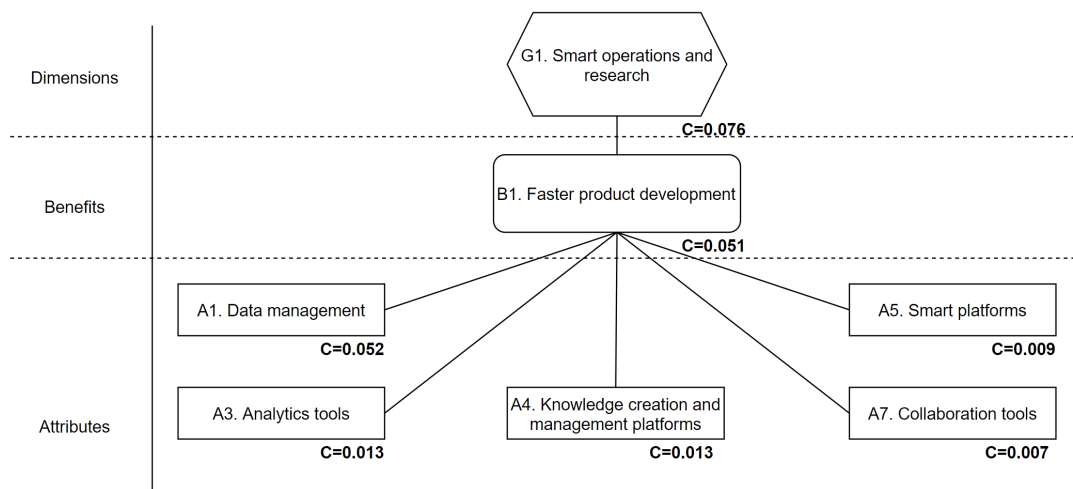


Fig. 3 Simplified ladder diagram for “Smart operations and research” (Faster product development benefit)

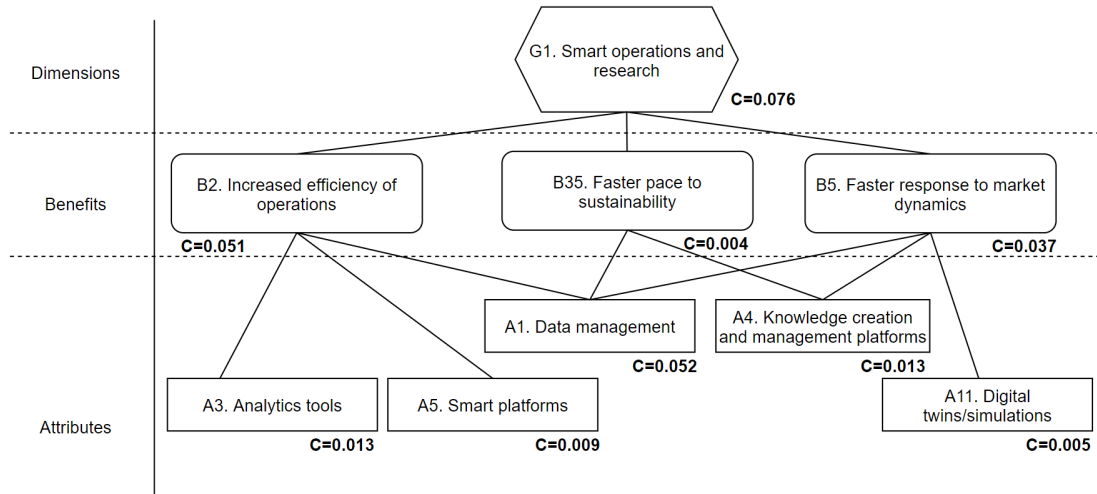


Fig. 4 Simplified ladder diagram for “Smart operations and research”

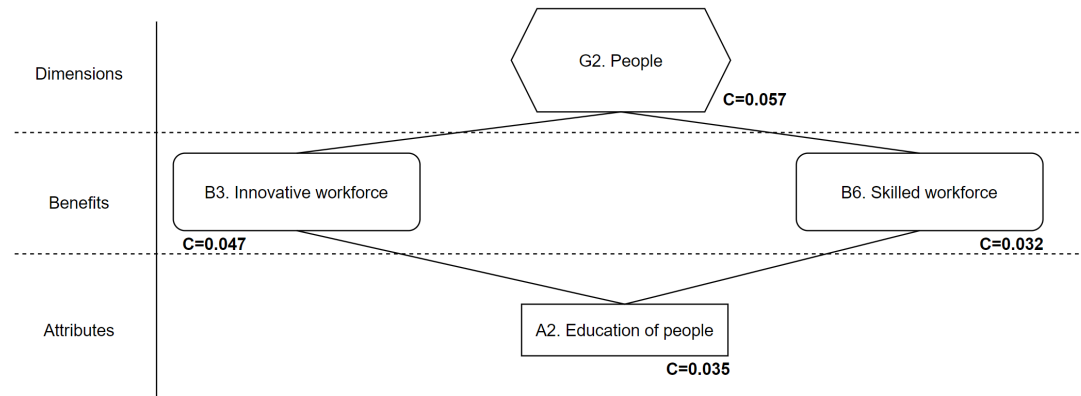


Fig. 5 Simplified ladder diagram for “People” dimension

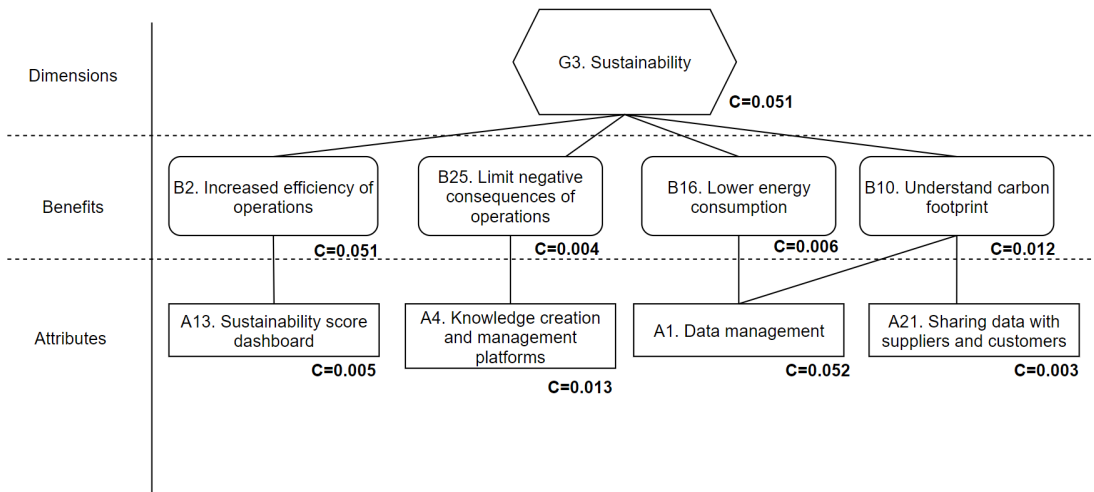


Fig. 6 Simplified ladder diagram for “Sustainability” dimension

It was evident again that “Data management” is a key attribute, contributing to lower energy consumption, by enabling data-driven decision-making. It also allows a better understanding of the carbon footprint. As it forms the foundation for digitalisation, it is an important contributor towards better sustainability.

In order to move to a higher stage of digital maturity, the data management (the attribute that comes with the highest centrality from all 59), supported by the analytics tools (the attribute that came third), should be the first ones considered when preparing the digital roadmap for the organisation. If the budget is limited and requires prioritisation, these should be the top priorities, contributing to most of the goals, including “Sustainability”.

Finally, the authors carried out a sensitivity analysis to understand how each single attribute influences the dimensions. For this, they calculated the values of the dimensions’ maturity separately for each attribute, setting its value to 1 (full influence on the dimensions) while setting all the other attributes’ values to 0 (no influence on dimensions). The result is shown in Fig. 7. Such analysis can be very useful for selecting the areas of focus when creating plans and planning the resources needed for achieving higher levels of maturity. For example, focusing solely on “Real-time data collecting and sharing” and investing most of the effort in improving the data management has a major positive influence on the overall digital maturity for most of the dimensions. It could be imagined that the creators of roadmaps and strategies could place a “Threshold line” on the diagram and use it to plan their activities: moving the threshold line up or down on the vertical scale could help in filtering the attributes and optimise between the desired maturity levels and the resources available to invest in the selected attributes.

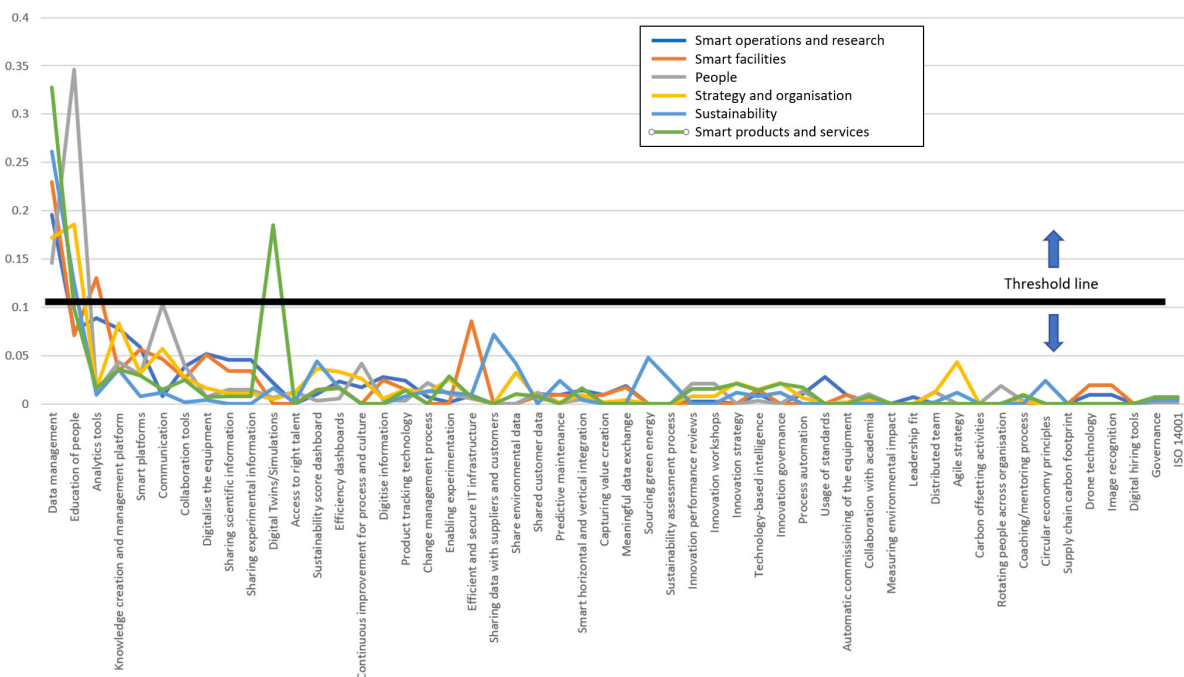


Fig. 7 Attributes’ influence on dimensions

Sustainability aspect

One of the observations after conducting the initial review was that currently available Digital Maturity or Industry 4.0 Readiness models do not include the sustainability aspect. The authors asked themselves the following question: “why is sustainability important, and should it be included in digitalisation activities at all?”

The conclusion was that it is impossible to be “digitally mature” without considering the sustainability aspect. This is true even more in the case of R&D organisations as they work to drive and secure the long-term future (and thus economic sustainability) of the company. This thinking was confirmed by the results from the interviews, where the dimension of “Sustainability” had the centrality of 0.045, placing it in third place after “Smart operations and research” and

“People” and before “Strategy and organisation”, “Smart facilities” and “Smart products and services”. This clearly demonstrates that it is high on the agenda of the experts. It is also natural to think that an organisation that progresses on the digital maturity journey will become more efficient, generating less waste, becoming naturally more friendly to the environment and to society. There are other, non-tangible motivations like the simple fact that people care about sustainability more than they used to years ago, knowing more about how operations impact the environment and society.

Such conclusions were also confirmed by emerging research which concludes that both digitalisation and sustainability are interconnected [8, 18, 19].

To further understand the current situation, separate interviews were conducted with both Sustainability and Digitalisation teams in one of the world’s leading manufacturing companies, concluding that even if companies include both Digital and Sustainability strategies in their operations, they are most likely executed in parallel by different teams. The skills of the teams are different or hardly overlapping, with the Digitalisation teams being more technical than the Sustainability teams. Another observation was that, while there is an initial appetite to merge both concepts from the Sustainability side, the Digitalisation tends to focus on narrower aspects related to shorter-term goals associated with ongoing projects like reducing energy consumption, CO₂ emissions, diffuse dust pollution, etc.)

6. Conclusion

In this study the authors attempted to determine the key elements of the Digital Maturity model applicable to R&D organisations, including the aspect of sustainability. Using the Means-End Chain method, the authors confirmed that digitalisation and sustainability are interconnected and that, by working together, they support each other. This is in line with conclusions from other research already available, including outcomes from studies carried out by Denicolai et al. [8] and Gupta et al. [19]. With this in mind, and the fact that the “Sustainability” dimension was the third most important one by centrality after “Smart operations and research” and “People”, the authors concluded that it should be included in the maturity model.

The following dimensions of the R&D Digital Maturity model emerged from the research, listed from largest to smallest centrality: “Smart operations and research”, “People”, “Sustainability”, “Strategy and organisation”, “Smart facilities” and “Smart products and services”. Interestingly, looking into the centrality gap between these elements, it can be determined that “Smart operations and research” should be the most important element to address. The gap between this element and the next two (“People” and “Sustainability”) was 0.019. Expert opinion clearly stated that the way in which R&D is organised, how it conducts the experiments, how it collects, stores and uses data, how it generates and shares knowledge, and the way it collaborates with both customers and partners are the key factors to accelerate research outcomes. The next areas to review when considering the digital maturity roadmap are “People” and “Sustainability”. The centrality gap between them was only 0.006, which indicates that they are both of equal importance. The second highest centrality for the “People” dimension clearly indicates that culture and the people factor must be considered together with the technology factor during the setting up of the transformation program. Sustainability had the third highest centrality score, showing its growing importance. The last three dimensions, “Strategy and Organisation”, “Smart Facilities” and “Smart Products and Services”, were separated from the three first by 0.027. Such gap splits the dimensions into two clusters which can be used as an indication for priority when building the digital transformation roadmaps. It is possible that such distribution is specific and only visible for R&D organisations, as they usually rely on human potential enabling creativity and innovation based on the solid foundation of technology.

Collaboration between digitalisation and sustainability is essential. R&D organisations should embrace and lead this effort as they are at the forefront of progress in all industries. The authors included the aspect of sustainability in the Digital Maturity model based on the results from the interviews, but also based on emerging trends, where both strategies are at the top of the agendas of companies as well as policy-makers in the majority of countries, companies and institu-

tions. The digitalisation will aid and accelerate the path to sustainability by the application of technologies, processes, and skills. Most likely those R&D organisations which progress on the digital maturity path and include the “Sustainability” dimension will be able to better carry out activities to innovate and introduce new products, services, and processes. They will also support their customers better and use innovative and effective ways to generate and share knowledge, which, in turn, will automatically help both their internal or external customers to become leaders in their respective markets and sectors.

When it comes to further research, the authors suggest two paths built on their initial work. Path 1 focuses on continuing to build the Digital Maturity model for R&D organisations by further nurturing the attributes and benefits leading to the model, including levels of maturity, scores and the process of assessing digital maturity, as well as the process of monitoring progress. This could result in an assessment tool that could be used by various organisations to assess their maturity and build their digital roadmaps. Path 2 relates to the Sustainability dimension to further nurture how technologies can accelerate it. It can be focused on all the aspects of digitalisation (for example, how predictive maintenance can extend the life of an asset, how a digital twin can eliminate the need for physical design, testing and monitoring, how IoT/IIoT can facilitate data science-based techniques and remote operations and monitoring, contributing towards such factors as health and safety, reducing waste and pollution and many others.

References

- [1] Huhtala, H., Parzefall, M.-R. (2007). A review of employee well-being and innovativeness: An opportunity for a mutual benefit, *Creativity and Innovation Management*, Vol. 16, No. 3, 299-306, [doi: 10.1111/j.1467-8691.2007.00442.x](https://doi.org/10.1111/j.1467-8691.2007.00442.x).
- [2] Medic, N., Anisic, Z., Lalic, B., Marjanovic, U., Brezocnik, M. (2019). Hybrid fuzzy multi-attribute decision making model for evaluation of advanced digital technologies in manufacturing: Industry 4.0 perspective, *Advances in Production Engineering & Management*, Vol. 14, No. 4, 483-493, [doi: 10.14743/apem2019.4.343](https://doi.org/10.14743/apem2019.4.343).
- [3] Kretschmer, T., Khashabi, P. (2020). Digital transformation and organization design: An integrated approach, *California Management Review*. Vol. 62, No. 4, 86-104, [doi: 10.1177/0008125620940296](https://doi.org/10.1177/0008125620940296).
- [4] Kane, G.C., Palmer, D., Nguyen-Phillips, A., Kiron, D., Buckley, N. (2017). Achieving digital maturity, MIT Sloan Management Review and Deloitte University Press, Vol. 59.
- [5] Martinčević, I., Kozina, G. (2021). Influence of digital technologies and its technological dynamics on company management, *Tehnički Vjesnik – Technical Gazette*, Vol. 28, No. 4, 1262-1267, [doi: 10.17559/TV-20200924091906](https://doi.org/10.17559/TV-20200924091906).
- [6] Lozano, R. (2015). A holistic perspective on corporate sustainability drivers: A holistic perspective on corporate sustainability drivers, *Corporate Social Responsibility and Environmental Management*, Vol. 22, No. 1, 32-44, [doi: 10.1002/csr.1325](https://doi.org/10.1002/csr.1325).
- [7] Hussain, S., Jahanzaib, M. (2018). Sustainable manufacturing – An overview and a conceptual framework for continuous transformation and competitiveness, *Advances in Production Engineering & Management*, Vol. 13, No. 3, 237-253, [doi: 10.14743/apem2018.3.287](https://doi.org/10.14743/apem2018.3.287).
- [8] Denicolai, S., Zucchella, A., Magnani, G. (2021). Internationalization, digitalization, and sustainability: Are SMEs ready? A survey on synergies and substituting effects among growth paths, *Technological Forecasting and Social Change*, Vol. 166, Article No. 120650, [doi: 10.1016/j.techfore.2021.120650](https://doi.org/10.1016/j.techfore.2021.120650).
- [9] Purba, H.H., Nindiani, A., Trimarjoko, A., Jaqin, C., Hasibuan, S., Tampubolon, S. (2021). Increasing Sigma levels in productivity improvement and industrial sustainability with Six Sigma methods in manufacturing industry: A systematic literature review, *Advances in Production Engineering & Management*, Vol. 16, No. 3, 307-325, [doi: 10.14743/apem2021.3.402](https://doi.org/10.14743/apem2021.3.402).
- [10] Fletcher, G., Griffiths, M. (2020). Digital transformation during a lockdown, *International Journal of Information Management*, Vol. 55, Article No. 102185, [doi: 10.1016/j.ijinfomgt.2020.102185](https://doi.org/10.1016/j.ijinfomgt.2020.102185).
- [11] Mohanty, V., Zunjur, A. (2022). Covid-19 pandemic preparedness of organizations and its impact on digital maturity, *Parikalpana: KIIT Journal of Management*, Vol. 18, No. 1, 134-144, [doi: 10.23862/kiit-parikalpana/2022/v18/i1/212351](https://doi.org/10.23862/kiit-parikalpana/2022/v18/i1/212351).
- [12] Kiel, D., Müller, J.M., Arnold, C., Voigt, K.-I. (2017). Sustainable industrial value creation: Benefits and challenges of Industry 4.0, *International Journal of Innovation Management*, Vol. 21, No. 8, Article No. 1740015, [doi: 10.1142/S1363919617400151](https://doi.org/10.1142/S1363919617400151).
- [13] Röglinger, M., Pöppelbuß, J., Becker, J. (2012). Maturity models in business process management, *Business Process Management Journal*, Vol. 18, No. 2, 328-346, [doi: 10.1108/14637151211225225](https://doi.org/10.1108/14637151211225225).
- [14] De Bruin, T., Rosemann, M., Freeze, R., Kulkarni, U. (2005). Understanding the main phases of developing a maturity assessment model, In: *Proceedings of 16th Australasian Conference on Information Systems, ACIS 2005*, Sydney, Australia, 8-19.

- [15] Kupilas, K.J., Rodriguez-Montequin, V., Villanueva-Balsera, J., Alvarez-Perez, C. (2020). Industry 4.0 and digital maturity, In: Zahera-Pérez (ed.), *Industria 4.0 y la Dirección e Ingeniería de proyectos. - Dirección e ingeniería de proyectos*; 3, Universidad de Cádiz, Cádiz, Spain, 66-102.
- [16] Brundtland, G.H., Khalid, M., Agnelli, S., Al-Athel, S., Chidzero, B., Fadika, L., de Botero, M.M. (1987). Our common future ("Brundtland report"), New York, United Nations, Report of the World Commission on Environment and Development, from https://www.unicas.it/media/2732719/Rapporto_Brundtland_1987.pdf, accessed December 15, 2021.
- [17] Khan, M.A. (1995). Sustainable development: The key concepts, issues and implications, *Sustainable Development*, Vol. 3, No. 2, 63-69, doi: 10.1002/sd.3460030203.
- [18] Javaid, M., Haleem, A., Singh, R.P., Suman, R., Gonzalez, E.S. (2022). Understanding the adoption of Industry 4.0 technologies in improving environmental sustainability, *Sustainable Operations and Computers*, Vol. 3, 203-217, doi: 10.1016/j.susoc.2022.01.008.
- [19] Gupta, S., Motlagh, M., Rhyner, J. (2020). The digitalization sustainability matrix: A participatory research tool for investigating digitainability, *Sustainability*, Vol. 12, No. 21, Article No. 9283, doi: 10.3390/su12219283.
- [20] Seele, P., Lock, I. (2017). The game-changing potential of digitalization for sustainability: Possibilities, perils, and pathways, *Sustainability Science*, Vol 12, 183-185, doi: 10.1007/s11625-017-0426-4.
- [21] Kitchenham, B., Charters, S.M. (2007). Guidelines for performing systematic literature reviews in software engineering, Technical report EBSE 2007-001, Keele University and University of Durham, Newcastle, Durham, United Kingdom, from https://www.researchgate.net/publication/302924724_Guidelines_for_performing_Systematic_Literature_Reviews_in_Software_Engineering, accessed December 15, 2021.
- [22] Kljajić Borštnar, M., Pucihar, A. (2021). Multi-attribute assessment of digital maturity of SMEs, *Electronics*, Vol. 10, No. 8, Article No. 885, doi: 10.3390/electronics10080885.
- [23] Ochoa-Urrego, R.-L., Peña-Reyes, J.-I. (2021). Digital maturity models: A systematic literature review, *Digitalization*, In: Schallmo, D.R.A., Tidd, J. (eds.), *Digitalization, Management for Professionals*, Springer, Cham, Switzerland, 71-85, doi: 10.1007/978-3-030-69380-0_5.
- [24] Cotrino, A., Sebastián, M.A., González-Gaya, C. (2020). Industry 4.0 roadmap: Implementation for small and medium-sized enterprises, *Applied Sciences*, Vol. 10, No. 23, Article No. 8566, doi: 10.3390/app10238566.
- [25] Gandhi, A., Sucahyo, Y.G. (2020). Towards a comprehensive exploration and mapping of maturity models in digital business, *DESIDOC Journal of Library & Information Technology*, Vol 40, No. 4, 253-261, doi: 10.14429/djlit.40.04.15673.
- [26] Teichert, R. (2019). Digital transformation maturity: A systematic review of literature, *Acta Universitatis Agricul-turae et Silviculturae Mendelianae Brunensis*. Vol. 67, No. 6, 1673-1687, doi: 10.11118/actaun201967061673.
- [27] Williams, C., Schallmo, D., Lang, K., Boardman, L. (2019). Digital maturity models for small and medium-sized enterprises: A systematic literature review, In: *Proceedings of The ISPIM Innovation Conference – Celebrating Innovation: 500 Years Since daVinci*, Florence, Italy.
- [28] Santos, R.C., Martinho, J.L. (2020). An Industry 4.0 maturity model proposal. *Journal of Manufacturing Technology Management*, Vol. 31, No. 5, 1023-1043, doi: 10.1108/JMTM-09-2018-0284.
- [29] Gökalp, E., Şener, U., Eren, P.E. (2017). Development of an assessment model for Industry 4.0: Industry 4.0-MM, In: Mas, A., Mesquida, A., O'Connor, R., Rout, T., Dorling, A. (eds.), *Software process improvement and capability determination. SPICE 2017. Communications in computer and information science*, Vol. 770, Springer, Cham, Switzerland, 128-142, doi: 10.1007/978-3-319-67383-7_10.
- [30] Lichtblau, K., Stich, V., Bertenrath, R., Blum, M., Bleider, M., Millack, A., Schmitt, K., Schmitz, E., Schröter, M. (2015). Industrie 4.0 Readiness, Impuls-Stiftung des VDMA, Aachen, Cologne, from <https://impuls-stiftung.de/wp-content/uploads/2022/05/Industrie-4.0-Readiness-english.pdf>, accessed August 15, 2021.
- [31] Geissbauer, R., Vedso, J., Schrauf, S. (2016). Industry 4.0: Building the digital enterprise: 2016 global Industry 4.0 survey, <https://www.pwc.com/gx/en/industries/industries-4.0/landing-page/industry-4.0-building-your-digital-enterprise-april-2016.pdf>, accessed August 15, 2021.
- [32] Leyh, C., Schäffer, T., Bley, K., Forstehäusler, S. (2016). SIMMI 4.0 – A maturity model for classifying the enterprise-wide IT and software landscape focusing on Industry 4.0, In: *Proceedings of the 2016 Federated Conference on Computer Science and Information Systems*, Poznań, Poland, 1297-1302, doi: 10.15439/2016F478.
- [33] Schuh, G., Anderl, R., Gausemeier, J., ten Hompel, M., Wahlster, W. (2017). *Industrie 4.0 maturity index, Managing the digital transformation of companies*, (acatech STUDY), Herbert Utz Verlag, Munich, Germany.
- [34] De Carolis, A., Macchi, M., Negri, E., Terzi, S. (2017). Guiding manufacturing companies towards digitalization a methodology for supporting manufacturing companies in defining their digitalization roadmap, In: *Proceedings of 2017 International Conference on Engineering, Technology and Innovation (ICE/ITMC)*, Madeira, Portugal, 487-495, doi: 10.1109/ICE.2017.8279925.
- [35] Schumacher, A., Erol, S., Sihn, W. (2016). A maturity model for assessing Industry 4.0 readiness and maturity of manufacturing enterprises, *Procedia CIRP*, Vol. 52, 161-166, doi: 10.1016/j.procir.2016.07.040.
- [36] Colli, M., Madsen, O., Berger, U., Møller, C., Wæhrens, B.V., Bockholt, M. (2018). Contextualizing the outcome of a maturity assessment for Industry 4.0, *IFAC-PapersOnLine*, Vol. 51, No. 11, 1347-1352, doi: 10.1016/j.ifacol.2018.08.343.
- [37] Verburg, R.M., Bosch-Sijtsema, P., Vartiainen, M. (2013). Getting it done: Critical success factors for project managers in virtual work settings, *International Journal of Project Management*, Vol. 31, No. 1, 68-79, doi: 10.1016/j.ijproman.2012.04.005.

- [38] Chen, C.-H., Wang, C.-L., Chen, P.-Y. (2018). Performance evaluation of the service industry innovation research program: The application of a means-end chain, *Technology in Society*, Vol. 54, 111-119, [doi: 10.1016/j.techsoc.2018.03.009](https://doi.org/10.1016/j.techsoc.2018.03.009).
- [39] Gutman, J. (1982). A means-end chain model based on consumer categorization processes, *Journal of Marketing*, Vol. 46, No. 2, 60-72, [doi: 10.1177/002224298204600207](https://doi.org/10.1177/002224298204600207).
- [40] van Rekom, J., Wierenga, B. (2007). On the hierarchical nature of means-end relationships in laddering data, *Journal of Business Research*, Vol. 60, No. 4, 401-410, [doi: 10.1016/j.jbusres.2006.10.004](https://doi.org/10.1016/j.jbusres.2006.10.004).
- [41] Reynolds, T.J., Gutman, J. (2001). Laddering theory, method, analysis, and interpretation, In: Reynolds, T.J., Olson, J.C. (eds.), *Understanding consumer decision making*, 1st Edition, Psychology Press, New York, USA, 40-79, [doi: 10.4324/9781410600844](https://doi.org/10.4324/9781410600844).
- [42] Grunert, K.G., Grunert, S.C. (1995). Measuring subjective meaning structures by the laddering method: Theoretical considerations and methodological problems, *International Journal of Research in Marketing*, Vol. 12, No. 3, 209-225, [doi: 10.1016/0167-8116\(95\)00022-T](https://doi.org/10.1016/0167-8116(95)00022-T).
- [43] Costa, A.I.A., Dekker, M., Jongen, W.M.F. (2004). An overview of means-end theory: Potential application in consumer-oriented food product design, *Trends in Food Science & Technology*, Vol. 15, No. 7-8, 403-415, [doi: 10.1016/j.tifs.2004.02.005](https://doi.org/10.1016/j.tifs.2004.02.005).
- [44] Pieters, R., Baumgartner, H., Allen, D. (1995). A means-end chain approach to consumer goal structures, *International Journal of Research in Marketing*, Vol. 12, No. 3, 227-244, [doi: 10.1016/0167-8116\(95\)00023-U](https://doi.org/10.1016/0167-8116(95)00023-U).
- [45] Guest, G., Bunce, A., Johnson, L. (2006). How many interviews are enough? An experiment with data saturation and variability, *Field Methods*, Vol. 18, No. 1, 59-82, [doi: 10.1177/1525822X05279903](https://doi.org/10.1177/1525822X05279903).
- [46] LadderUX, Home, from <https://ladderux.org/>, accessed August 15, 2022.
- [47] Arsil, P., Li, E., Bruwer, J. (2016). Using means-end chain analysis to reveal consumers' motivation for buying local foods: An exploratory study, *Gadjah Mada International Journal of Business*, Vol. 18, No. 3, 285-300, [doi: 10.22146/gamaijb.6061](https://doi.org/10.22146/gamaijb.6061).
- [48] Wahyuni, N. (2016). Effect of education and training, career development and job satisfaction of employee performance at the department of education office of Gowa, *Journal of Education and Vocational Research*, Vol. 7, No. 1, 14-20, [doi: 10.22610/jevr.v7i1.1217](https://doi.org/10.22610/jevr.v7i1.1217).

Supply chain coordination based on the probability optimization of target profit

Jian, M.^a, Liu, T.^{a,*}, Hayrutdinov, S.^b, Fu, H.^a

^aSchool of Transportation and Logistics, Southwest Jiaotong University, Chengdu, P.R. China

^bManagement Development Institute of Singapore in Tashkent, Uzbekistan

ABSTRACT

Supply chain management decision-making study mainly based on the expected utility theory and most of the studies are obtaining the average values in the statistical sense. For Supply Chain (SC) decision-making individuals the statistical-based optimal profitability brings decision conflicts in the particular market within a specific period. Moreover, the small and medium outsourcing participants face unexpected outcomes which are the main cause of SCs disruption. This study proposes a contractual coordination model that maximizes the probability of a pre-determined Profit Target (PT). The purpose of this paper is to reduce the influence of demand uncertainty with the high risk of unexpected outcomes. We constructed the Revenue Sharing (RS) and buyback contract models within the SC participants' PT conditions and then discussed the SC overall performance. We simulated and analyzed the coordination conditions and the decision-making preferences of SC participants under the two contracts. From the comparison, under the PT strategy, the retailer is more willing to adopt the RS contract rather than the buyback contract. But the SC upstream supplier's contract selection decision depends on the specific contract parameters. Finally, numerical results indicated the contract selection decisions with the given PT of both SC participants.

ARTICLE INFO

Keywords:

Supply chain;
Coordination;
Contractual coordination;
Revenue-sharing contract;
Buyback contract;
Profit target;
Optimization;
Probability optimization

*Corresponding author:

liutong_60@163.com
(Liu, T.)

Article history:

Received 14 February 2022

Revised 8 August 2022

Accepted 12 August 2022



Content from this work may be used under the terms of the Creative Commons Attribution 4.0 International License (CC BY 4.0). Any further distribution of this work must maintain attribution to the author(s) and the title of the work, journal citation and DOI.

1. Introduction

Fast-growing market competition is increasing the SC market demand uncertainty which is one of the main causes of SCs disruption. Moreover, the healthcare industry and short life-cycle products' SCs face unpredictable and unexpected market returns caused by the combination of industry competitiveness and perishability. The management of SC with the Profit Target based on decision-makers' incentivization has multiple advantages in today's marketplace. The stability of a SC under the PT is one of the main advantageous motivations. Today's healthcare industry requires a new strategy to deal with high risks and ensure their market's satisfaction stability. Moreover, the SCs engaged in socially responsible activities and jointly intend to exhibit Corporate Social Responsibility (CSR) with a pre-determined PT may be a compromise solution. The CSR participant's profit may be negative and to keep their stability, the management of SC requires a PT level. However, the SCs with CSR solutions are under pressure of social and environmental issues [1]. The channels with a specific PT have unique profitability influence and the SCs who fail to

maximize their adoption of a new strategy will be disrupted by the market uncertainty. Additionally, a SC under the PT orientation can also ensure the profitability of chain participants within the demand uncertainty. PT might help the SC participants reduce risk and loss with a specified level of profit. PT is part of management strategies that SC participants use to manage the risks. *"A profit target is a pre-determined point at which the SC participants can initiate conditional orders in a predictable and specified level as well as maximum loss constraints"*.

The existing research in SC are mainly based on the expected utility theory, with the utility maximization as the decision-making goal. The expected utility theory is a statistical-based mean concept, which brings unexpected outcomes for SC decision-makers. Therefore, decision-making studies based on PT are promising new approaches. In the SC decision-making study with the PT, the probability of realizing a PT is maximized as the decision-making goal. Compared with the expected utility theory, the SC decision-maker can cooperate more intuitively, and it can effectively reduce the loss caused by market fluctuations.

The newsboy model is a single item inventory controlling problem within the single-period stochastic demand, where demand uncertainty is the main industry issue under inventory, pricing, and overall operational management studies [2]. Khouja investigated and reviewed the different single-period problem-based extensions [3]. The research on supply chain can be summarized into the following categories. The first is the research on the supply chain structure, which can be divided into two-level supply chain [4], three-level supply chain [5], and two-channel supply chain [6]. On this basis, there are also literature studies on the optimization of channel structure [7]. The second is to study the uncertainty risk in the supply chain [8]. Then there is the research on information asymmetry [9]. Lee *et al.* [10] defined the content of information sharing in the supply chain and constructed the basic model of information sharing in the supply chain [11]. Finally, the relevant research is based on the preference of decision makers. The common preferences are risk aversion [12], waste aversion [13], fairness concern [14], test aversion [15] and green preference [16].

The single-period problem or newsboy model-based first PT investigation with a two-product SC extension was proposed in [17]. Their study constructed a two-product SC model with a newsboy problem and investigated the effects of SC participants' decision-making on achieving the PT. The newsboy problem-based research with pricing was proposed in [18]. Yang *et al.* research considered both profit and revenue targets under the single-period problem, the study discussed the effects of profit and revenue targets on the expected profits and the probability of achieving PT or revenue target respectively [19].

Available literature mainly considered the single decision maker's behavior in a SC with the PT and the influence of various newsboy products on a SC. None of the literature considers the joint strategical decision-making of the SC participants in-between an upstream and a downstream chain participant with their PT. However, most of the research with the newsboy problem is concerned with profit maximization. Additionally, there is a lack of studies simultaneously engaged with the stability of a SC under the PT and profit maximization.

Contractual coordination provides a viable alternative as a mechanism for coordination of the SC and proves to be an interesting research direction. Various decentralized SC processes have been coordinated aiming to improve the functionality. The concept of contractual coordination in improving the SC processes have been widely investigated. Researchers and practitioners used incentivization to motivate and coordinate their SC performance [20]. The contractual coordination mechanisms are important to have the decentralized SC's decision-makers pursue channel coordination. The existing SC contractual coordination mechanism with the newsboy problem is proposed by Arrow and Harris [21]. The most common applied contractual coordination mechanisms include wholesale price contracts [21], RS contracts [22], buyback contracts [23], and quantity flexibility contracts [24]. Considering contractual coordination under the newsboy problem, the buyback contract is incentivizing to increase an order quantity by sharing the inventory risk of downstream in a SC. The RS contract with the newsvendor problem plays an important role in the coordination of SC and most of the studies focused on newsvendor given with exogenous retailing price. Several extensions to the earlier contract model with newsboy have been developed [25]. Upstream supplier maximizes the profit of whole decentralized SC as the coordinator, in this

case, the RS contract model can efficiently coordinate SC members' performance. The position guarantees a contractual coordination improvement, whereas the sharing parameter determines SC total profit distribution in between members [26]. The literature on SC contract mainly focuses on profit allocation. No research investigates the PT orientated SC under the contractual coordination theory to reduce the influence of demand uncertainty.

This study constructs a contractual coordination model based on the PT oriented chain participants' incentivization. We analyzed the RS and buyback contract models with a SC participant's PT and then discussed the contract selection within SC participants' PT. Then, we characterized the decision-makers' optimal profit realization and the contract selection conditions, to reduce the influence of demand uncertainty with the risk of unexpected loss. This paper expands the existing research scenarios of supply chain contracts, which is closer to the actual production situation of the market for decision makers, and also provides a reference for the design of diverse contracts.

The rest of this paper is organized as follows. Section 2 provides the basic model description, establishment, and assumptions. Section 3 analyses of the RS contract with a specific PT and coordination conditions of SC. Section 4 provides the analyses under the buyback contract with SC PT and coordination conditions. Section 5 presents the numerical analysis of contract selection with the given PT. Section 6 summarizes and concludes the study results.

2. The basic model, description, and assumptions

In this section, we construct a basic contract model with a PT similar to *Yang et al.* [19]. Consider a two-stage SC consisting of one upstream supplier and one downstream retailer. The market demand during the single-season is stochastic. To avoid an unexpected random demand outcome that will cause chain disruption, the SC participants will set a PT. The PT is pre-determined and expected to be achieved in advance. The probability of achieving a PT is SC participants' decision-making variable as the self-interested on the stability and adoption in a SC.

To facilitate this model, this paper has the following assumptions:

- Assumption 1:* The SC upstream and downstream participants are rational decision-makers.
Assumption 2: The SC participants will determine the optimal order quantity and the maximum probability of achieving the PT based on the pre-determined target point.
Assumption 3: The SC shortage lost is not considered.
Assumption 4: The SC downstream retailer has only one opportunity to decide the ordering variable. As the classical newsboy problem, there is only one chance to order at the beginning of a single season.

We consider the SC contract parameters with a unit wholesale price w , a unit selling price p , and a unit salvage value v . The market demand is x and we denote $F(x)$ as the distribution function of x with its density $f(x)$.

Expected profit of downstream retailer

For the comparison, we first characterized a benchmark case with the retailer's profit function. Within the classical newsboy problem, SC downstream retailer's order quantity q is under the conditions of:

$$\prod r = \begin{cases} px + v(q - x) - wq & x < q \\ pq - wq & x \geq q \end{cases} \quad (1)$$

Then, the expected profit of a SC downstream retailer under the newsboy problem is as follow:

$$E_{\pi_r} = \int_0^q (px + v(q - x) - wq)f(x)dx + \int_q^{+\infty} (pq - wq)f(x)dx \quad (2)$$

For the retailer's profit analysis, where the downstream retailer set a PT, we donate the constraint conditions of order quantity. When $x < q$ the retailer's profit increases with the increase of market demand; else when $x \geq q$ the retailer's profit does not change with the change of market demand and the maximum profit can be reached when $x = q$. If the retailer has a PT t_r to

achieve, it cannot exceed the maximum profit, as $t_r \leq pq - wq$ and $q \geq \frac{t_r}{p-w}$. Thus, if $q < \frac{t_r}{p-w}$, then $t_r > pq - wq$, the probability of achieving the PT is 0. When $q \geq \frac{t_r}{p-w}$, in order to achieve the PT, the condition needs to satisfy $px + v(q - x) - wq \geq t_r$. Hence, we can get $x \geq \frac{(w-v)q+t_r}{(p-v)}$ and the probability of $x \geq \frac{(w-v)q+t_r}{(p-v)}$ is $1 - F\left(\frac{(w-v)q+t_r}{(p-v)}\right)$. Therefore, the probability of the SC retailer's

$$PT \text{ is: } P(t_r) = \begin{cases} 0 & q < \frac{t_r}{p-w} \\ 1 - F\left(\frac{(w-v)q+t_r}{(p-v)}\right) & q \geq \frac{t_r}{p-w} \end{cases}$$

When $q < \frac{t_r}{p-w}$, the probability of the SC retailer's PT is 0; when $q \geq \frac{t_r}{p-w}$, the probability of the retailer achieving the PT increases with the increase of q . The optimal order quantity of the retailer can be obtained as $\frac{t_r}{p-w}$ where the probability of the retailer's PT is $1 - F\left(\frac{t_r}{p-w}\right)$.

Definition 1: In the SC downstream retailer's decision on maximizing the probability, he first sets a PT t_r based on his actual situation. In order to achieve a PT, the retailer's optimal order quantity is $\frac{t_r}{p-w}$ and the probability of achieving the PT is maximum $1 - F\left(\frac{t_r}{p-w}\right)$.

Expected profit of upstream supplier

SC upstream supplier has a unit production cost c and the total profit of the supplier can be expressed as follow:

$$\prod s = wq - cq \tag{3}$$

Where the expected profit of the SC upstream supplier under the newsboy problem is as follow:

$$E\pi_s = \int_0^{+\infty} (wq - cq)f(x)dx \tag{4}$$

For the SC upstream supplier, who does not face the market demand directly, the profit will not change with the change of market demand. Therefore, the profit that the supplier can achieve is $wq - cq$, and the probability of achieving her PT is 100%.

From the basic model analysis, we can get the following three aspects of the problem:

- Comparing to the SC downstream retailer conditions, the upstream supplier does not bear the market risk, and her profit will not change with the change of market demand. The supplier only incentivized to get the downstream retailer's order as much as possible, so that she can achieve higher profit;
- When the SC retailer determines the PT, it can increase the probability of achieving the PT by adjusting his order quantity. There is an optimal order quantity under each specific PT for retailer, but the SC downstream's order quantity is not optimal from the point of supplier and the overall SC.
- For the SC retailer and supplier, the level of PT that can be achieved by both participants are less under the decentralized decision-making control.

Thus, the research of PT oriented SC contracts analyzes both participants' decision-making in order to find the overall SC coordination conditions.

Definition 2: When the SC participants are making an uniform decision in order to maximize their probability of achieving PT with an optimal order quantity, we define this condition as the SC coordination.

3. Revenue-sharing contract with a specific profit target

In this section, we construct the RS contract with PT oriented SC retailer and supplier, then we consider the coordination conditions under the RS contract from the perspective of SC participants' PT. The downstream retailer is a SC leader and the upstream supplier is a follower.

Based on the *Definition 1*, the events of the decision-making process under the RS contract with SC participants' PT and based on the *Definition 2*, the analyzes of the coordination conditions under the RS contract with SC participants' PT are as follows:

- 1) SC downstream retailer and upstream supplier set their PT.
- 2) SC upstream supplier is committed to providing for the retailer a lower wholesale price, while the downstream retailer is committed to returning a certain percentage of sales revenue.
- 3) SC retailer and supplier will determine their PT and set the optimal order quantity.
- 4) According to Definition 2, obtaining the PT based RS contract coordination conditions.
- 5) Analyzing the RS contract conditions for the improvement of the overall SC profitability.

3.1 Analysis of the retailer's decision

Under the RS contract, the supplier charges wholesale price w_φ per unit product while the downstream retailer is committed to returning a certain percentage $(1 - \varphi)$ of sales revenue to the supplier for making up for the supplier's profit loss due to the lower wholesale price to the retailer. Thus, the total profit of the downstream retailer can be expressed as:

$$\prod r = \begin{cases} \varphi[px + v(q - x)] - w_\varphi q & x < q \\ \varphi pq - w_\varphi q & x \geq q \end{cases} \quad (5)$$

Where φ assumed to be in the range of $0 < \varphi < 1$, and the expected profit of the downstream retailer under the newsboy problem is as follow:

$$E\pi_r = \int_0^q (\varphi(px + v(q - x)) - w_\varphi q) f(x) dx + \int_q^{+\infty} (\varphi pq - w_\varphi q) f(x) dx \quad (6)$$

For the retailer's PT analysis, when $t_r > (\varphi p - w_\varphi)q$, we have $P(t_r) = 0$, that is, when $q < \frac{t_r}{\varphi p - w_\varphi}$ $P(t_r) = 0$; when $t_r = (\varphi p - w_\varphi)q$, which is $q = \frac{t_r}{\varphi p - w_\varphi}$, we have $P(t_r) = 1 - F(q)$; and when $t_r \leq (\varphi p - w_\varphi)q$, or equivalently $q > \frac{t_r}{\varphi p - w_\varphi}$, we have $P(t_r) = 1 - F\left(\frac{(w_\varphi - \varphi v)q + t_r}{\varphi(p - v)}\right)$. Therefore, the

probability of the retailer's PT under RS contracts is: $P(t_r) = \begin{cases} 0 & q < \frac{t_r}{\varphi p - w_\varphi} \\ 1 - F\left(\frac{(w_\varphi - \varphi v)q + t_r}{\varphi(p - v)}\right) & q \geq \frac{t_r}{\varphi p - w_\varphi} \end{cases}$.

Theorem 1: Under the RS contract, the optimal order quantity of the SC retailer is $\frac{t_r}{\varphi p - w_\varphi}$ and the probability of achieving PT is $1 - F\left(\frac{t_r}{\varphi p - w_\varphi}\right)$.

Proof of Theorem 1: In the case where $q < \frac{t_r}{\varphi p - w_\varphi}$ the probability of achieving retailer's PT is 0. In the case where $q \geq \frac{t_r}{\varphi p - w_\varphi}$, $w_\varphi - \varphi v > 0$ we have $\frac{(w_\varphi - \varphi v)q + t_r}{\varphi(p - v)}$ which is increases with the increase of q . $1 - F\left(\frac{(w_\varphi - \varphi v)q + t_r}{\varphi(p - v)}\right)$ decreases with the increase of order quantity q . $F(x)$ is an increasing function. Therefore, the retailer's optimal order quantity is $\frac{t_r}{\varphi p - w_\varphi}$, and the probability of achieving PT is $1 - F\left(\frac{t_r}{\varphi p - w_\varphi}\right)$.

Corollary 1: Under RS contract condition, $\varphi > \frac{p - w + w_\varphi}{p}$ ($w > w_\varphi$), retailers can increase the probability of achieving PT by increasing the RS contract coefficient φ .

Proof: To increase the probability of SC retailer's PT achievement, the conditions of $1 - F\left(\frac{t_r}{\varphi p - w\varphi}\right) > 1 - F\left(\frac{t_r}{p-w}\right)$ must be satisfied. It is equivalent to $\frac{t_r}{p-w} > \frac{t_r}{\varphi p - w\varphi}$, thus we have $\varphi > \frac{p-w+w\varphi}{p}$ ($w > w_\varphi$). By taking the derivative of $1 - F\left(\frac{t_r}{\varphi p - w\varphi}\right)$ with respect to φ , we have $f\left(\frac{t_r}{\varphi p - w\varphi}\right) * \frac{pt_r}{(-w+p\varphi)^2} > 0$ for any φ . Therefore, the probability of achieving PT $1 - F\left(\frac{t_r}{\varphi p - w\varphi}\right)$ increases with the increase of RS contract coefficient φ .

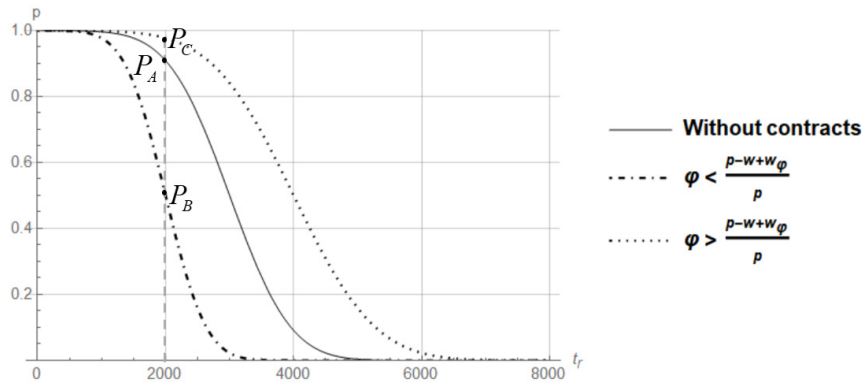


Fig. 1 The probability of achieving the PT: different sharing coefficient vs. no contract

Fig. 1 illustrates a comparison of the SC retailer's probability of achieving the PT under different contract parameters and no contract case, where P_A represents the probability of achieving the PT with no contract case; P_B represents the probability of achieving a PT under the condition where the RS contract coefficient satisfied $\varphi < \frac{p-w+w\varphi}{p}$. P_C represents the probability of achieving a PT under where the RS contract coefficient is larger, i.e., $\varphi > \frac{p-w+w\varphi}{p}$. From Fig. 1 we can get the conditions of $P_C > P_A > P_B$.

Fig. 2 illustrates a comparison of retailer's probability of achieving PT under different targets and no contract case respectively, where $t_{01} = t_{r1} < t_{02} = t_{r2}$. Consequently, Figs. 1 and 2 indicate that if $\varphi < \frac{p-w+w\varphi}{p}$ retailer's probability of achieving its PT will be significantly reduced. On the contrary, i.e., if $\varphi > \frac{p-w+w\varphi}{p}$ retailer's probability of achieving its PT will increase. Thus, the retailers prefer to use RS contract to increase their probability of achieving a PT when $\varphi > \frac{p-w+w\varphi}{p}$. Moreover, it can be seen from Fig. 1 that the condition where RS coefficient is larger, the retailer's probability of obtaining PT increases.

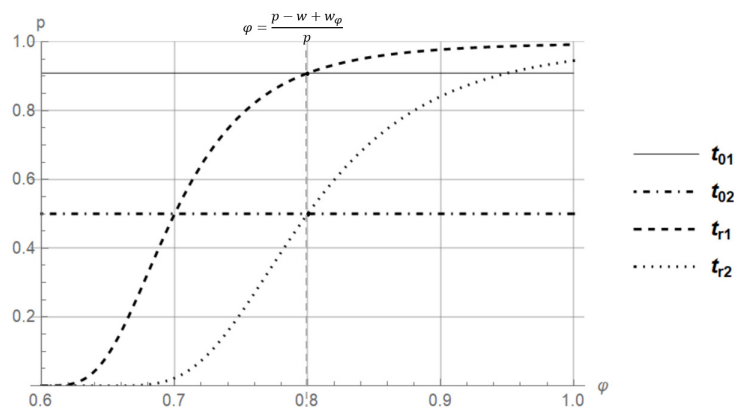


Fig. 2 The probability of achieving the PT: different PT vs. no contract

3.2 Analysis of the supplier's decision

Under RS contract the total profit condition of SC upstream supplier can be expressed as follow:

$$\prod^s = \begin{cases} (1-\varphi)[px + v(q-x)] + w_\varphi q - cq & x < q \\ (1-\varphi)pq + w_\varphi q - cq & x \geq q \end{cases} \quad (7)$$

Let t_s denote the expected PT of the supplier. For further analysis of the supplier's profit function, we know: when $t_s > [(1-\varphi)p + w_\varphi - c]q$ equivalently $q < \frac{t_s}{(1-\varphi)p + w_\varphi - c}$, where the probability is equal $P(t_s) = 0$; and when $t_s = [(1-\varphi)p + w_\varphi - c]q$ which is equivalent to $q = \frac{t_s}{(1-\varphi)p + w_\varphi - c}$, we have the probability of $P(t_s) = 1 - F(q)$; where $P(t_s) = 1 - F\left(\frac{(c-w_\varphi)q - (1-\varphi)vq + t_s}{(1-\varphi)(p-v)}\right)$, which indicates $q > \frac{t_s}{(1-\varphi)p + w_\varphi - c}$, where we have $P(t_s) = 1 - F\left(\frac{(c-w_\varphi)q - (1-\varphi)vq + t_s}{(1-\varphi)(p-v)}\right)$. Thus, we have the supplier's PT probability: $P(t_s) = \begin{cases} 0 & q < \frac{t_s}{(1-\varphi)p + w_\varphi - c} \\ 1 - F\left(\frac{(c-w_\varphi)q - (1-\varphi)vq + t_s}{(1-\varphi)(p-v)}\right) & q \geq \frac{t_s}{(1-\varphi)p + w_\varphi - c} \end{cases}$.

Theorem 2: Under the RS contract, the optimal order quantity of the upstream supplier is $\frac{t_s}{(1-\varphi)p + w_\varphi - c}$, and the probability of achieving the PT is $1 - F\left(\frac{t_s}{(1-\varphi)p + w_\varphi - c}\right)$.

Proof of Theorem 2: For a given order quantity, where q is $q < \frac{t_s}{(1-\varphi)p + w_\varphi - c}$, the supplier's probability of achieving the PT is equal to 0. When $q \geq \frac{t_s}{(1-\varphi)p + w_\varphi - c}$ the inequation $(c - w_\varphi - (1-\varphi)v) > 0$ always holds. Therefore, $\frac{(c-w_\varphi)q - (1-\varphi)vq + t_s}{(1-\varphi)(p-v)}$ increases with the increase of q . And $1 - F\left(\frac{(c-w_\varphi)q - (1-\varphi)vq + t_s}{(1-\varphi)(p-v)}\right)$ decreases with the increase of the order quantity q . $F(x)$ is an increasing function. Thus, the SC supplier's optimal order quantity is $\frac{t_s}{(1-\varphi)p + w_\varphi - c}$ and the probability of achieving the PT is $1 - F\left(\frac{t_s}{(1-\varphi)p + w_\varphi - c}\right)$.

Corollary 2: With the increase of RS coefficient φ supplier's probability of achieving PT decreases.

Proof: By taking the derivative of $1 - F\left(\frac{t_s}{(1-\varphi)p + w_\varphi - c}\right)$ with respect to φ , we have $-f\left(\frac{t_s}{(1-\varphi)p + w_\varphi - c}\right) * \frac{pt_s}{(c-w_\varphi + p(-1+\varphi))^2} < 0$ for any φ . Thus, the probability of achieving the PT $1 - F\left(\frac{t_s}{(1-\varphi)p + w_\varphi - c}\right)$ decreases with the increase of the RS contract coefficient φ .

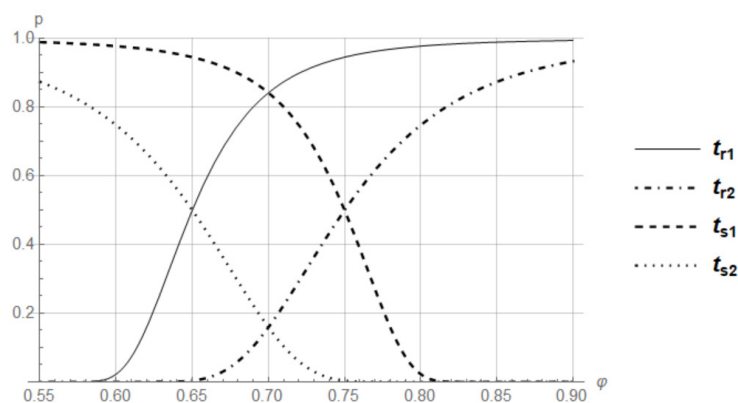


Fig. 3 SC participant's probability of achieving the PT under RS coefficient

Fig. 3 illustrates a comparison of the SC participants' PT probabilities with the RS coefficient changes. As can be seen from the Fig. 3 above, the probability of achieving the PT of the retailer increases with the increase of the RS coefficient, while the probability of achieving the PT of the supplier decreases. Moreover, the increasing probability point where the SC participants have the same PT decreases the actual PT. Therefore, an appropriate and coordinated PT will help to achieve a win-win situation.

3.3 Coordination conditions under the revenue-sharing contract

In this subsection, we discussed the SC coordination conditions under the RS contract. To achieve overall SC coordination, the optimal order quantity of the SC participants should be coherent with their PT, so that the optimal order quantity based on the probability of achieving the PT. In this case, under the RS contract conditions, the SC participants can reach their optimal order quantity at the same time they both get the highest probability of achieving their PT. Considering the coordination conditions of the RS contract, we have the following *Theorem 3*.

Theorem 3: Under the RS contract with SC participants' PT, the SC coordination condition is $t_r = -\frac{t_s(p\varphi-w_\varphi)}{c-p+p\varphi-w_\varphi}$ where $0 < (p\varphi - w_\varphi) < p - c$ If the condition falls to $0 < (p\varphi - w_\varphi) < \frac{p-c}{2}$, the SC retailer can achieve the higher PT than the upstream supplier; otherwise, i.e., $\frac{p-c}{2} < (p\varphi - w_\varphi) < p - c$, the PT of retailer is less than that of the SC upstream supplier.

Proof of Theorem 3: Under the conditions where the SC is coordinated, the optimal order quantity that the SC upstream supplier and downstream retailer can achieve the PT are equal $\frac{t_r}{\varphi p - w_\varphi} = \frac{t_s}{(1-\varphi)p + w_\varphi - c}$. Thus, we obtain $t_r = -\frac{t_s(p\varphi-w_\varphi)}{c-p+p\varphi-w_\varphi}$. For $t_r > 0, t_s > 0$, we have $\frac{(p\varphi-w_\varphi)}{p-c-(p\varphi-w_\varphi)} > 0$, which is $0 < (p\varphi - w_\varphi) < p - c$ or $p - c < (p\varphi - w_\varphi) < 0$. However, $p - c < 0$ it does not hold; thus, we have $0 < (p\varphi - w_\varphi) < p - c$. When $0 < (p\varphi - w_\varphi) < \frac{p-c}{2}$ we have $t_r > t_s$; when $\frac{p-c}{2} < (p\varphi - w_\varphi) < p - c$, therefore $t_r < t_s$.

According to Section 2 basic model analysis with the three aspects of the problem, this section analyzed the improved conditions of PT oriented SC under the RS contract.

Fig. 4 illustrates SC participants' probability of achieving PT under different conditions. The horizontal axes represent the PT and the order quantity, respectively. The vertical axes represent the probability of achieving PT. P_1, P_2 indicate the maximum probability that the retailer will achieve his PT when no contract condition and under RS contract, respectively; P_3 indicates the maximum probability that the supplier will achieve her PT under the RS contract condition; P_4, P_5 indicate the probability of retailer's achieving his PT under the different order quantity, when no contract condition and the RS contract condition, respectively; q_1, q_2 indicate the retailer's optimal order quantity to achieve a specific PT, under the no-contract condition and the RS contract condition, respectively; P_{r0}, P_{r1} indicate the retailer's probability of achieving a specific PT under the no-contract condition and the RS contract condition, respectively; $\lambda_{s0}, \lambda_{s1}$ indicate the range of PT that the supplier can achieve under the no-contract condition and the RS contract condition, respectively; $\lambda_{r0}, \lambda_{r1}$ indicate the range of PT that the SC retailer can achieve under the no-contract condition and the RS contract condition, respectively.

From the Fig. 4, the following conclusions can be seen:

- For the SC retailer, under the RS contract the probability of achieving a specific PT is higher, $P_{r1} > P_{r0}$; the range of PT that the retailer can achieve under the RS contract will also increase $\lambda_{r1} > \lambda_{r0}$;
- For the supplier, under the no-contract condition the probability of achieving specific PT is 100%, under RS contract condition the range of PT that the supplier can achieve will also increase $\lambda_{s1} > \lambda_{s0}$;
- Under the RS contract condition the SC retailer's optimal order quantity q_2 is less than the optimal order quantity q_1 when non-contractual condition. However, the SC retailer's probability of achieving his PT will increase, because of the supplier's RS portion.

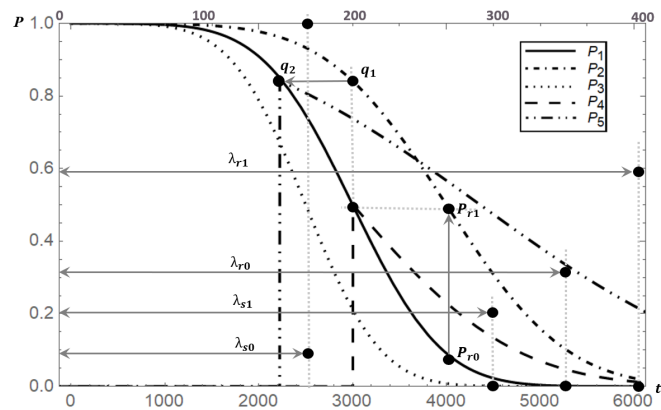


Fig. 4 Analysis of PT oriented SC coordination conditions under the RS contract.

4. Buyback contract with a specific profit target

In this section, we discussed the buyback contract under the SC participants' PT. Firstly, we constructed the buyback contract conditions for the SC downstream retailer and upstream supplier respectively. Then we analyzed the coordination conditions under the buyback contract within SC participants' PT.

Based on the *Definition 1*, the events of the decision-making process under the buyback contract with SC participants' PT and based on the *Definition 2*, the analyzes of the coordination conditions under the buyback contract with SC participants' PT are as follows:

- 1) SC downstream retailer and upstream supplier set their PTs;
- 2) The upstream supplier shares the market risk and will buy back the unsold products.
- 3) SC retailer and supplier will determine their PT and set the optimal order quantity.
- 4) According to Definition 2, obtaining the PT based RS contract coordination conditions.
- 5) Analyzing the RS contract conditions for the improvement of the overall SC profitability.

4.1 Analysis of the retailer's decision

Under the buyback contract, the supplier charges a retailer wholesale price w_b for each unit ordered product and provides the buyback credit b for each unit remaining product at the end of a selling season. Thus, the profit conditions of the SC downstream retailer can be expressed as follow:

$$\prod_r = \begin{cases} px + (b + v)(q - x) - w_bq & x < q \\ pq - w_bq & x \geq q \end{cases} \tag{8}$$

Considering the contract conditions within PT probability we can get the followings. When the retailer's PT is $t_r > (p - w_b)q$ which is $q < \frac{t_r}{p - w_b}$, the retailer's PT probability is equal to $P(t_r) = 0$. When PT is $t_r = (p - w_b)q$, which is $q = \frac{t_r}{p - w_b}$, we have the retailer's PT probability $P(t_r) = 1 - F(q)$ when $t_r \leq (p - w_b)q$ i.e. $q > \frac{t_r}{p - w_b}$ we have $P(t_r) = 1 - F\left(\frac{(w_b - b - v)q + t_r}{p - b - v}\right)$. Thus, we have overall

probability condition of retailer's PT as follow:
$$P(t_r) = \begin{cases} 0 & q < \frac{t_r}{p - w_b} \\ 1 - F\left(\frac{(w_b - b - v)q + t_r}{p - b - v}\right) & q \geq \frac{t_r}{p - w_b} \end{cases}$$

Theorem 4: Under the buyback contract, the SC retailer's optimal order quantity with his PT is $\frac{t_r}{p - w_b}$, and the probability of achieving the PT is $1 - F\left(\frac{t_r}{p - w_b}\right)$.

Proof of Theorem 4: In the case where order quantity $q < \frac{t_r}{p - w_b}$, retailer's probability of achieving the PT is equal to 0. In the next case where order quantity $q \geq \frac{t_r}{p - w_b}$, the probability $\frac{w_b - b - v}{p - b - v} > 0$.

Thus, $\frac{(w_b-b-v)q+t_r}{p-b-v}$ increases with the increase of q . And $1 - F\left(\frac{(w_b-b-v)q+t_r}{p-b-v}\right)$ decreases with increase of order quantity q . $F(x)$ is an increasing function. Therefore, retailer's optimal order quantity is $\frac{t_r}{p-w_b}$ and the probability of achieving PT is $1 - F\left(\frac{t_r}{p-w_b}\right)$.

Corollary 3: The SC retailer's probability of achieving his PT cannot increase under the buyback contract conditions.

Proof: In case of no contract, the supplier charges downstream retailer with the wholesale price w for unit product. While under the buyback contract, supplier charges downstream retailer the wholesale price w_b for unit product and provides buyback credit b for remaining product at the end of selling season. Compared to the case where the contract is not applied, the supplier will generate a transfer payment to the downstream retailer at the end of selling season due to the buyback contract conditions. Therefore, to ensure the profit, the upstream supplier must charge higher wholesale price, i.e., $w_b > w$. Similarly, under the RS contract, the upstream supplier will receive a portion of the retailer's revenue for each unit sold, so the supplier will be willing to sell at a lower wholesale price, i.e., $w_\varphi < w$. Consequently, we have $w_\varphi < w < w_b$.

In order to increase the retailer's PT probability, the contract condition has to satisfy $1 - F\left(\frac{t_r}{p-w_b}\right) > 1 - F\left(\frac{t_r}{p-w}\right)$, that is $\frac{t_r}{p-w} > \frac{t_r}{p-w_b}$. Thus, we have $w_b < w$ which is a contradiction with the premise $w_\varphi < w < w_b$. Hence, the probability that the retailer achieves his PT cannot increase using a buyback contract. Therefore, compared with the situation under the RS and buyback contracts, the SC downstream retailer prefers to choose the RS contract rather than the buyback contract.

4.2 Analysis of the supplier's decision

Under the buyback contract the total profit of the SC upstream supplier within the newsboy problem can be expressed as follow:

$$\prod_s = \begin{cases} -b(q-x) + w_bq - cq & x < q \\ w_bq - cq & x \geq q \end{cases} \tag{9}$$

With the supplier's PT, when $t_s > (w_b - c)q$, i.e., $q < \frac{t_s}{(w_b - c)}$, we have $P(t_s) = 0$; and when $t_s = (w_b - c)q$, i.e., $q = \frac{t_s}{(w_b - c)}$, we have $P(t_s) = 1 - F(q)$; finally, when the supplier's PT is $t_s \leq (w_b - c)q$, i.e., $q > \frac{t_s}{(w_b - c)}$, we have $P(t_s) = 1 - F\left(\frac{(w_b-b-c)q+t_s}{b}\right)$. Thus, we have the supplier's PT probability: $P(t_s) = \begin{cases} 0 & q < \frac{t_s}{(w_b - c)} \\ 1 - F\left(\frac{(w_b-b-c)q-t_s}{b}\right) & q \geq \frac{t_s}{(w_b - c)} \end{cases}$.

Theorem 5: Under the buyback contract, the optimal order quantity for the supplier is $q = \frac{t_s}{(w_b - c)}$ and the SC supplier's PT probability is $P(t_s) = 1 - F\left(\frac{t_s}{(w_b - c)}\right)$.

Proof of Theorem 5: For given order quantity q , when $q < \frac{t_s}{(w_b - c)}$ SC upstream supplier's probability of PT is equal to 0. When $q \geq \frac{t_s}{(w_b - c)}$ the inequation $(w_b - b - c) > 0$ always holds. Therefore, $\frac{(w_b-b-c)q-t_s}{b}$ increases with the increase of order quantity. $1 - F\left(\frac{(w_b-b-c)q-t_s}{b}\right)$ decreases with the increase of order quantity q . $F(x)$ is an increasing function. Thus, the supplier's optimal order quantity is $\frac{t_s}{(w_b - c)}$ and the probability of achieving PT is $1 - F\left(\frac{t_s}{(w_b - c)}\right)$.

Compared to the case under RS contract where the supplier's optimal order quantity is $\frac{t_s}{(1-\varphi)p+w_\varphi-c}$ the probability of achieving PT is $1 - F\left(\frac{t_s}{(1-\varphi)p+w_\varphi-c}\right)$.

When $w_b > (1 - \varphi)p + w_\varphi$ the supplier's probability of PT under the buyback contract is greater than under the usage of a RS contract, otherwise, i.e., $w_b < (1 - \varphi)p + w_\varphi$, the supplier's probability of PT under the buyback contract is less than the RS contract condition.

4.3 Coordination condition under the buyback contract

PT oriented SC coordination conditions under the buyback contract are the same as the RS contract condition, where the optimal order quantity of the SC participants should be coherent with their predetermined PT. In this case, the SC participants can reach their optimal order quantity and achieve a higher probability of their PT.

Theorem 6: Under the buyback contract parameters within the PT, the SC coordination condition is $t_r = \frac{t_s(p-w_b)}{(w_b-c)}$. When $w_b > \frac{p+c}{2}$ the SC downstream retailer's achieving PT is higher than the upstream supplier; otherwise, i.e., $w_b < \frac{p+c}{2}$, the downstream retailer's achieving PT is smaller.

Proof of Theorem 6: When SC is coordinated under the buyback contract, the optimal order quantity that the SC participants can achieve the PT is equal, i.e., $\frac{t_r}{p-w_b} = \frac{t_s}{(w_b-c)}$. Thus, the coordination condition is $t_r = \frac{t_s(p-w_b)}{(w_b-c)}$. When $w_b > \frac{p+c}{2}$, the SC retailer can achieve a higher PT than the upstream supplier, i.e., $t_r > t_s$; When $w_b < \frac{p+c}{2}$, the PT of the downstream retailer is less than that of the SC upstream supplier, i.e., $t_r < t_s$.

5. Numerical analysis

In this section, we numerically analyzed the contract selection with the given PT for both SC participants. We assumed that $c = 30$, $p = 50$, $v = 15$ and market demand x is uniformly distributed with $U(0,200)$. The density function and the cumulative distribution function of the stochastic demand x are respectively $f(x) = \frac{1}{200}$, $F(x) = \frac{x}{200}$. We assumed that the SC downstream retailer's PT is $t_r = 800$ and the upstream supplier's PT is $t_s = 1000$. Following the *Theorem 3*, we assumed with the difference of $t_r = 800 < t_s = 1000$, where $\frac{p-c}{2} < (p\varphi - w_\varphi) < p - c$, and where we have $30 < w_\varphi < 40$.

For the RS contract analysis, the SC downstream retailer's optimal order quantity is assumed as $\frac{800}{50\varphi-w_\varphi}$ following to *Theorem 1*. Where the probability of achieving the PT of 800 is $1 - \frac{4}{50\varphi-w_\varphi}$; For the SC upstream supplier, following to *Theorem 2* the optimal order quantity is $\frac{1000}{50(1-\varphi)+w_\varphi-30}$ and the probability of achieving the PT of 1000 is $1 - \frac{5}{50(1-\varphi)+w_\varphi-30}$. Thus, we can analyze the RS condition $\varphi = \frac{80+9w_\varphi}{450}$.

In Table 1, the first-row numerical values show the condition where the RS contract can coordinate the PT based SC. In this case, the probability that the SC retailer and supplier can achieve their PT are equal. With the same wholesale price but under the different RS coefficient the probability of the SC retailer's PT is increasing with the increase of the RS coefficient. The probability of supplier's PT decreases with the increase of the RS coefficient and increases with the increase of the wholesale price. This table shows that retailers prefer the contract parameters combination with high revenue sharing coefficient and low wholesale price, while suppliers prefer the opposite.

For the buyback contract analysis, the SC downstream retailer's optimal order quantity is assumed as $\frac{800}{50-w_b}$ following to *Theorem 4*. Where the probability of achieving PT of 800 is $1 - \frac{4}{50-w_b}$; For the SC upstream supplier, following to *Theorem 5* the optimal order quantity is $\frac{1000}{(w_b-30)}$ and the probability of achieving the PT of 1000 is $1 - \frac{5}{(w_b-30)}$. Then, according to *Theorem 6*, we can analyze the coordination condition under buyback contract as $w_b = \frac{370}{9}$.

Table 1 SC participants PT probabilities within the RS contract parameters

w_φ	φ	q^*	$P(t_r)$	$P(t_s)$
35.00	0.88	90.00	0.55	0.55
35.00	0.89	84.21	0.58	0.52
35.00	0.90	80.00	0.60	0.50
35.00	0.91	76.19	0.62	0.47
35.00	0.92	72.73	0.64	0.44
35.00	0.93	69.57	0.65	0.41
35.00	0.94	66.67	0.67	0.38
35.00	0.95	64.00	0.68	0.33
35.00	0.96	61.54	0.69	0.29
35.50	0.88	94.12	0.53	0.57
36.00	0.88	100.00	0.50	0.58
36.50	0.88	106.67	0.47	0.60
37.00	0.88	114.29	0.43	0.62
37.50	0.88	123.08	0.38	0.63
38.00	0.88	133.33	0.33	0.64
38.50	0.88	145.45	0.27	0.66
39.00	0.88	160.00	0.20	0.67

Table 2 SC participants PT probabilities within the buyback contract parameters

w_b	q^*	$P(t_r)$	$P(t_s)$
41.11	90.00	0.55	0.55
40.50	84.21	0.58	0.52
40.00	80.00	0.60	0.50
39.50	76.19	0.62	0.47
39.00	72.73	0.64	0.44
38.50	69.57	0.65	0.41
38.00	66.67	0.67	0.38
37.50	64.00	0.68	0.33
37.00	61.54	0.69	0.29
36.50	59.26	0.70	0.23
36.00	57.14	0.71	0.17

In Table 2, the first-row numerical values show the condition where the buyback contract can achieve coordination. At this point, the probabilities that the SC participants can achieve their PT are equal. Table 2 shows that under the buyback contract parameter w_b , the probability of SC downstream retailer's PT increases with the increase of the wholesale price, while the probability of the SC upstream supplier PT decreases. This table shows that retailers prefer contract parameters with high wholesale prices, while suppliers prefer the opposite.

6. Conclusion

The traditional SC research is based on the expected utility theory, where the expected utility maximization as the decision-making goal. Most of the studies are based on the statistical average value and thus cannot avoid the low returns or large fluctuations in profitability. For decision-makers, maximizing the probability of achieving the PT can effectively reduce their own risk. However, from the perspective of SC, each decision-maker has its own goal. There is a certain conflict between the goal of decentralized decision-making and the overall optimization of the SC. Therefore, this paper proposes the research of SC contracts based on PT.

In this study, we investigated the RS and buyback contracts based on the SC participants' PT. Different from the traditional SC contracts, it has valuable advantages for SC participants to deal with market risk. Through the research of SC contractual coordination under the PT, our main findings can be summarized as follows:

- This study analyzed the RS contract and buyback contract with PT and obtained the optimal order quantity and the probability of achieving PT for both SC participants. Additionally, we analyzed the coordination conditions of the RS contract and buyback contract with the PT.
- When the RS coefficient of the contract is within a certain range, the probability of achieving the PT can be increased for both SC participants. As the RS coefficient increases, the probability of SC retailer's PT increases, and the upstream supplier's probability of PT decreases.
- From the comparison, it can be seen that under the buyback contract a SC retailer cannot increase the probability of achieving the PT by adjusting the contract parameters. Therefore, under the PT strategy, the retailer is more willing to adopt the RS contract rather than the buyback contract.
- Under the buyback contract, the SC supplier can adjust the contract parameters within a certain range to increase the probability of achieving her PT. Compared with the RS contract, the SC upstream supplier's contract selection decision depends on the specific contract parameters.
- Coordination conditions analyses under the two main contracts proved that the PT of the SC participants can be achieved based on the contracts' parameters. This study found the unique condition where both SC participants can achieve their PT and coordinate overall SC.

Acknowledgment

The authors would like to thank to all referees, for their constructive comments and useful suggestions that help us to improve the quality of the paper. This work is supported by The National Social Science Fund of China (No. 18BGL104).

References

- [1] Panda, S., Modak, N.M. (2016). Exploring the effects of social responsibility on coordination and profit division in a supply chain, *Journal of Cleaner Production*, Vol. 139, 25-40, doi: [10.1016/j.jclepro.2016.07.118](https://doi.org/10.1016/j.jclepro.2016.07.118).
- [2] Yue, J., Chen, B., Wang, M.-C. (2006). Expected value of distribution information for the newsvendor problem, *Operations Research*, Vol. 54, No. 6, 1128-1136, doi: [10.1287/opre.1060.0318](https://doi.org/10.1287/opre.1060.0318).
- [3] Khouja, M. (1999). The single-period (news-vendor) problem: Literature review and suggestions for future research, *Omega*, Vol. 27, No. 5, 537-553, doi: [10.1016/S0305-0483\(99\)00017-1](https://doi.org/10.1016/S0305-0483(99)00017-1).
- [4] Pundoor, G., Chen, Z.-L. (2009). Joint cyclic production and delivery scheduling in a two-stage supply chain, *International Journal of Production Economics*, Vol. 119, No. 1, 55-74, doi: [10.1016/j.ijpe.2009.01.007](https://doi.org/10.1016/j.ijpe.2009.01.007).
- [5] Manzari Tavakoli, E., Mirzaee, M. (2014). Coordination of a three-level supply chain under disruption using profit sharing and return policy contracts, *International Journal of Industrial Engineering Computations*, Vol. 5, 139-150, doi: [10.5267/j.ijiec.2013.09.001](https://doi.org/10.5267/j.ijiec.2013.09.001).
- [6] Hu, H., Wu, Q., Han, S., Zhang, Z. (2020). Coordination of dual-channel supply chain with perfect product considering sales effort, *Advances in Production Engineering & Management*, Vol. 15, No. 2, 192-203, doi: [10.14743/apem2020.2.358](https://doi.org/10.14743/apem2020.2.358).
- [7] Zeng, L., Wang, J., Hu, Y. (2018). Retailer channel decisions of consumer electronics supply chain in a competitive environment, *Tehnički Vjesnik – Technical Gazette*, Vol. 25, No. 6, 1819-1828, doi: [10.17559/TV-20181101140915](https://doi.org/10.17559/TV-20181101140915).
- [8] Hou, J., Zeng, A.Z., Sun, L. (2017). Backup sourcing with capacity reservation under uncertain disruption risk and minimum order quantity, *Computers & Industrial Engineering*, Vol. 103, 216-226, doi: [10.1016/j.cie.2016.11.011](https://doi.org/10.1016/j.cie.2016.11.011).
- [9] Chen, Y., Özer, Ö. (2018). Supply chain contracts that prevent information leakage, *Management Science*, Vol. 65, No. 12, 5619-5650, doi: [10.1287/mnsc.2018.3200](https://doi.org/10.1287/mnsc.2018.3200).
- [10] Lee, H.L., Whang, S. (2000). Information sharing in a supply chain, *International Journal of Manufacturing Technology and Management*, Vol. 1, No. 1, 79-93, doi: [10.1504/IJMTM.2000.001329](https://doi.org/10.1504/IJMTM.2000.001329).
- [11] Türker, Y.A., Tunacan, T., Torkul, O. (2021). The impact of information sharing on different performance indicators in a multi-level supply chain, *Tehnički Vjesnik – Technical Gazette*, Vol. 28, No. 6, 1960-1974, doi: [10.17559/TV-20200108205821](https://doi.org/10.17559/TV-20200108205821).
- [12] Chen, X., Shum, S., Simchi-Levi, D. (2014). Stable and coordinating contracts for a supply chain with multiple risk-averse suppliers, *Production and Operations Management*, Vol. 23, No. 3, 379-392, doi: [10.1111/poms.12073](https://doi.org/10.1111/poms.12073).
- [13] Muzaffar, A., Deng, S., Malik, M.N. (2020). Contracting mechanism with imperfect information in a two-level supply chain, *Operational Research*, Vol. 20, 349-368, doi: [10.1007/s12351-017-0327-4](https://doi.org/10.1007/s12351-017-0327-4).
- [14] Haitao Cui, T., Raju, J.S., Zhang, J. (2007). Fairness and channel coordination, *Management Science*, Vol. 53, No. 8, 1303-1314, doi: [10.1287/mnsc.1060.0697](https://doi.org/10.1287/mnsc.1060.0697).
- [15] Hu, H., Wu, Q., Zhang, Z., Han, S. (2019). Effect of the manufacturer quality inspection policy on the supply chain decision-making and profits, *Advances in Production Engineering & Management*, Vol. 14, No. 4, 472-482, doi: [10.14743/apem2019.4.342](https://doi.org/10.14743/apem2019.4.342).

- [16] Fang, I.W., Lin, W.-T. (2021). A multi-objective optimal decision model for a green closed-loop supply chain under uncertainty: A real industrial case study, *Advances in Production Engineering & Management*, Vol. 16, No. 2, 161-172, doi: [10.14743/apem2021.2.391](https://doi.org/10.14743/apem2021.2.391).
- [17] Lau, A.H.-L., Lau, H.-S. (1988). Maximizing the probability of achieving a target profit in a two-product newsboy problem, *Decision Sciences*, Vol. 19, No. 2, 392-408, doi: [10.1111/j.1540-5915.1988.tb00275.x](https://doi.org/10.1111/j.1540-5915.1988.tb00275.x).
- [18] Petruzzi, N.C., Dada, M. (1999). Pricing and the newsvendor problem: A review with extensions, *Operations Research*, Vol. 47, No. 2, 183-194, doi: [10.1287/opre.47.2.183](https://doi.org/10.1287/opre.47.2.183).
- [19] Yang, S., Shi, C.V., Zhao, X. (2011). Optimal ordering and pricing decisions for a target oriented newsvendor, *Omega*, Vol. 39, No. 1, 110-115, doi: [10.1016/j.omega.2010.04.003](https://doi.org/10.1016/j.omega.2010.04.003).
- [20] Govindan, K., Popiuc, M.N., Diabat, A. (2013). Overview of coordination contracts within forward and reverse supply chains, *Journal of Cleaner Production*, Vol. 47, 319-334, doi: [10.1016/j.jclepro.2013.02.001](https://doi.org/10.1016/j.jclepro.2013.02.001).
- [21] Arrow, K.J., Harris, T. (1974). Optimal inventory policy (1951), In: *Economic information, decision, and prediction. theory and decision library*, Vol 7-2, Springer, Dordrecht, Netherlands, doi: [10.1007/978-94-010-9278-4_2](https://doi.org/10.1007/978-94-010-9278-4_2).
- [22] Cachon, G.P., Lariviere, M.A. (2005). Supply chain coordination with revenue-sharing contracts: Strengths and limitations, *Management Science*, Vol. 51, No. 1, 30-44, doi: [10.1287/mnsc.1040.0215](https://doi.org/10.1287/mnsc.1040.0215).
- [23] Pasternack, B.A. (2008). Commentary - Optimal pricing and return policies for perishable commodities, *Marketing Science*, Vol. 27, No. 1, 131-132, doi: [10.1287/mksc.1070.0347](https://doi.org/10.1287/mksc.1070.0347).
- [24] Tsay, A.A., Lovejoy, W.S. (1999). Quantity flexibility contracts and supply chain performance, *Manufacturing & Service Operations Management*, Vol. 1, No. 2, 89-111, doi: [10.1287/msom.1.2.89](https://doi.org/10.1287/msom.1.2.89).
- [25] Zhao, T., Xu, X., Chen, Y., Liang, L., Yu, Y., Wang, K. (2020). Coordination of a fashion supply chain with demand disruption, *Transportation Research Part E: Logistics and Transportation Review*, Vol. 134, Article No. 101838, doi: [10.1016/j.tre.2020.101838](https://doi.org/10.1016/j.tre.2020.101838).
- [26] Cachon, G.P. (2003). Supply chain coordination with contracts, *Handbooks in Operations Research and Management Science*, Vol. 11, 227-339, doi: [10.1016/S0927-0507\(03\)11006-7](https://doi.org/10.1016/S0927-0507(03)11006-7).

A bi-objective optimization of airport ferry vehicle scheduling based on heuristic algorithm: A real data case study

Han, X.^a, Zhao, P.X.^{a,*}, Kong, D.X.^a

^aSchool of Management, Shandong University, Jinan, Shandong, P.R. China

ABSTRACT

The optimization of ferry vehicle scheduling is the key factor to improve the punctuality of flights and passenger satisfaction at airports. Based on the airport reality, a bi-objective mixed integer linear programming model for airport ferry vehicle scheduling is proposed in this paper, in which the first objective is to minimize the number of vehicles used, and the second objective is to minimize the maximum number of flights per ferry vehicle serving under the constraint that the first objective takes the optimal value. For the optimization model of the second objective, this paper designs three heuristic algorithms: strict equalization algorithm, relaxed equalization algorithm and transplantation algorithm, and integrates them into a main algorithm. The actual flight data of Beijing Capital International Airport are used for numerical examples, and all the examples tested can obtain the exact solution or high-quality approximate solution using the designed algorithm, which verifies the effectiveness of the algorithm. This study can be used to inform decisions on the efficient and balanced use of airport ferry vehicles. Despite the system presented in the paper is designed for airport, it can be applied to solve similar vehicle scheduling problems.

ARTICLE INFO

Keywords:
Ferry vehicle;
Vehicle routing;
Bi-objective optimization;
Heuristic algorithm;
Strict equalization algorithm;
Relaxed equalization algorithm;
Transplantation algorithm

**Corresponding author:*
pxzhao@sdu.edu.cn
(Zhao, P.X.)

Article history:
Received 10 May 2022
Revised 9 August 2022
Accepted 16 August 2022



Content from this work may be used under the terms of the Creative Commons Attribution 4.0 International License (CC BY 4.0). Any further distribution of this work must maintain attribution to the author(s) and the title of the work, journal citation and DOI.

1. Introduction

In recent years, the rapid development of the civil aviation industry has made the scheduling and management of the limited ground resources at airports, such as parking positions, runways and ground support vehicles, gradually become important and complex. Among them, the ground support vehicles are special vehicles that provide a series of ground services for the aircraft, such as refuelling, air catering and ferrying. However, at present, the scheduling of airport ground support vehicles is still mainly manual, which is inefficient and easy to cause flight delays [1]. Flights parked at remote stands need ferry vehicles to transport passengers, so the scheduling level of ferry vehicles not only affects the punctuality of flights, but also directly affects the experience of passengers. The ferry service is characterized by time-consuming and different number of vehicles required for flights, which makes the ferry vehicle resources even more tight. In addition to completing all ferry services on time with as few ferry vehicles as possible, balancing the workload of each ferry vehicle as far as possible also facilitates driver scheduling and vehicle maintenance.

The research on flight ground service scheduling mainly includes the scheduling optimization of ground service crew [2-8] and ground support vehicles. The ground support vehicle scheduling problem is a kind of vehicle routing problem, and the vehicle routing problem is widely used in the scheduling of vehicles such as electric vehicles [9], automated guided vehicles [10] and logistics vehicles [11]. For example, Norin *et al.* designed a greedy randomized adaptive search procedure to solve the de-icing vehicle scheduling problem [12]. Du *et al.* designed a column generation heuristic algorithm to solve the tractor scheduling problem [13]. Schyns designed an ant colony algorithm to solve the refuelling truck scheduling problem [14]. Padrón *et al.* proposed a decomposition framework and a sequence iterative method to solve the collaborative scheduling problem of multiple ground support vehicles [15]. Padrón and Guimarans [16] improved the algorithm proposed by Padrón *et al.* [15]. This paper focuses on the studies on ferry vehicle scheduling, as detailed in Table 1.

As can be seen from Table 1, although there are existing studies involving optimization objectives in terms of balancing the workload of ferry vehicles, they are all nonlinear objective functions, which are solved using solvers or meta-heuristic algorithms. Solvers have difficulty solving large-scale nonlinear integer programming problems, and meta-heuristic algorithms often have difficulty obtaining the accuracy of the resulting solutions. This paper constructs a bi-objective optimization model for ferry vehicle scheduling, in which the first objective is to minimize the number of ferry vehicles used, and the programming model is a two-index arc-flow model based on a directed acyclic network, which is easy to obtain the optimal solution. The second objective is to minimize the maximum number of flights served by a single ferry vehicle under the constraint of using the minimum number of ferry vehicles, and the programming model is a three-index mixed integer linear programming model. Since the model of the second optimization objective has large number of variables and is difficult to solve directly, three heuristic algorithms are designed and integrated into a main algorithm to solve the model. The analysis of numerical examples shows that the algorithm can solve 42 out of 60 examples to the optimum, and the Gap of the remaining examples is also very small.

The rest of the paper is organized as follows. Section 2 constructs a bi-objective optimization model for ferry vehicle scheduling. Section 3 presents several heuristic algorithms for solving the optimization model of the second objective. Section 4 uses the actual flight data of Beijing Capital International Airport for numerical examples to verify the effectiveness of the designed heuristic algorithms. Section 5 provides conclusions and some possible directions for future research.

Table 1 Studies related to ferry vehicle scheduling

Literature	Optimization goal	Programming model	Solving method
[17]	Maximize robustness	ILP	Column generation
[18]	Minimize total costs, including vehicle usage costs and driving costs	LP	Shortest augmenting path algorithm
[19]	Minimize the variance of the number of flights per ferry vehicle serving	QP	Gurobi
[20]	Minimize the number of vehicles, the total vehicle mileage and the variance of the number of flights per ferry vehicle serving	Three-objective IP	Two-stage heuristic algorithm
[21]	Minimize the number of vehicles and the total deviation of the number of flights per ferry vehicle serving	Bi-objective MIP	Particle swarm optimization
[22]	Minimize the number of vehicles	MILP, LP	CPLEX
[1]	Minimize the number of vehicles, the total vehicle mileage and the difference between the vehicle arrival time and the earliest service time	Three-objective MIP	Non-dominated sorting genetic algorithm
[23]	Minimize the number of vehicles and the total vehicle idle time	Bi-objective MIP	Non-dominated sorting genetic algorithm
[24]	Minimize the number of vehicles	ILP, LP	Lingo

2. Problem description and model construction

Let there be $|N|$ flights requiring ferry services at an airport during a certain time period (including arriving flights and departing flights; if a flight arrives and then departs during this time

period, it is considered as two flights), where N is the set of these flights. Ferry vehicles for arriving flights are required to transport passengers from the parking positions to the terminal, while ferry vehicles for departing flights do the opposite. Let the time required for the ferry vehicle to travel from the end position of the ferry service of flight $i \in N$ (the terminal if i is an arriving flight, otherwise the parking position of i) to the start position of the ferry service of flight $j \in N$ (the parking position of j if j is an arriving flight, otherwise the terminal) be t_{ij} . Let the ferry service start time window for flight $i \in N$ be $[a_i, b_i]$ and the required service time be $serv_i$, where a_i and b_i are determined according to the Scheduled Time of Arrival (STA) or Scheduled Time of Departure (STD) of flight i . Depending on the aircraft type, let the number of ferry vehicles required for flight $i \in N$ be D_i (if relevant data on the number of passengers on the flight are available, the number of passengers can be used instead of the aircraft type to determine the number of ferry vehicles required for the flight more accurately).

To facilitate the algorithm design, this paper transforms the research problem into a vehicle scheduling problem with only one ferry vehicle for each flight by setting up virtual flights. Let flight $i \in N$ correspond to D_i virtual flights with the same time window, service time and other relevant time parameters as i . Denote the set of all virtual flights as N^V [19, 22, 24]. We use the service sequence and service time compatibility information in the flight service time window to construct the underlying network $G = (V, A)$ of the ferry vehicle scheduling model, where $V = \{0, |N^V| + 1\} \cup \{i | i \in N^V\}$ (Nodes 0 and $|N^V| + 1$ can be regarded as ferry vehicle depot), $A = \{(i, j) | Ad_{ij} = 1, i, j \in V\}$. Ad_{ij} is an element of the adjacency matrix Ad of network G . Ad_{ij} is calculated as follows.

$$Ad_{ij} = \begin{cases} 1, & \text{if } i = 0 \text{ and } j \in N^V \\ 1, & \text{if } j = |N^V| + 1 \text{ and } i \in N^V \\ 1, & \text{if } i, j \in N^V \text{ and } a_i + serv_i + t_{ij} \leq b_j \\ 0, & \text{otherwise} \end{cases} \quad (1)$$

For the ferry vehicle, the inequality $serv_i + t_{ij} \geq b_i - a_i$ holds for $\forall i, j \in N^V$, then G is a directed acyclic network [22, 25].

The first objective of the ferry vehicle scheduling optimization is to minimize the number of ferry vehicles used. The decision variable $x_{ij} \in \{0, 1\}$ decides whether a ferry vehicle serves node j immediately after serving node i , and the decision variable $t_i \in [a_i, b_i]$ decides the service start time of flight i . The two-index mixed integer linear programming model for the first optimization objective is constructed as follows.

$$\min \sum_{(0,j) \in A} x_{0j} \quad (2)$$

$$\sum_{j|(i,j) \in A} x_{ij} = 1, \forall i \in N^V \quad (3)$$

$$\sum_{j|(j,i) \in A} x_{ji} = 1, \forall i \in N^V \quad (4)$$

$$a_i \leq t_i \leq b_i, \forall i \in N^V \quad (5)$$

$$t_i + serv_i + t_{ij} \leq t_j + M(1 - x_{ij}), \forall (i, j) \in A, i, j \in N^V \quad (6)$$

$$x_{ij} \in \{0, 1\}, \forall (i, j) \in A \quad (7)$$

The objective function Eq. 2 in the above model is to minimize the number of ferry vehicles dispatched. Constraints Eqs. 3 to 4 indicate that each virtual flight is served only once. Constraints Eqs. 5 to 6 are time window constraints.

The second optimization objective is to minimize the maximum number of flights served by a single ferry vehicle under the constraint of using the minimum number of ferry vehicles. Let the optimal value of model 2 to 7 be K , that is, at least K ferry vehicles are needed to serve all flights on time. The second programming model uses the three-index decision variable x_{ij}^k to decide whether ferry vehicle k serves node j immediately after serving node i , and introduces a new

decision variable z to represent the maximum number of flights served by a single ferry vehicle. The mixed integer linear programming model for the second optimization objective is constructed as follows.

$$\min z \tag{8}$$

$$\sum_{i,j|(i,j) \in A} x_{ij}^k \leq z + 1, \forall k \in \{1,2, \dots, K\} \tag{9}$$

$$\sum_{i|i \in N^V} x_{0i}^k = 1, \forall k \in \{1,2, \dots, K\} \tag{10}$$

$$\sum_{k=1}^K \sum_{j|(i,j) \in A} x_{ij}^k = 1, \forall i \in N^V \tag{11}$$

$$\sum_{j|(i,j) \in A} x_{ij}^k = \sum_{j|(j,i) \in A} x_{ji}^k, \forall i \in N^V, k \in \{1,2, \dots, K\} \tag{12}$$

$$e_i \leq t_i \leq l_i, \forall i \in N^V \tag{13}$$

$$t_i + serv_i + t_{ij} \leq t_j + M(1 - x_{ij}^k), \forall k \in \{1,2, \dots, K\}, (i,j) \in A \text{ and } i,j \in N^V \tag{14}$$

$$x_{ij}^k \in \{0,1\}, \forall k \in \{1,2, \dots, K\}, (i,j) \in A \tag{15}$$

The objective function Eq. 8 and constraint Eq. 9 in the above model minimize the maximum number of flights served by a single ferry vehicle. Constraint Eq. 10 indicates that each ferry vehicle is dispatched only once. Constraint Eq. 11 indicates that each virtual flight is served only once. Constraint Eq. 12 is the flow balance condition of the virtual flight node. Constraints Eqs. 13 to 14 are time window constraints. Obviously, $\lceil \frac{|N^V|}{K} \rceil$ is a lower bound for the optimal value of model in Eqs. 8 to 15.

3. Proposed approach: A heuristic algorithm

Models in Eq. 2 to 7 can be solved quickly using the solver to obtain the exact solution [22]. Models 8 to 15 is a three-index arc-flow model with a large number of variables, which is difficult to solve directly using the solver for flight data with a 24-hour planning period. In this paper, three heuristic algorithms (see Algorithms 1, 2, and 3) are designed and integrated into a main algorithm (see Algorithm 0) to solve models in 8 to 15. The symbols involved in the algorithms are shown in Table 2.

Table 2 The symbols used in the algorithms

Symbol	Meaning
popsize	The number of solutions
$solu(u, i)$	The ferry vehicle serving flight i in solution $u, u = 1,2, \dots, popsize, i = 1,2, \dots, N^V $
$st(u, i)$	The service start time of flight i in solution $u, u = 1,2, \dots, popsize, i = 1,2, \dots, N^V $
$fv1(u, k)$	The last flight that ferry vehicle k has served in solution $u, u = 1,2, \dots, popsize, k = 1,2, \dots, K$
$fv2(u, k)$	The service start time of the last flight that ferry vehicle k has served in solution $u, u = 1,2, \dots, popsize, k = 1,2, \dots, K$
$fv3(u, k)$	The number of flights that ferry vehicle k has served in solution $u, u = 1,2, \dots, popsize, k = 1,2, \dots, K$
ava_i	The set of ferry vehicles that can serve flight i
ava'_i	The set of ferry vehicles whose number of served flights satisfies a specific condition among ferry vehicles available for flight i
$fea(u)$	The number of flights served in solution u
$opt(u)$	The maximum number of flights served by a single ferry vehicle in solution u
$solu0(i)$	The ferry vehicle serving flight i in the optimal solution of models 2 to 7
$st0(i)$	The service start time of flight i in the optimal solution of models 2 to 7
$solu'$	The set of solutions with the largest number of served flights
UF	The set of unserved flights in the solutions with the largest number of served flights
UF^{max}	The last flight unserved in the solutions with the largest number of served flights

Firstly, all the flights in N^V are sorted in ascending order according to a_i and respectively numbered as flight $1,2, \dots, |N^V|$. Then, if two flights are served by the same ferry vehicle, the vehicle must serve the flight with the smaller number first. Algorithms 1-3 all ensure that the con-

straints on the time window and the number of ferry vehicles are not violated, then the resulting solution, if infeasible, is due to the fact that some flights are not served. Algorithm 2 has looser restrictions than Algorithm 1 in terms of the equilibrium degree of the ferry vehicle workload, so the main algorithm executes Algorithm 1 first, and if no feasible solution is obtained, Algorithm 2 is executed. If Algorithm 2 still fails to obtain a feasible solution, the time windows of the unserved flights are generally in the peak period of flight take-off and landing, during which there are fewer feasible vehicle scheduling schemes. Algorithm 3 transplants part of the ferry vehicle scheduling arrangement from the optimal solution of models 2 to 7, while taking into account the equilibrium degree of the ferry vehicle workload. If neither Algorithm 1 nor Algorithm 2 can get a feasible solution, Algorithm 3 can be executed.

Algorithm 0: Main algorithm

```

Input: popsize,  $K$ ,  $|N^V|$ ,  $a_i$ ,  $b_i$ ,  $serv_i$ ,  $t_{ij}$ ,  $solu0(i)$ ,  $st0(i)$ 
1 Execute Algorithm 1, return  $solu(u, i)$ ,  $st(u, i)$ ,  $fea(u)$ ,  $opt(u)$ ;
2 If  $\max_{u \in \{1, 2, \dots, \text{popsize}\}} \{fea(u)\} < |N^V|$ 
3   Execute Algorithm 2, return  $solu(u, i)$ ,  $st(u, i)$ ,  $fea(u)$ ,  $opt(u)$ ;
4   If  $\max_{u \in \{1, 2, \dots, \text{popsize}\}} \{fea(u)\} < |N^V|$ 
5      $solu' \leftarrow \{solu(u, i) \mid i \in \{1, 2, \dots, |N^V|\}, fea(u) = \max_{u \in \{1, 2, \dots, \text{popsize}\}} \{fea(u)\}\};$ 
6      $UF \leftarrow \{i \in \{1, 2, \dots, |N^V|\} \mid solu(u, i) \in solu', solu(u, i) = 0\};$ 
7      $UF^{\max} \leftarrow \max_{i \in UF} \{i\};$ 
8     Execute Algorithm 3, return  $solu(u, i)$ ,  $st(u, i)$ ,  $fea(u)$ ,  $opt(u)$ ;
9 Return  $solu(u, i)$ ,  $st(u, i)$ ,  $fea(u)$ ,  $opt(u)$ 

```

Algorithm 1 first makes ferry vehicles 1, 2, ..., K serve flights 1, 2, ..., K respectively (lines 1-7 of Algorithm 1). For flights $K + 1, K + 2, \dots, |N^V|$, the set ava_i of the ferry vehicles that can serve it is determined in turn, and from the set, a ferry vehicle that has served the least number of flights is randomly selected to serve it (lines 8-18 of Algorithm 1). The time complexity of Algorithm 1 is $O(\text{popsize} \times (|N^V| - K) \times K^2)$.

Algorithm 1: Strict equalization algorithm

```

Input: popsize,  $K$ ,  $|N^V|$ ,  $a_i$ ,  $b_i$ ,  $serv_i$ ,  $t_{ij}$ 
1 For  $u \leftarrow 1, 2, \dots, \text{popsize}$ 
2   For  $i \leftarrow 1, 2, \dots, K$ 
3      $solu(u, i) \leftarrow i;$ 
4      $st(u, i) \leftarrow a_i;$ 
5      $fv1(u, i) \leftarrow i;$ 
6      $fv2(u, i) \leftarrow a_i;$ 
7      $fv3(u, i) \leftarrow 1;$ 
8 For  $u \leftarrow 1, 2, \dots, \text{popsize}$ 
9   For  $i \leftarrow K + 1, K + 2, \dots, |N^V|$ 
10     $ava_i \leftarrow \{k \in \{1, 2, \dots, K\} \mid fv2(u, k) + serv_{fv1(u, k)} + t_{fv1(u, k), i} \leq b_i\};$ 
11    If  $ava_i \neq \emptyset$ 
12       $ava'_i \leftarrow \{k \in ava_i \mid fv3(u, k) = \min_{k \in ava_i} \{fv3(u, k)\}\};$ 
13      Randomly select a ferry vehicle in  $ava'_i$ , denote as  $k$ ;
14       $solu(u, i) \leftarrow k;$ 
15       $st(u, i) \leftarrow \max \{fv2(u, k) + serv_{fv1(u, k)} + t_{fv1(u, k), i}, a_i\};$ 
16       $fv2(u, k) \leftarrow \max \{fv2(u, k) + serv_{fv1(u, k)} + t_{fv1(u, k), i}, a_i\};$ 
17       $fv1(u, k) \leftarrow i;$ 
18       $fv3(u, k) \leftarrow fv3(u, k) + 1;$ 
19  $fea(u) \leftarrow \sum_{k=1}^K fv3(u, k); opt(u) \leftarrow \max_{k \in \{1, 2, \dots, K\}} \{fv3(u, k)\};$ 
20 Return  $solu(u, i)$ ,  $st(u, i)$ ,  $fea(u)$ ,  $opt(u)$ 

```

The difference between Algorithm 2 and Algorithm 1 is that for flights $K + 1, K + 2, \dots, |N^V|$, if there are ferry vehicles with the number of served flights less than or equal to $\lfloor \frac{|N^V|}{K} \rfloor$ in set ava_i , then a ferry vehicle is randomly selected from them (from the ferry vehicles with the number of served flights less than or equal to $\lfloor \frac{|N^V|}{K} \rfloor$) to serve flight i . Otherwise, the factor of ferry vehicle task volume is no longer considered, and a ferry vehicle is randomly selected from ava_i to serve flight i (lines 9-27 of Algorithm 2). The time complexity of Algorithm 2 is $O(\text{popsize} \times (|N^V| - K) \times K)$.

Algorithm 2: Relaxed equalization algorithm

```

Input: popsize,  $K$ ,  $|N^V|$ ,  $a_i$ ,  $b_i$ ,  $serv_i$ ,  $t_{ij}$ 
1  For  $\forall u \in \{1,2, \dots, \text{popsize}\}, i \in \{1,2, \dots, |N^V|\}$ , set  $solu(u, i) \leftarrow 0$ ;
2  For  $u \leftarrow 1,2, \dots, \text{popsize}$ 
3      For  $i \leftarrow 1,2, \dots, K$ 
4           $solu(u, i) \leftarrow i$ ;
5           $st(u, i) \leftarrow a_i$ ;
6           $fv1(u, i) \leftarrow i$ ;
7           $fv2(u, i) \leftarrow a_i$ ;
8           $fv3(u, i) \leftarrow 1$ ;
9  For  $u \leftarrow 1,2, \dots, \text{popsize}$ 
10     For  $i \leftarrow K + 1, K + 2, \dots, |N^V|$ 
11          $ava_i \leftarrow \{k \in \{1,2, \dots, K\} | fv2(u, k) + serv_{fv1(u,k)} + t_{fv1(u,k),i} \leq b_i\}$ ;
12         If  $ava_i \neq \emptyset$ 
13              $ava'_i \leftarrow \{k \in ava_i | fv3(u, k) \leq \lfloor \frac{|N^V|}{K} \rfloor\}$ ;
14             If  $ava'_i \neq \emptyset$ 
15                 Randomly select a ferry vehicle in  $ava'_i$ , denote as  $k$ ;
16                  $solu(u, i) \leftarrow k$ ;
17                  $st(u, i) \leftarrow \max \{fv2(u, k) + serv_{fv1(u,k)} + t_{fv1(u,k),i}, a_i\}$ ;
18                  $fv2(u, k) \leftarrow \max \{fv2(u, k) + serv_{fv1(u,k)} + t_{fv1(u,k),i}, a_i\}$ ;
19                  $fv1(u, k) \leftarrow i$ ;
20                  $fv3(u, k) \leftarrow fv3(u, k) + 1$ ;
21             If  $ava'_i = \emptyset$ 
22                 Randomly select a ferry vehicle in  $ava_i$ , denote as  $k$ ;
23                  $solu(u, i) \leftarrow k$ ;
24                  $st(u, i) \leftarrow \max \{fv2(u, k) + serv_{fv1(u,k)} + t_{fv1(u,k),i}, a_i\}$ ;
25                  $fv2(u, k) \leftarrow \max \{fv2(u, k) + serv_{fv1(u,k)} + t_{fv1(u,k),i}, a_i\}$ ;
26                  $fv1(u, k) \leftarrow i$ ;
27                  $fv3(u, k) \leftarrow fv3(u, k) + 1$ ;
28      $fea(u) \leftarrow \sum_{k=1}^K fv3(u, k)$ ;  $opt(u) \leftarrow \max_{k \in \{1,2, \dots, K\}} \{fv3(u, k)\}$ ;
29     Return  $solu(u, i), st(u, i), fea(u), opt(u)$ 

```

Algorithm 3 relies on the optimal solution of models 2 to 7 and the parameter UF^{\max} determined by the solution obtained by Algorithm 2. For flights $1, 2, \dots, UF^{\max}$, the results of the ferry vehicle assignment for these flights in the optimal solution of models 2 to 7 are directly transplanted (lines 2-8 of Algorithm 3). For flights $UF^{\max} + 1, UF^{\max} + 2, \dots, |N^V|$, the ferry vehicles continue to be assigned as in Algorithm 2. The time complexity of Algorithm 3 is $O(\text{popsize} \times (|N^V| - UF^{\max}) \times K)$.

Algorithm 3: Transplantation algorithm

```

Input: popsize,  $K$ ,  $|N^V|$ ,  $a_i$ ,  $b_i$ ,  $serv_i$ ,  $t_{ij}$ ,  $UF^{\max}$ ,  $solu0(i)$ ,  $st0(i)$ 
1  For  $\forall u \in \{1,2, \dots, \text{popsize}\}, k \in \{1,2, \dots, K\}$ , set  $fv3(u, k) \leftarrow 0$ ;
2  For  $u \leftarrow 1,2, \dots, \text{popsize}$ 
3      For  $i \leftarrow 1,2, \dots, UF^{\max}$ 
4           $solu(u, i) \leftarrow solu0(i)$ ;
5           $st(u, i) \leftarrow st0(i)$ ;
6           $fv1(u, solu0(i)) \leftarrow i$ ;
7           $fv2(u, solu0(i)) \leftarrow st0(i)$ ;
8           $fv3(u, solu0(i)) \leftarrow fv3(u, solu0(i)) + 1$ ;
9  For  $u \leftarrow 1,2, \dots, \text{popsize}$ 
10     For  $i \leftarrow UF^{\max} + 1, UF^{\max} + 2, \dots, |N^V|$ 
11          $ava_i \leftarrow \{k \in \{1,2, \dots, K\} | fv2(u, k) + serv_{fv1(u,k)} + t_{fv1(u,k),i} \leq b_i\}$ ;
12         If  $ava_i \neq \emptyset$ 
13              $ava'_i \leftarrow \{k \in ava_i | fv3(u, k) \leq \lfloor \frac{|N^V|}{K} \rfloor\}$ ;
14             If  $ava'_i \neq \emptyset$ 
15                 Randomly select a ferry vehicle in  $ava'_i$ , denote as  $k$ ;
16                  $solu(u, i) \leftarrow k$ ;
17                  $st(u, i) \leftarrow \max \{fv2(u, k) + serv_{fv1(u,k)} + t_{fv1(u,k),i}, a_i\}$ ;
18                  $fv2(u, k) \leftarrow \max \{fv2(u, k) + serv_{fv1(u,k)} + t_{fv1(u,k),i}, a_i\}$ ;
19                  $fv1(u, k) \leftarrow i$ ;
20                  $fv3(u, k) \leftarrow fv3(u, k) + 1$ ;
21             If  $ava'_i = \emptyset$ 

```

```

22 Randomly select a ferry vehicle in  $ava_i$ , denote as  $k$ ;
23  $solu(u, i) \leftarrow k$ ;
24  $st(u, i) \leftarrow \max \{fv2(u, k) + serv_{fv1(u, k)} + t_{fv1(u, k), i}, a_i\}$ ;
25  $fv2(u, k) \leftarrow \max \{fv2(u, k) + serv_{fv1(u, k)} + t_{fv1(u, k), i}, a_i\}$ ;
26  $fv1(u, k) \leftarrow i$ ;
27  $fv3(u, k) \leftarrow fv3(u, k) + 1$ ;
28  $fea(u) \leftarrow \sum_{k=1}^K fv3(u, k)$ ;  $opt(u) \leftarrow \max_{k \in \{1, 2, \dots, K\}} \{fv3(u, k)\}$ ;
29 Return  $solu(u, i), st(u, i), fea(u), opt(u)$ 

```

4. Numerical examples: Results and discussion

This section takes 24 hours (0:00-23:59) as the planning period, and uses the flight data of Beijing Capital International Airport for 60 days from February 1 to April 1, 2018 as the numerical examples. The average number of virtual flights for these 60 data sets is 900. Models 2 to 7 can be solved directly using the CPLEX solver, and the results are shown in Table 3. The running conditions are a 2.7 GHz PC (Intel® Core™ i7-7500U CPU), Windows 7 operating system, running with 8 GB RAM, and using CPLEX 12.9 solver.

Table 3 Results of solving models 2 to 7

Serial number	Number of virtual flights	Solving time (s)	Objective value	Serial number	Number of virtual flights	Solving time (s)	Objective value
1	957	34.04	76	31	905	68.16	66
2	815	64.27	58	32	844	94.07	67
3	878	133.89	61	33	889	131.92	72
4	870	102.51	74	34	876	38.92	70
5	856	45.35	60	35	884	129.76	64
6	901	137.72	72	36	968	152.71	78
7	885	216.34	61	37	844	120.32	54
8	912	105.71	75	38	898	59.25	72
9	968	34.63	76	39	839	21.14	68
10	894	121.24	62	40	1029	180.03	70
11	746	42.99	55	41	1040	226.7	77
12	825	91.09	64	42	1054	269.23	70
13	855	89.62	57	43	878	117.8	59
14	876	81.09	72	44	832	72.57	64
15	832	19.94	74	45	947	32.96	80
16	878	124.16	62	46	856	99.97	71
17	856	80.29	64	47	904	104.13	80
18	888	113.24	72	48	902	27.81	64
19	859	102.35	54	49	770	226.68	57
20	997	278.51	72	50	979	203.46	67
21	933	170.15	65	51	877	107.53	63
22	990	214.33	64	52	862	106.35	57
23	1016	271.08	62	53	845	105.75	56
24	931	183.39	64	54	888	135.85	63
25	923	157.87	64	55	880	130.92	58
26	884	132.13	56	56	1012	175.3	78
27	838	102.57	66	57	1068	181.98	70
28	897	106.77	66	58	1033	177.51	74
29	858	125.05	62	59	791	1806.15	49
30	841	75.93	60	60	939	4276.94	54

As can be seen from Table 3, for models 2 to 7, the optimal solutions can be obtained for all 60 groups of data, and the average time to solve the problem is 200 seconds. The optimal solutions for 58 groups of data can be obtained within 5 minutes. Algorithm 0 designed in Section 3 is implemented using MATLAB R2017b and used for these 60 groups of data. The solving results of models 8 to 15 are obtained as shown in Table 4 (popsize is set to 300).

As can be seen from Table 4, the heuristic algorithms designed are very suitable for solving models 8 to 15. Among these 60 groups of data, the exact optimal solutions can be obtained for 42 groups of data (all obtained by Algorithm 1), and for the other 18 groups of data, the objective value differs from the lower bound $\lceil \frac{|N^V|}{K} \rceil$ of the model by only 1. There are 11 groups of data

that need to use Algorithm 2 and only 4 groups of data that need to use Algorithm 3, all of which can obtain the approximate optimal solution, and the maximum Gap with the lower bound of the model is only 7.69 %.

Take the 60th group of data as an example to show the results of ferry vehicle scheduling. This group of data has a total of 939 virtual flights using 54 ferry vehicles with the $\lceil \frac{|N^V|}{K} \rceil$ value of 18. The 60th group of data uses Algorithm 3 to obtain the final solution with the UF^{\max} value of 255, and a single ferry vehicle serves up to 19 virtual flights. The number of flights served by each ferry vehicle is shown in Table 5.

Table 4 Results of solving models 8 to 15

Serial number	$\lceil \frac{ N^V }{K} \rceil$	Algorithm used	Objective value	Gap (%)	Serial number	$\lceil \frac{ N^V }{K} \rceil$	Algorithm used	Objective value	Gap (%)
1	13	1	13	0.00	31	14	1	14	0.00
2	15	1	15	0.00	32	13	1	13	0.00
3	15	1	15	0.00	33	13	1	13	0.00
4	12	1	12	0.00	34	13	1	13	0.00
5	15	1	15	0.00	35	14	1	14	0.00
6	13	1	13	0.00	36	13	1	13	0.00
7	15	1	15	0.00	37	16	1	16	0.00
8	13	1	13	0.00	38	13	1	13	0.00
9	13	1	13	0.00	39	13	1	13	0.00
10	15	1	15	0.00	40	15	1	15	0.00
11	14	1	14	0.00	41	14	1	14	0.00
12	13	1	13	0.00	42	16	1	16	0.00
13	15	1	15	0.00	43	15	1	16	6.25
14	13	1	13	0.00	44	13	1	14	7.14
15	12	1	12	0.00	45	12	1	13	7.69
16	15	1	15	0.00	46	13	2	14	7.14
17	14	1	14	0.00	47	12	2	13	7.69
18	13	1	13	0.00	48	15	2	16	6.25
19	16	1	16	0.00	49	14	2	15	6.67
20	14	1	14	0.00	50	15	2	16	6.25
21	15	1	15	0.00	51	14	2	15	6.67
22	16	1	16	0.00	52	16	2	17	5.88
23	17	1	17	0.00	53	16	2	17	5.88
24	15	1	15	0.00	54	15	2	16	6.25
25	15	1	15	0.00	55	16	2	17	5.88
26	16	1	16	0.00	56	13	2	14	7.14
27	13	1	13	0.00	57	16	3	17	5.88
28	14	1	14	0.00	58	14	3	15	6.67
29	14	1	14	0.00	59	17	3	18	5.56
30	15	1	15	0.00	60	18	3	19	5.26

Table 5 Results of ferry vehicle scheduling on a certain day

Ferry vehicle	Number of flights served	Ferry vehicle	Number of flights served	Ferry vehicle	Number of flights served
1	15	19	18	37	18
2	18	20	13	38	16
3	17	21	18	39	19
4	19	22	18	40	18
5	19	23	14	41	15
6	19	24	19	42	17
7	18	25	18	43	19
8	15	26	18	44	16
9	14	27	17	45	15
10	18	28	18	46	17
11	17	29	18	47	16
12	19	30	19	48	19
13	19	31	19	49	16
14	19	32	19	50	15
15	18	33	19	51	17
16	19	34	15	52	15
17	19	35	17	53	18
18	19	36	19	54	16

5. Conclusion

This paper proposes a bi-objective optimization model for airport ferry vehicle scheduling to optimize the number of vehicles used and the equilibrium degree of the vehicle workload, in which the objective function designed for the second objective is to minimize the maximum number of flights served by a single ferry vehicle. For the second optimization objective, three concise and efficient heuristic algorithms are designed and tested using the actual flight data from an airport. The analysis of numerical examples shows that Algorithms 1 and 2, which do not depend on the optimal solution of the first optimization objective, have been able to solve most of the examples, and the effectiveness of these algorithms is verified by the fact that all three algorithms can obtain exact solutions or high-quality approximate solutions.

Although the bi-objective optimization in this paper is designed for airports, its algorithms can also be applied to solve similar vehicle scheduling problems that balance the workload of vehicles. Possible future research directions also include the problem of real-time scheduling of ferry vehicles considering uncertain and unexpected conditions.

Acknowledgement

This work was supported by the National Natural Science Foundation of China (grant numbers 72071122, 72134004); the Natural Science Foundation of Shandong Province (grant number ZR2020MG002); and the Social Science Planning Research Project of Shandong Province (grant number 20CGLJ11).

References

- [1] Zeng, Z.H., Jia, L.Q. (2020). Research on airport special vehicle scheduling problem, In: *Proceedings of 2020 International Conference on Virtual Reality and Intelligent Systems (ICVRIS)*, Zhangjiajie, China, 1076-1078.
- [2] Lv, H., Qin, Y., Tang, R., Luo, C. (2011). Multi-population co-evolutionary memetic algorithm for multi-objective airport ground services scheduling problem, In: *Proceedings of 2011 3rd International Workshop on Intelligent Systems and Applications*, Wuhan, China, 1-4, doi: [10.1109/ISA.2011.5873292](https://doi.org/10.1109/ISA.2011.5873292).
- [3] Ip, W.H., Wang, D., Cho, V. (2013). Aircraft ground service scheduling problems and their genetic algorithm with hybrid assignment and sequence encoding scheme, *IEEE Systems Journal*, Vol. 7, No. 4, 649-657, doi: [10.1109/JSYST.2012.2196229](https://doi.org/10.1109/JSYST.2012.2196229).
- [4] Trabelsi, S.F., Mora-Camino, F., Padrón Astorga, S.P. (2013). A decentralized approach for ground handling fleet management at airports, In: *Proceedings of 2013 International Conference on Advanced Logistics and Transport*, Sousse, Tunisia, 302-307, doi: [10.1109/ICAadLT.2013.6568476](https://doi.org/10.1109/ICAadLT.2013.6568476).
- [5] Tang, F., Liu, S., Dong, X., Cui, B. (2017). Aircraft ground service scheduling problems and Partheno-genetic algorithm with hybrid heuristic rule, In: *Proceedings of 2017 IEEE 7th Annual International Conference on CYBER Technology in Automation, Control, and Intelligent Systems (CYBER)*, Honolulu, USA, 551-555, doi: [10.1109/CYBER.2017.8446518](https://doi.org/10.1109/CYBER.2017.8446518).
- [6] Fink, M., Desaulniers, G., Frey, M., Kiermaier, F., Kolisch, R., Soumis, F. (2019). Column generation for vehicle routing problems with multiple synchronization constraints, *European Journal of Operational Research*, Vol. 272, No. 2, 699-711, doi: [10.1016/j.ejor.2018.06.046](https://doi.org/10.1016/j.ejor.2018.06.046).
- [7] Gök, Y.S., Guimarans, D., Stuckey, P.J., Tomasella, M., Ozturk, C. (2020). Robust resource planning for aircraft ground operations, In: Hebrard, E., Musliu, N. (eds.), *Integration of constraint programming, artificial intelligence, and operations research, CPAIOR 2020, Lecture notes in computer science*, Vol. 12296, Springer, Cham, Switzerland, 222-238, doi: [10.1007/978-3-030-58942-4_15](https://doi.org/10.1007/978-3-030-58942-4_15).
- [8] Gök, Y.S., Tomasella, M., Guimarans, D., Ozturk, C. (2020). A simheuristic approach for robust scheduling of airport turnaround teams, In: *Proceedings of 2020 Winter Simulation Conference (WSC)*, Orlando, USA, 1336-1347, doi: [10.1109/WSC48552.2020.9383947](https://doi.org/10.1109/WSC48552.2020.9383947).
- [9] Huang, A.Q., Zhang, Y.Q., He, Z.F., Hua, G.W., Shi, X.L. (2021). Recharging and transportation scheduling for electric vehicle battery under the swapping mode, *Advances in Production Engineering & Management*, Vol. 16, No. 3, 359-371, doi: [10.14743/apem2021.3.406](https://doi.org/10.14743/apem2021.3.406).
- [10] Shi, W., Tang, D.B., Zou, P. (2021). Multi-objective automated guided vehicle scheduling based on MapReduce framework, *Advances in Production Engineering & Management*, Vol. 16, No. 1, 37-46, doi: [10.14743/apem2021.1.383](https://doi.org/10.14743/apem2021.1.383).
- [11] Zhao, P.X., Luo, W.H., Han, X. (2019). Time-dependent and bi-objective vehicle routing problem with time windows, *Advances in Production Engineering & Management*, Vol. 14, No. 2, 201-212, doi: [10.14743/apem2019.2.322](https://doi.org/10.14743/apem2019.2.322).
- [12] Norin, A., Yuan, D., Granberg, T.A., Värbrand, P. (2012). Scheduling de-icing vehicles within airport logistics: A heuristic algorithm and performance evaluation, *Journal of the Operational Research Society*, Vol. 63, No. 8, 1116-1125, doi: [10.1057/jors.2011.100](https://doi.org/10.1057/jors.2011.100).

- [13] Du, J.Y., Brunner, J.O., Kolisch, R. (2014). Planning towing processes at airports more efficiently, *Transportation Research Part E: Logistics and Transportation Review*, Vol. 70, 293-304, doi: [10.1016/j.tre.2014.07.008](https://doi.org/10.1016/j.tre.2014.07.008).
- [14] Schyns, M. (2015). An ant colony system for responsive dynamic vehicle routing, *European Journal of Operational Research*, Vol. 245, No. 3, 704-718, doi: [10.1016/j.ejor.2015.04.009](https://doi.org/10.1016/j.ejor.2015.04.009).
- [15] Padrón, S., Guimarans, D., Ramos, J.J., Fitouri-Trabelsi, S. (2016). A bi-objective approach for scheduling ground-handling vehicles in airports, *Computers & Operations Research*, Vol. 71, 34-53, doi: [10.1016/j.cor.2015.12.010](https://doi.org/10.1016/j.cor.2015.12.010).
- [16] Padrón, S., Guimarans, D. (2019). An improved method for scheduling aircraft ground handling operations from a global perspective, *Asia-Pacific Journal of Operational Research*, Vol. 36, No. 4, Article No. 1950020, doi: [10.1142/S0217595919500209](https://doi.org/10.1142/S0217595919500209).
- [17] Diepen, G., Pieters, B.F.I., van den Akker, J.M., Hoogeveen, J.A. (2013). Robust planning of airport platform buses, *Computers & Operations Research*, Vol. 40, No. 3, 747-757, doi: [10.1016/j.cor.2011.08.002](https://doi.org/10.1016/j.cor.2011.08.002).
- [18] Weiszer, M., Chen, J., Locatelli, G. (2015). An integrated optimisation approach to airport ground operations to foster sustainability in the aviation sector, *Applied Energy*, Vol. 157, 567-582, doi: [10.1016/j.apenergy.2015.04.039](https://doi.org/10.1016/j.apenergy.2015.04.039).
- [19] Li, Q., Bi, J., Li, Z. (2017). Research on ferry vehicle scheduling problem within airport operations, In: *Proceedings of 2017 10th International Symposium on Computational Intelligence and Design (ISCID)*, Hangzhou, China, 248-251, doi: [10.1109/ISCID.2017.153](https://doi.org/10.1109/ISCID.2017.153).
- [20] Liu, Y., Zhang, J., Ding, C., Bi, J. (2019). Modeling and heuristic algorithm of ground ferry vehicle scheduling in large airports, In: *Proceedings of the 19th COTA International Conference of Transportation Professionals*, Nanjing, China, 159-170, doi: [10.1061/9780784482292.015](https://doi.org/10.1061/9780784482292.015).
- [21] Zhao, P.X., Gao, W.Q., Han, X., Luo, W.H. (2019). Bi-objective collaborative scheduling optimization of airport ferry vehicle and tractor, *International Journal of Simulation Modelling*, Vol. 18, No. 2, 355-365, doi: [10.2507/IJSIMM18\(2\)CO9](https://doi.org/10.2507/IJSIMM18(2)CO9).
- [22] Han, X., Zhao, P., Meng, Q., Yin, S., Wan, D. (2020). Optimal scheduling of airport ferry vehicles based on capacity network, *Annals of Operations Research*, Vol. 295, No. 1, 163-182, doi: [10.1007/s10479-020-03743-0](https://doi.org/10.1007/s10479-020-03743-0).
- [23] Liu, Y., Wu, J., Tang, J., Wang, W., Wang, X. (2022). Scheduling optimisation of multi-type special vehicles in an airport, *Transportmetrica B: Transport Dynamics*, Vol. 10, No. 1, 954-970, doi: [10.1080/21680566.2021.1983484](https://doi.org/10.1080/21680566.2021.1983484).
- [24] Zhao, P., Han, X., Wan, D. (2021). Evaluation of the airport ferry vehicle scheduling based on network maximum flow model, *Omega*, Vol. 99, Article No. 102178, doi: [10.1016/j.omega.2019.102178](https://doi.org/10.1016/j.omega.2019.102178).
- [25] Bertsimas, D., Jaillet, P., Martin, S. (2019). Online vehicle routing: The edge of optimization in large-scale applications, *Operations Research*, Vol. 67, No. 1, 143-162, doi: [10.1287/opre.2018.1763](https://doi.org/10.1287/opre.2018.1763).

Ultrasonic abrasive polishing of additive manufactured parts: An experimental study on the effects of process parameters on polishing performance

Liu, X.^a, Wang, J.^{a,*}, Zhu, J.^a, Liew, P.J.^b, Li, C.^c, Huang, C.^d

^aMarine Engineering College, Dalian Maritime University, Ganjingzi District, Dalian, P.R. China

^bFakulti Kejuruteraan Pembuatan, Universiti Teknikal Malaysia Melaka, Hang Tuah Jaya, Durian Tunggal, Melaka, Malaysia

^cXinyu Key Laboratory of Materials Technology and Application for Intelligent Manufacturing, Xinyu University, P.R. China

^dCollege of Marine Engineering, Jimei University, Fujian, P.R. China

ABSTRACT

The rough surface of metal parts produced by the powder-based layered Additive Manufacturing (AM) technology such as Selective Laser Melting (SLM) is an important problem that needs to be solved. This study introduces obvious improvements in the surface quality of the AM parts by means of ultrasonic abrasive polishing (UAP), which uses cavitation collapse and micro-cut of abrasive particles for finishing surfaces. Experiments were conducted using the orthogonal experimental design method with an $L_9(3^4)$ orthogonal array to investigate the effects of ultrasonic power, machining time, abrasive particle size, and particle concentration on surface roughness Ra and material removal rate (MRR). The wear of the abrasive particles in the slurry was also studied. IN625 nickel-based alloy specimen manufactured by Selective Laser Melting (SLM) was chosen as the target workpiece. The results show that when the ultrasonic output power was too high, both surface quality and machining efficiency were deteriorated. And the surface roughness Ra was not further improved by just increasing the machining time. Severe cavitation erosion occurred in the polishing process and created leftover pits on the workpiece surface, which has a large influence on Ra . The size and amount of the abrasive particles should be within a certain range, which is helpful for material removal and improving the polishing performance. The work is useful for studying the influential process parameters involved in UAP and finding out the appropriate conditions.

ARTICLE INFO

Keywords:

Additive manufacturing;
3D printing;
Selective laser melting (SLM);
Ultrasonic abrasive polishing;
Process parameters;
Surface roughness;
Material removal rate;
Orthogonal array tests

*Corresponding author:

wjs@dlnu.edu.cn
(Wang, J.)

Article history:

Received 19 January 2022

Revised 14 August 2022

Accepted 21 August 2022



Content from this work may be used under the terms of the Creative Commons Attribution 4.0 International Licence (CC BY 4.0). Any further distribution of this work must maintain attribution to the author(s) and the title of the work, journal citation and DOI.

1. Introduction

Additive Manufacturing (AM) technology is a process of joining materials layer by layer to make parts based on a pre-designed three-dimensional model data, which is distinguished from traditional subtractive machining techniques [1]. The manufactured components have high dimensional accuracy and long-term dimensional stability [2, 3]. Therefore, the AM technology greatly reduces waste material, part weight, and production time. In addition, manufacturing components with no geometric limitations makes it attractive in various fields such as automotive, aerospace, and medicine [4-8].

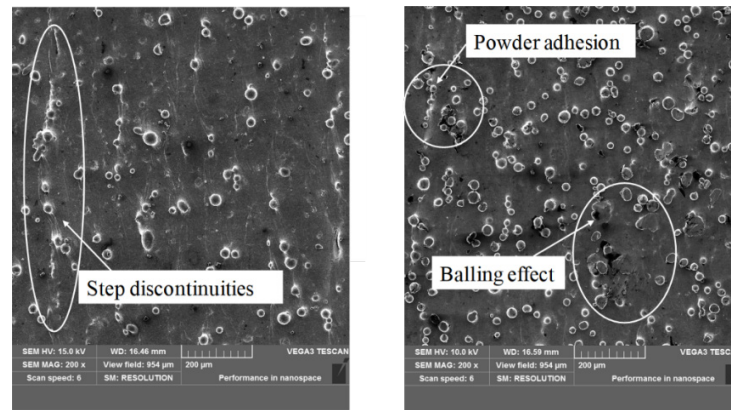


Fig. 1 Stair-stepping effect, balling effect, and powder adhesion in SLM

A laser beam can be focused to a small size which makes the energy density high and can minimize the molten pool and heat-affected zone. Therefore, lasers have been widely utilized in AM processes, especially for the metallic materials with high melting points [9-12]. The laser-based AM processes are classified into two categories [13]. One is the laser-based directed energy deposition (L-DED), where the material can be either wire or powder, and is melted and deposited simultaneously. The other one is the laser-based powder bed fusion (L-PBF), where the laser source selectively melts metallic powders layer by layer. Even though the L-DED has faster built speeds, the L-PBF is more popular due to its better manufacturing capability for producing compact features with greater geometrical accuracy and high specific strength [10, 12].

Selective laser melting (SLM) and Selective laser sintering (SLS) are typical L-PBF technologies. SLS technology has relatively low strength sintered parts. In addition, the mechanical properties and forming accuracy of SLS sintered parts are lower than that of SLM due to voids in process entities [14]. SLM acts as one of the most popular AM processes for metallic materials in industry now. However, the surface roughness of the SLM parts is still too high for direct uses. In the SLM process, stair-stepping effect, balling effect, and powder adhesion [15-18] are the three main factors leading to the poor quality as shown in Fig. 1. These not only affect the aesthetics, but also greatly limits the functional performance of the parts including fatigue life and friction properties [19].

To improve the surface quality of AM parts for practical uses, various post-process finishing techniques are implemented [20]. Today, manual polishing is still the main polishing method for AM parts, but it needs long operating time and high labor costs, and the accuracy is dependent on the experience of the personnel. Chemical polishing, electrochemical polishing, laser polishing, and abrasive flow machining have shown their capabilities in finishing AM parts [21-23]. However, they have their respective advantages and shortcomings when applied to surface polishing of AM parts. The larger thermal damage caused by laser polishing leads to the deformation of metal parts more easily. In the same way, chemical polishing causes great chemical damage. While electrochemical polishing is not suitable for polishing metal parts with deep inner holes. Abrasive flow machining is potential for surface finishing of internal channels, but it still has the limitations include damage to thin-walled structures due to excessive pumping pressures and abrasive contamination in the internal channels.

The principle of ultrasonic abrasive polishing, abbreviated as UAP here, was proved effective in improving surface quality of AM parts in some recent studies [21, 24-26]. In this process, the materials are removed by the combination of cavitation and micro-cut of abrasive particles, which is feasible for finishing various AM parts with complex external and internal surfaces. Mass and dimensional losses are only significant for initially rough surfaces with numerous surface irregularities. Therefore, UAP has the potential to finish the surface without alteration of the original AM dimensions, which distinguishes it from other surface finishing techniques. Nevertheless, the machining capability of UAP for finishing AM surfaces is not totally understood. Many input parameters exist in UAP which would influence the polishing performance, and there is a lack of systematic study on this. In this study, UAP experiments of SLM manufactured

IN625 alloy specimen were conducted using the orthogonal experimental design method with an $L_9(3^4)$ orthogonal array to investigate the effects of ultrasonic power, machining time, abrasive size, and abrasive concentration on polishing results. The work is useful for studying the influential process parameters involved in UAP and improving the machining performance.

2. Basic principle of ultrasonic abrasive polishing (UAP)

UAP uses an ultrasonic tool (horn) in conjunction with abrasive particles suspended in a liquid slurry for surface polishing, the ultrasonic tool tip should be at a specific distance away from the specimen surface to prevent a contact between them. According to the previous studies, three main material removal modes in the polishing process were concluded [25, 27] and schematically shown in Fig. 2. They include:

- Cavitation erosion from the abrasive slurry, which is effective for removing partially melting powders on the AM surfaces.
- Abrasion by the impact of the abrasive particles against the workpiece accelerated by the force of cavitation collapse.
- Small-scale material removal by high frequency impact of abrasive particles excited by ultrasonic vibration of the tool.

In addition, the cavitation effect is helpful for the circulation of abrasives and chip removal of the workpiece materials, which facilitate the material removal in UAP.

The cavitation is mainly influenced by ultrasonic amplitude, ultrasonic frequency, and physical parameters of the liquid. Generally, ultrasonic frequency ranged from 20-40 kHz is appropriate for cavitation. The cavitation intensity increases with the increase of the ultrasonic amplitude. And an increase of the liquid viscosity would suppress the cavitation. On the other hand, the frequency and intensity of the abrasive impact would also be influenced by the input ultrasonic parameters and the characteristics of the particles.

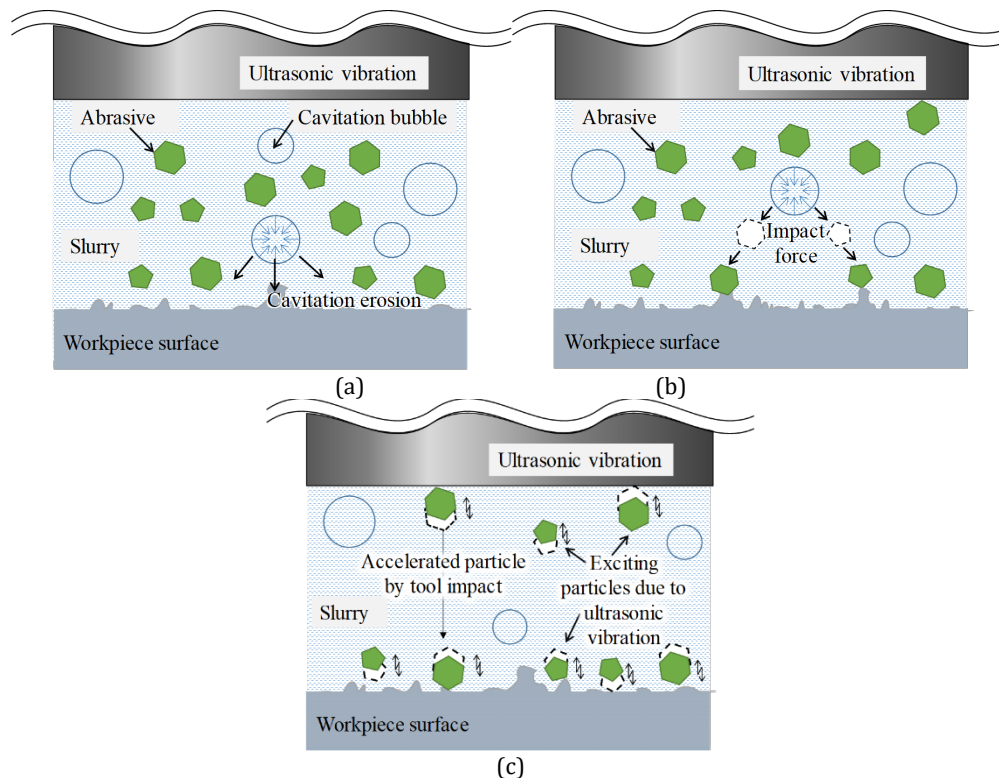


Fig. 2 Schematic view of material removal in UAP: (a) cavitation erosion, (b) abrasive impact accelerated by cavitation collapse, (c) abrasive impact excited by ultrasonic vibration of the tool

Therefore, both the settings of the ultrasonic parameters and the composition of the slurry are important for the material removal in UAP, and accordingly influence the polishing efficiency and the surface quality. In the following sections, UAP experiments are introduced, discussions are also conducted based on the experimental results and previous studies.

3. Materials and methods

3.1 Materials

The slurry composed of silicon carbide abrasive particles and purified water. The IN625 specimen was a cube with a side length of 20 mm, which was manufactured by a SLM equipment (FARSOON) with the scanning speed of 7.6 m/s. The metal powder size ranges from 15 μm to 53 μm . The powder-bed depth is 0.1 mm, and the material parameters are illustrated in Table 1. Surfaces built at 90° orientation were treated with UAP process.

Table 1 Material parameters

Element	C	Si	Mn	S	P	Cr	Ni	Mo	Al	Ti	Nb+Ta	Co	Fe
wt %	≤ 0.1	≤ 0.5	≤ 0.5	≤ 0.015	≤ 0.015	20.0-23.0	≥ 58.0	8.8-10.0	≤ 0.4	≤ 0.4	3.15-4.15	< 1.0	< 5.0

3.2 Experimental setup

An ultrasonic generator with the output power ranging from 800-1800 W (Ningbo Scientz Biotechnology) was used in this work. The frequency is 19.5-20.5 kHz. The diameter of the horn tip is 25 mm. The ultrasonic amplitude can be adjusted purposely by changing the output power.

3.3 Design of experiments

In this study, the surface roughness Ra and the material removal rate (MMR) were used for evaluating the polishing performance of UAP. To obtain the appropriate condition covering a wide range of factors in a more efficient way, the orthogonal experimental design was applied to reduce the number of experiments. Table 2 lists the specific conditions of an $L_9(3^4)$ orthogonal array used in this work, corresponding to four factors of three levels. As shown in Table 2, three levels of ultrasonic power were 900, 1200 and 1500 W. Three levels of machining time were 10 min, 20 min and 30 min. Three levels of abrasive size were 800, 1200, and 2000 grit sizes. Three levels of abrasive concentration were 5 %, 10 % and 15 %.

Table 2 Experimental design using the L_9 orthogonal array

Experimental number	Factors			
	A (Ultrasonic power)	B (Machining time)	C (Abrasive size)	D (Abrasive concentration)
1	900	10	800	5
2	900	20	1200	10
3	900	30	2000	15
4	1200	10	1200	15
5	1200	20	2000	5
6	1200	30	800	10
7	1500	10	2000	10
8	1500	20	800	15
9	1500	30	1200	5

The orthogonal experimental results were studied with the range analysis, which is a statistical method to determine the sensitivity of the factors and to obtain the optimal process conditions. The analyzing process of range analysis is as follows:

$$k_{Xm} = K_{Xm} / 3 \quad (1)$$

$$R = \max(k_{X1}, k_{X2}, k_{X3}) - \min(k_{X1}, k_{X2}, k_{X3}) \quad (2)$$

K_{Xm} and k_{Xm} means the sum and the average value of the experimental results of factor X with level m . R means the influence degree of the factor X , and the higher the value R is, the greater

the influence degree of factor X is. The tendency charts showing the influence of each parameter on the surface roughness and the MRR were also drawn based on the range analysis.

3.4 Experimental procedure

As shown in Fig. 3, the workpiece to be polished was fixed in a container filled with the abrasive slurry. The ultrasonic tool was immersed in the slurry, the distance between the tool tip and the workpiece was adjusted to guarantee efficient polishing and prevent direct contact between the two. Meanwhile, cooling system was applied during the process to avoid a drastic increase in temperature of the horn. Repeated polishing experiments were conducted for each condition as shown in Table 2. After polishing, the surface roughness was tested by a hand-held roughness meter with the measurement accuracy of $0.002 \mu\text{m}$ (Mitutoyo), and the surface was observed with a scanning electron microscope (TESCAN). Due to the high standard deviations of AM surface, as least as 5 measurements of each specimen were conducted to calculate the average Ra value. The weight of the workpiece before and after polishing was measured by an electronic balance with the measurement accuracy of 0.1 mg . Thus, the MRR can be calculated as the difference of weight over the polishing time. In addition, the particle size distribution before and after machining was examined by a particle size analysis device (Mastersizer 3000, Malvern Panalytical) to study the wear of abrasive particles.

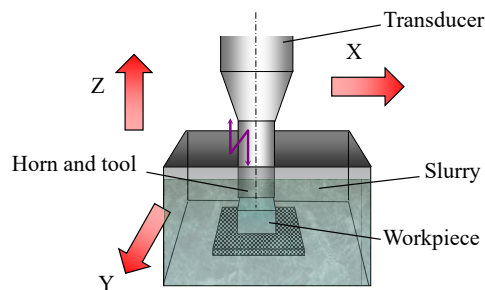


Fig. 3 Schematic view of the experimental process

4. Results and discussions

The obtained surface roughness Ra and MRR after ultrasonic polishing experiments are as shown in Table 3. The initial average Ra of the target SLM surface is $9.48 \mu\text{m}$. After polishing, the surface roughness was decreased obviously ranging from $5.01 \mu\text{m}$ to $6.80 \mu\text{m}$. The MRR ranges from 1.14 mg/min to 3.0 mg/min .

Table 3 Results of surface roughness and MRR

Experimental number	Surface roughness Ra (μm)	MRR (mg/min)
1	5.58	2.40
2	5.92	2.15
3	6.05	1.86
4	6.20	1.84
5	5.66	2.71
6	6.22	1.57
7	5.01	3.00
8	6.80	1.14
9	6.20	1.57

Range analysis results of surface roughness and MRR were presented in Table 4 and Table 5, respectively. K_j and k_j represents the sum and average value of the measurement results of the roughness and the MRR for each factor (each column) with level j , $j = 1, 2, 3$, respectively. The results show that the main influence factor on surface roughness is abrasive concentration, and the influence order of different process parameters on Ra is: abrasive concentration > abrasive size > machining time > ultrasonic power based on the value R . The main influence factor on MRR is abrasive size, and the influence order of the parameters is: abrasive size > machining time > abrasive concentration > ultrasonic power using the same analysis method. In this work,

the surface roughness value is required to be as small as possible, which means the surface quality is improved. On the other hand, the MRR should be high, which is important to increase the machining efficiency. When the combination of the four process parameters is ultrasonic power at 900 W, machining time of 10 min, grit size at 2000, and abrasive concentration at 10 %, the analysis results show smallest R_a value (the corresponding level of minimum k for each factor) and highest MRR (the corresponding level of maximum k for each factor).

Table 4 Range analysis on surface roughness

	Ultrasonic power (W)	Machining time (min)	Abrasive size (μm)	Abrasive concentration (% wt)
K_1	17.55	16.79	18.60	17.44
K_2	18.08	18.38	18.32	17.15
K_3	18.01	18.47	16.72	19.05
k_1	5.850	5.597	6.200	5.813
k_2	6.027	6.127	6.107	5.717
k_3	6.003	6.157	5.573	6.350
R	0.177	0.560	0.627	0.633
Order of priority	Abrasive concentration > Abrasive size > Machining time > Ultrasonic power			
Optimal level	900	10	2000	10
Optimal combination	900 W, 10 min, 2000 grit, 10 %			

Table 5 Range analysis on MRR

	Ultrasonic power (W)	Machining time (min)	Abrasive size (μm)	Abrasive concentration (% wt)
K_1	6.41	7.24	5.11	6.68
K_2	6.12	6.00	5.56	6.72
K_3	5.71	5.00	7.57	4.84
k_1	2.137	2.413	1.703	2.227
k_2	2.040	2.000	1.853	2.240
k_3	1.903	1.667	2.523	1.613
R	0.233	0.747	0.820	0.627
Order of priority	Abrasive size > Machining time > Abrasive concentration > Ultrasonic power			
Optimal level	900	10	2000	10
Optimal combination	900 W, 10 min, 2000 grit, 10 %			

4.1 Effects of ultrasonic power

Fig. 4 shows the effects of ultrasonic power on surface roughness and MRR. When the output power of the ultrasonic generator was 900 W, better surface roughness R_a and larger MRR were obtained compared to 1200 W and 1500 W. Based on our former research [25], when the ultrasonic power is among 400 W to 600 W, the surface becomes smoother with the increase of ultrasonic power. It is considered that with the increase of ultrasonic power, the cavitation intensity is enhanced which strengthens the cavitation erosion effects on the work surface and accordingly facilitates the removal of partially melted powders. In addition, abrasion against the work-piece due to the impact of abrasive particle that accelerated by cavitation collapse is also enhanced, so irregularities on the initially rough AM surfaces can be gradually smoothed. However, in this work, it is found that a too high ultrasonic power deteriorates both the surface quality and the machining efficiency. Existed studies have shown that the cavitation erosion effects on a solid surface increase with ultrasonic power up to a threshold and then decrease [28, 29]. The presence of a maximum in the ultrasonically enhanced erosion effects with increasing power is attributed to a peak in the cavitation intensity, which is supposed to increase with the enhancement of ultrasonic power if the collapse time allows the cavitation bubble to grow [30, 31]. Therefore, the condition produces maximum of cavitation erosion effects must be a function of power as well as frequency. On the other hand, it is commonly believed that the horn amplitude (here is controlled by the output power) has a significant effect on ultrasonic machining [32]. In this work, the output power has minimal impact on R_a and MRR compared to the other factors, which may be related to the choice of the three high output power levels.

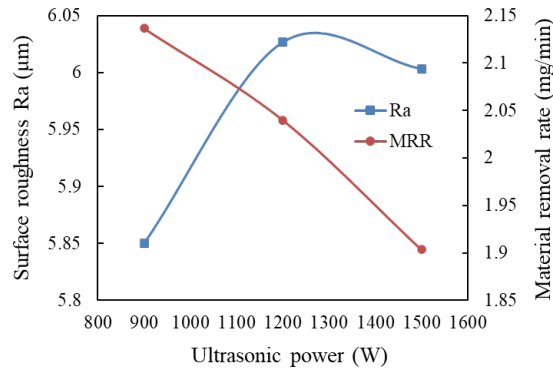


Fig. 4 Effects of ultrasonic power on surface roughness and MRR

The wear of abrasive particles under 900 W and 1500 W were compared by examining particle size distribution before and after polishing process. Other conditions are the same: 2000 grit size abrasive particles, 5 % abrasive concentration, machining time of 20 min. The results are shown in Fig. 5. The maximum particle size that can be detected becomes smaller as indicated with the ellipse marks after polishing (maximum value shifted to the left). The mean particle size before polishing was found to be 8.98 μm, according to the measurement report. After polishing with 900 W and 1500 W, the mean particle size reduces to 8.74 μm and 8.16 μm, respectively. The wear of abrasive particles is increased due to the stronger cavitation effect at higher ultrasonic power. Therefore, more motion energy of the abrasive particles was consumed in the wear between the particles but not the material removal of the workpiece when the ultrasonic power was 1500 W, which accordingly influences the polishing efficiency and the surface quality.

Fig. 6(a) shows the typical surface characteristics of the workpiece before polishing, and Fig. 6(b) is the same area after polishing. Obvious improvement of surface quality can be confirmed. The partially melted powders were almost removed as indicated in area A, and some larger discontinuities were also smoothed as shown in area B. On the other hand, tightly attached balls and irregular structures were challenging to be removed. In addition, some leftover pits due to cavitation erosion are found on the polished surface as shown in area C. With the increase of ultrasonic power, severe cavitation erosion may occur, which can leave more such leftover structures on work surface and increase the *Ra* value.

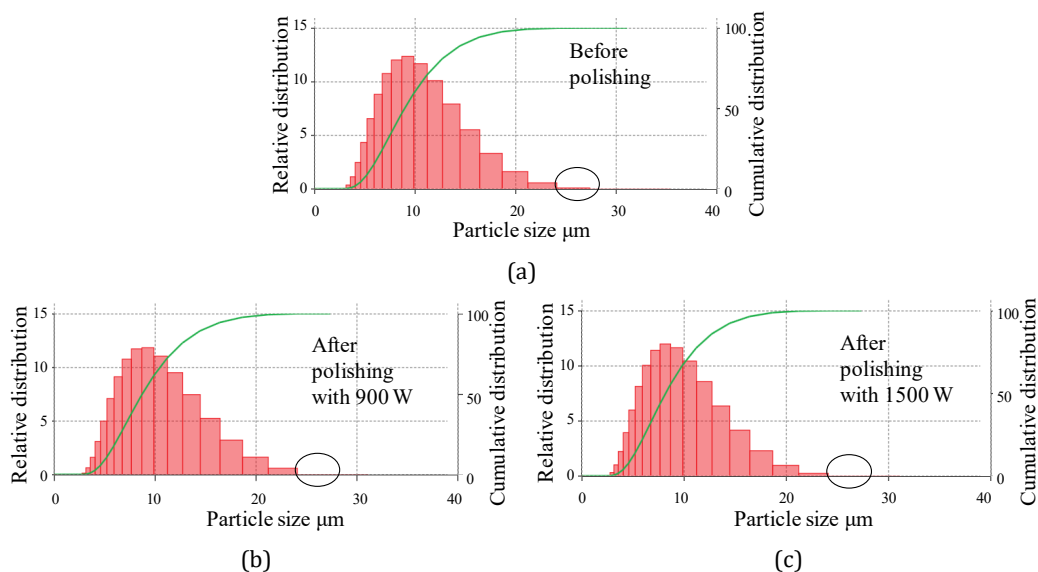


Fig. 5 Particle size distribution before (a) and after polishing with (b) 900 W and (c) 1500 W

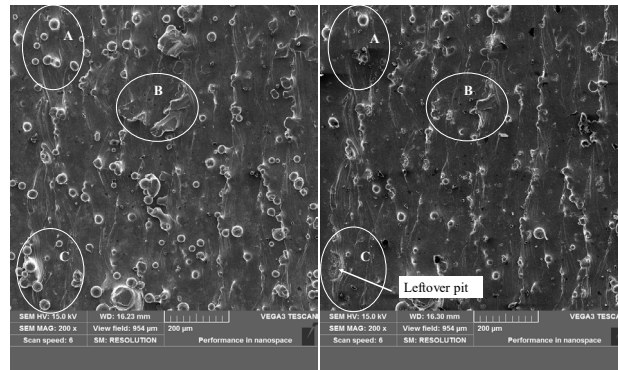


Fig. 6 SEM images of the surfaces: (a) as-manufactured AM workpiece surface; (b) surface after ultrasonic abrasive polishing

Therefore, although the machining capability of UAP could be enhanced at higher power, the increase in wear of abrasives and excessive erosion of surface occur simultaneously, which strongly influences the polishing process. In addition, large number of cavitation bubbles and broken abrasive particles between the horn and the workpiece may play a screening role that inhibits effective cavitation erosion and abrasion of particles against the workpiece at higher power. All these lead to the better surface roughness Ra and larger MRR at 900 W than 1200 W and 1500 W in this work.

4.2 Effects of machining time

Fig. 7 shows the effects of machining time on surface roughness Ra and MRR. The machining time of 10 min resulted in minimum Ra and maximum MRR compared to 20 min and 30 min. At the initial stage of polishing, the partially melted powders were removed quickly, and the peak of material surface was easily to be ground. Therefore, the Ra value rapidly reduced, and the MRR was high. With the increase of polishing time, the peak of the surface was smoothed and became flat, which slowed down the MRR. And we found the similar tendency in the previous work [25] that the partially melted powders were predominately removed in the first several minutes and only slight material removal occurred in the remaining machining time. The surface was significantly modified in the initial stage (around several minutes or less) and converge to an equilibrium state.

Normally, the Ra should not be worse because more powders and irregular structures might be removed with the increase of the machining time. However, the results show an obvious increase in the Ra value after 20 min and 30 min. The workpiece was an AM manufactured part and has its own surface features, large pits may be left on the surface as introduced in area C of Fig. 6 after the removal of tightly attached large balls and irregular structures due to severe cavitation erosion. This has a large effect on the surface roughness Ra . In addition, the existence of these pits may further negatively affect the polishing performance because it is easier to deepen the pits under cavitation erosion and abrasive impacts than to flatten them. It seems more necessary to finding out appropriate conditions to facilitate effective polishing action for further reducing the Ra value.

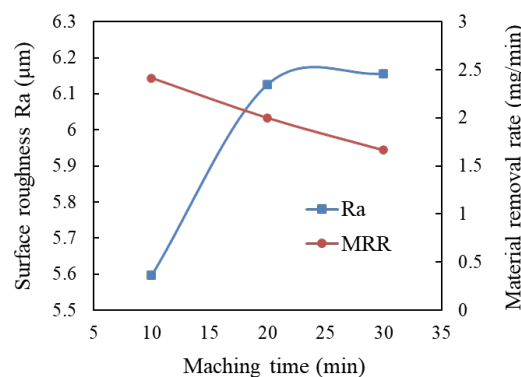


Fig. 7 Effects of machining time on surface roughness and MRR

On the other hand, with the increase of processing time, the wear of abrasive becomes more and more serious, which weakens the grinding capability of abrasive particles. And in the experiments, no new slurry was introduced in the machining area, the continuous high-power ultrasonic work leads to severe wear of abrasive particles and affects the UAP process.

4.3 Effects of abrasive size

Fig. 8 shows the effects of abrasive size on surface roughness R_a and MRR. Using abrasive particles of 2000 grit size resulted in minimum R_a and maximum MRR compared to 1200 and 800 grit sizes. The abrasive particles act as bubble nucleation sites, compared to smaller particles, the larger particles have larger surface areas to compete for bubble nucleation, so the cavitation erosion against workpiece may be inhibited in the presence of larger particles. Accordingly, material removal process is influenced.

The wear of abrasive particles of 2000 and 800 grit sizes were compared by examining particle size distribution before and after polishing process, respectively. Other conditions are the same: 900 W ultrasonic power, 5 % abrasive concentration, and machining time of 20 min. The results are shown in Fig. 9, the particles become smaller due to the wear for both cases. The mean particle size of 2000 and 800 grit abrasive particles decrease from 8.98 μm and 19 μm to 8.74 μm and 17.7 μm , respectively. A decrease of 2.7 % and 6.8 % in mean particle size for 2000 and 800 grit abrasive particles is confirmed. Therefore, more motion energy was consumed in abrasive broken for larger abrasive particles, and accordingly influences the polishing process. In addition, the larger size particle could act as a physical barrier on the specimen surface to avoid the impact of micro-jets induced by cavitation collapse and affect the material removal [21]. The diameters of the micro-jets are around 10-30 μm [33]. The mean particle size of 1200 and 800 grit abrasive particles are 13.8 μm and 19 μm , respectively, which would screen the micro-jets and inhibit material removal. Therefore, when using abrasives of 1200 and 800 grit sizes, both surface quality and machining efficiency are deteriorated.

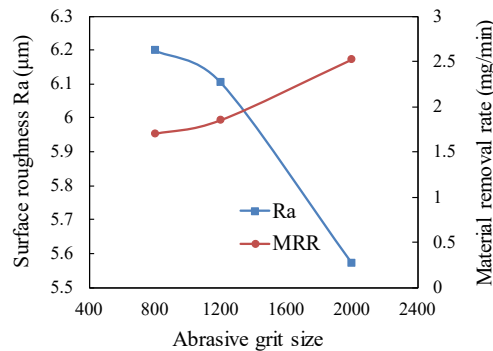


Fig. 8 Effects of abrasive size on surface roughness and MRR

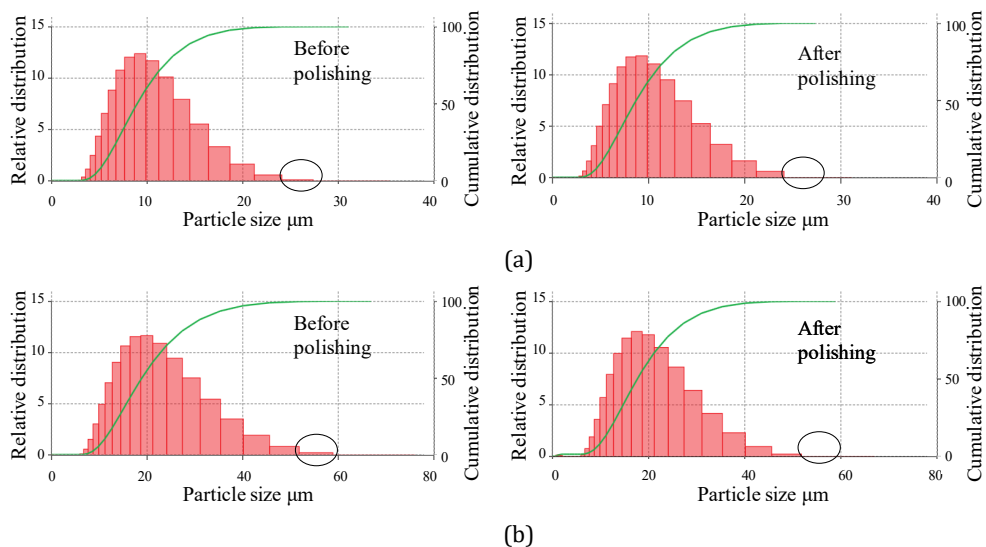


Fig. 9 Particle size distribution before and after polishing: (a) 2000 and (b) 800 grit sizes

4.4 Effects of abrasive concentration

Fig. 10 shows the effects of abrasive concentration on surface roughness Ra and MRR. The abrasive concentration at 10 % resulted in minimum Ra and maximum MRR compared to 5 % and 15 %. The former studies [21, 25] also showed that the surface roughness is improved with the increase of abrasive concentration in a certain range, then the Ra value cannot get better with a further increase in abrasive concentration. And the MRR also showed the same tendency. When the abrasive concentration is too high, the interference between the abrasive particles increases. It is supposed that more motion energy of the abrasive particles would be consumed in the impact between the particles but not the material removal of the workpiece, which would accordingly affect the polishing performance. Furthermore, a large number of abrasive particles would act competing nucleation sites, which may inhibit the cavitation erosion against the workpiece, resulting in the reduction of material removal.

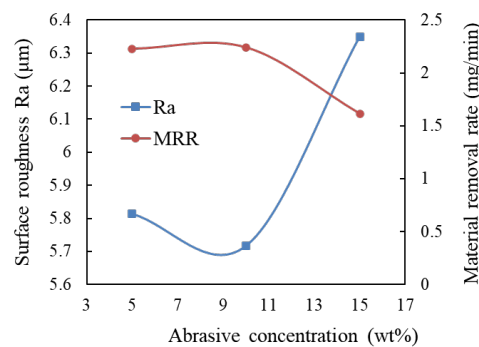


Fig. 10 Effects of abrasive concentration on surface roughness and MRR

5. Conclusion

Since ultrasonic process is cost effective and applicable to the manufacturing of micro-to macro-scale structures, it may lead to new applications in specially designed surface treatment by controlling the process parameters appropriately. In this work, the machining capability of UAP which used ultrasonic cavitation in an abrasive slurry was studied. Polishing experiments on SLM manufactured IN625 alloy specimen were conducted using the orthogonal experimental design method with an $L_9(3^4)$ orthogonal array. Range analysis was performed on the experimental results to investigate the effects of ultrasonic power, machining time, abrasive size, and abrasive concentration on polishing performance. The work is useful for studying the influential process parameters involved in ultrasonic abrasive polishing and optimizing the process parameters. The following conclusions can be drawn:

- When the ultrasonic power is too high, both abrasive wear and cavitation bubbles increase, which may play a screening role that inhibits cavitation erosion and abrasion of particles against the workpiece. Therefore, the surface quality and the machining efficiency would be deteriorated.
- During polishing process, severe cavitation erosion can occur and create leftover pits on the workpiece surface, which has a large influence on Ra .
- The AM surface is significantly modified in the initial polishing stage because the partially melted powders and some peak irregular structures are removed.
- Using too large abrasive particles is not helpful for material removal. The larger particles have larger surface areas to compete for bubble nucleation and act as physical barriers on the workpiece surface to inhibit the material removal of the workpiece. And the severe wear of large abrasive particles also influences the polishing performance.
- Both the surface quality and the MRR were improved when the abrasive concentration increased within a certain range. While the abrasive concentration is too high, the interference between the abrasive particles increases, the material removal is suppressed, and the surface quality is also deteriorated.

- Based on the range analysis, the influence order of different process parameters on R_a was abrasive concentration > abrasive size > machining time > ultrasonic power, while the influence order of the parameters on MRR was abrasive size > machining time > abrasive concentration > ultrasonic power in this study. When the ultrasonic power, machining time, grit size and abrasive concentration are 900 W, 10 min, 2000 grit size, and 10 %, respectively, the analysis results show smallest R_a value and highest MRR.

Funding

This work is supported by China Postdoctoral Science Foundation [Grant no. 2019M651093], the Natural Science Foundation of Liaoning Province (China) [Grant no. 2021-MS-135], Dalian Science and Technology Development Funds of China [Grant no. 2020RQ092], the National Natural Science Foundation of China [Grant no. 51805067], Fundamental Research Funds for the Central Universities of China [Grant no. 3132019366].

Conflicts of Interest

The authors declare no conflict of interest.

References

- [1] ASTM International. (2015). ISO/ASTM52900-15 Standard terminology for additive manufacturing-general principles- terminology, West Conshohocken, PA: ASTM International.
- [2] Mandić, M., Galeta, T., Raos, P., Jugović, V. (2016). Dimensional accuracy of camera casing models 3D printed on Mcor IRIS: A case study, *Advances in Production Engineering & Management*, Vol. 11, No. 4, 324-332, doi: [10.14743/apem2016.4.230](https://doi.org/10.14743/apem2016.4.230).
- [3] Mendricky, R., Soni, R.D. (2022). Geometric stability of parts produced by 3D printing, *Tehnički Vjesnik – Technical Gazette*, Vol. 29, No. 1, 23-29, doi: [10.17559/TV-20191101110214](https://doi.org/10.17559/TV-20191101110214).
- [4] Han, X., Zhu, H., Nie, X., Wang, G., Zeng, X. (2018). Investigation on selective laser melting AlSi10Mg cellular lattice strut: Molten pool morphology, surface roughness and dimensional accuracy, *Materials*, Vol. 11, No. 3, Article No. 392, doi: [10.3390/ma11030392](https://doi.org/10.3390/ma11030392).
- [5] Calignano, F., Peverini, O.A., Addamo, G., Iuliano, L. (2020). Accuracy of complex internal channels produced by laser powder bed fusion process, *Journal of Manufacturing Processes*, Vol. 54, 48-53, doi: [10.1016/j.jmapro.2020.02.045](https://doi.org/10.1016/j.jmapro.2020.02.045).
- [6] Calignano, F., Manfredi, D., Ambrosio, E.P., Biamino, S., Lombardi, M., Atzeni, E., Salmi, A., Minetola, P., Iuliano, L., Fino, P. (2017). Overview on additive manufacturing technologies, *Proceedings of the IEEE*, Vol. 105, No. 4, 593-612, doi: [10.1109/JPROC.2016.2625098](https://doi.org/10.1109/JPROC.2016.2625098).
- [7] Polanec, B., Kramberger, J., Glodež, S. (2020). A review of production technologies and materials for manufacturing of cardiovascular stents, *Advances in Production Engineering & Management*, Vol. 15, No. 4, 390-402, doi: [10.14743/apem2020.4.373](https://doi.org/10.14743/apem2020.4.373).
- [8] Patalas-Maliszewska, J., Topczak, M. (2021). A new management approach based on Additive Manufacturing technologies and Industry 4.0 requirements, *Advances in Production Engineering & Management*, Vol. 16, No. 1, 125-135, doi: [10.14743/apem2021.1.389](https://doi.org/10.14743/apem2021.1.389).
- [9] Wei, C., Zhang, Z., Cheng, D., Sun, Z., Zhu, M., Li, L. (2021). An overview of laser-based multiple metallic material additive manufacturing: From macro-to micro-scales, *International Journal of Extreme Manufacturing*, Vol. 3, No. 1, Article No. 012003, doi: [10.1088/2631-7990/abce04](https://doi.org/10.1088/2631-7990/abce04).
- [10] DebRoy, T., Wei, H.L., Zuback, J.S., Mukherjee, T., Elmer, J.W., Milewski, J.O., Beese, A.M., Wilson-Heid, A., De, A., Zhang, W. (2018). Additive manufacturing of metallic components – Process, structure and properties, *Progress in Materials Science*, Vol. 92, 112-224, doi: [10.1016/j.pmatsci.2017.10.001](https://doi.org/10.1016/j.pmatsci.2017.10.001).
- [11] Lewandowski, J.J., Seifi, M. (2016). Metal additive manufacturing: A review of mechanical properties, *Annual Review of Materials Research*, Vol. 46, 151-186, doi: [10.1146/annurev-matsci-070115-032024](https://doi.org/10.1146/annurev-matsci-070115-032024).
- [12] Gao, W., Zhang, Y., Ramanujan, D., Ramani, K., Chen, Y., Williams, C.B., Wang, C.C.L., Shin, Y.C., Zhang, S., Zavattieri, P.D. (2015). The status, challenges, and future of additive manufacturing in engineering, *Computer-Aided Design*, Vol. 69, 65-89, doi: [10.1016/j.cad.2015.04.001](https://doi.org/10.1016/j.cad.2015.04.001).
- [13] ASTM International. (2013). *Standard Terminology for Additive Manufacturing Technologies*, ASTM International 2013 F2792-12a.
- [14] Koziar, T. (2020). Rheological properties of polyamide PA 2200 in SLS technology, *Tehnički Vjesnik – Technical Gazette*, Vol. 27, No. 4, 1092-1100, doi: [10.17559/TV-20190225122204](https://doi.org/10.17559/TV-20190225122204).
- [15] Wang, J., Liu, S., Fang, Y., He, Z. (2020). A short review on selective laser melting of H13 steel, *International Journal of Advanced Manufacturing Technology*, Vol. 108, 2453-2466, doi: [10.1007/s00170-020-05584-4](https://doi.org/10.1007/s00170-020-05584-4).
- [16] Strano, G., Hao, L., Everson, R.M., Evans, K.E. (2013). Surface roughness analysis, modelling and prediction in selective laser melting, *Journal of Materials Processing Technology*, Vol. 213, No. 4, 589-597, doi: [10.1016/j.jmatprotec.2012.11.011](https://doi.org/10.1016/j.jmatprotec.2012.11.011).

- [17] Bhaduri, D., Penchev, P., Batal, A., Dimov, S., Soo, S.L., Sten, S., Harrysson, U., Zhang, Z., Dong, H. (2017). Laser polishing of 3D printed mesoscale components, *Applied Surface Science*, Vol. 405, 29-46, doi: [10.1016/j.apsusc.2017.01.211](https://doi.org/10.1016/j.apsusc.2017.01.211).
- [18] Cabanettes, F., Joubert, A., Chardon, G., Dumas, V., Rech, J., Grosjean, C., Dimkovski, Z. (2018). Topography of as built surfaces generated in metal additive manufacturing: A multi scale analysis from form to roughness, *Precision Engineering*, Vol. 52, 249-265, doi: [10.1016/j.precisioneng.2018.01.002](https://doi.org/10.1016/j.precisioneng.2018.01.002).
- [19] Gordon, E.R., Shokrani, A., Flynn, J.M., Goguelin, S., Barclay, J., Dhokia, V. (2016). A surface modification decision tree to influence design in additive manufacturing, In: Setchi, R., Howlett, R., Liu, Y., Theobald, P. (eds.), *Sustainable design and manufacturing 2016. SDM 2016. Smart innovation, systems and technologies*, Vol. 52, Springer, Cham, Switzerland, doi: [10.1007/978-3-319-32098-4_36](https://doi.org/10.1007/978-3-319-32098-4_36).
- [20] Kumbhar, N.N., Mulay, A.V. (2018). Post processing methods used to improve surface finish of products which are manufactured by additive manufacturing technologies: A review, *Journal of The Institution of Engineers (India): Series C, Mechanical, Production, Aerospace and Marine Engineering*, Vol. 99, 481-487, doi: [10.1007/s40032-016-0340-z](https://doi.org/10.1007/s40032-016-0340-z).
- [21] Tan, K.L., Yeo, S.H. (2020). Surface finishing on IN625 additively manufactured surfaces by combined ultrasonic cavitation and abrasion, *Additive Manufacturing*, Vol. 31, Article No. 100398, doi: [10.1016/j.addma.2019.100938](https://doi.org/10.1016/j.addma.2019.100938).
- [22] Nagalingam, A.P., Yuvaraj, H.K., Yeo, S.H. (2020). Synergistic effects in hydrodynamic cavitation abrasive finishing for internal surface-finish enhancement of additive-manufactured components, *Additive Manufacturing*, Vol. 33, Article No. 101110, doi: [10.1016/j.addma.2020.101110](https://doi.org/10.1016/j.addma.2020.101110).
- [23] Zhao, C., Qu, N., Tang, X. (2021). Removal of adhesive powders from additive-manufactured internal surface via electrochemical machining with flexible cathode, *Precision Engineering*, Vol. 67, 438-452, doi: [10.1016/j.precisioneng.2020.11.003](https://doi.org/10.1016/j.precisioneng.2020.11.003).
- [24] Lee, J.-Y., Nagalingam, A.P., Yeo, S.H. (2020). A review on the state-of-the-art of surface finishing processes and related ISO/ASTM standards for metal additive manufactured components, *Virtual and Physical Prototyping*, Vol. 16, No. 1, 68-96, doi: [10.1080/17452759.2020.1830346](https://doi.org/10.1080/17452759.2020.1830346).
- [25] Wang, J., Zhu, J., Liew, P.J. (2019). Material removal in ultrasonic abrasive polishing of additive manufactured components, *Applied Sciences*, Vol. 9, No. 24, Article No. 5359, doi: [10.3390/app9245359](https://doi.org/10.3390/app9245359).
- [26] Tan, K.L., Yeo, S.H. (2017). Surface modification of additive manufactured components by ultrasonic cavitation abrasive finishing, *Wear*, Vol. 378-379, 90-95, doi: [10.1016/j.wear.2017.02.030](https://doi.org/10.1016/j.wear.2017.02.030).
- [27] Ichida, Y., Sato, R., Morimoto, Y., Kobayashi, K. (2005). Material removal mechanisms in non-contact ultrasonic abrasive machining, *Wear*, Vol. 258, No. 1-4, 107-114, doi: [10.1016/j.wear.2004.05.016](https://doi.org/10.1016/j.wear.2004.05.016).
- [28] Whillock, G., Harvey, B.F. (1997). Ultrasonically enhanced corrosion of 304L stainless steel II: The effect of frequency, acoustic power and horn to specimen distance, *Ultrasonics Sonochemistry*, Vol. 4, No. 1, 33-38, doi: [10.1016/S1350-4177\(96\)00015-6](https://doi.org/10.1016/S1350-4177(96)00015-6).
- [29] Virost, M., Chave, T., Nikitenko, S.I., Shchukin, D.G., Zemb, T., Möhwald, H. (2010). Acoustic cavitation at the water-glass interface, *Journal of Physical Chemistry C*, Vol. 114, No. 30, 13083-13091, doi: [10.1021/jp1046276](https://doi.org/10.1021/jp1046276).
- [30] Couppis, E.C., Klinzing, G.E. (1974). Effect of cavitation on reacting systems, *AIChE Journal*, Vol. 20, No. 3, 485-491, doi: [10.1002/aic.690200308](https://doi.org/10.1002/aic.690200308).
- [31] Shchukin, D.G., Skorb, E., Belova, V., Möhwald, H. (2011). Ultrasonic cavitation at solid surfaces, *Advanced Materials*, Vol. 23, No. 17, 1922-1934, doi: [10.1002/adma.201004494](https://doi.org/10.1002/adma.201004494).
- [32] Bhosale, S.B., Pawade, R.S., Brahmankar, P.K. (2014). Effect of process parameters on MRR, TWR and surface topography in ultrasonic machining of alumina-zirconia ceramic composite, *Ceramics International*, Vol. 40, No. 8, Part B, 12831-12836, doi: [10.1016/j.ceramint.2014.04.137](https://doi.org/10.1016/j.ceramint.2014.04.137).
- [33] Tzanakis, I., Eskin, D.G., Georgoulas, A., Fytanidis, D.K. (2014). Incubation pit analysis and calculation of the hydrodynamic impact pressure from the implosion of an acoustic cavitation bubble, *Ultrasonics Sonochemistry*, Vol. 21, No. 2, 866-878, doi: [10.1016/j.ultsonch.2013.10.003](https://doi.org/10.1016/j.ultsonch.2013.10.003).

Machinability analysis and multi-response optimization using NSGA-II algorithm for particle reinforced aluminum based metal matrix composites

Umer, U.^{a,*}, Mohammed, M.K.^a, Abidi, M.H.^a, Alkhalefah, H.^a, Kishawy, H.A.^b

^aAdvanced Manufacturing Institute, King Saud University, Riyadh, Saudi Arabia

^bMachining Research Laboratory, University of Ontario Institute of Technology, Oshawa, ON, Canada

ABSTRACT

In this study the effects of reinforcement particle size and cutting parameters on machining performance variables like cutting force, maximum tool-chip interface temperature and surface roughness of the machined surface have been investigated while machining Aluminum based metal matrix composites (MMCs). MMC bars with silicon carbide reinforcement having 10 % volume fraction and particle sizes of 5 μm , 10 μm and 15 μm are machined with polycrystalline diamond (PCD) inserts. Experiments are performed using central composite design (CCD) having four parameters with three levels. Response surfaces for each performance variables are generated using polynomial models. Single variable and interaction effects have been investigated using principal component analysis and 3D response charts. Multi-response optimization has been performed to minimize surface roughness and maximum tool-chip interface temperature using non-dominated sorting genetic algorithm II (NSGA-II). In addition, constraints have been applied to the optimization search to filter design points with high cutting forces and low material removal rate. Most of the optimal solutions are found to be with moderate cutting speeds, low feed rate and low depth of cuts.

ARTICLE INFO

Keywords:

Metal Matrix Composites (MMC);
Machining;
Reinforcement particle;
Machinability;
Multi-objective optimization;
Non-dominated sorting genetic algorithm (NSGA-II)

*Corresponding author:

uumer@ksu.edu.sa
(Umer, U.)

Article history:

Received 8 March 2022

Revised 31 August 2022

Accepted 31 August 2022



Content from this work may be used under the terms of the Creative Commons Attribution 4.0 International License (CC BY 4.0). Any further distribution of this work must maintain attribution to the author(s) and the title of the work, journal citation and DOI.

1. Introduction

1.1 General

Metal matrix composites (MMCs) are gaining popularity in different fields such as automotive, aerospace, biomedical and electronics. They are gradually replacing conventional metals and alloys owing to their superior properties e.g., strength to weight ratio and wear resistance. They are usually made by net-shape manufacturing techniques. However, to obtain the required accuracy and surface finish, secondary processes such as machining cannot be avoided. Machining of MMCs is different and quite challenging as compared to the traditional metals and alloys due to the presence of hard reinforcement particles. The interactions between reinforcement particles and cutting tools result in excessive tool wear. The debonding and fracture of these reinforcement particles leads to poor surface integrity of the machined surface. The choice of optimum cutting parameters becomes more complex and depends on several factors like shape, size, volume fraction and distribution of these reinforcement particles.

There have been many attempts to analyze machinability of particle reinforced MMCs with respect to cutting forces, chip morphology, surface finish, sub-surface damages and tool wear. The effect of reinforcement particle size on tool wear and surface finish was analyzed by Ciftci *et al.* [1] during machining of Aluminum based MMC with silicon carbide reinforcement (Al/SiCp). They utilized both coated and uncoated carbide tools. MMCs were made up of 30 μm , 45 μm and 110 μm particle sizes and volume fraction of 16 %. They reported that both tool wear and surface finish deteriorate with increasing particle size. Similar findings were reported by Kannan *et al.* [2] also while machining Al/Al₂O₃p MMC having different particle sizes and volume fractions. It was noted that high volume fraction of reinforcement particles also results in an increased tool wear that ultimately leads to poorer finish on the machined surface. High volume fraction of reinforcement particles leads to higher frequency of tool-particle interactions which result in accelerated tool wear. In another study Al/SiCp MMC were machined with 5 %, 10 % and 15 % volume fraction. They concluded that machinability of MMC was severely affected by the cutting speed and volume fraction of reinforcement particles [3]. The effects of cutting speed, feed rate, tool inclination angle and volume fraction of reinforcement particles for Al/SiCp MMC using carbide tool were investigated by Joshi *et al.* [4]. They developed a relationship between flank wear and cutting time and showed that the cutting speed and volume fraction of reinforcement particles are mainly responsible for increased tool wear.

Rai *et al.* [5] performed machinability analysis for different reinforcement materials when cutting Aluminum based MMC with TiC, TiAl₃ and Si particles. They evaluated cutting forces and surface roughness for each material and compared with the non-reinforced one. MMC with TiC reinforcement are found to be better and showed lowest cutting forces and reduced surface roughness. The authors reported absences of built-up-edge in case of Al/TiCp MMC which results in low tool wear by attrition as compared to other MMCs. The machinability of aluminum based MMC with B₄C reinforcement particles was analyzed by Karakas *et al.* [6]. They investigated the formation of built-up-edge and tool wear while machining with coated and uncoated tungsten carbide tools. Flank wear and BUE formation was found to be significant for uncoated tools at all cutting speeds. Cheung *et al.* [7] studied the effect of volume fraction of reinforcement on the surface roughness of the machined surface. Tool marks and surface roughness are found to increase as volume fraction increases. They suggested that this might be due to the pronounced spring back effect of the tool cutting edge when it strikes to the hard reinforcement particles. The effect of reinforcement particle size was investigated by Chandrasekaran and Johansson [8] and found that for each particle size there is an optimum feed rate and volume fraction of the reinforcement particles. In another research conducted by Xiaoping and Seah [9] both particle size and volume fraction of reinforcement particles are found to be significant for tool life. They reported that there is a critical value of volume fraction for each particle size above which tool wear increases at a rapid rate. This critical volume found to decrease as particle size increases.

According to researchers, surface integrity of the machined MMC is greatly dependent on the size, shape, volume fraction, bonding strength, and distribution pattern of the reinforcement particles. Lin *et al.* [10] reported that a good quality surface is not easier to achieve for MMCs as fractured and debonded reinforcement particles abrade the surface and cutting tool that leads to pits and tool marks on the machined surface. The effects of shape of the reinforcement (particles and whiskers) on the quality of the machined MMC were analyzed by Cheung *et al.* [7] when cutting Al/SiCp MMC using diamond tools. They examined the tool-particle interactions and reported that cut-through particles leave a good surface finish as compared to the debonded particles as later are mainly responsible for cracking and pits on the machined surface. It was noted that the cut-through mechanism is dominant in whiskers as compared to the particle based MMCs.

Sub-surface damages and surface roughness examinations for machining with particle reinforced MMCs were done by El-Gallab and Sklad [11]. They plotted microhardness profiles for the sub-surface damages and showed that damage is mostly located 60 μm to 100 μm beneath the machined surface. Transmission electron microscopic (TEM) examinations revealed that sub-surface damage is associated with piling up of dislocations in smaller grains areas. Dandekar and

Shin [12] developed a 3D finite element (FE) model with cohesive elements to predict sub-surface damage due to particle debonding while machining Al/SiCp MMC. They calculated debonding energy for SiC particles and showed that the damage depth increases with feed rate which also results in higher cutting forces. Machinability analysis for MMCs with different tools was investigated by Hung *et al.* [13]. They measured the sub-surface damage by testing the microhardness of the plastically deformed machined surfaces. Microscopic examinations of the machined surfaces showed that CBN and PCD tools fractured the reinforced particles along their crystallographic planes resulting in low plastic deformation. In contrast machining with other tools resulted in particles debonding resulted in higher sub-surface damage.

Pramanik *et al.* [14] compared residual stresses for the non-reinforced alloy and MMC. It was noted that longitudinal residual stresses for the non-reinforced alloys are tensile in nature and increases with both cutting speed and feed rate. For MMC the residual stresses are found to be compressive and showing very little dependency on the cutting parameters, i.e. almost constant by changing cutting speed and feed rate. As residual stresses in machining are mainly due to plastic deformation and temperature gradients inside the material, these phenomena are somewhat altered by the presence of hard reinforcement particles. From authors perspective this might be due to constrained matrix flow, hammering effect of the reinforcement particles and compression of the matrix between the cutting tool and hard ceramic particles.

The effect of reinforcement particles during MMC machining was studied by Cheung *et al.* [7] using quick stop test. They observed semi-continuous chips and believed that it is a result of reduction in ductility of the matrix due to hard reinforcement particles. It has also been observed that during cutting the reinforcement particles accumulate along the shear plane. The debonding of the particles and stress concentration accelerate the process of crack propagation resulting in serrated or semi-continuous chips [15]. Similar findings are reported in other studies while turning [11, 16] and drilling [17] Al/SiCp MMCs. Olivas *et al.* [18] reported that tensile residual stresses present on the surface of the ductile matrix generated during fabrication of MMC also facilitate this crack propagation/formation of semi-continuous chips.

The relationships between thrust force, torque and tool wear were examined by Morin *et al.* [19] while drilling non-reinforced aluminum alloy and MMC. They reported almost equal thrust force and torque for aluminum alloy and MMC and concluded that it is the matrix which controls the forces and not the particles. Nonetheless, it was noted that the overall force signal profile over the entire cutting length is much dependent on the size, volume and bonding strength of the reinforcement particles. Sikder and Kishawy [20] developed an analytical force model when machining Aluminum based MMCs with different sizes and volume fractions of alumina (Al_2O_3) particles. They showed that debonding energy and hence cutting force increases with particle size due to increase in surface area of the debonding particle. In contrast Sun *et al.* [21] reported reduction in cutting forces while machining Al/SiCp MMC. However, their study focused on comparatively big particle sizes (15 μm to 60 μm) and large volume fractions (20 % to 50 %).

Various optimization techniques have been used by researchers for machining MMCs and other metallic alloys. However evolutionary algorithms and heuristic optimizers are found to be dominant over gradient based methods. Muthukrishnan and Davim [27] did a surface roughness optimization study using analysis of variance (ANOVA) and artificial neural network (ANN). The study showed that feed rate is the dominant factor to control the surface roughness of the machined MMC in comparison to the depth of cut and cutting speed. They suggested the most optimal cutting parameters to minimize surface roughness. Regression model for tool wear was developed by Seeman *et al.* [28] while machining MMC. Built-up edge (BUE) formation was detected at low cutting speeds resulting in high tool wear. Microscopic examination revealed the presence of both abrasive and adhesive wear at low cutting speeds. Flank wear is found to be more dependent on the cutting speed and feed rate as compared to the depth of cut. Second order response surface models for cutting force, power and specific cutting force for machining Al/SiCp MMC were developed by Gaitonde *et al.* [29]. The developed models showed that variation of cutting force with respect to feed rate is almost same for any value of cutting speed. In addition, they found that an increase in cutting speed resulted in reduction of the cutting force. This is found to be more pronounced at higher feed rates in comparison to lower values. Antonio *et al.*

[30] performed optimization using genetic algorithm (GA) considering multiple objectives while machining aluminum based MMC with 20 % volume of SiC reinforced particles. The output variables considered in the study were machining forces, tool wear and surface roughness. All forces are found to increase with the tool wear whilst cutting force showing marked increase. With other parameters kept constant, surface roughness is found to increase with decrease in cutting speed. The optimum cutting parameters reported with cutting speed of 350 m/min, feed rate of 0.1mm/rev and cutting time equals to 19 min.

In view of the above it is evident that machinability studies in MMC involving temperature measurement are rare. In addition, the interaction effects of particle size with cutting parameters are not explicitly presented in the open literature. This study aims to perform machinability optimization for cutting temperatures and surface roughness while machining MMCs with different particle sizes. The interaction effects of particle size and cutting parameters on maximum tool-chip interface temperature, surface roughness of the machined surface and cutting force has been described in details and finally optimum parameters are suggested for each particle size's MMC.

2. Materials and methods

Aluminum based MMC bars of SupremEx® grade supplied by Materion, UK were utilized for turning operations. These composite bars were made using powder metallurgy and mechanical alloying process route and 100 % compaction is achieved using hot isostatic pressing. Reinforcement particles were made of silicon carbide (SiC) having an average size of 5 μm , 10 μm and 15 μm with 10 % volume fraction. A Kistler piezoelectric quartz dynamometer (9257B) was employed for measuring the cutting forces F_c during machining of MMCs. Before converting the analog force signals to digital ones, a dual mode charge amplifier (Kistler 5017B) was connected that converts low charge signals to proportional voltage signals. Dynoware® was used to acquire and save the data for further analysis. An Optris 640 thermal imaging camera was selected to capture maximum tool-chip interface temperature T during MMC machining. The camera was mounted on the tool-post as shown in the Fig. 1 and it was set to record maximum temperature during the cutting. The surface quality parameter R_a of the turned surfaces was measured using a Taylor Hobson Surtronic S100 tester at three locations after each experimental run and the average value was noted. For the design of experiment (DOE) study, a central composite design CCD-25 with four factors and 3 levels was selected for the study. The factors and their levels are shown in Table 1.



Fig. 1 Experimental setup for MMC turning with thermal imaging camera

Table 1 Factors and their levels for the DOE

Factors	Levels		
Particle size, p (μm)	0	1	2
Cutting speed, v (m/min)	5	10	15
Feed rate, f (mm/rev)	60	120	180
Depth of cut, d (mm)	0.1	0.15	0.2
	1.0	1.5	2.0

Using DOE results response surfaces are generated based on 2nd degree polynomials for all the three input variables. These response surfaces are used by the optimization solver in order to predict output variables for the experimental runs not available in the DOE matrix. For optimization, Non-dominated Sorting Genetic Algorithm II (NSGA-II) has been utilized [31]. NSGA-II is a fast and elitist genetic algorithm for multi-response optimization. Elitism improves converges and avoids local optima and guides towards the real pareto optimal design points. There are no penalty parameters for constraints implementation. In fact, the method utilizes a modified dominance method to cater for constraint handling. Though other methods can also be utilized and compared with NSGA-II, the main goal of the study is to select and apply an efficient and robust optimization technique that can handle multiple objectives and constraint considering the population size. The optimization work and other statistical analysis are carried with the help of a general purpose optimization software modeFrontier® developed by Esteco [32]. The workflow involving all elements for the optimization problem is shown in Fig. 2. The optimization problem is set to minimize maximum tool-chip interface temperature and surface roughness on the machined surface with the consideration of constraints on cutting force and material removal rate. The optimization problem is illustrated in Table 2.

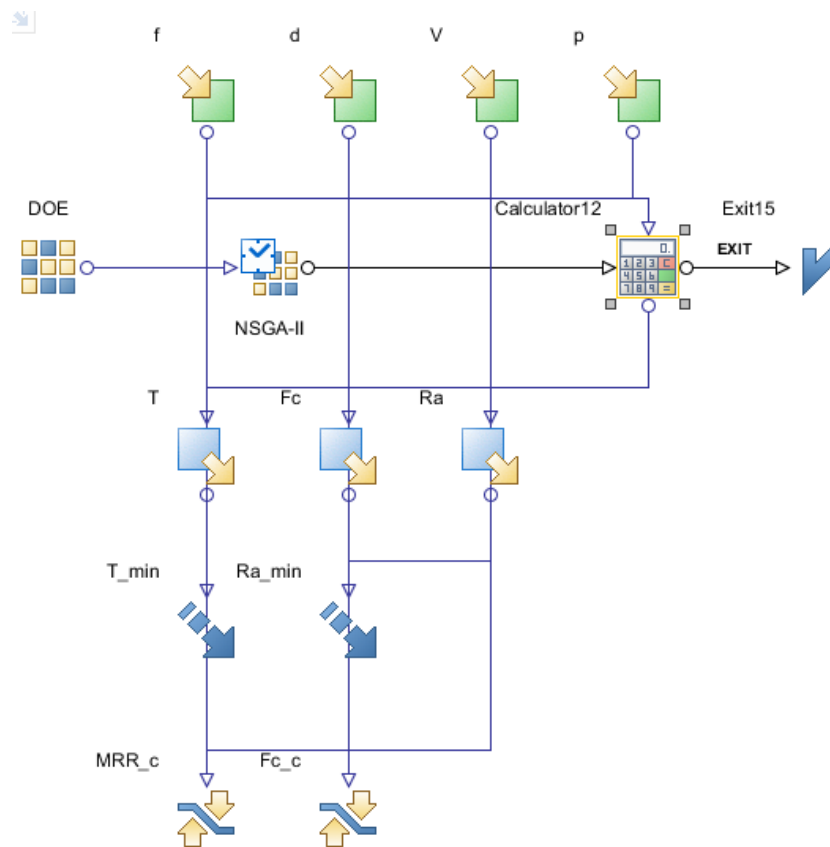


Fig. 2 Optimization workflow with all inputs, outputs, objectives and constraints

Table 2 Optimization problem’s objectives and constraints

Objectives	Minimize T Minimize Ra
Constraints	$MRR \geq 200 \text{ mm}^3/\text{s}$ $F_c \leq 800 \text{ N}$

3. Results and discussions

The CCD-25 design matrix with the resulting output variables, i.e. cutting force F_c , maximum tool chip interface temperature T , and surface roughness Ra are shown in Table 3.

Table 3 The CCD-25 design matrix with output variables

Id	p (μm)	v (m/min)	f (mm/rev)	d (mm)	F_c (N)	T ($^{\circ}\text{C}$)	R_a (μm)
0	5	60	0.1	1	287	323.5	2.12
1	5	60	0.2	1	522	393.2	1.62
2	5	60	0.1	2	841	435.2	1.91
3	5	60	0.2	2	1092	466.5	1.52
4	5	180	0.1	1	262	530.3	0.76
5	5	180	0.2	1	489	538.4	1.69
6	5	180	0.1	2	816	610	0.83
7	5	180	0.2	2	1066	698.1	1.69
8	5	120	0.15	1.5	766	543.3	1.18
9	10	60	0.15	1.5	857	407.7	2.53
10	10	180	0.15	1.5	841	638.2	1.53
11	10	120	0.15	1	431	492.9	1.56
12	10	120	0.15	2	1028	581.8	2.04
13	10	120	0.1	1.5	691	529	1.03
14	10	120	0.2	1.5	967	572.4	1.97
15	10	120	0.15	1.5	854	569.2	2.17
16	15	60	0.1	1	357	302.5	1.57
17	15	60	0.2	1	621	392.7	2.53
18	15	60	0.1	2	904	428.5	2.49
19	15	60	0.2	2	1214	537.2	3.07
20	15	180	0.1	1	339	560.1	1.33
21	15	180	0.2	1	598	608.2	2.4
22	15	180	0.1	2	887	732.4	1.9
23	15	180	0.2	2	1196	781.2	2.39
24	15	120	0.15	1.5	864	543.1	2.16

To investigate relationships between input and output variables the spearman's rank correlation coefficient is evaluated and depicted in Fig. 3. It is quite evident that maximum tool-chip interface temperature is highly dependent on cutting speed followed by depth of cut and feed rate. Particle size's effect on temperature is comparatively low but cannot be ignored as tool's crater wear is found to be highly sensitive with respect to maximum tool-chip interface temperature. Surface roughness is found to be severely affected by the size of particle, followed by cutting speed and feed rate. As discussed in the literature review, debonding of particles leave pits and cracks on the machined surface. With large reinforcement particles size of pits increases resulting in poor surface finish. The negative rank for cutting speed indicates reduction in surface roughness with higher cutting speed. This is a common observation in machining as this eliminates BUE resulting in low tool wear and good surface integrity. Finally, the coefficients for cutting force show that it is mainly controlled by depth of cut and feed rate. However the effect of particle size cannot be ignored and the cutting force is found to increase with particle size as observed by Sikder and Kishawy [20]. Cutting force is not much affected by the cutting speed as both strain hardening and thermal softening increases with the cutting speed. Hence both effects neutralize each other.

The interaction effects of the input variables on surface roughness of the machined surface are shown in Fig. 4. The highest interaction effect is provided by feed rate and particle size followed by depth of cut and particle size. With the increase in feed rate, the tool marks on the machined surface becomes more pronounced and hence results in poor surface finish. Similarly due to fracture and debonding of large reinforcement particles, the waviness on the machined surface increases. In contrast the interaction effect of cutting speed and particle size has negligible effect due to their inverse effects on R_a when examining individually.

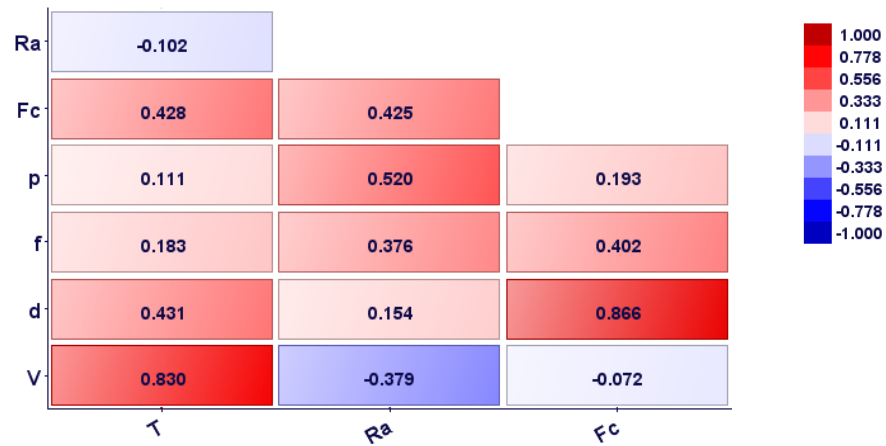


Fig. 3 Spearman's rank correlation matrix

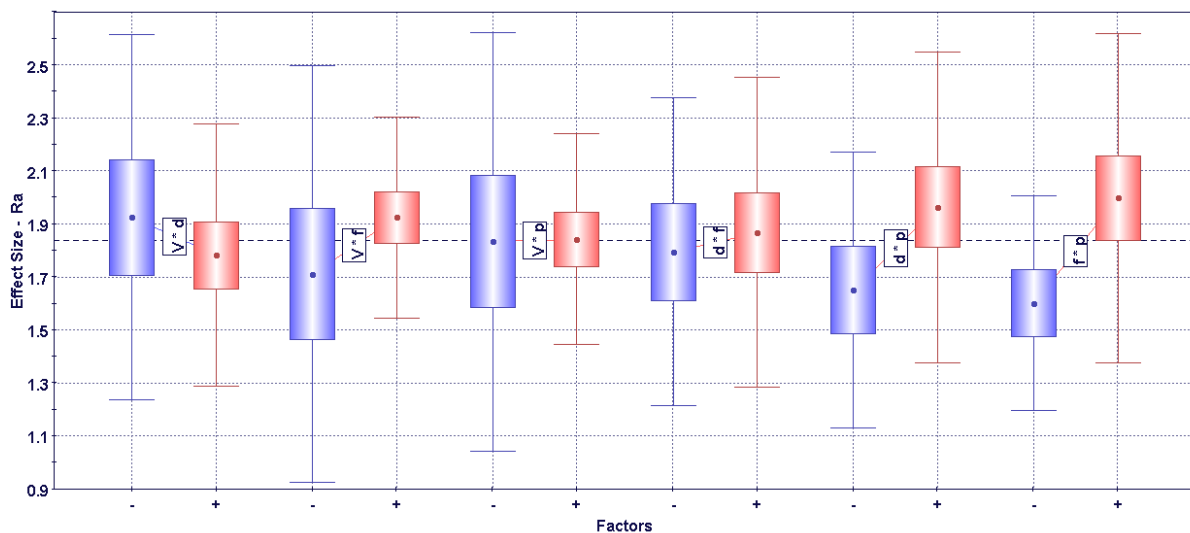


Fig. 4 Interaction effects of input variables on surface roughness

Fig. 5 highlights interaction effect of particle size and cutting parameters on maximum tool-chip interface temperature. The maximum tool-chip interface temperature is an important performance indicator in machining as it is strongly coupled with tool performance and surface integrity of the workpiece. It can be inferred from the figure that maximum interaction effect is provided by the combination of cutting speed and particle size followed by the combination of cutting speed and depth of cut. As it is well known fact in machining that temperatures are mostly affected by cutting speed due to increase in rate of plastic deformation. Hence temperature rises in the primary shear zone. With large reinforcement particles at higher cutting speed, the kinetic energy of the hard reinforcement particles increases [32]. This escalates abrasive wear on the cutting tool resulting in higher frictional stresses at the tool-chip interface and hence, temperature rises at the secondary shear zone.

The interaction effects of input variables on cutting force are depicted in Fig. 6. The interaction effect of depth of cut and feed rate is found to be highest followed by the interaction effect of depth of cut and particle size. With the increase in feed rate and depth of cut the chip cross sectional area or the chip load increases on the tool rake face which results in higher cutting and radial forces. In addition, the debonding energy required for the cutting action increases with big sized particles. Similarly, as discussed above tool wear accelerates with increase in particle size. Both phenomena give rise to higher cutting forces.

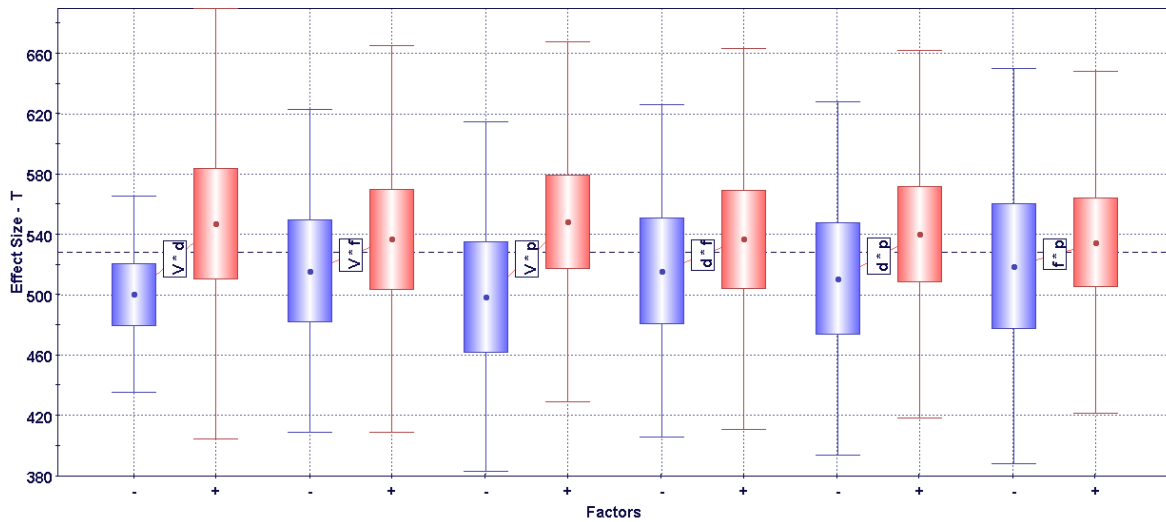


Fig. 5 Interaction effects of input variables on maximum tool-chip interface temperature

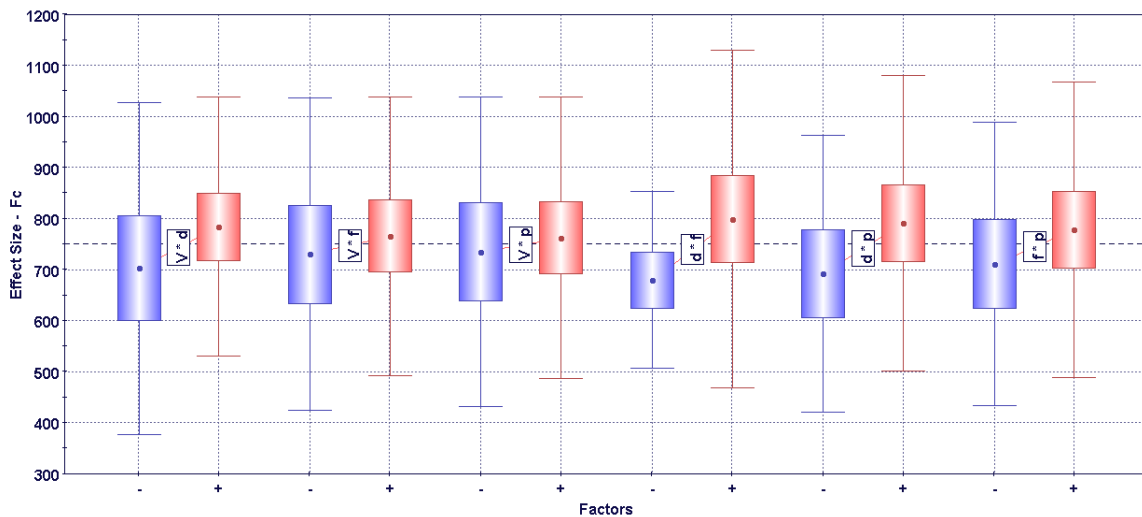


Fig. 6 Interaction effects of input variables on cutting force

The relationships between all the input and output variables can be visualized by principal component analysis as shown in Fig. 7. In this method multidimensional data is reduced to 2 or 3 dimensions of maximum variability called principal components. Here the data is plotted against to principal components $PC1$ and $PC2$ as depicted in Fig. 7. $PC1$ corresponds to 37 % variation in the data whereas $PC2$ corresponds to 28.6 % variation in data. The arrows show the dependency of the input or output variables on the variability of the principal components. Those are collinear with $PC1$ show 100 % dependency and orthogonal ones show null dependency. In this way the relationship between variables could be analyzed by observing their directions or their components in principal directions. It can be seen that F_c and d have large components along $PC1$. Similarly, R_a , v and T are strongly dependent on $PC2$. As d is found to be closer to F_c as compared to f and p , this suggests a strong correlation between F_c and d . In this way, R_a is found to be more dependent on p as compared to f and d . Also, T shows a strong dependency on v in comparison to d and f .

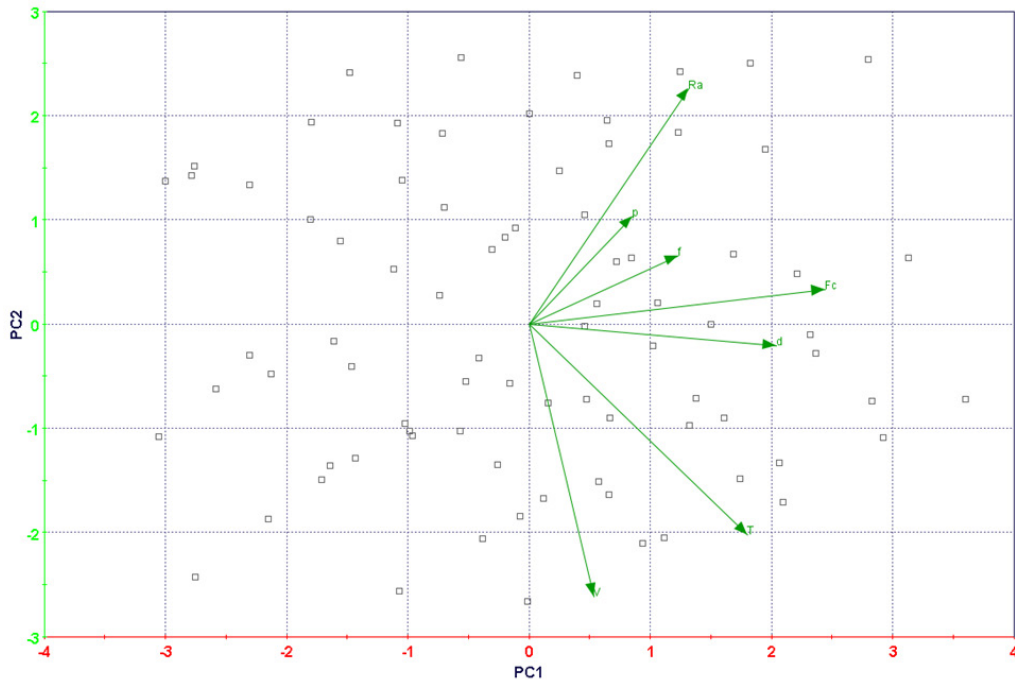


Fig. 7 Principal component analysis (PCA) for all input and output variables

The combined effect of feed rate and reinforcement particle size on surface roughness is shown in Fig. 8. The effect of reinforcement particle size on surface roughness at low feed rate is almost negligible and it increases gradually with feed rate. Similarly with small reinforcement the effect of feed rate on surface roughness is quite low. However, it is increasing with particle size and marked increase in surface roughness can be observed with particle size of 15 μm . Thus, maximum surface roughness is found to be with large reinforcement particles and higher feed rates. Feed marks parallel to the direction of the cutting velocity are more pronounced with increasing feed rate. Also, it has been observed that the reinforcement particles are partially or totally fractured or debonded from the machined surface during cutting. This aggravates further with large reinforcement particles, thus results in poor surface finish.

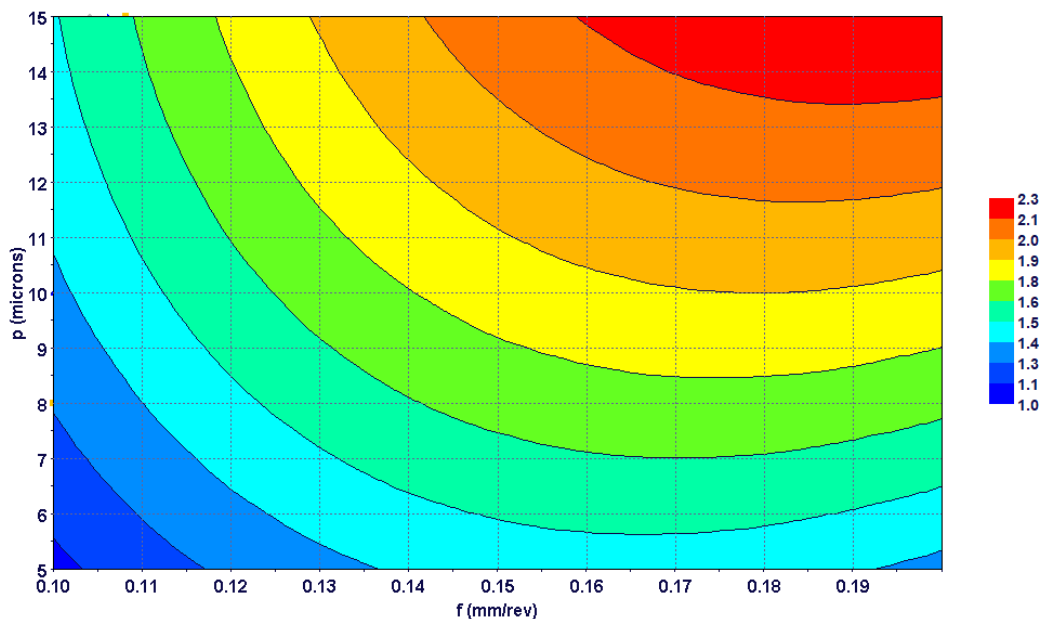


Fig. 8 Effects of feed rate and particle size on surface roughness

Fig. 9 shows the combined effect of depth of cut and reinforcement particle size on cutting force during MMC machining. The effect of reinforcement particle size on cutting force is marginally very low as compared to the depth of cut, though both factors contribute positively as shown in figure. Maximum cutting force is obtained at the top right corner, i.e. with large depth of cut and big reinforcement particles. As cutting force is proportional to the depth of cut due to increase in chip load, the debonding energy increases with particle size that leads to further escalation in cutting force as depicted in Fig. 9.

The combined effect of feed rate and reinforcement particle size on maximum tool-chip interface temperature is shown in Fig. 10. It is depicted that maximum tool-chip interface temperature increases with both feed rate and reinforcement particle size. Increase in particle size at low feed rate results in approximately 5.6 % rise in temperature. Whereas a jump of 8.8 % is observed at higher feed rate as shown in figure. The plastic energy consumed at the primary shear zone is proportional to the uncut chip thickness, i.e. feed rate. Thus, higher feed rates result in high heat dissipation which escalates temperature at the tool-chip interface. Similarly large reinforcement particles give rise to rapid tool wear which increases friction and heat generation at the secondary shear zone, thus resulting in higher tool-chip interface temperature.

Large reinforcement particles are also responsible for high abrasive wear on the tool flank face. This is due to increase in kinetic energy for the large particles which increases their rolling and sliding actions on the tool's surface. Effects of particle size on tool's flank wear can be analyzed in Fig. 11 (Scanning electrons photomicrographs) showing high abrasive wear on tool's flank face with 15 μm MMC. Welded aluminum can be seen on the tool's edges as it is a common problem when machining at dry conditions with higher speeds and low feed rates.

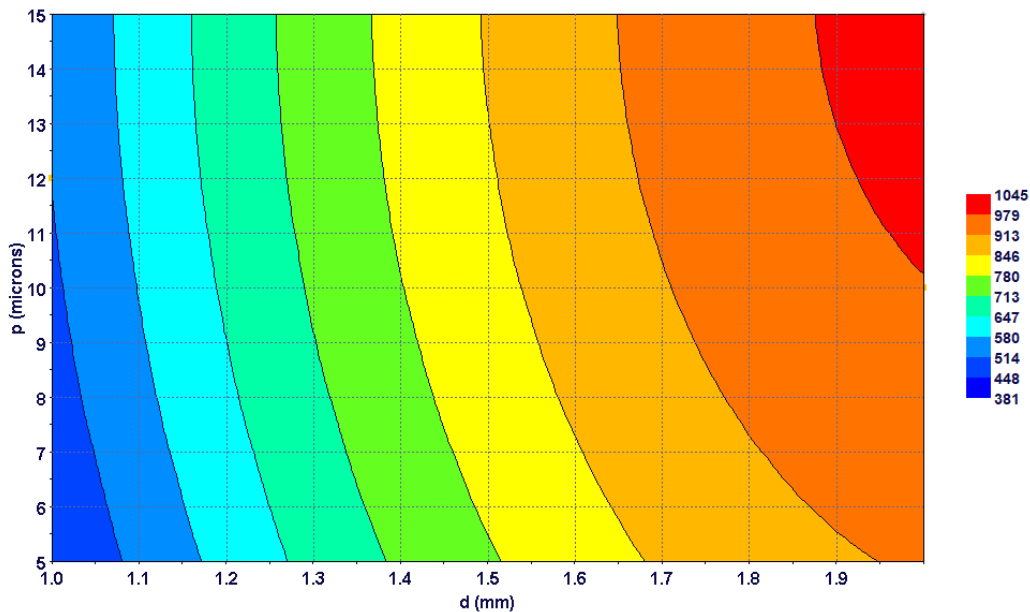


Fig. 9 Effects of depth of cut and particle size on cutting force

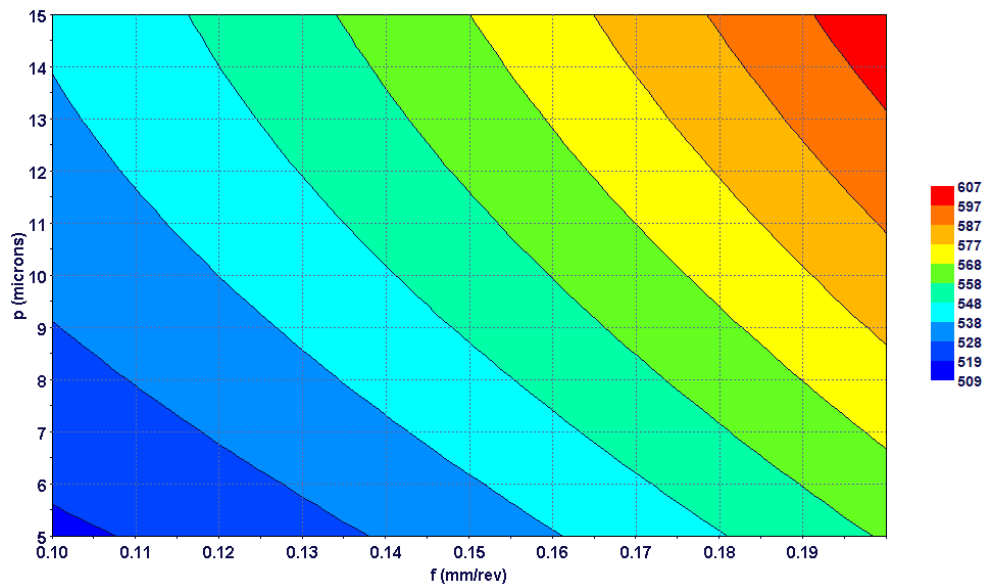


Fig. 10 Effects feed rate and particle size on maximum tool-chip interface temperature

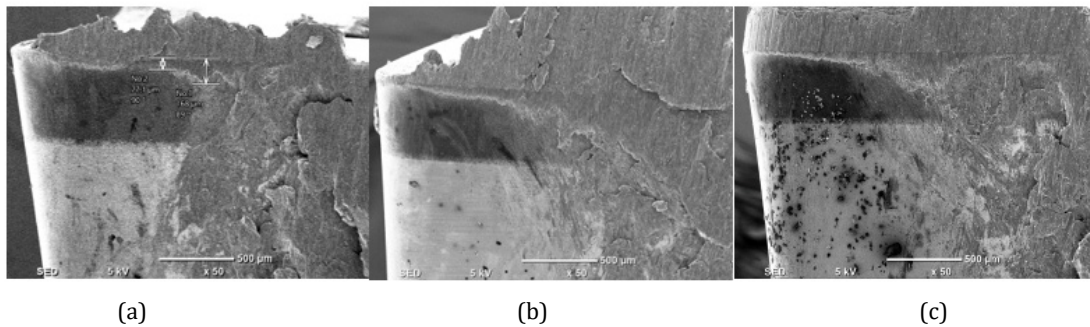


Fig. 11 Tool wear when machining MMC: (a) 5 μm , (b) 10 μm , (c) 15 μm
 $v = 180 \text{ m/min}$, $f = 0.10 \text{ mm/rev}$, $d = 1.0 \text{ mm}$, cutting time = 10 min

All the experimental runs obtained after optimization are shown in a 3D bubble chart as illustrated in Fig. 12. They are plotted against the two objectives, i.e. surface roughness R_a and maximum tool chip interface temperature T . The size of the bubble indicates reinforcement particle size. The design points with yellow colors are considered as unfeasible, i.e. violating at least one constraint in the optimization problem. The solid ones are said to be real as they are from the DOE matrix, whereas hollow bubbles represent virtual design point obtained via response surfaces. As the objective is to minimize both surface roughness and maximum tool-chip interface temperature, the optimal design points should be at the lower left corner of the diagram. A pareto-front can be drawn for each particle size to find out the optimal design points. Using the pareto front for 5 μm particle size three design points A5, B5 and C5 can be marked as candidates for optimal solution. Similarly, A10 and B10 can be marked as optimal for 10 μm particle size MMC. For 15 μm MMC, only one feasible design point is found in the optimal area and marked as A15 as shown in figure. The feasible design points marked with letter B are characterized by low feed rate, low depth of cut and moderate cutting speed. Similarly design point A5 have higher cutting speed and relatively higher MMR as compared to design points B5. The details of all the possible optimal solutions are shown in Table 4.

The relationship between four variables at a time can be visualized by a 4D bubble chart as shown in Fig. 13. Similar to the 3D bubble chart as explained above, the design points are plotted against the two objectives R_a and T . Cutting speed v is represented by color of the bubble whereas feed rate f is represented by the size of the bubble. It can be seen that higher temperatures are mostly contributed by high cutting speed and high interactions effects of the remaining input variables, i.e. $f \cdot d$, $f \cdot p$ and $d \cdot p$. Similarly poor surface finish is found to be associated with low cutting speed, moderate and high feed rate or depth of cut and large reinforcement particles.

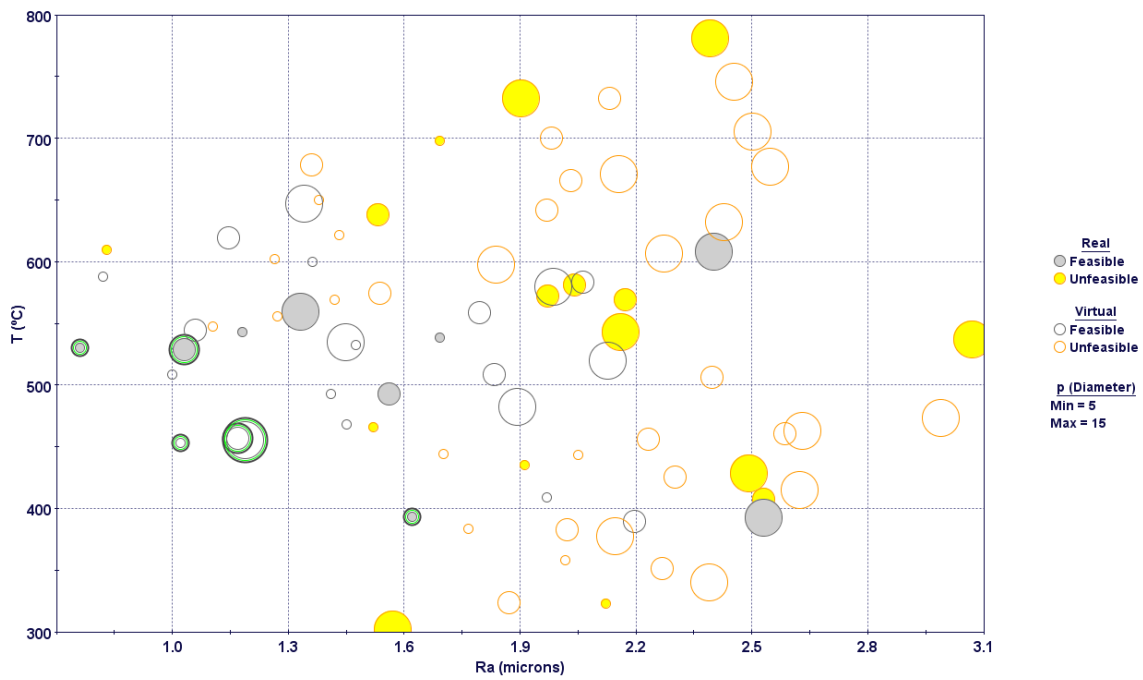


Fig. 12 3D bubble charts showing design points against the two objectives

Table 4 Details of optimal solutions

Id	p (μm)	v (m/min)	f (mm/rev)	d (mm)	F_c (N)	T ($^{\circ}\text{C}$)	Ra (μm)
A5	5	180	0.1	1.0	262	530.3	0.76
B5	5	120	0.1	1.0	262	453.5	1.02
C5	5	60	0.2	1.0	522	393.2	1.62
A10	10	120	0.1	1.5	691	529.0	1.03
B10	10	120	0.1	1.0	316	457.1	1.17
A15	15	120	0.1	1.0	329	455.8	1.19

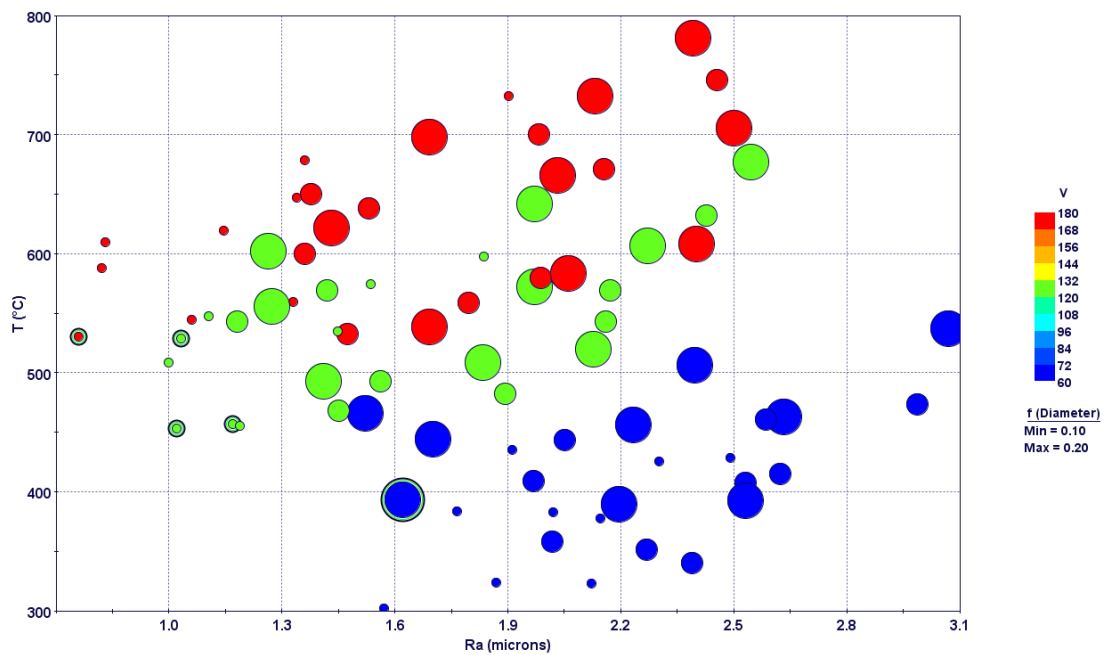


Fig. 13 4D bubble charts showing design points with four variables at a time

4. Conclusions

Machinability analysis and multi-objective optimization for particle reinforced aluminium based MMC have been performed during machining with PCD inserts. Effects of particle size on cutting force, surface roughness and maximum tool-chip interface temperature have been investigated with some qualitative analysis for the flank wear on PCD inserts. Following conclusions can be drawn:

- It has been noticed that particle size main and interaction effects contribute significantly towards the machinability of particle reinforced aluminium based MMCs.
- Surface roughness of the machined MMCs is found to be highly affected by the size of the reinforcement particles. Large reinforcement particles lead to poorer surface finish.
- As feed rates increase surface roughness more aggressively than other cutting parameters, the highest interaction effect is provided by the combination of particle size and feed rate.
- Large reinforcement particles are also found responsible for higher cutting temperatures. The interaction effect of cutting speed and particle size is found to be significant in controlling the maximum tool-chip interface temperature.
- Cutting force is found to be mainly influenced by depth of cut and feed rate. Particle size effect is found to be low for the volume fraction selected in the study. However, its effect cannot be ignored when other parameters are kept constant.
- The interaction effect of depth of cut and particle size is found significant for the cutting force. The debonding energy of the reinforced particles increases with size during machining. Hence results in escalation of the cutting force.
- Most of the optimal solutions are found to be with moderate cutting speed, low depth of cut and low feed rates.

Acknowledgement

This project was funded by the National Plan for Science, Technology, and Innovation (MAARIFAH), King Abdulaziz City for Science and Technology, Kingdom of Saudi Arabia, Award No. 13-ADV-971-02.

References

- [1] Ciftci, I., Turker, M., Seker, U. (2004). Evaluation of tool wear when machining SiC_p-reinforced Al-2014 alloy matrix composites, *Materials & Design*, Vol. 25, No. 3, 251-255, doi: [10.1016/j.matdes.2003.09.019](https://doi.org/10.1016/j.matdes.2003.09.019).
- [2] Kannan, S., Kishawy, H.A., Balazinski, M. (2005). Flank wear progression during machining metal matrix composites, *Journal of Manufacturing Science and Engineering*, Vol. 128, No. 3, 787-791, doi: [10.1115/1.2164508](https://doi.org/10.1115/1.2164508).
- [3] Ozben, T., Kilickap, E., Çakır, O. (2008). Investigation of mechanical and machinability properties of SiC particle reinforced Al-MMC, *Journal of Materials Processing Technology*, Vol. 198, No. 1-3, 220-225, doi: [10.1016/j.jmatprotec.2007.06.082](https://doi.org/10.1016/j.jmatprotec.2007.06.082).
- [4] Joshi, S.S., Ramakrishnan, N., Nagarwalla, H.E., Ramakrishnan, P. (1999). Wear of rotary carbide tools in machining of Al/SiC_p composites, *Wear*, Vol. 230, No. 2, 124-132, doi: [10.1016/S0043-1648\(99\)00092-7](https://doi.org/10.1016/S0043-1648(99)00092-7).
- [5] Rai, R.N., Datta, G.L., Chakraborty, M., Chattopadhyay, A.B. (2006). A study on the machinability behaviour of Al-TiC composite prepared by in situ technique, *Materials Science and Engineering: A*, Vol. 428, No. 1-2, 34-40, doi: [10.1016/j.msea.2005.11.040](https://doi.org/10.1016/j.msea.2005.11.040).
- [6] Karakaş, M.S., Acır, A., Übeyli, M., Ögel, B. (2006). Effect of cutting speed on tool performance in milling of B₄C_p reinforced aluminum metal matrix composites, *Journal of Materials Processing Technology*, Vol. 178, No. 1-3, 241-246, doi: [10.1016/j.jmatprotec.2006.04.005](https://doi.org/10.1016/j.jmatprotec.2006.04.005).
- [7] Cheung, C.F., Chan, K.C., To, S., Lee, W.B. (2002). Effect of reinforcement in ultra-precision machining of Al6061/SiC metal matrix composites, *Scripta Materialia*, Vol. 47, No. 2, 77-82, doi: [10.1016/S1359-6462\(02\)00097-0](https://doi.org/10.1016/S1359-6462(02)00097-0).
- [8] Chandrasekaran, H., Johansson, J.-O. (1996). On the behaviour of fibre/particle reinforced aluminium alloy matrix composites in milling and grinding, In: *Proceedings of 2nd International Conference on Machining of Advanced Materials*, Aachen, Germany, 463-478.
- [9] Li, X., Seah, W.K.H. (2001). Tool wear acceleration in relation to workpiece reinforcement percentage in cutting of metal matrix composites, *Wear*, Vol. 247, No. 2, 161-171, doi: [10.1016/S0043-1648\(00\)00524-X](https://doi.org/10.1016/S0043-1648(00)00524-X).
- [10] Lin, J.T., Bhattacharyya, D., Ferguson, W.G. (1998). Chip formation in the machining of SiC-particle-reinforced aluminium-matrix composites, *Composites Science and Technology*, Vol. 58, No. 2, 285-291, doi: [10.1016/S0266-3538\(97\)00126-7](https://doi.org/10.1016/S0266-3538(97)00126-7).

- [11] El-Gallab, M., Sklad, M. (1998). Machining of Al/SiC particulate metal matrix composites: Part II: Workpiece surface integrity, *Journal of Materials Processing Technology*, Vol. 83, No. 1-3, 277-285, doi: [10.1016/S0924-0136\(98\)00072-7](https://doi.org/10.1016/S0924-0136(98)00072-7).
- [12] Dandekar, C.R., Shin, Y.C. (2009). Multi-step 3-D finite element modeling of subsurface damage in machining particulate reinforced metal matrix composites, *Composites Part A: Applied Science and Manufacturing*, Vol. 40, No. 8, 1231-1239, doi: [10.1016/j.compositesa.2009.05.017](https://doi.org/10.1016/j.compositesa.2009.05.017).
- [13] Hung, N.P., Boey, F.Y.C., Khor, K.A., Phua, Y.S., Lee, H.F. (1996). Machinability of aluminum alloys reinforced with silicon carbide particulates, *Journal of Materials Processing Technology*, Vol. 56, No. 1-4, 966-977, doi: [10.1016/0924-0136\(95\)01908-1](https://doi.org/10.1016/0924-0136(95)01908-1).
- [14] Pramanik, A., Zhang, L.C., Arsecularatne, J.A. (2008). Machining of metal matrix composites: Effect of ceramic particles on residual stress, surface roughness and chip formation, *International Journal of Machine Tools and Manufacture*, Vol. 48, No. 15, 1613-1625, doi: [10.1016/j.ijmactools.2008.07.008](https://doi.org/10.1016/j.ijmactools.2008.07.008).
- [15] Iuliano, L., Settineri, L., Gatto, A. (1998). High-speed turning experiments on metal matrix composites, *Composites Part A: Applied Science and Manufacturing*, Vol. 29, No. 12, 1501-1509, doi: [10.1016/S1359-835X\(98\)00105-5](https://doi.org/10.1016/S1359-835X(98)00105-5).
- [16] Kannan, S., Kishawy, H.A. (2008). Tribological aspects of machining aluminium metal matrix composites, *Journal of Materials Processing Technology*, Vol. 198, No. 1-3, 399-406, doi: [10.1016/j.jmatprotec.2007.07.021](https://doi.org/10.1016/j.jmatprotec.2007.07.021).
- [17] Tosun, G., Muratoglu, M. (2004). The drilling of an Al/SiC_p metal-matrix composites. Part I: microstructure, *Composites Science and Technology*, Vol. 64, No. 2, 299-308, doi: [10.1016/S0266-3538\(03\)00290-2](https://doi.org/10.1016/S0266-3538(03)00290-2).
- [18] Olivas, E.R., Swadener, J.G., Shen, Y.-L. (2006). Nanoindentation measurement of surface residual stresses in particle-reinforced metal matrix composites, *Scripta Materialia*, Vol. 54, No. 2, 263-268, doi: [10.1016/j.scriptamat.2005.09.021](https://doi.org/10.1016/j.scriptamat.2005.09.021).
- [19] Morin, E., Masounave, J., Laufer, E.E. (1995). Effect of drill wear on cutting forces in the drilling of metal-matrix composites, *Wear*, Vol. 184, No. 1, 11-16, doi: [10.1016/0043-1648\(94\)06541-1](https://doi.org/10.1016/0043-1648(94)06541-1).
- [20] Sikder, S., Kishawy, H.A. (2012). Analytical model for force prediction when machining metal matrix composite, *International Journal of Mechanical Sciences*, Vol. 59, No. 1, 95-103, doi: [10.1016/j.ijmecsci.2012.03.010](https://doi.org/10.1016/j.ijmecsci.2012.03.010).
- [21] Sun, W., Duan, C., Yin, W. (2021). Modeling of force and temperature in cutting of particle reinforced metal matrix composites considering particle effects, *Journal of Materials Processing Technology*, Vol. 290, Article No. 116991, doi: [10.1016/j.jmatprotec.2020.116991](https://doi.org/10.1016/j.jmatprotec.2020.116991).
- [22] Klancnik, S., Hrelja, M., Balic, J., Brezocnik, M. (2016). Multi-objective optimization of the turning process using a Gravitational Search Algorithm (GSA) and NSGA-II approach, *Advances in Production Engineering & Management*, Vol. 11, No. 4, 366-376, doi: [10.14743/apem2016.4.234](https://doi.org/10.14743/apem2016.4.234).
- [23] Duplak, J., Hatala, M., Duplakova, D., Steranka, J. (2018). Comprehensive analysis and study of the machinability of a high strength aluminum alloy (EN AW-AlZn5.5MgCu) in the high-feed milling, *Advances in Production Engineering & Management*, Vol. 13, No. 4, 455-465, doi: [10.14743/apem2018.4.303](https://doi.org/10.14743/apem2018.4.303).
- [24] Xu, E.B., Yang, M.S., Li, Y., Gao, X.Q., Wang, Z.Y., Ren, L.J. (2021). A multi-objective selective maintenance optimization method for series-parallel systems using NSGA-III and NSGA-II evolutionary algorithms, *Advances in Production Engineering & Management*, Vol. 16, No. 3, 372-384, doi: [10.14743/apem2021.3.407](https://doi.org/10.14743/apem2021.3.407).
- [25] Aljinović, A., Bilić, B., Gjeldum, N., Mladineo, M. (2021). Prediction of surface roughness and power in turning process using response surface method and ANN, *Tehnički Vjesnik – Technical Gazette*, Vol. 28, No. 2, 456-464, doi: [10.17559/TV-20190522104029](https://doi.org/10.17559/TV-20190522104029).
- [26] Can, A., Üniüvar, A. (2017). Optimization of process parameters in drilling of SMC composites using Taguchi method, *Tehnički Vjesnik – Technical Gazette*, Vol. 24, No. 2, 435-442, doi: [10.17559/TV-20160103215256](https://doi.org/10.17559/TV-20160103215256).
- [27] Muthukrishnan, N., Davim, J.P. (2009). Optimization of machining parameters of Al/SiC-MMC with ANOVA and ANN analysis, *Journal of Materials Processing Technology*, Vol. 209, No. 1, 225-232, doi: [10.1016/j.jmatprotec.2008.01.041](https://doi.org/10.1016/j.jmatprotec.2008.01.041).
- [28] Seeman, M., Ganesan, G., Karthikeyan, R., Velayudham, A. (2010). Study on tool wear and surface roughness in machining of particulate aluminum metal matrix composite-response surface methodology approach, *International Journal of Advanced Manufacturing Technology*, Vol. 48, 613-624, doi: [10.1007/s00170-009-2297-z](https://doi.org/10.1007/s00170-009-2297-z).
- [29] Gaitonde, V.N., Karnik, S.R., Davim, J.P. (2009). Some studies in metal matrix composites machining using response surface methodology, *Journal of Reinforced Plastics and Composites*, Vol. 28, No. 20, 2445-2457, doi: [10.1177/0731684408092375](https://doi.org/10.1177/0731684408092375).
- [30] António, C.A.C., Davim, J.P. (2002). Optimal cutting conditions in turning of particulate metal matrix composites based on experiment and a genetic search model, *Composites Part A: Applied Science and Manufacturing*, Vol. 33, No. 2, 213-219, doi: [10.1016/S1359-835X\(01\)00094-X](https://doi.org/10.1016/S1359-835X(01)00094-X).
- [31] Deb, K., Pratap, A., Agarwal, S., Meyarivan, T. (2002). A fast and elitist multi-objective genetic algorithm: NSGA-II, *IEEE Transactions on Evolutionary Computation*, Vol. 6, No. 2, 182-197, doi: [10.1109/4235.996017](https://doi.org/10.1109/4235.996017).
- [32] modeFrontier, from <https://engineering.esteco.com/modefrontier>, accessed February 1, 2022.
- [33] Kannan, S., Kishawy, H.A., Deiab, I.M., Surappa, M.K. (2006). On the role of reinforcements on tool performance during cutting of metal matrix composites, *Journal of Manufacturing Processes*, Vol. 8, No. 2, 67-75, doi: [10.1016/S1526-6125\(07\)00006-0](https://doi.org/10.1016/S1526-6125(07)00006-0).

Supply chain coordination contract design: The case of farmer with capital constraints and behavioral preferences

Wang, Y.L.^{a,b}, Yin, X.M.^b, Zheng, X.Y.^b, Cai, J.R.^{a,b,*}, Fang, X.^c

^aResearch Center for Enterprise Management, Chongqing Technology and Business University, Chongqing, P.R. China

^bSchool of Business Administration, Chongqing Technology and Business University, Chongqing, P.R. China

^cSchool of Management Science and Engineering, Chongqing Technology and Business University, Chongqing, P.R. China

ABSTRACT

Coordination mechanism design is an important issue in agricultural supply chain. This study investigates agricultural supply chain coordination contracts in the presence of output uncertainty. It considers a two-level supply chain comprising a farmer and a retailer, where the farmer faces capital constraints and shows stockout-averse (SA), waste-averse (WA), or stockout- and waste-averse (SW) preferences. The results show that the retailer order, production input, and supply chain expected utility in the decentralized decision framework are lower than those realized under the centralized decision model; hence, the wholesale price contract cannot coordinate the supply chain. Nevertheless, the designed coordination contract mechanism coordinates the supply chain efficiently and realizes a flexible distribution of benefits between the farmer and the retailer. Furthermore, when the revenue-sharing coefficient meets specific conditions, both the farmer and the retailer achieve a win-win situation. Finally, we verify the coordination contract design using numerical simulations and analyze the effects of SA and WA preferences on decision-making and the supply chain expected utility. This study provides theoretical guidance for the coordination mechanism design of agricultural supply chain with capital constraints and behavioral preferences.

ARTICLE INFO

Keywords:

Supply chain;
Supply chain coordination;
Contract design;
Capital constraints;
Waste-averse preferences;
Stockout-averse preferences;
Behavioral preferences

*Corresponding author:

caijr@ctbu.edu.cn
(Cai, J.R.)

Article history:

Received 9 February 2022

Revised 8 August 2022

Accepted 13 August 2022



Content from this work may be used under the terms of the Creative Commons Attribution 4.0 International License (CC BY 4.0). Any further distribution of this work must maintain attribution to the author(s) and the title of the work, journal citation and DOI.

1. Introduction

Agricultural production is influenced by uncertain environmental factors (such as the weather, war crisis, human factors, etc.). Hence, farmers are cautious regarding the amount of production input needed. Before the production season, retailers pre-order agricultural products from farmers based on the predicted market demand. Then, farmers organize the agricultural production according to the retailer's orders. However, uncertainty in the output may lead to a mismatch between agricultural output and retailer orders. Overproduction or underproduction generates losses to farmers; hence, they may become waste-averse (WA) or stockout-averse (SA) [1]. In addition, some farmers have limited funds; due to the long production cycle of agricultural products, they may face capital constraints. Therefore, designing an effective supply chain coordination contract mechanism is crucial for managing farmers' financial constraints and behavioral preferences.

When faced with capital constraints, farmers may seek financing from formal financial institutions or other legal channels [2], such as trade credit and bank credit [3-6], advance payment discounts (advance payment) [7-9], and purchase order financing [9]. Therefore, research has begun focusing on financing services and financing strategies [10-13]. However, a financing strategy may benefit the individual but may not the entire supply chain. Hence, a coordination contract mechanism is needed for achieving coordination in the supply chain and a "win-win" situation for all participants. The literatures indicate that the wholesale price contract [14], option contract [15], revenue-sharing contract and buyback contract [16-19], output penalty contract and cost-sharing contract [19], general contract based on risk compensation [20], and two-way revenue-sharing contract [21] may coordinate the supply chain efficiently.

However, when addressing supply chain coordination problems in the presence of financial constraints, the above literatures assume that the output is determined, and participants are risk neutral. Therefore, this study's original contribution lies in the following three aspects:

- The output is assumed to be randomly determined owing to the uncertainty in the agricultural production.
- Agricultural products may be in excess or insufficient; hence, we consider that the farmer may have behavioral preferences: stockout- and waste-averse (SW), WA, or SA preferences.
- We design a supply chain coordination contract mechanism and analyze the influence of behavioral preferences on participants' decision-making and the expected utility of the supply chain.

The remainder of this paper is organized as follows. Section 2 describes the problems, assumptions, and notations. Section 3 presents the model. Section 4 introduces the design of the coordinated contract mechanism. Section 5 provides a numerical simulation analysis, and Section 6 provides our concluding remarks.

2. Model's setup, assumptions, and notations

2.1 Problem description

We address the case of a two-level supply chain comprising a financially constrained farmer and a retailer. According to the predicted market demand, the retailer books agricultural products Q to the farmer in advance. The farmer determines its production input q according to the retailer's order. Since the output of agricultural products is randomly determined, the farmer's output is uq , where u is the random output factor, with $u \in (0, B)$ [22]. In the sales season, the farmer sells agricultural products to the retailer at the unit wholesale price w agreed in the contract. The retailer resells them to consumers at unit price p , satisfying consumer demand. This mechanism is shown in Fig. 1.

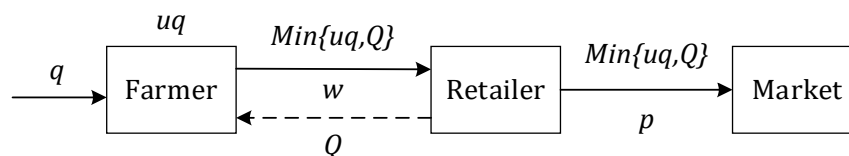


Fig. 1 Schematic diagram of the study structure

2.2 Model assumptions

Assumption 1: The market price of agricultural products p is inversely proportional to the number of agricultural products $\min\{Q, uq\}$, namely, $p = A - \min\{Q, uq\}$ [23]. A is the highest price that consumers are willing to pay, and $\min\{Q, uq\}$ is the transaction volume of the farmer and retailer, namely:

$$\min\{Q, uq\} = \begin{cases} Q, & Q \leq uq \\ uq, & Q > uq \end{cases}$$

Assumption 2: The farmer has SA preferences when the production cannot meet the retailer's order, as $Q > uq$. In the case of insufficient production, an additional penalty $\lambda(Q - uq)^+$ is generated; λ is the shortage aversion coefficient. On the other hand, the farmer has WA preferences when the output is in excess, namely, $Q < uq$. In this case, an additional penalty $\beta(uq - Q)^+$ is imposed on the excess production; β is the WA coefficient. Similar assumptions are made in the literature [1].

Assumption 3: Since farmers may have different behavioral preferences, we consider situations where the farmer has WA, SA and SW preferences.

Assumption 4: We consider a scenario in which a farmer faces capital constraints, namely, $cq > T$. To supplement the insufficient funds $(cq - T)^+$, the farmer obtains financing from a third party. The financing rate is r , and the financing cost is $r(cq - T)^+$; c is the unit production cost of agricultural products, and T indicates the funds held by the farmer.

Assumption 5: $p > w > c$.

Assumption 6: The farmer and the retailer have symmetrical information.

2.3 Notations

All the symbols used in this article are summarized in Table 1.

Table 1 The listing of notations

Symbols	Descriptions	Symbols	Descriptions
c	Unit production cost	λ	Stockout-aversion coefficient
w	Wholesale price	β	Waste-aversion coefficient
p	Retail price	C (top right corner)	Centralized decision model
q	Production input	B (top right corner)	Decentralized decision model
Q	Order quantity	H (top right corner)	Coordination contract mechanism
u	Random output factor	SA	Stockout-aversion
$F(u)$	Cumulative distribution function of u	WA	Waste-aversion
$f(u)$	Probability density function of u	SW	Stockout- and waste-averse
T	Funds held by the farmer	r	Financing rate
Π_R^j	Retailer's expected profit	*	Optimal value
Π_i^j	Supply chain expected utility	U_F^j	The farmer's expected utility

$i \in \{SW, SA, WA\}, j \in \{C, B, H\}$

3. Alternative models

3.1 Centralized decision model

In the centralized decision-making framework, the farmer and retailer belong to the same collective, and both aim to maximize the expected utility of the entire supply chain. When the farmer has SW preferences, the utility of the supply chain is:

$$\pi_{SW}^C = (A - \min\{Q, uq\}) \min\{Q, uq\} - \lambda(Q - uq)^+ - \beta(uq - Q)^+ - cq - r(cq - T)^+ \quad (1)$$

In Eq. 1, $(A - \min\{Q, uq\}) \min\{Q, uq\}$ represents sales revenue, and $\lambda(Q - uq)^+$ and $\beta(uq - Q)^+$ are punishments for production shortage and overproduction, respectively; cq is the production cost, and $r(cq - T)^+$ is the financing interest cost.

According to Eq. 1, the expected utility of the supply chain is:

$$\Pi_{SW}^C = (A + \lambda + \beta) \left[Q - q \int_0^{\frac{Q}{q}} F(u) du \right] + 2q^2 \int_0^{\frac{Q}{q}} F(u) du - Q^2 - \lambda Q - [\beta\mu + (1 + r)c]q + rT \quad (2)$$

The first partial derivatives of Π_{SW}^C with respect to Q and q are, respectively:

$$\frac{\partial \Pi_{SW}^C}{\partial Q} = (A + \lambda + \beta) \left[1 - F\left(\frac{Q}{q}\right) \right] - 2 \left[Q - q \left(\frac{Q}{q}\right) \right] - \lambda = 0 \quad (3)$$

$$\frac{\partial \Pi_{SW}^C}{\partial q} = (4q - A - \lambda - \beta) \int_0^{\frac{Q}{q}} F(u) du + \frac{(A + \lambda + \beta - 2q)Q}{q} F\left(\frac{Q}{q}\right) - \beta\mu - (1 + r)c = 0 \quad (4)$$

By solving Eqs. 3 and 4 simultaneously, we obtain the optimal order quantity Q_{SW}^{C*} and production input quantity q_{SW}^{C*} in the centralized decision framework:

$$\begin{cases} (A + \lambda + \beta) \left[1 - F\left(\frac{Q_{SW}^{C*}}{q_{SW}^{C*}}\right) \right] - 2 \left[Q_{SW}^{C*} - q_{SW}^{C*} F\left(\frac{Q_{SW}^{C*}}{q_{SW}^{C*}}\right) \right] - \lambda = 0 \\ (4q_{SW}^{C*} - A - \lambda - \beta) \int_0^{\frac{Q_{SW}^{C*}}{q_{SW}^{C*}}} F(u) du + \frac{(A + \lambda + \beta - 2q_{SW}^{C*})Q_{SW}^{C*}}{q_{SW}^{C*}} F\left(\frac{Q_{SW}^{C*}}{q_{SW}^{C*}}\right) - \beta\mu - (1 + r)c = 0 \end{cases} \quad (5)$$

We then obtain the optimal expected utility of the supply chain, as follows:

$$\begin{aligned} \Pi_{SW}^{C*} = & (A + \lambda + \beta) \left[Q_{SW}^{C*} - q_{SW}^{C*} \int_0^{\frac{Q_{SW}^{C*}}{q_{SW}^{C*}}} F(u) du \right] + 2q_{SW}^{C*} \int_0^{\frac{Q_{SW}^{C*}}{q_{SW}^{C*}}} F(u) du - Q_{SW}^{C*}{}^2 - \lambda Q_{SW}^{C*} \\ & - [\beta\mu + (1 + r)c]q_{SW}^{C*} + rT \end{aligned} \quad (6)$$

If the farmer only has SA preferences, $\lambda > 0$, and $\beta = 0$; however, if the farmer only has WA preferences, $\lambda = 0$ and $\beta > 0$. The optimal decision and the supply chain expected utility in the centralized decision framework may be obtained in the same way; this analysis step is, therefore, omitted.

3.2 Decentralized decision model

In the decentralized decision framework, the farmer determines the amount of production input q to maximize their expected utility, and the retailer determines the order quantity Q to maximize their expected profit. We assume that the farmer and retailer have the same decisional power; hence, they play a Cournot game. When the farmer has SW preferences, the expected utility of the farmer and the expected profit of the retailer are as follows:

$$U_F^B = E[w \min\{Q, uq\} - \lambda(Q - uq)^+ - \beta(uq - Q)^+ - cq - r(cq - T)] = (w + \beta)Q - \beta\mu q - q(w + \lambda + \beta) \int_0^{\frac{Q}{q}} F(u) du - cq - r(cq - T) \quad (7)$$

$$\Pi_R^B = E[(A - \min\{Q, uq\}) \min\{Q, uq\} - w \min\{Q, uq\}] = (A - w)Q - Q^2 - (A - w)q \int_0^{\frac{Q}{q}} F(u) du + 2q^2 \int_0^{\frac{Q}{q}} F(u) du \quad (8)$$

The first and second partial derivatives of U_F^B with respect to q are:

$$\frac{\partial U_F^B}{\partial q} = (w + \lambda + \beta) \left(\frac{Q}{q} F\left(\frac{Q}{q}\right) - \int_0^{\frac{Q}{q}} F(u) du \right) - \beta\mu - (1 + r)c \quad (9)$$

$$\frac{\partial^2 U_F^B}{\partial q^2} = -\frac{Q^2}{q^3} (w + \lambda + \beta) f\left(\frac{Q}{q}\right) < 0 \quad (10)$$

The first and second partial derivatives of Π_R^B with respect to Q are:

$$\frac{\partial \Pi_R^B}{\partial Q} = (A - w) \left[1 - F\left(\frac{Q}{q}\right) \right] - 2 \left[Q - qF\left(\frac{Q}{q}\right) \right] \quad (11)$$

$$\frac{\partial^2 \Pi_R^B}{\partial Q^2} = -\frac{(A - w)}{q} f\left(\frac{Q}{q}\right) - 2 \left[1 - f\left(\frac{Q}{q}\right) \right] < 0 \quad (12)$$

Since $\frac{\partial^2 U_F^B}{\partial q^2} < 0$, and $\frac{\partial^2 \Pi_R^B}{\partial Q^2} < 0$, when $\frac{\partial U_F^B}{\partial q} = 0$, and $\frac{\partial \Pi_R^B}{\partial Q} = 0$, in the decentralized decision framework, the optimal order quantity Q_{SW}^{B*} and production input quantity q_{SW}^{B*} may be obtained as follows:

$$\begin{cases} (A - w) \left[1 - F\left(\frac{Q_{SW}^{B*}}{q_{SW}^{B*}}\right) \right] - 2 \left[Q_{SW}^{B*} - q_{SW}^{B*} F\left(\frac{Q_{SW}^{B*}}{q_{SW}^{B*}}\right) \right] = 0 \\ (w + \lambda + \beta) \left(\frac{Q_{SW}^{B*}}{q_{SW}^{B*}} F\left(\frac{Q_{SW}^{B*}}{q_{SW}^{B*}}\right) - \int_0^{\frac{Q_{SW}^{B*}}{q_{SW}^{B*}}} F(u) du \right) - \beta\mu - (1 + r)c = 0 \end{cases} \quad (13)$$

Under decentralized decisions, the optimal expected utility of the farmer, the optimal expected profit of the retailer, and the optimal expected utility of the supply chain are, respectively:

$$U_F^{B*} = (w + \beta)Q_{SW}^{B*} - \beta\mu q_{SW}^{B*} - q_{SW}^{B*}(w + \lambda + \beta) \int_0^{\frac{Q_{SW}^{B*}}{q_{SW}^{B*}}} F(u) du - c(1 + r)q_{SW}^{B*} + rT \quad (14)$$

$$\Pi_R^{B*} = (A - w)Q_{SW}^{B*} - Q_{SW}^{B*2} - (A - w)q_{SW}^{B*} \int_0^{\frac{Q_{SW}^{B*}}{q_{SW}^{B*}}} F(u) du + 2q_{SW}^{B*2} \int_0^{\frac{Q_{SW}^{B*}}{q_{SW}^{B*}}} F(u) du \quad (15)$$

$$\begin{aligned} \Pi_{SW}^{B*} = & (A + \lambda + \beta) \left[Q_{SW}^{B*} - q_{SW}^{B*} \int_0^{\frac{Q_{SW}^{B*}}{q_{SW}^{B*}}} F(u) du \right] + 2q_{SW}^{B*2} \int_0^{\frac{Q_{SW}^{B*}}{q_{SW}^{B*}}} F(u) du - Q_{SW}^{B*2} - \lambda Q_{SW}^{B*} \\ & - [\beta\mu + (1 + r)c]q_{SW}^{B*} + rT \end{aligned} \quad (16)$$

If the farmer only has SA preferences, $\lambda > 0$, and $\beta = 0$; however, if the farmer has WA preferences, $\lambda = 0$, and $\beta > 0$. The optimal decision behavior and supply chain expected utility under decentralized decision may be obtained using the above procedure; hence, this analysis step is omitted.

The above model analysis suggests the following proposition:

Proposition 1: Supply chain coordination under decentralized decisions cannot be realized.

Proof: Under decentralized decisions, if the supply chain realizes coordination, $Q_{SW}^{B*} = Q_{SW}^{C*}$, and $q_{SW}^{B*} = q_{SW}^{C*}$. A comparison between Eqs. 5 and 13 indicates that supply chain coordination may only be realized when both $w = -\beta$ and $w = -(\lambda + \beta)$ are satisfied, which contradicts $w > 0$; thus, supply chain coordination cannot be realized in this context.

4. Coordination contract mechanism design

In the decentralized decision-making framework, both the farmer and the retailer aim to maximize their interests, ignoring the best interests of the entire supply chain. Therefore, to maximize the expected utility of the supply chain, an effective coordination contract mechanism is needed, so that both the farmer and the retailer are willing to participate in the mechanism.

Inspired by the literature [16, 19, 24], we design a coordination contract mechanism in which the retailer gives Φ ($0 \leq \Phi \leq 1$) times of their sales income to farmers, and the retailer shares Δ ($0 \leq \Delta \leq 1$) times of the shortage punishment, θ ($0 \leq \theta \leq 1$) times the overproduction punishment, and k ($0 \leq k \leq 1$) times the financing interest costs of the farmer.

Under the proposed coordination contract mechanism, if the farmer has SA and WA preferences, the farmer's expected utility and the retailer's expected profit are, respectively:

$$U_F^H = E[w \min\{Q, uq\} + \Phi(A - \min\{Q, uq\}) \min\{Q, uq\} - (1 - \Delta)\lambda(Q - uq)^+ - (1 - \theta)\beta(uq - Q)^+ - cq - (1 - k)r(cq - T)] \quad (17)$$

$$\Pi_R^H = E[(1 - \Phi)(A - \min\{Q, uq\}) \min\{Q, uq\} - w \min\{Q, uq\} - kr(cq - T) - \Delta\lambda(Q - uq)^+ - \theta\beta(uq - Q)^+] \quad (18)$$

Hence, we obtain the following proposition:

Proposition 2:

- Under the proposed coordination contract mechanism, if the coefficient satisfies Eq. 19, the supply chain may be coordinated;
- the farmer's behavioral preferences do not affect the coordination contract mechanism design:

$$\begin{cases} \theta = 1 + \frac{w}{\beta} - \Phi \\ \Delta = 1 - \Phi \\ k = \frac{w\mu + (1 - \Phi)(1 + r)}{rc} \end{cases} \quad (19)$$

Proof: Substituting Eq. 19 into Eqs. 17 and 18, we obtain:

$$\begin{cases} U_F^H = \Phi \Pi_{SW}^c + \frac{(w\mu + \Phi c - c)T}{c} \\ \Pi_R^H = (1 - \Phi) \Pi_{SW}^c - \frac{(w\mu + \Phi c - c)T}{c} \end{cases} \quad (20)$$

Eq. 20 indicates that $\frac{\partial U_F^H}{\partial q} = \frac{\partial \Pi_{SW}^c}{\partial q} = 0$ and $\frac{\partial \Pi_R^H}{\partial q} = \frac{\partial \Pi_{SW}^c}{\partial q} = 0$ are both valid; hence, $Q_{SW}^{H*} = Q_{SW}^{C*}$ and $q_{SW}^{H*} = q_{SW}^{C*}$, achieving coordination in the supply chain. In addition, Eq. 19 also shows that θ, Δ, k are independent of λ and β ; in other words, the behavioral preferences of the farmer do not affect the design of the coordination contract mechanism.

The premise that the farmer and retailer are willing to participate in the coordination contract mechanism is a Pareto improvement of benefits; we, thus, derive Eq. 21, and we obtain the following proposition:

$$\begin{cases} U_F^H = \Phi \Pi_{SW}^c + \frac{(w\mu + \Phi c - c)T}{c} > U_F^{B*} \\ \Pi_R^H = (1 - \Phi) \Pi_{SW}^c - \frac{(w\mu + \Phi c - c)T}{c} > \Pi_R^{B*} \end{cases} \quad (21)$$

Proposition 3: If the revenue-sharing coefficient Φ meets $\Phi_1 \leq \Phi \leq \Phi_2$, both the farmer and retailer are willing to participate in the coordination contract mechanism, and both achieve a win-win situation, where Φ_1 and Φ_2 satisfy Eqs. 22 and 23:

$$\begin{cases} \Phi_1 = \frac{c(T + U_F^{B*}) - Tw\mu}{c(T + \Pi_{SW}^{C*})} \\ \Phi_2 = \frac{c(T + \Pi_{SW}^{C*} - \Pi_R^{B*}) - Tw\mu}{c(T + \Pi_{SW}^{C*})} \end{cases} \quad (22)$$

$$\Phi_1 - \Phi_2 = \frac{U_F^{B*} + \Pi_R^{B*} - \Pi_{SW}^{C*}}{T + \Pi_{SW}^{C*}} < 0 \quad (23)$$

5. Results and discussion: numerical simulation

We resort to the numerical simulation method to further verify the correctness of the above conclusions and obtain more robust findings. Without loss of generality, the parameters are set as follows: $A = 100, r = 0.1, B = 2, c = 1, w = 3, T = 5, \lambda = \beta = 1$.

Table 2 Calculation results under different models

Model	Φ	Q	q	Farmer's expected utility	Retailer's expected profit	Expected utility of supply chain
Centralized decision model	—	86.36	300.95	—	—	3729.91
Decentralized decision model	—	26.34	34.17	26.43	1655.64	1682.07
Coordination contract mechanism	0	86.36	300.95	10	3719.91	3729.91
	0.1	86.36	300.95	383.49	3346.42	3729.91
	0.2	86.36	300.95	756.98	2972.93	3729.91
	0.4	86.36	300.95	1503.96	2225.95	3729.91
	0.8	86.36	300.95	2997.93	731.98	3729.91

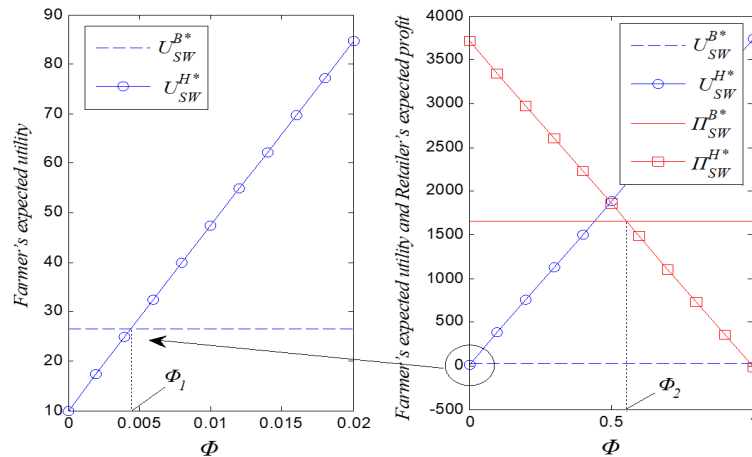


Fig. 2 Effect of Φ on farmer's expected utility and retailer's expected profit

5.1 Analysis of the coordination contract

Table 2 and Fig. 2 indicate that the optimal order, production input, and expected supply chain utility in the decentralized decision framework are lower than those realized under the centralized decision model. The designed coordination contract mechanism coordinates the supply chain and realizes a flexible distribution of benefits between the farmer and retailer. In particular, when the revenue-sharing coefficient is $0.0044 < \Phi < 0.5527$, the farmer and retailer achieve a win-win situation.

5.2 Sensitivity analysis

To further understand the impact of farmers' behavior preferences on decision-making and the expected utility of the supply chain, we separately analyze three different scenarios.

Analysis of SW preferences

If the farmer has SW preferences, namely, $\lambda > 0$ and $\beta > 0$, we obtain the findings reported in Figs. 3-7. The following five conclusions may be drawn:

- In the centralized decision model, the optimal order, production input, and expected supply chain utility are greater than those realized under the decentralized decision model.
- The optimal order in the centralized and decentralized decision models decreases with WA coefficient β .
- The optimal order in the centralized decision model decreases with SA coefficient λ , while the retailer order in the decentralized decision framework increases with SA coefficient λ .
- Whether in a centralized or decentralized decision model, the optimal production input is an increasing and decreasing function of SA coefficient λ and WA coefficient β , respectively.
- Whether in a centralized decision model or decentralized decision model, the expected utility of the supply chain is an increasing and decreasing function of SA coefficient λ and WA coefficient β , respectively.

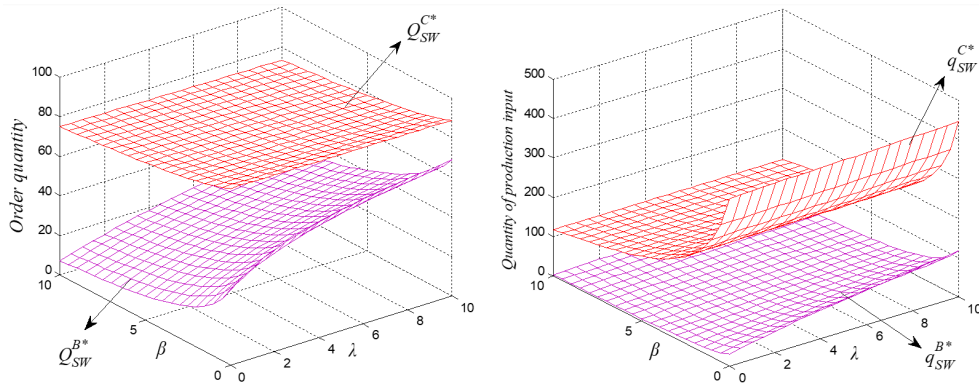


Fig. 3 Effect of λ and β on retailer's order and farmer's production input

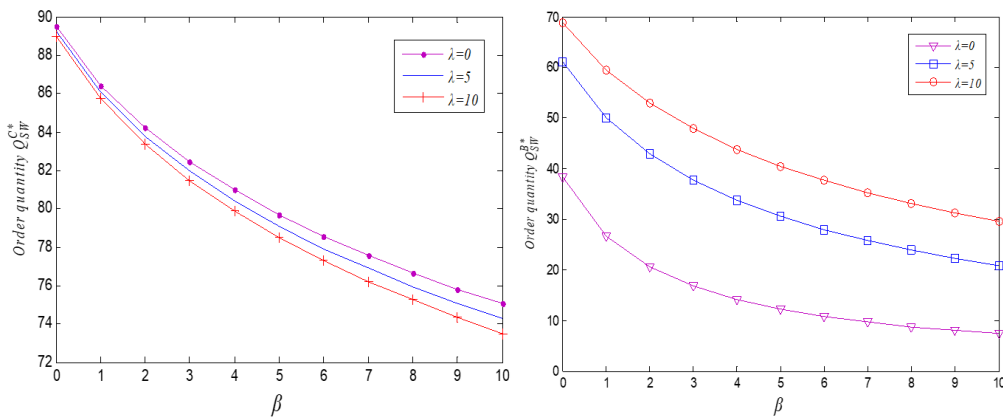


Fig. 4 Effect of λ and β on retailer's order under centralized decision and decentralized decision model

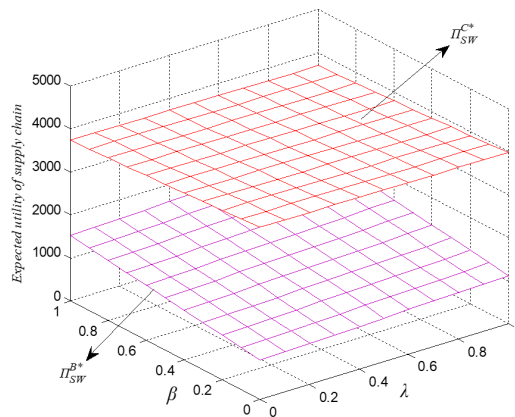


Fig. 5 Effect of λ and β on expected utility of supply chain under centralized decision and decentralized decision model

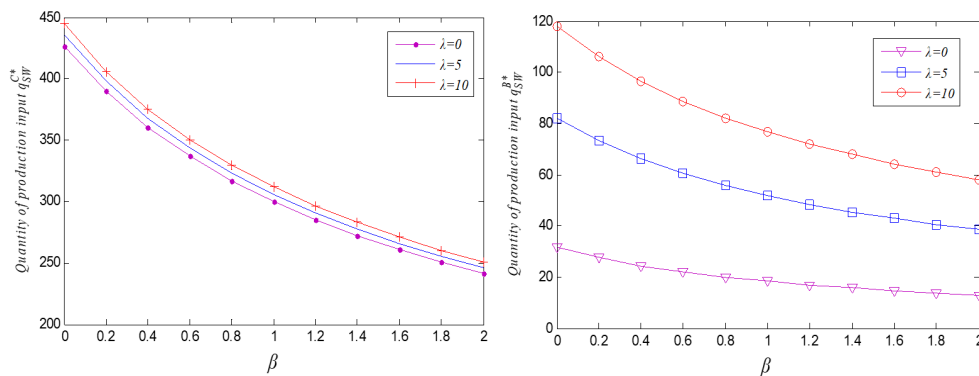


Fig. 6 Effect of λ and β on farmer's production input under centralized decision and decentralized decision model

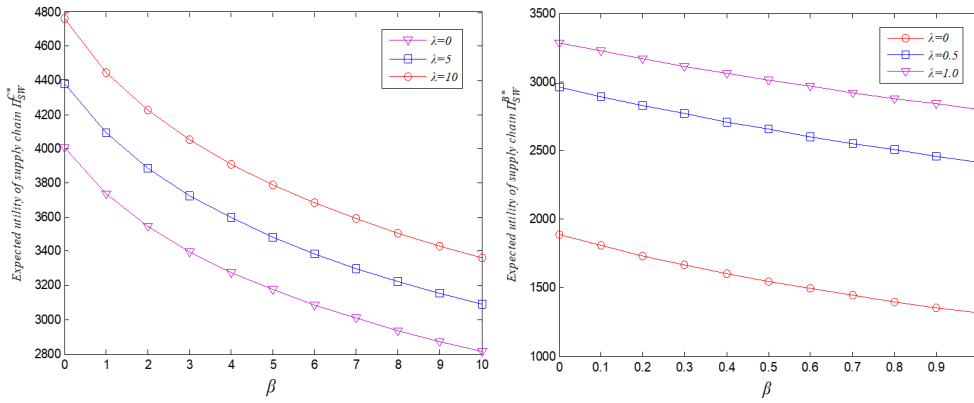


Fig. 7 Effect of λ and β on expected utility of supply chain under centralized decision and decentralized decision model

Analysis of SA preferences

If the farmer has SA preferences, that is, $\lambda > 0$ and $\beta = 0$, we obtain the results reported in Figs. 8 and 9. Therefore, the following three conclusions can be drawn:

- The optimal order (expected supply chain utility) in the decentralized decision model increases with SA coefficient λ , while the opposite result is obtained in the centralized decision model.
- Whether in the centralized or decentralized decision model, the optimal production input increases with the SA coefficient λ .
- The optimal order, production input, and expected supply chain utility in the centralized decision model are greater than those realized under the decentralized decision framework.

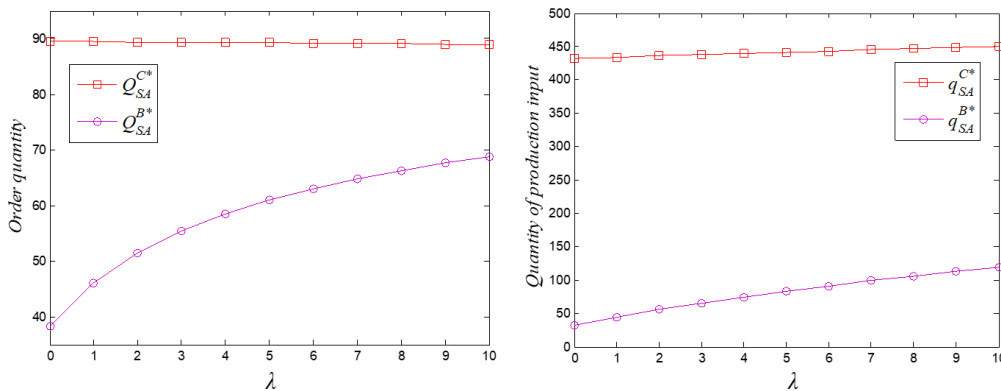


Fig. 8 Effect of λ on retailer's order and farmer's production input under centralized decision and decentralized decision model

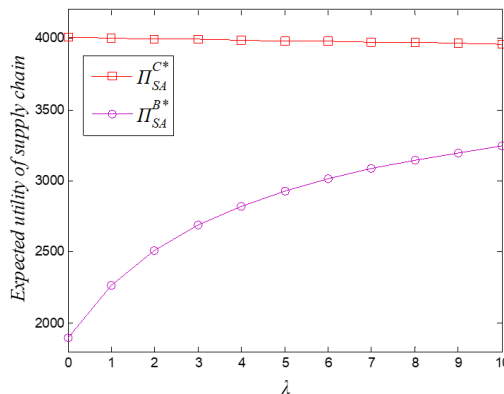


Fig. 9 Effect of λ on expected utility of supply chain under centralized decision and decentralized decision model

Analysis of WA preferences

If the farmer only WA preferences, that is, $\lambda = 0$ and $\beta > 0$, we obtain the results reported in Figs. 10 and 11. The following two conclusions can be drawn:

- Whether in the centralized or decentralized decision model, the optimal order, production input, and expected utility of supply chain decrease with WA coefficient β .
- The optimal order, production input, and expected supply chain utility in the centralized decision model are greater than those realized under the decentralized decision framework.

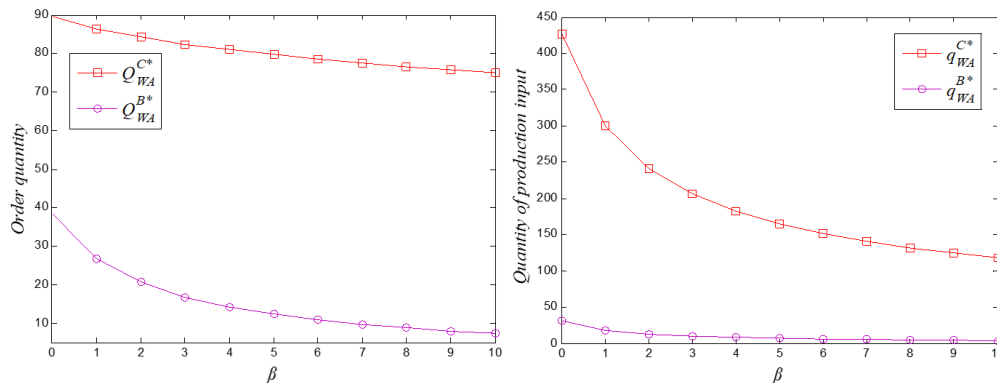


Fig. 10 Effect of β on retailer's order and farmer's production input under centralized decision and decentralized decision model

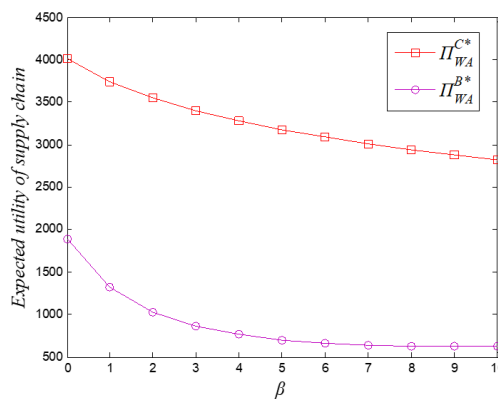


Fig. 11 Effect of β on expected utility of supply chain under centralized decision and decentralized decision model

6. Conclusion

This study examines the design of supply chain coordination contracts in the presence of farmer's capital constraints and behavioral preferences. It addresses the case of a two-level supply chain comprising a farmer and a retailer. The farmer faces capital constraints, seeks financing from a third party, and may have SW, SA, and WA preferences. The full-text analysis suggests the following conclusions:

- In the decentralized decision framework, the supply chain cannot be coordinated. However, the designed coordination contract mechanism coordinates the supply chain efficiently and realizes a flexible distribution of benefits between the farmer and the retailer. Furthermore, when the revenue-sharing coefficient is small ($0.0044 < \Phi < 0.5527$), both the farmer and the retailer achieve a win-win situation.
- In the centralized decision model, regardless of the behavioral preferences of the farmer, the optimal order, production input, and expected utility of the supply chain are always greater than those realized under the decentralized decision scheme.

- The farmer's optimal production input is always an increasing and decreasing function of SA coefficient λ and WA coefficient β , respectively.
- In the centralized decision model, the retailer's optimal order always decreases with SA coefficient λ , but the opposite result holds in the decentralized decision framework. The retailer's order always decreases with WA coefficient β .
- The expected utility of the supply chain is always an increasing and decreasing function of SA coefficient λ and WA coefficient β , respectively.

The coordination method proposed in this paper can be applied in other industries with similar backgrounds. However, it may not be applicable in the cases of random demand, supply chain competition, and information asymmetry. These are all future research directions.

Acknowledgement

This work was supported by the Humanities and Social Science Research Project of Ministry of Education of China (20XJC630007), the Humanities and Social Sciences Foundation of Chongqing Education Commission of China (22SKJD103), the Project of Science and Technology Research Program of Chongqing Education Commission of China (KJQN202000809), and the Open Project of Research Center for Enterprise Management of Chongqing Technology and Business University in 2021.

References

- [1] Jian, M., Wang, Y.L. (2018). Decision-making strategies in supply chain management with a waste-averse and stockout-averse manufacturer, *Advances in Production Engineering & Management*, Vol. 13, No. 3, 345-357, doi: [10.14743/apem2018.3.295](https://doi.org/10.14743/apem2018.3.295).
- [2] Vanaga, R., Sloka, B. (2020). Financial and capital market commission financing: Aspects and challenges, *Journal of Logistics, Informatics and Service Science*, Vol. 7, No. 1, 17-30, doi: [10.33168/LISS.2020.0102](https://doi.org/10.33168/LISS.2020.0102).
- [3] Yu, X., Wan, Z. (2020). Supply chain financing model under a new mechanism of bankruptcy guarantee, *Economic Computation and Economic Cybernetics Studies and Research*, Vol. 54, No. 2, 243-262, doi: [10.24818/18423264/54.2.20.15](https://doi.org/10.24818/18423264/54.2.20.15).
- [4] Hua, S., Liu, J., Cheng, T.C.E., Zhai, X. (2019). Financing and ordering strategies for a supply chain under the option contract, *International Journal of Production Economics*, Vol. 208, 100-121, doi: [10.1016/j.ijpe.2018.10.008](https://doi.org/10.1016/j.ijpe.2018.10.008).
- [5] Kouvelis, P., Zhao, W. (2018). Who should finance the supply chain? Impact of credit ratings on supply chain decisions, *Manufacturing & Service Operations Management*, Vol. 20, No. 1, 19-35, doi: [10.1287/msom.2017.0669](https://doi.org/10.1287/msom.2017.0669).
- [6] Jin, W., Zhang, Q., Luo, J. (2019). Non-collaborative and collaborative financing in a bilateral supply chain with capital constraints, *Omega*, Vol. 88, 210-222, doi: [10.1016/j.omega.2018.04.001](https://doi.org/10.1016/j.omega.2018.04.001).
- [7] Shah, N., Shah, P., Patel, M. (2020). Inventory policies with retailer's flexible payment time and customer's fixed credit time for manufacturer-retailer supply chain, *Economic Computation and Economic Cybernetics Studies and Research*, Vol. 54, No. 4, 87-102, doi: [10.24818/18423264/54.4.20.06](https://doi.org/10.24818/18423264/54.4.20.06).
- [8] Jin, W., Luo, J., Zhang, Q. (2018). Optimal ordering and financing decisions under advance selling and delayed payment for a capital-constrained supply chain, *Journal of the Operational Research Society*, Vol. 69, No. 12, 1978-1993, doi: [10.1080/01605682.2017.1415643](https://doi.org/10.1080/01605682.2017.1415643).
- [9] Zhao, L., Huchzermeier, A. (2019). Managing supplier financial distress with advance payment discount and purchase order financing, *Omega*, Vol. 88, 77-90, doi: [10.1016/j.omega.2018.10.019](https://doi.org/10.1016/j.omega.2018.10.019).
- [10] Zhang, L.-L., Kim, H.-K. (2020). The influence of financial service characteristics on use intention through customer satisfaction with mobile fintech, *Journal of System and Management Sciences*, Vol. 10, No. 2, 82-94, doi: [10.33168/JSMS.2020.0206](https://doi.org/10.33168/JSMS.2020.0206).
- [11] Hua, S., Liu, J., Cheng, T.C.E., Zhai, X. (2019). Financing and ordering strategies for a supply chain under the option contract, *International Journal of Production Economics*, Vol. 208, 100-121, doi: [10.1016/j.ijpe.2018.10.008](https://doi.org/10.1016/j.ijpe.2018.10.008).
- [12] Jin, W., Luo, J., Zhang, Q. (2018). Optimal ordering and financing decisions under advance selling and delayed payment for a capital-constrained supply chain, *Journal of the Operational Research Society*, Vol. 69, No. 12, 1978-1993, doi: [10.1080/01605682.2017.1415643](https://doi.org/10.1080/01605682.2017.1415643).
- [13] Yang, H., Zhuo, W., Shao, L. (2017). Equilibrium evolution in a two-echelon supply chain with financially constrained retailers: The impact of equity financing, *International Journal of Production Economics*, Vol. 185, 139-149, doi: [10.1016/j.ijpe.2016.12.027](https://doi.org/10.1016/j.ijpe.2016.12.027).
- [14] Yan, N., Sun, B. (2013). Coordinating loan strategies for supply chain financing with limited credit, *OR Spectrum*, Vol. 35, 1039-1058, doi: [10.1007/s00291-013-0329-4](https://doi.org/10.1007/s00291-013-0329-4).
- [15] Liang, Y., Qiao, P.L., Luo, Z.Y., Song, L.L. (2016). Constrained stochastic joint replenishment problem with option contracts in spare parts remanufacturing supply chain, *International Journal of Simulation Modelling*, Vol. 15, No. 3, 553-565, doi: [10.2507/IJSIMM15\(3\)C013](https://doi.org/10.2507/IJSIMM15(3)C013).

- [16] Moon, I., Feng, X.-H., Ryu, K.-Y. (2015). Channel coordination for multi-stage supply chains with revenue-sharing contracts under budget constraints, *International Journal of Production Research*, Vol. 53, No. 16, 4819-4836, doi: [10.1080/00207543.2014.993438](https://doi.org/10.1080/00207543.2014.993438).
- [17] Feng, X., Moon, I., Ryu, K. (2015). Supply chain coordination under budget constraints, *Computers & Industrial Engineering*, Vol. 88, 487-500, doi: [10.1016/j.cie.2015.08.005](https://doi.org/10.1016/j.cie.2015.08.005).
- [18] Shi, J., Du, Q., Lin, F., Li, Y., Bai, L., Fung, R.Y.K., Lai, K.K. (2020). Coordinating the supply chain finance system with buyback contract: A capital-constrained newsvendor problem, *Computers & Industrial Engineering*, Vol. 146, Article No.106587, doi: [10.1016/j.cie.2020.106587](https://doi.org/10.1016/j.cie.2020.106587).
- [19] Xu, X., Cheng, X., Sun, Y. (2015). Coordination contracts for outsourcing supply chain with financial constraint, *International Journal of Production Economics*, Vol. 162, 134-142, doi: [10.1016/j.ijpe.2015.01.016](https://doi.org/10.1016/j.ijpe.2015.01.016).
- [20] Phan, D.A., Vo, T.L.H., Lai, A.N. (2019). Supply chain coordination under trade credit and retailer effort, *International Journal of Production Research*, Vol. 57, No. 9, 2642-2655, doi: [10.1080/00207543.2019.1567950](https://doi.org/10.1080/00207543.2019.1567950).
- [21] Zhao, L., Li, L., Song, Y., Li, C., Wu, Y. (2018). Research on pricing and coordination strategy of a sustainable green supply chain with a capital-constrained retailer, *Complexity*, Vol. 2018, Article ID 6845970, doi: [10.1155/2018/6845970](https://doi.org/10.1155/2018/6845970).
- [22] Fang, X., Wang, R., Yuan, F.J., Gong, Y., Cai, J.R., Wang, Y.L. (2020). Modelling and simulation of fresh-product supply chain considering random circulation losses, *International Journal of Simulation Modelling*, Vol. 19, No. 1, 169-177, doi: [10.2507/IJSIMM19-1-CO5](https://doi.org/10.2507/IJSIMM19-1-CO5).
- [23] Cachon, G.P., Lariviere, M.A. (2005). Supply chain coordination with revenue-sharing contracts: Strengths and limitations, *Management Science*, Vol. 51, No. 1, 30-44, doi: [10.1287/mnsc.1040.0215](https://doi.org/10.1287/mnsc.1040.0215).
- [24] Yan, K., Cui, L., Zhang, H., Liu, S., Zuo, M. (2022). Supply chain information coordination based on blockchain technology: A comparative study with the traditional approach, *Advances in Production Engineering & Management*, Vol. 17, No. 1, 5-15, doi: [10.14743/apem2022.1.417](https://doi.org/10.14743/apem2022.1.417).

Numerical study of racking resistance of timber-made double-skin façade elements

Kozem Šilih, E.^a, Premrov, M.^{a,*}

^aUniversity of Maribor, Faculty of Civil Engineering, Transportation Engineering and Architecture, Maribor, Slovenia

ABSTRACT

The use of a double-skin façade (DSF) is a quite new approach in the building renovation process, complementing conventional renovation strategies. A double-skin façade is an envelope wall construction that consists of two transparent surfaces separated by a cavity and can essentially improve the thermal and acoustic resistance of the building envelope. The main double-skin wall components are usually composed of a hardened external single glazing pane and a double or triple thermal insulating internal glass pane, which are connected to the frame structure. Recently, many studies have analysed the thermal and acoustic performance of DSF elements, but almost none in terms of structural behaviour, especially in terms of determining the racking resistance of such wall elements. Moreover, with a view to reduce the global warming potential, an eco-friendly timber frame instead of a commonly used steel, aluminium or plastic frame is studied in this analysis. However, structurally combining timber and glass to develop an appropriate load-bearing structural element is a very complex process involving a combination of two materials with different material properties, where the type of bonding can be selected as a crucial parameter affecting the racking resistance range. Since the costs of experiments performed on such full-scale DSF elements are very high and such experiments are time-consuming, it is crucial to develop special mathematical models for analysing the influence of the most important parameters. Therefore, the main goal of this paper is to develop the finite element mathematical model of the studied DSF structural elements with a highly ecological solution by using a timber frame. In the second step, the developed model is further implemented in the numerical analysis of racking stiffness and followed by a comprehensive parametric numerical study on different parameters influencing the horizontal load-bearing capacity of such DSF timber elements. The obtained results indicate that the new approach of the developed load-bearing prefabricated timber DSF elements can essentially improve racking resistance and stiffness compared with the widely studied timber-glass single-skin wall elements and can thus be fully recommended especially in the structural renovation process of old buildings.

ARTICLE INFO

Keywords:

Timber;
Glass;
Double-skin façades;
Racking resistance;
Mathematical modelling;
Numerical analysis;
Finite Elements Methods (FEM)

*Corresponding author:

miroslav.premrov@um.si
(Premrov, M.)

Article history:

Received 2 December 2021
Revised 12 August 2022
Accepted 19 August 2022



Content from this work may be used under the terms of the Creative Commons Attribution 4.0 International License (CC BY 4.0). Any further distribution of this work must maintain attribution to the author(s) and the title of the work, journal citation and DOI.

1. Introduction

In the past few decades, climate change has prompted experts to urgently call for action to remove the causes and alleviate the consequences of climate change that affect the environment, and design new buildings primarily with eco-friendly materials. Therefore, the field of energy consumption is witnessing a global trend aiming is to reduce greenhouse gas emissions. Consequently, a new strategy to design buildings with net zero emissions has to be adopted not only for new buildings, but also for building renovations, [1-4]. Since most energy flux is transmitted through

building envelope elements [5, 6], the façade upgrade with essential thermal transmittance decrease can be one of the most effective interventions to improve the thermal efficiency and aesthetic appeal of existing buildings, [4]. In this sense, the advantages of wood and glass have led to the development of so-called timber-glass wall elements, in which single-layer outer and thermal insulated inner double or triple glass panes are rigidly connected to the timber frame with a bonding line, [2, 4, 5]. Since such DSF wall elements were developed primarily as external building envelope elements to enhance solar heat gains of the building during the heating period, they are usually placed on the south façade of the building. The proper orientation of such transparent façade elements enables the utilisation of solar energy for heating and internal illumination of the building [7-11]. However, the consequent asymmetrical layout of such transparent wall elements can result in many problems with the horizontal stability of the whole building. Their asymmetrical position can cause a serious plan irregularity problem, which may result in high torsional actions caused by heavy seismic or wind loads. The contribution of such DSF wall elements to the horizontal carrying capacity of the whole building is usually neglected and has not yet been implemented in any standards.

Moreover, the hybrid steel-glass or timber-glass shear wall system can be created to realise hybrid structures with glass as the main stabilising material. Various hybrid glass component solutions are currently being studied mainly in the academic context, [12]. It was demonstrated in many experimental [4, 13, 14] and numerical studies [15] performed on full-scale single-skin timber-glass load-bearing structural wall elements that triple insulating glazing can foster higher racking resistance and stiffness compared with the single glazing. However, the racking stiffness is not in a range with the timber-framed walls with conventional sheathing boards, such as OSB or fibre-plaster boards, which are prescribed as primary load-bearing racking structural wall elements by standards. However, the goal of the design process in the comprehensive renovation of old buildings is also to improve the thermal standard of the building, and the sound and the racking resistance of the load-bearing envelope façade elements. Consequently, the concept of a specially developed double-skin façade (DSF) elements with an additional single-layer outer glass pane added to the commonly used triple insulating inner glazing rigidly connected to the frame structure and separated by a cavity could be a good and useful approach [16-18]. Such a solution can significantly decrease the U-value of such transparent envelope wall elements, and considerably improve the sound resistance.

Combining timber and glass to make an appropriate load-bearing structural element is a very complex process involving a combination of two materials with different material properties, where the bonding line can be selected as a crucial parameter affecting the obtained load-bearing range [14], [19-26]. It is important to point out that only the load-bearing approach to the racking resistance and stiffness of such timber DSF elements will be numerically analysed in this paper as an upgrade of the already published experimental [5, 13, 14] and numerical studies [15, 27] performed on full-scale timber-glass wall elements with double and triple insulating glazing, but only as a concept of single-skin façade (SSF) elements. No energy, LCA or acoustic studies on DSF elements will be performed in the presented study.

It should be emphasised that, to our knowledge, no special studies have been published on the topic of the racking resistance of timber DSF elements. In the broader study in [18], the structural approach to timber DSF was studied, but only for the vertical load impact. In [28], an experimental analysis of the racking resistance and stiffness of DSF elements was carried out as part of a national research project in two different specially selected full-scale test groups, varying the type of the adhesive connecting the insulating inner glazing to the timber frame (polyurethane and epoxy). As mentioned before, there are many different parameters which significantly influence the racking resistance and stiffness of timber DSF elements, especially the type of the bonding line between the glass pane and the timber frame, and the type and thickness of the glass panes. Since the experiments performed on such full-scale DSF elements are very time-consuming and also the costs are very high, it is crucial to develop special mathematical models to be used to further analyse the influence of most important parameters, and based on these results, to develop special simple final expressions for the racking resistance and stiffness of timber DSF elements to be suitable also for simple engineering usage.

The main goal of this paper is to develop a mathematical model of the studied DSF structural elements with a highly ecological solution by using a timber frame (Section 3). The developed finite element model can be further implemented in the numerical analysis of the racking resistance and stiffness (Section 4) and followed by a broad parametric numerical study on different most important parameters influencing the horizontal load-bearing capacity of such DSF elements (Section 5). Special attention will be dedicated to analysing the influence of the thickness t_a and width w_a of the bonding line, and to the thickness of the outer and inner glass pane t_{gl} . Based on our previous experimental [5, 13, 14, 25, 26] and numerical studies [15, 27] performed on conventional single-skin façade (SSF) timber-glass wall elements and certain findings from experiments performed on full-scale DSF elements [28], only a case with a polyurethane adhesive in the bonding line between the insulating inner glazing and the timber frame is analysed in the presented study as the most appropriate and useful bonding solution (Fig. 1).

2. Main concept of timber double-skin façade wall elements

According to [16], a double-skin façade (DSF) is an envelope element that consists of two transparent surfaces rigidly connected to a frame structure and separated by a cavity. The cavity is used as an air channel and can be naturally or mechanically ventilated and thus it does not offer an occupied space. The width of the cavity can vary from 200 mm to over 2 m. Solar shading systems can be integrated within the cavity. The insulating glazing is usually placed on the inner side of the façade, while the extra skin is placed on the external side to significantly improve the thermal transmittance of the wall element, and reduce the energy demand for heating and cooling, [16-18], [29-36]. The extra skin can reduce the cooling demand in the summer and the heating demand in the winter. Therefore, DSF elements have been proposed as a promising passive building technology to enhance energy efficiency and improve indoor thermal comfort [29]. Simulations of different envelope scenarios in the Mediterranean climate [36] have shown that the most energy efficient DSF is with low-e glazing as the outer layer. It is concluded in [17], however, that in warm climates its benefit in the summer is limited. Such a constructed envelope element also demonstrates better sound resistance [29, 35, 36] in comparison with widely used SSF elements and can, therefore, be suitable for high noise areas where a high level of sound insulation is required.

The exterior glazing primarily consists of a hardened fully tempered single glass pane, while ordinary annealed glass is usually used for the thermal-insulating double or triple inner glazing, as schematically presented in Fig. 1. As already mentioned in the introduction, the type of the bonding line with appropriate adhesive dimensions was the crucial parameter in the structural behaviour of experimentally and numerically tested single-skin timber-glass façade wall elements against a horizontal load impact. Additionally, there are many types of adhesives to choose from, such as silicone, polyurethane, acrylate and epoxy.

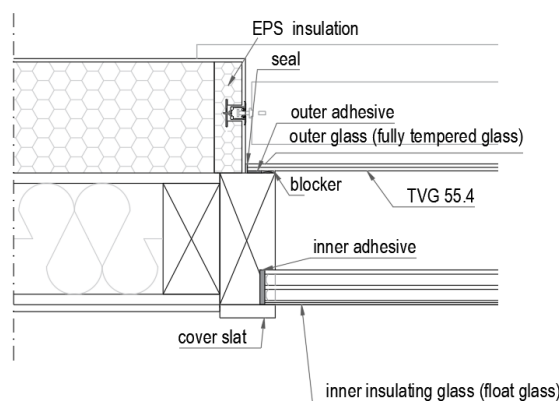


Fig. 1 Schematic presentation of the timber DSF wall element

Basically, the frame structure can be made from many different materials, but it is mainly made from steel, aluminium or plastic. However, it is obvious that, for this specific building typology to reach the zero energy building targets, mere energy conserving strategies involving decreases with the DSF elements energy demand for heating and cooling, as stated before, may not suffice. Renewable energy sources and technologies should be additionally considered as integral parts of the building envelope and systems [36]. Bearing in mind an eco-friendly renovation approach, the use of low-carbon materials is one of the most acknowledged mitigation measures for carbon reduction. Therefore, the adoption of timber as the main structural frame material can potentially further reduce the overall embodied carbon, [18]. Consequently, our study will be limited to the approach using a timber frame.

In addition to the foreseen structural advantages, the DSF envelope wall elements improve the sound insulation of the building envelope and energy performance compared to the regular triple insulating glazing [17, 18, 29], therefore they can be very useful especially in renovation process by upgrading of the envelope elements in old existing buildings, compared also with commonly used single-skin façade solutions. However, most studies do not address structural solutions, instead focusing on energy analyses and their impact on the LCA results or analyses of sound insulation compared to single façade transparent elements. The numerical study in [18] is focused only on the vertical load impact but does not address the racking resistance range as the most important if the DSF elements are considered bracing structural elements.

3. Mathematical model

The studied DSF wall elements have been modelled and analysed by using the commercial finite element model (FEM) computer program SAP2000 Nonlinear v 17.0.0 [37]. In the computational model, the timber frame was modelled by 1-dimensional (beam) finite elements, while the glazing boards were modelled using 2-dimensional finite elements of the “composite shell” type, which allows for the simulating of composite multi-layer shells. The adhesive bonding of the glazing panes to the timber frame was modelled using linear link elements (springs). As in reality, the adhesive bonding is provided continuously over the whole perimeter, the stiffness properties of the discrete spring elements were defined based on the spacing of the springs in the computational model using Eqs. 1 and 2 [15, 22, 38] for the inner and outer type of the bonding line:

$$K_1 = \frac{E_a \cdot A_a}{t_a} = \frac{E_a \cdot (w_a \cdot l_a)}{t_a} \quad (1)$$

$$K_2 = \frac{G_a \cdot A_a}{t_a} = \frac{G_a \cdot (w_a \cdot l_a)}{t_a} \quad (2)$$

where K_1 is the stiffness in the direction normal to the connected plane, while K_2 is the shear stiffness in the two perpendicular directions in the connected plane. E_a and G_a are the modulus of elasticity and the shear modulus of the adhesive material, respectively, t_a and w_a designate the thickness and the width of the adhesive layer, respectively, while l_a is the impact length for a single spring element and is equal to the spacing between the springs. According to the scheme in Fig. 2b in our study, the bonding line between the inner glazing and the timber frame is marked with $t_{a,inn}$ and $w_{a,inn}$ variable parameters for the springs in Eqs. 1 and 2, while the parameters $t_{a,out}$ and $w_{a,out}$ are used for the outer bonding in the modelling process.

The present study was performed for the case of the double-skin timber-glass wall system DSF-P (double-skin façade) with full-scale dimensions of 1.25 m × 2.34 m (Fig. 2a), taken from the experimental analysis performed in [28]. The geometry and the typical cross-section of the DSF wall element with all adhesive types are shown in Fig. 2. As stated, two different types of adhesives were used, i.e. polyurethane (Ködiglaze P, [39]) for the inner triple insulation glazing, and silicone (Ködiglaze S, [40]) for the outer single glazing. The timber frame is composed of glue-laminated timber GL24h according to the EN 1194 classification [41]. For the inner triple insulating glazing, float glass (44.2) is used [42], i.e. glass panes 2, 3 and 4 in Fig. 2b, while a thermally toughened soda lime silicate safety glass (TVG 55.4) is used for the single outer glazing [43], i.e. glass pane 1 in Fig. 2b. It is important to point out that only the linear-elastic behaviour of all material components will be considered at this stage of modelling.

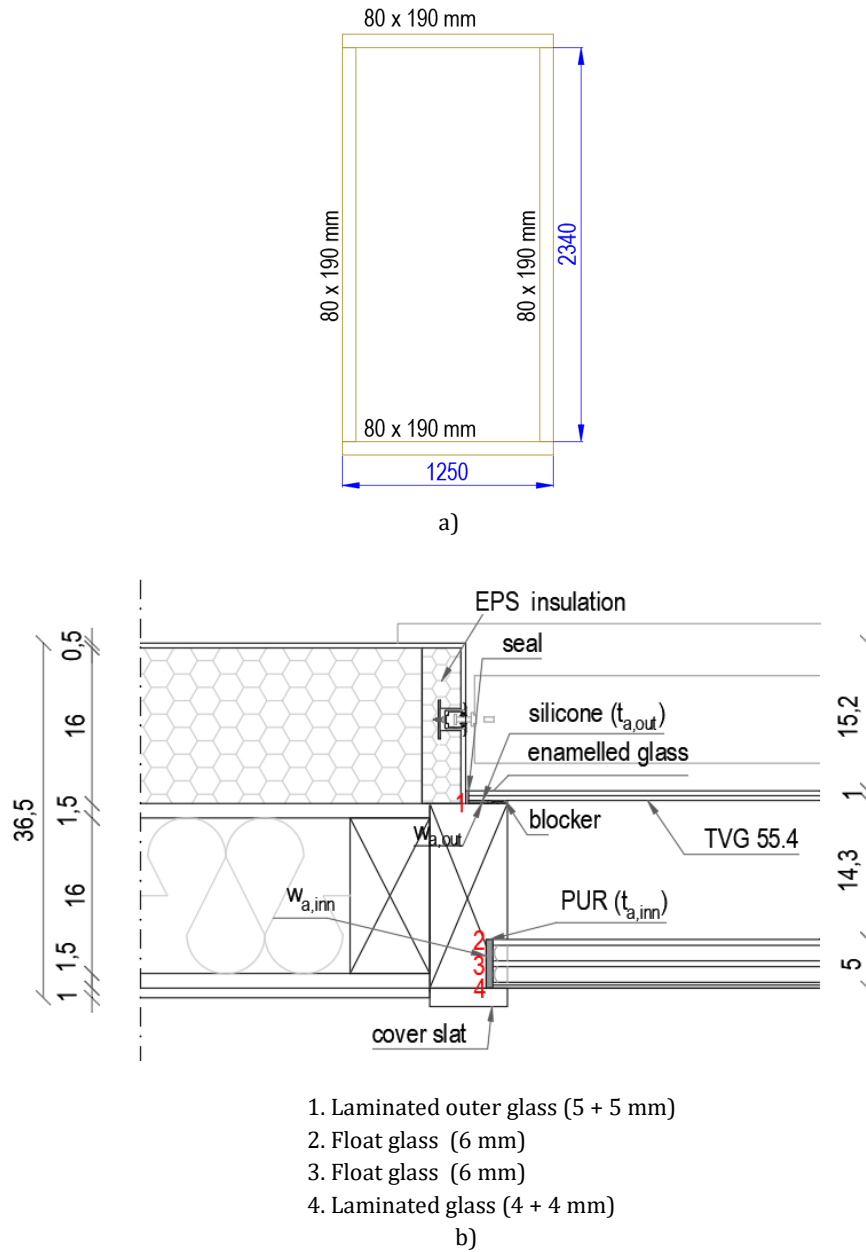


Fig. 2 External dimensions of the wall samples and dimensions of the timber frame elements (a), and the system cross-section with installation details (b)

Table 1 Material properties of the adhesives [39, 40]

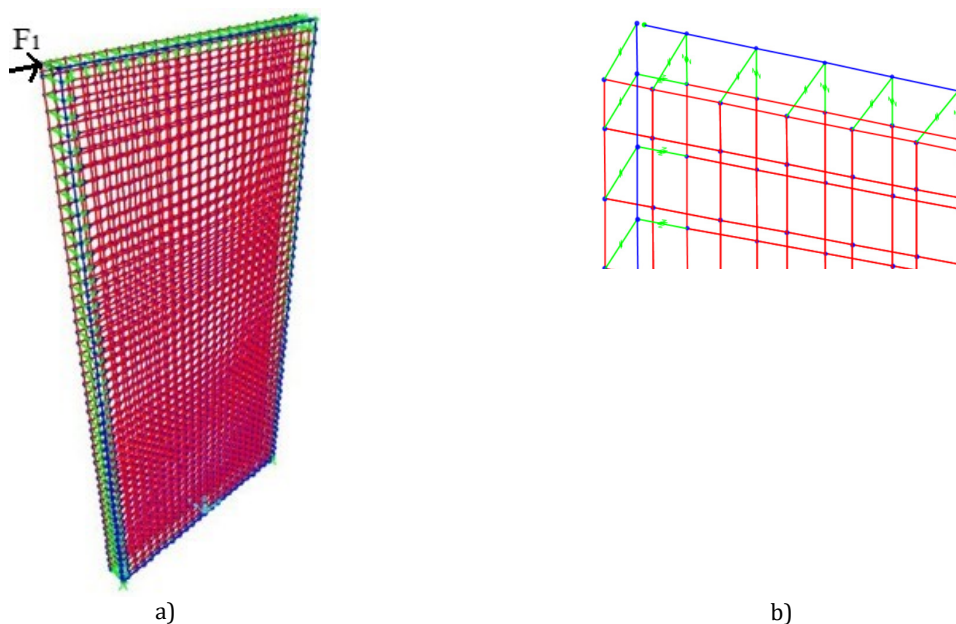
	Poisson's ratio ν	Shear modulus G_s (MPa)	Elastic modulus E_0 (MPa)	Decay time t_d (s)	Decay constant β
Silicone (Ködiglaze S)	0.5	0.351	1,053	100	0.0026
Polyurethane (Ködiglaze P)	0.49	0.454	1,354	290	0.0016

The input data for two types of adhesives, and the material properties of the glass and timber are listed in Tables 1 and 2, respectively.

Table 2 Material properties of the timber [41] and glass components [42, 43]

	Timber frame GL24h [41]	Float glass [42]	Thermally toughened glass [43]
Standard	EN 1194	EN 12150	EN 12150
E (MPa)	II 11,600 I 720	70,000	70,000
ν (-)	II 0.25 I 0.45	0.23	0.23
G (MPa)	II 720 I 35	0.45	0.45
f_t (MPa)	II 14 I 0.5	45	120
f_c (MPa)	II 14 I 0.5	500	500
ρ (kg/m ³)	380	2,500	2,500

The developed numerical finite element model of the whole composite DSF wall element as established in SAP 2000 [37] is shown in Fig. 3a. The timber material was considered as an isotropic elastic material (with the modulus of elasticity $E_{0,mean}$) and the elements of the timber frame were modelled as the simple plane-stress elements. Both glass panes were modelled using the linear shell elements offered by the SAP2000 software. While glass is a very brittle material it was therefore modelled as acting linearly elastic in tension and compression. The schematic presentation of the detail bonding line modelling simulating the adhesive bonding between the timber frame and both glazings by using discrete two-dimensional spring elements with perpendicular stiffness properties K_1 and K_2 is presented in Fig. 3b. It is important to point out that the bonding lines for the outer and inner glazing are modelled and simulated separately with different values of K_1 and K_2 according to Eqs. 1 and 2. The tensile (left bottom) support was arranged using three M16 bolts and two steel plates (one on each side of the wall element). The steel plates were connected to a rigid steel frame. In the numerical model, the bolts were considered as linear elastic spring supports with the stiffness equal to the slip modulus K_{ser} for bolts. It should be noted that the steel plates were not included in the numerical model. The compressive (right bottom) support was modelled using rigid point supports.

**Fig. 3** a) DSF-P finite element model, and b) the presentation of the spring/link elements

4. Numerical analysis and discussion of results

In the numerical analysis, the model was loaded with a vertical load in the first phase, followed by the second phase with a gradual increase of the horizontal load (“step by step analysis”). Based on the ratio between the horizontal force and the calculated displacement, the racking stiffness R was determined. Subsequently, the results were compared with the results of the experimental tests performed in [28].

Fig. 4 shows a comparison between the results of the experimental tests [28] performed on three full-scale test samples with the polyurethane adhesive for the inner glazing (DSF-P1, DSF-P2 and DSF-P3) and the numerical analysis performed on the test samples with exactly the same all dimensions presented in Fig. 2 and all material properties listed in Tables 1 and 2.

The diagram shows a very good agreement between the numerical and experimental results of three full-scale test samples regarding the behaviour of the structure in the elastic range until irreversible non-linear deformations appear. However, it should be mentioned that the test samples in [28] were experimentally tested pending the total failure of the element and the yielding of both adhesives occurred by the forces of approximately $F_1 = 28$ kN. This yielding stage of the adhesive was not modelled with our developed mathematical model, as in the first phase of the developed new structural DSF elements, it is assumed to be used only as a bracing element for buildings, where the wind load is decisive as the horizontal load impact and the structure thus has to be dimensioned only in the linear-elastic range.

The horizontal displacement u_1 at a force of $F_1 = 10$ kN and the calculated racking stiffness R for both experimental test and the numerical simulation are presented in Table 3. For the experimental results, the average value of all three test samples is calculated [28].

It is obvious from the presented results that the numerical results exhibit a very good agreement with the experimental ones. Therefore, it can be concluded that the developed FE model can be used for further parametrical studies with different parameters, which can significantly affect the racking resistance of DSF wall elements.

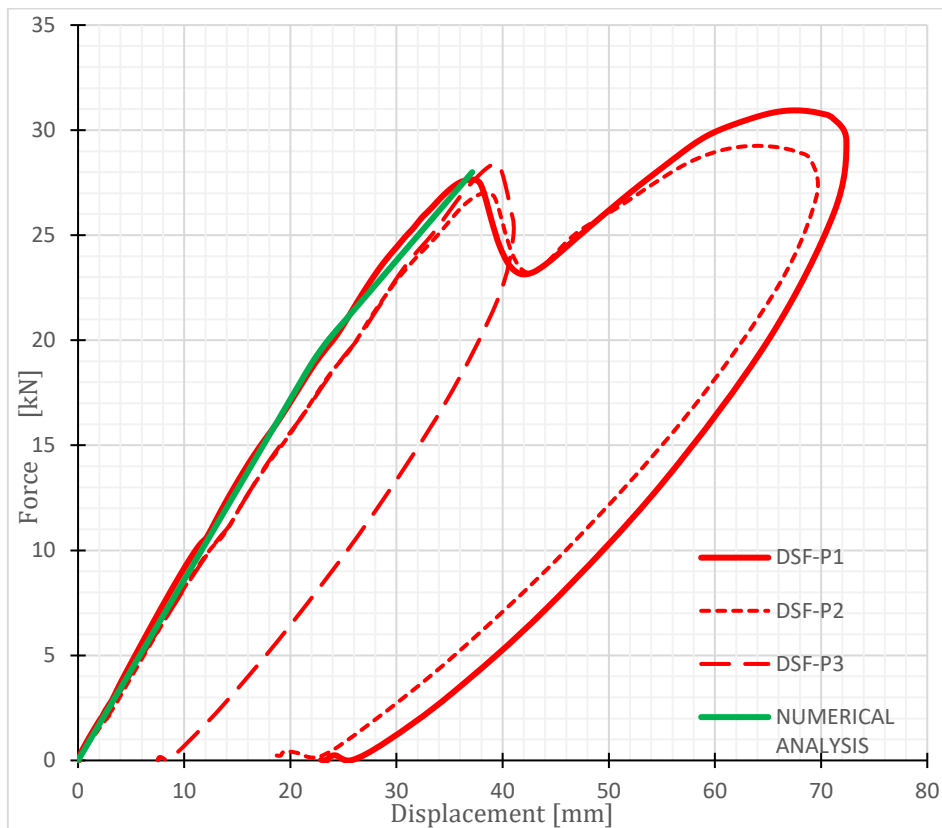


Fig. 4 Experimental and numerical force-displacement diagrams for the DSF-P wall element

Table 3 Experimental and numerical displacements at an acting force of $F_1 = 10$ kN and racking stiffness R

Model type	DSF-P
Displacement u_1 (mm) at $F_1 = 10$ kN – numerical	11.67
Displacement u_1 (mm) at $F_1 = 10$ kN – experimental [28]	11.00
Numerical stiffness: $R = F_1 / u_1$ (N/mm)	857
Experimental stiffness [28]: $R = F_1 / u_1$ (N/mm)	909

5. Parametric numerical analysis of the horizontal load-bearing capacity and stiffness of DSF-P wall elements

The parametric analysis was performed on the DSF-P model, in which the polyurethane adhesive thickness of the inner insulating glazing $t_{a,inn}$ was varied first, while the other parameters, such as silicone adhesive thickness of the outer glazing, glass thickness t_{gl} and the width of the adhesive layer w_a , remained unchanged. The thickness of the outer single glass (Glass 1) and the thickness of the triple inner insulating glass (Glass 2, 3, 4) according to Fig. 2b were further varied. In this case, the widths of the adhesive layer changed depending on the thickness of Glasses 2 and 3.

5.1 Analysis of the influence of the adhesive thickness on the horizontal load-bearing capacity of DSF wall panels

In the first parametric study, the thickness of the polyurethane adhesive bonding the triple insulating glazing to the timber frame was parametrically changed ($t_{a,inn} = 3 \text{ mm}, 5 \text{ mm}, 7 \text{ mm}, 9 \text{ mm}$), while the thickness of the silicone bonding the outer glass pane to the timber frame was constant $t_{a,out} = 3 \text{ mm}$ in all cases.

Table 4 and Fig. 5 show the results of displacements at an acting horizontal force of $F_1 = 10 \text{ kN}$ and the calculated racking stiffness as a function of the thickness of the variable polyurethane adhesive.

As expected, the racking stiffness of the wall element almost hyperbolically decreases with the increasing thickness of the polyurethane adhesive, since a greater thickness of adhesive represents a greater yielding of the joint between the timber frame and the glass. Very similar conclusions on the influence of the adhesive thickness were also obtained in the numerical study in [15] performed on single-skin façade elements with only triple or double insulating glazing.

Table 4 Displacements u and stiffnesses R at different thicknesses of the polyurethane adhesive $t_{a,inn}$

$t_{a,inn}$ (mm)	u at $F_1 = 10 \text{ kN}$ (mm)	R (N/mm)
3	6.40	1,563
5	9.26	1,080
7	11.67	857
9	13.07	765

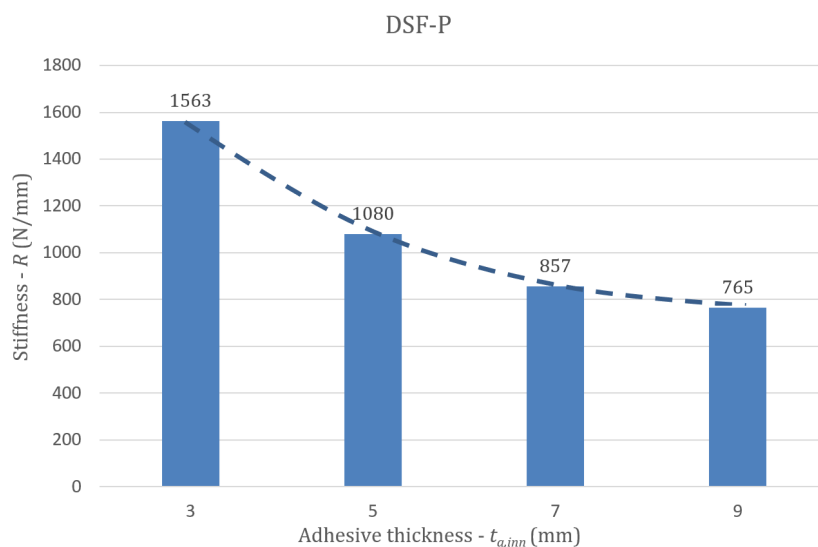


Fig. 5 Racking stiffness values for the parametrical selected adhesive thicknesses $t_{a,inn}$

5.2 Analysis of the influence of the glass thickness on the horizontal load-bearing capacity of DSF wall elements

Parametric analyses were also carried out, varying the thickness of the outer Glass 1 $t_{gl,out}$ and of the inner glasses 2, 3, 4 $t_{gl,inn}$ and taking into account the respective constant width of the polyurethane adhesive layer $w_a = 28$ mm for the inner glazing. The layout of the glasses is shown in Fig. 6.

Table 5 shows the results for different thicknesses of the outer single Glass 1 $t_{gl,out}$ at an acting horizontal force of $F_1 = 10$ kN with a constant adhesive thickness of $t_{a,inn} = 7$ mm and width $w_{a,out} = 20$ mm for the fixing of the triple inner insulating glass to the timber frame. The silicone adhesive of the constant thickness of $t_{a,out} = 3$ mm was used to fix the single outer insulating glass to the timber frame. The thicknesses of the inner triple glazing (Glasses 2, 3, 4) are constant and the same as used in the experimental analysis [28].

It is evident from the listed results that the glass thickness $t_{gl,out}$ has almost no impact on the racking resistance if the width of the bonding line $w_{a,out}$ is not adequately changed. Therefore, the width of the adhesive in the bonding line w_a will be systemically changed with the increasing thickness of the glass panes t_{gl} in our further analysis.

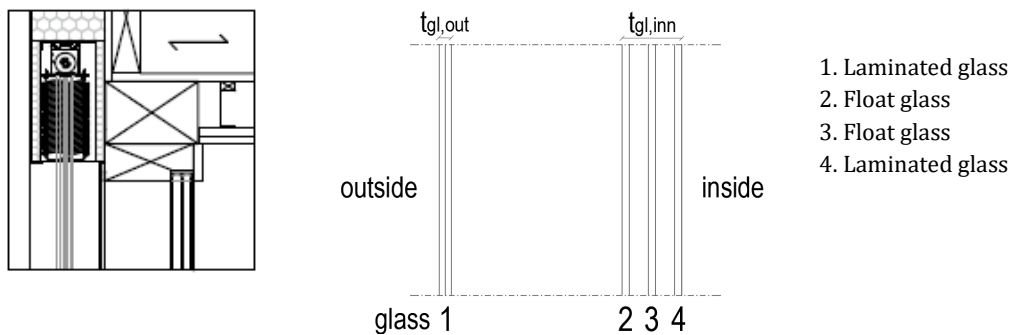


Fig. 6 Illustration of the glass layout and thickness of the DSF-P wall element

Table 5 Calculated displacements u and stiffness R for different glass thicknesses of outer Glass 1 $t_{gl,out}$

Glass pane	Thicknesses of the outer glass $t_{gl,out}$ and inner glass $t_{gl,inn}$ (mm)			
	Example 1	Example 2	Example 3	Example 4
1 - outer	4 + 4	5 + 5	6 + 6	7 + 7
$w_{a,out}$ (mm)	20	20	20	20
2 - inner	6	6	6	6
3 - inner	6	6	6	6
4 - inner	4 + 4	4 + 4	4 + 4	4 + 4
u (mm) at $F_1 = 10$ kN	11.68	11.67	11.66	11.64
R (N/mm)	856.16	856.90	857.63	859.11

5.3 Analysis of the influence of the adhesive layer width on the horizontal load-bearing capacity of DSF wall elements

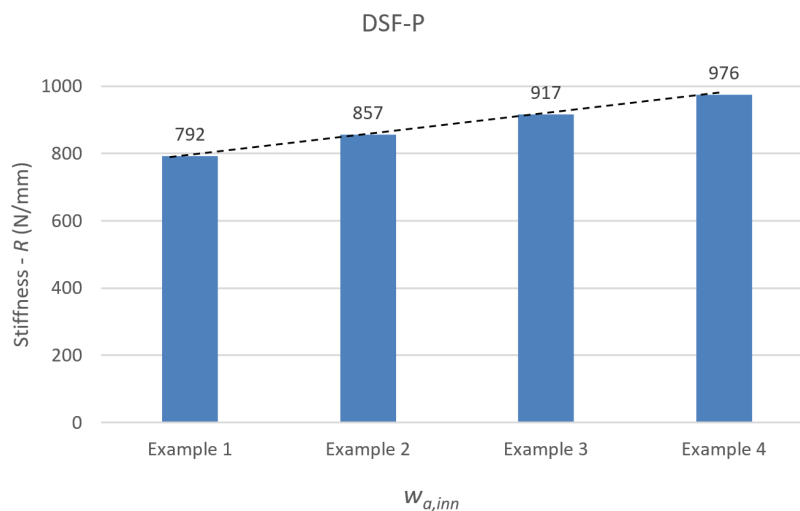
Table 6 shows the obtained numerical results for different parametrically selected thicknesses of the triple inner insulating glass (glasses 2, 3, 4) at an acting force of $F_1 = 10$ kN. The inner glazing is bonded to the timber frame with a polyurethane adhesive with a constant thickness of $t_{a,inn} = 7$ mm. The thickness of the silicone adhesive fixing of the outer single glass (Glass 1) to the timber frame remained unchanged $t_{a,out} = 3$ mm and the thickness of the outer Glass 1 $t_{gl,out}$ remained constant (5 + 5 mm) as used in the experimental study [28].

The calculation of the spring stiffness takes into account the influence of the adhesive layer width w_a and varies according to the thickness of glasses 2, 3 and 4. Consequently, the values $w_{a,inn}$ systematically increase from 24 mm in Example 1 to 36 mm in Example 4.

The calculated results are graphically presented in Fig. 7. The linear approximation is marked with the dashed line.

Table 6 Displacements u and stiffness R for different glass thicknesses 2, 3, 4

Glass pane	Thicknesses of the outer glass $t_{gl,out}$ and inner glass $t_{gl,inn}$ (mm)			
	Example 1	Example 2	Example 3	Example 4
1 – outer	5 + 5	5 + 5	5 + 5	5 + 5
2 – inner	4	6	8	10
3 – inner	4	6	8	10
4 – inner	3 + 3	4 + 4	5 + 5	6 + 6
$w_{a,inn}$ (mm)	24	28	32	36
u (mm) at $F_1 = 10$ kN	12.62	11.67	10.90	10.25
R (N/mm)	792	857	917	976

**Fig. 7** Stiffness for different cases of the considered width of the adhesive

The results evidently demonstrate that the thickness of the outer single Glass 1 has practically no influence on the racking stiffness of the wall element if the corresponding width of the adhesive is not changed. On the other hand, increasing the thickness of the inner insulating glasses 2, 3 and 4, but considering the corresponding increasing width of the adhesive layer w_a in Eqs. 1 and 2, increases the overall DSF racking stiffness in an almost linear way, and has an important positive effect on the horizontal load-bearing capacity of the wall element.

6. Conclusion

The paper presents the finite element model developed and used for the numerical analysis of the resistance and stiffness of double-skin façade (DSF) elements. Respecting the known facts from different experimental and numerical analyses performed on single-skin timber-glass wall elements, there are many various parameters which significantly affect the racking resistance of such elements and can be further implemented to double-skin timber glass façade elements. Considering that the costs of the experiments performed on such full-scale DSF elements are very high and such experiments are time-consuming, an extensive parametric numerical study of various main parameters influencing the horizontal load carrying capacity of such DSF elements was performed. Particular attention was paid to the analysis of the influence of the adhesive thickness and the width of the bonding line as well as the thickness of the outer and inner glazing panel.

The computational analyses carried out on individual load-bearing DSF wall elements have shown a considerable influence of the adhesive layer width bonding the glass pane to the timber frame with almost linear behaviour approximation (Fig. 7), while the second important parameter, i.e. the adhesive thickness, exhibited almost hyperbolic influence (Fig. 5). On the other hand, the glass thickness was found to be a less important parameter, which becomes relevant only if the width of the adhesive layer increased simultaneously and adequately with the glass thickness.

The obtained results indicate that the new approach of the developed load-bearing prefabricated timber DSF elements can essentially improve racking resistance and stiffness compared

with the widely studied timber-glass single-skin wall elements and can thus be fully recommended especially in the structural renovation process of old buildings.

However, the presented spring FE model is maybe still complex for practical engineering usage, but very useful for parametrical research studies. Therefore, our future work will be focused to development of a simple mathematical model with fictive diagonals [27] also for DSF elements to be used in simple computational FEM programs. Due to its simplicity such a model than it can be used for modelling with simpler and cheaper programs.

References

- [1] Jensen, P.A., Maslesa, E., Berg, J.B., Thuesen, C. (2018). 10 questions concerning sustainable building renovation, *Building and Environment*, Vol. 143, 130-137, doi: [10.1016/j.buildenv.2018.06.051](https://doi.org/10.1016/j.buildenv.2018.06.051).
- [2] Abdul Hamid, A., Farsäter, K., Wahlström, Å., Wallentén, P. (2018). Literature review on renovation of multifamily buildings in temperate climate conditions, *Energy and Buildings*, Vol. 172, 414-431, doi: [10.1016/j.enbuild.2018.04.032](https://doi.org/10.1016/j.enbuild.2018.04.032).
- [3] Ascione, F., Bianco, N., De Masi, R.F., Mauro, G.M., Vanoli, G.P. (2017). Energy retrofit of educational buildings: Transient energy simulations, model calibration and multi-objective optimization towards nearly zero-energy performance, *Energy and Buildings*, Vol. 144, 303-319, doi: [10.1016/j.enbuild.2017.03.056](https://doi.org/10.1016/j.enbuild.2017.03.056).
- [4] Žegarac Leskovar, V., Premrov, M. (2019). *Integrative approach to comprehensive building renovations*, Springer, Cham, Switzerland, doi: [10.1007/978-3-030-11476-3](https://doi.org/10.1007/978-3-030-11476-3).
- [5] Žegarac Leskovar, V., Premrov, M. (2013). *Energy-efficient timber-glass houses*, Springer, London, United Kingdom doi: [10.1007/978-1-4471-5511-9](https://doi.org/10.1007/978-1-4471-5511-9).
- [6] Rules on efficient use of energy in buildings (2010). Official Gazette, Republic of Slovenia, 52/2010, from <http://www.pisrs.si/Pis.web/pregledPredpisa?id=PRAV14331>, accessed November 13, 2021.
- [7] Inanici, M.N., Demirbilek, F.N. (2000). Thermal performance optimization of building aspect ratio and south window size in five cities having different climatic characteristic of Turkey, *Building and Environment*, Vol. 35, No. 1, 41-52, doi: [10.1016/S0360-1323\(99\)00002-5](https://doi.org/10.1016/S0360-1323(99)00002-5).
- [8] Chiras D. (2002). *The solar house: Passive heating and cooling*, Chelsea Green Publishing, White River Junction, Vermont, USA.
- [9] Persson, M.-L., Roos, A., Wall, M. (2006). Influence of window size on the energy balance of low energy houses, *Energy and Buildings*, Vol. 38, No. 3, 181-188, doi: [10.1016/j.enbuild.2005.05.006](https://doi.org/10.1016/j.enbuild.2005.05.006).
- [10] Hachem, C., Athientitis, A., Fazio, P. (2011). Parametric investigation of geometric form effects on solar potential of housing units, *Solar Energy*, Vol. 85, No. 9, 1864-1877, doi: [10.1016/j.solener.2011.04.027](https://doi.org/10.1016/j.solener.2011.04.027).
- [11] Premrov, M., Žigart, M., Žegarac Leskovar, V. (2018). Influence of the building shape on the energy performance of timber-glass buildings located in warm climatic regions, *Energy*, Vol. 149, 496-504, doi: [10.1016/j.energy.2018.02.074](https://doi.org/10.1016/j.energy.2018.02.074).
- [12] Feldmann, M., Kasper, R., Abeln, B., Cruz, P., Belis, J., Beyer, J., Colvin, J., Ensslen, F., Eliasova, M., Galuppi, L., Gessler, A., Grenier, C., Haese, A., Hoegner, H., Kruijs, R., Lanosch, K., Louter, C., Manara, G., Morgan, T., Neugebauer, J., Rajcic, V., Royer-Carfagni, G., Schneider, J., Schula, S., Siebert, G., Sulcova, Z., Wellershoff, F., Zarnic, R. (2014). *Guidance for European structural design of glass components*, European Commission, Joint Research Centre, Institute for the Protection and Security of the Citizen, Ispra, Italy.
- [13] Premrov, M., Dujič, B., Ber, B. (2013). Glazing influence on the seismic resistance of prefabricated timber-framed buildings, In: Belis, J., Louter, C. (eds.), *COST action TU0905 mid-term conference on structural glass*, CRC Press, Boca Raton, Florida, USA, 25-32.
- [14] Premrov, M., Serrano, E., Winter, W., Fadai, A., Nicklisch, F., Dujič, B., Sustersic, I., Brank, B., Strukelj, A., Drzecnik, M., Buyuktasgin, H.A., Erol, G., Ber, B. (2015). Workshop report *WP 6: Testing on life-size specimen components: shear walls, beams and columns including long-term behaviour*: WoodWisdom-net, research project, load bearing timber-glass-composites, 2012-2014, 15.
- [15] Ber, B., Finžgar, G., Premrov, M., Štrukelj, A. (2018). On parameters affecting the racking stiffness of timber-glass walls, *Glass Structures & Engineering*, No. 4, 69-82, doi: [10.1007/s40940-018-0086-5](https://doi.org/10.1007/s40940-018-0086-5).
- [16] Saelens, D. (2002). *Energy performance assessment of single-storey multiple-skin facades*, Catholic University of Leuven, Belgium, PhD Dissertation, from <https://bwk.kuleuven.be/bwf/PhDs/PhDSaelens>, accessed November 15, 2021.
- [17] Alibaba, H.Z., Ozdeniz, M.B. (2016). Energy performance and thermal comfort of double-skin and single-skin facades in warm-climate offices, *Journal of Asian Architecture and Building Engineering*, Vol. 15, No. 3, 635-642, doi: [10.3130/jaabe.15.635](https://doi.org/10.3130/jaabe.15.635).
- [18] Pomponi, F., D'Amico, B. (2017). Holistic study of a timber double skin façade: Whole life carbon emissions and structural optimization, *Building and Environment*, Vol. 124, 42-56, doi: [10.1016/j.buildenv.2017.07.046](https://doi.org/10.1016/j.buildenv.2017.07.046).
- [19] Niedermaier, P. (2003). Shear-strength of glass panel elements in combination with timber frame constructions, In: *Proceedings of the 8th International Conference on Architectural and Automotive Glass (GPD)*, Tampere, Finland, 262-264.

- [20] Cruz, P.J.S., Pacheco, J.A.L., Pequeno, J.M.B. (2007). Experimental studies on structural timber glass adhesive bonding, In: *COST E34, Bonding of Timber, 4th Workshop »Practical Solutions for Furniture & Structural Bonding*, Larnaca, Cyprus, 67-75.
- [21] Neubauer, G., Schober, P. (2008). *Holz-Glas-Verbundkonstruktionen*, Weiterentwicklung und Herstellung von Holz-Glas-Verbundkonstruktionen durch statisch wirksames Verkleben von Holz und Glas zum Praxiseinsatz im Holzhausbau (Impulsprojekt V2 des Kind Holztechnologie), Endbericht, Holzforschung Austria, Vienna, Austria.
- [22] Hochhauser, W. (2011). *A contribution to the calculation and sizing of glued and embedded timber-glass composite panes*, PhD Thesis, Vienna University of Technology, Austria.
- [23] Blyberg, L. (2011). *Timber/glass adhesive bonds for structural applications*, Licentiate thesis, Linnaeus University, School of Engineering, Växjö, Sweden, from <http://www.diva-portal.org/smash/get/diva2:447937/FULLTEXT01.pdf>, accessed November 15, 2021.
- [24] Blyberg, L., Serrano, E., Enquist, B., Sterley, M. (2012). Adhesive joints for structural timber/glass applications: Experimental testing and evaluation methods, *International Journal of Adhesion and Adhesives*, Vol. 35, 76-87, doi: [10.1016/j.ijadhadh.2012.02.008](https://doi.org/10.1016/j.ijadhadh.2012.02.008).
- [25] Ber, B., Premrov, M., Štrukelj, A., Kuhta, M. (2014). Experimental investigations of timber-glass composite wall panels, *Construction and Building Materials*, Vol. 66, 235-246, doi: [10.1016/j.conbuildmat.2014.05.044](https://doi.org/10.1016/j.conbuildmat.2014.05.044).
- [26] Štrukelj, A., Ber, B., Premrov, M. (2015). Racking resistance of timber-glass wall elements using different types of adhesives, *Construction and Building Materials*, Vol. 93, 130-143, doi: [10.1016/j.conbuildmat.2015.05.112](https://doi.org/10.1016/j.conbuildmat.2015.05.112).
- [27] Premrov, M., Ber, B., Kozem Šilih, E. (2021). Study of load-bearing timber-wall elements using experimental testing and mathematical modelling, *Advances in Production Engineering & Management*, Vol. 16, No. 1, 67-81, doi: [10.14743/apem2021.1.385](https://doi.org/10.14743/apem2021.1.385).
- [28] Premrov, M., Zegarac Leskovic, V., Ber, B., Kozem Šilih, E., Vogrinec, K., Lesnik, M. (2021). *Razvoj multifunkcijskega klimatsko aktivnega nosilnega ovoja objektov - DOM+: zaključno poročilo raziskovalnega projekta: delovni paket A1.2 Raziskava nosilnosti in togosti DSF stenskih elementov* (UM FGPA, TRL 3-4): trajanje projekta (TRL 3-4): 1. 3. 2019-28. 2. 2021. Maribor: Univerza v Mariboru, Fakulteta za gradbeništvo, prometno inženirstvo in arhitekturo, Slovenia.
- [29] Ghaffarianhoseini, A., Ghaffarianhoseini, A., Berardi, U., Tookey, J., Li, D.H.W., Kariminia, S. (2016). Exploring the advantages and challenges of double-skin facades (DSFs), *Renewable and Sustainable Energy Reviews*, Vol. 60, 1052-1065, doi: [10.1016/j.rser.2016.01.130](https://doi.org/10.1016/j.rser.2016.01.130).
- [30] Poirazis, H. (2004). *Double skin façades for office buildings*, Literature review, Department of Construction and Architecture, Lund University, Lund, Sweden.
- [31] Xu, L., Ojima, T. (2007). Field experiments on natural energy utilization in a residential house with a double skin façade system, *Building and Environment*, Vol. 42, No. 5, 2014-2023, doi: [10.1016/j.buildenv.2005.07.026](https://doi.org/10.1016/j.buildenv.2005.07.026).
- [32] Chan, A.L.S., Chow, T.T., Fong, K.F., Lin, Z. (2009). Investigation on energy performance of double skin façade in Hong Kong, *Energy and Buildings*, Vol. 41, No. 11, 1135-1142, doi: [10.1016/j.enbuild.2009.05.012](https://doi.org/10.1016/j.enbuild.2009.05.012).
- [33] Haase, M., Marques da Silva, F., Amato, A. (2009). Simulation of ventilated facades in hot and humid climates, *Energy and Buildings*, Vol. 41, No. 4, 361-373, doi: [10.1016/j.enbuild.2008.11.008](https://doi.org/10.1016/j.enbuild.2008.11.008).
- [34] Tijjani Musa, B., Alibaba, H.Z. (2016). Evaluating the use of double skin facade systems for sustainable development, *International Journal of Recent Research in Civil and Mechanical Engineering*, Vol. 2, No. 2, 151-159.
- [35] Huckemann, V., Borges Leão, É., Leão, M. (2009). Acoustic comfort in office buildings with double skin glass facades, *Bauphysik*, Vol. 31, No. 5, 305-312, doi: [10.1002/bapi.200910040](https://doi.org/10.1002/bapi.200910040).
- [36] Saroglou, T., Theodosiou, T. Givoni, B., Meir, I.A. (2019). A study of different envelope scenarios towards low carbon high-rise buildings in the Mediterranean climate - can DSF be part of the solution?, *Renewable and Sustainable Energy Reviews*, Vol. 113, Article No. 109237, doi: [10.1016/j.rser.2019.06.044](https://doi.org/10.1016/j.rser.2019.06.044).
- [37] CSI. SAP2000 (v17.0.0). (2010). *Linear and nonlinear static and dynamic analysis and design of three-dimensional structures*. Berkeley: Computer & Structures, Inc.
- [38] Kreuzinger, H., Niedermaier, P. (2005). *Glas als Schubfeld*, Tagungsband Ingenieurholzbau, Karlsruher Tage.
- [39] Kömmerling, Product Information Ködiglaze P (2008). Special adhesive for bonding insulating glass units into the window sash.
- [40] Kömmerling, Product Information Ködiglaze S (2008). Special adhesive for structural and direct glazing.
- [41] European Committee for Standardization, (2003). EN 1194:2003: Timber structures – glued laminated timber strength classes and determination of characteristic values, Brussels.
- [42] European Committee for Standardization, (2004). EN 572-2:2004: Glass in building – Basic soda lime silicate glass products – Part 2: Float glass, Brussels.
- [43] European Committee for Standardization, (2000). EN 12150-1:2000: Glass in building – Thermally toughened soda lime silicate safety glass – Part 1: Definition and description, Brussels.

A Plant Simulation approach for optimal resource utilization: A case study in the tire manufacturing industry

Butrat, A.^a, Supsomboon, S.^{b,*}

^{a,b}The Sirindhorn International Thai-German Graduate School of Engineering, King Mongkut's University of Technology North Bangkok, Bangkok, Thailand

ABSTRACT

In this study, the resource allocation and vital manufacturing processes in the tire manufacturing industry was comprehensively optimized. The paper deals in detail with the Banbury mixing process, which produces homogeneous rubber materials for tire components. In addition, the mixing process models were established by the Plant Simulation software to validate and compare scenarios and experiments with realistic production constraints. Discrete empirical distribution (dEmp) was proposed for population data. Various scenarios were created for different resource and process. Experiments were set as different group of compound set. Experiment manager was used as a tool to set up scenarios and the experiments to provide alternative results. The study results display the production time and machine utilization. The shortest production time of experiment results represents the best group of each scenario. As results, the scenario, which BB1 is changed from non-productive Banbury mixer to special Banbury mixer along with the normal process is combined with second special process, provides the suitable production volume which can reduce of total production time for 8.06 %. Our study provides a variety of the resource utilization of a Banbury mixing process and suggests an efficient optimization method for production performance improvement.

ARTICLE INFO

Keywords:
Manufacturing;
Resource utilization;
Bottleneck;
Optimization;
Simulation modelling;
Discrete-event simulation (DES);
Discrete empirical distribution;
Tires;
Rubber;
Banbury mixer;
Tecnomatix Plant Simulation

**Corresponding author:*
Srisawat.s@tggs.kmutnb.ac.th
(Supsomboon, S.)

Article history:
Received 22 November 2021
Revised 1 March 2022
Accepted 13 June 2022



Content from this work may be used under the terms of the Creative Commons Attribution 4.0 International Licence (CC BY 4.0). Any further distribution of this work must maintain attribution to the author(s) and the title of the work, journal citation and DOI.

1. Introduction

Many companies face problems of the production capacity, bottleneck analysis is widely used to solve such problem. Bottleneck is a capacity constraint resource (CCR) whose available capacity limits the ability to meet the product volume of the system. The bottleneck identification is performed to find the bottleneck process which provides the highest machine utilization because of unbalance amount of batch [1, 2]. The production process is analysed according to the time operations. After the bottleneck process is defined, the technique to reduce the processing time of the bottleneck process and balance the processing time in a line process called Line balancing is applied. This technique assigns the work to stations in a line process in order to achieve the desired output rate with the smallest number of workstations [3].

Recently, many companies apply digital manufacturing program to optimize their production system with respect to time, cost and quality [4]. These programs can be used to increase productivity and optimize production systems by applying visual commissioning to manufacturing process and increasing production flexibility [5]. The simulation processes model is created to test new ideas and propose options in various scenarios before actual implementation. Simulation models are created to explicitly visualize how an existing operation might perform under varied inputs and how a new or proposed operations might behave under the same or different situation: material flows and plant layouts [6]. Moreover, to increase the production rate, the optimization of production lines using line balance and discrete event simulation approach can be considered [7].

A software named Plant simulation is performed using discrete event simulation tools. This software allows the use of simulation techniques to identify and minimize various problems related to production systems [8-10]. For production planners, the use of dynamic production system simulations can improve the productivity of existing resources and reduce the cost of planning for new production resources. They can also optimize system variables under complicated constraints [11-16].

In this study, the case studied company is the tire company. Their products include Truck and Bus Radial Tire (TBR) and Private Car Radial Tire (PCR). Due to the increase of demand, the company production capacity had reached its limit. The basic analysis of the company showed that the bottleneck of the production system was Banbury mixing process. This mixing process is the process combining carbon black, natural and synthetic rubber and other various types of chemicals which are used to produce a homogeneous rubber material for tire components called Productive compound (Pro). Productive compound is produced by 1-4 steps of Banbury mixing process. The outcome of each Banbury mixing process in each step which cannot use to produce tire components is called Non-productive compound (Non-pro). The Banbury mixer can be divided into 3 types: Non-pro BB, Pro BB and Special BB. Non-pro BB is used to produce Non-productive compound. Pro BB is used to produce Productive compound. Special BB can be used to produce less step of Non-productive compound and produce Productive compound in 1 step (some compound). There are 6 Banbury mixer in the production lines shown in Fig. 1. BB1, BB3 and BB4 are Non-pro BB. BB5 and BB6 are Pro BB. BB2 is Special BB.

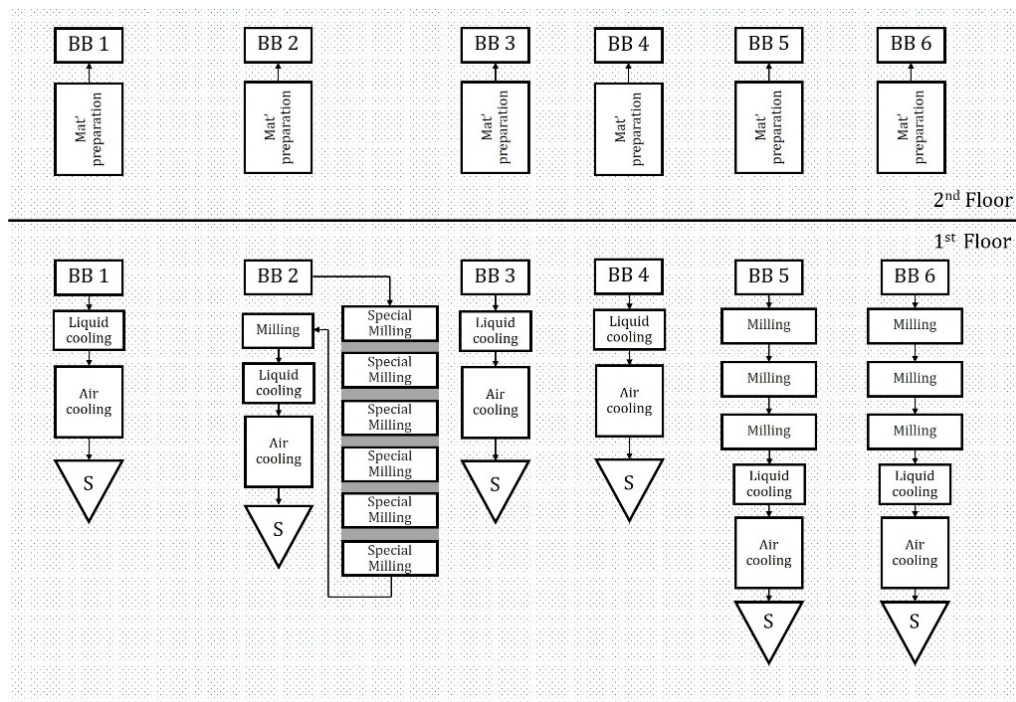


Fig. 1 Banbury mixing process flow chart and layout

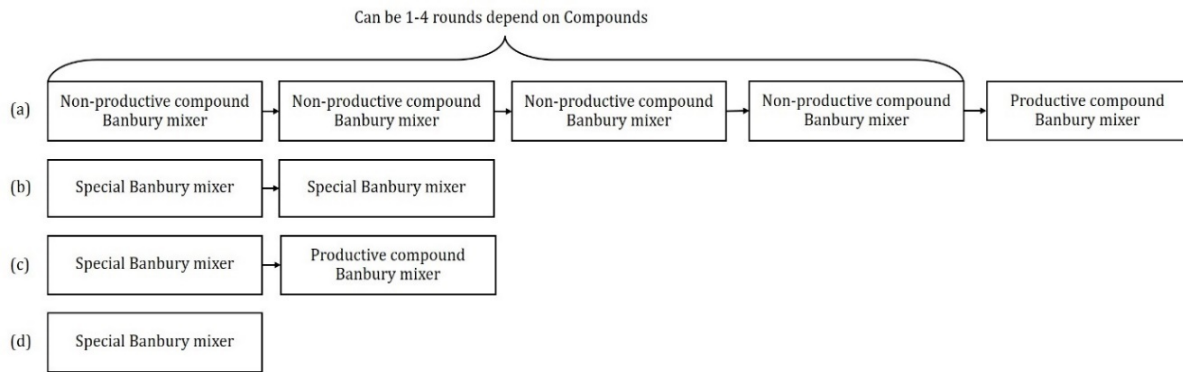


Fig. 2 Banbury mixing processes, (a) normal process, (b) first special process, (c) second special process, (d) third special process

The normal Banbury mixing process is usually done in five steps. The first four steps of mixing provide non-productive compounds and the last step provides productive compounds. However, there are some special Banbury mixing processes which can provide productive compounds in less numbers of steps. The Banbury mixing processes are described as follows.

Normal Banbury mixing process (N) is to assign Non-pro BB to mix 1 to 4 steps, depending on each compound, and Pro BB to mix 1 step as shown in Fig. 2(a). The first special Banbury mixing process (1st) is to assign Special BB to mix 2 steps as shown in Fig. 2(b). The second special Banbury mixing process (2nd) is to assign Special BB to mix 1 step and Pro BB to mix 1 step as shown in Fig. 2(c). The third special Banbury mixing process (3rd) is to assign Special BB to mix 1 step as shown in Fig. 2(d).

Because productive compounds are usually the last step in all Banbury mixing processes, the numbers of productive compound steps can be defined to a specific number. For example, if 5 compounds are needed and each compound requires 10 batches, the number of steps for productive compounds is 50 steps. However, for the same 5 compounds, the number of steps for non-productive compounds is different. Its number of steps can be 0 to 4 based on the mixing process. For example, if the normal process is chosen, 4 steps for non-productive compound and 1 step for productive compound can be performed. However, by the same compound, if the second special process is chosen, 1 step for non-productive compound and 1 step for productive compound can be performed. In addition, each compound could not be applied to all Banbury mixing processes. There were 11 compounds from 31 compounds which could be produced by special process.

To simplify sets of compounds, it was defined into 5 sets based on Banbury mixing processes. First set was the 20 compounds which could only be produced by normal process. Second set was the 1 compound which could be produced by normal or first special process. Third set was the 4 compounds which could be produced by normal or second special process. Fourth set was the 5 compounds which could be produced by normal or third special process. Fifth set was the 1 compound which could be produced by normal, first or second special process. Moreover, the compound in the first set was called normal type (20 compounds) and the rest of compound was called special type (11 compounds).

Due to the above factors, workload balance between each Banbury mixer was the critical issue when a production planner needed to design the production volume to meet the demand. This study presents the optimization of manufacturing operations by balancing production line. The concept of balancing the production line is to design the best group of Banbury mixing processes.

With simulation technique, all the types of the production process data were analysed. The input data included processing time, setting-up time, batch size, time between batch and total demand. The output data included machine utilization, total setting-up time proportion, total time between batch proportion and total production time. The simulation scenarios were created as different plans for resource allocation. The simulation experiments were set as various of total production planning of pro, non-pro and special compounds. This part of the process is

important for every simulation model because it involves various sources of system randomness. Moreover, the simulation study performed discrete empirical distribution because a standard theoretical distribution could not be found. It provided a good representation of our data while population data had been used [17, 18].

In this study, a Plant Simulation approach for optimal resource utilization: a case study in the tire manufacturing industry is presented. The outline is organized as follows. Section 2 illustrates the current performance of Banbury mixing process. Section 3 illustrates the simulation scenarios and experiments, the scenario results comparisons and estimation of production cost saving. Section 4 summarizes the conclusions and provides suggestions for future work, respectively.

2. Current performance of Banbury mixing process

After the problem was defined, the current production system was carefully analysed. The Banbury mixing process 3D simulation model was created in the Tecnomatix Plant Simulation as shown in Fig. 3. This model was called “Current capacity”, described the existing state of the production capacity of each Banbury mixer. It was created with the help of tables containing recorded data concerning the time in the current production plan.

The special milling method of Special BB created in simulation model is presented in Fig. 4(b). The special method was used to order queue of the special mill machines (MM) shown in Fig. 4(a). This method was coded to check whether which MM was empty before transferring WIP to the empty MM. Fig. 5 shows that the WIP compound which is transferred from BB waits for its destination. The destination of WIP compound receives from the first row of “OrderQueue” list. After that, a MM is set as the destination of the WIP compound, then the MM is deleted from the OrderQueue list. The MM is returned after it is already empty and waits for the next WIP compound.

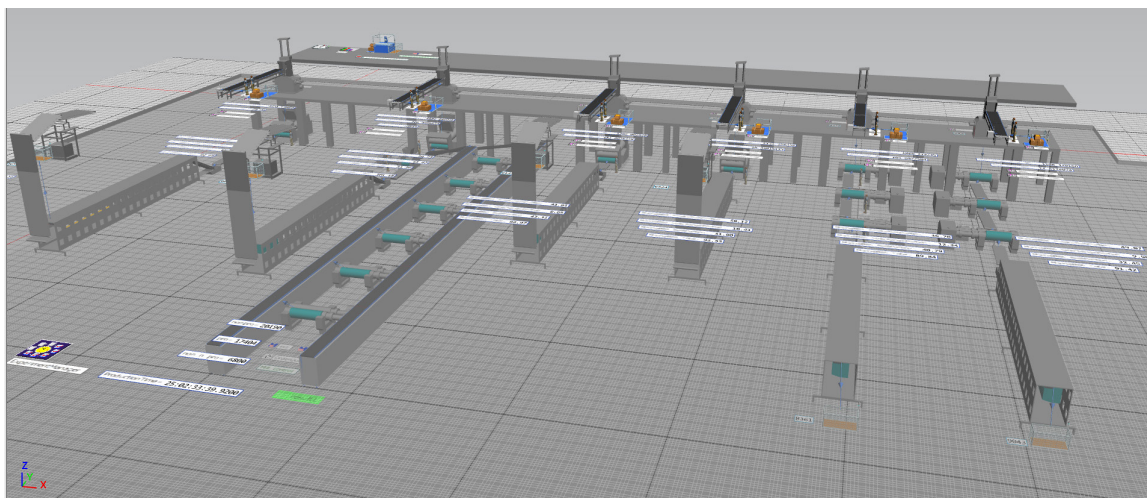


Fig. 3 The Banbury mixing process 3D simulation model

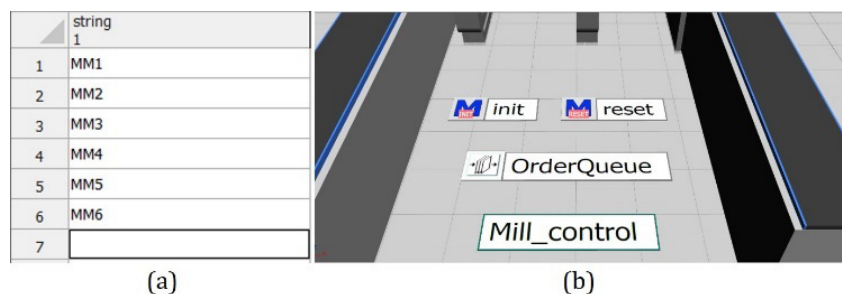


Fig. 4 (a) Special milling order queue, (b) Special milling in Special BB control

Procedure 1 Special milling method

- 1: **Waituntil** OrderQueue list ≥ 1 **then**
- 2: set WIP destination as first OrderQueue list
- 3: Remove first OrderQueue list
- 4: Move WIP to the target Special milling
- 5: Waituntil the milling process finish
- 6: Move WIP to milling
- 7: **Pop** the target Special milling to OrderQueue list

Fig. 5 Special milling operation method

The Banbury operation time including size change time (SC), processing time (PT) and time between batch (BwB) was considered. The sequence of mixing process is described in Fig. 6. The size change time starts when a worker setting up the Banbury mixer. Then, the processing time starts when the front gate of Banbury mixer opens to feed raw materials in and finishes when the back gate of Banbury mixer opens to feed a work-in-process out. The time between batch is the waiting time between feeding the work-in-process out and feeding the next raw materials in. Batch size is the number of batches between 2 size changes. Total production volume is the total number of batches in a month.

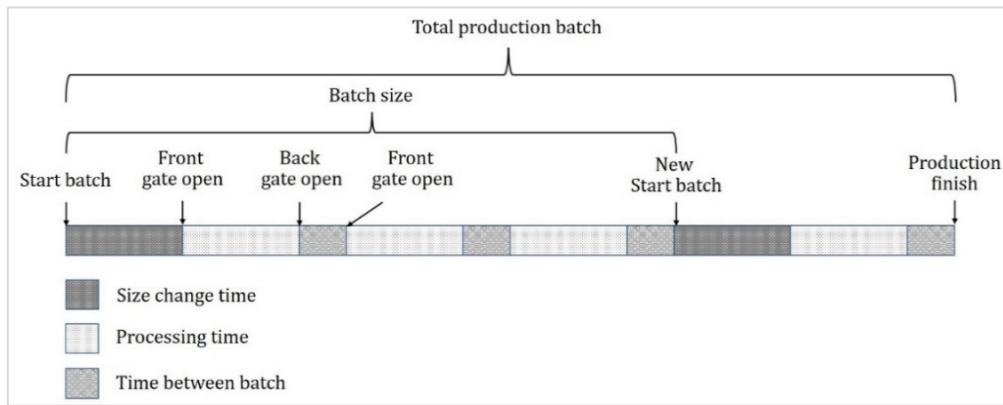


Fig. 6 Mixing process sequence

According to the described above, the system is the Banbury mixing process with the 3 types of the time consumption in the mixers. The simulation models are proposed under these 4 assumptions:

- 1) The system will not break down and is completely reliable.
- 2) Due to automation record of time, the input time is population data, the statistic theory will be Discrete empirical distribution.
- 3) The model will finish after passing 31 days without any break.
- 4) The number of areas to place the finished product (Non-pro, Pro compound) is unlimited.

Table 1 Banbury mixing process time and production volume data

Data	Banbury mixer						
	BB1	BB2	BB3	BB4	BB5	BB6	
Processing time (PT)	Mode (s)	125	180	113	133	107	131
	Mode frequency (times)	531	407	482	294	1166	471
	Max (s)	467	482	288	340	380	232
	Min (s)	83	131	94	91	63	68
Time between batch (BwB)	Mode (s)	22	23	150	32	24	30
	Mode frequency (times)	1083	807	829	521	1103	2175
	Max (s)	1093	4306	186	4898	4923	3980
	Min (s)	16	18	41	21	12	13
Size change time (SC)	Mode (s)	1017	1845	1296	1544	521	1729
	Mode frequency (times)	3	3	3	3	3	3
	Max (s)	4544	4779	4743	3442	4409	4332
	Min (s)	122	175	112	111	208	110
Average batch size (batch)		38	47	46	35	34	48
Total production volume (batch)		6042	6800	7242	6906	8935	8469

Table 2 The machine utilization and the production time

Banbury mixer	Machine utilization				Production time (days)
	Processing time (PT) (%)	Set-up time (SC) (%)	Recovery time (BwB) (%)	Total (%)	
BB1	42.83	10.04	10.76	63.62	31
BB2	45.48	9.22	26.29	81.00	
BB3	39.15	7.64	39.99	86.77	
BB4	40.55	8.56	24.84	73.96	
BB5	32.61	10.77	35.00	78.38	
BB6	37.75	7.48	24.29	69.52	

The Banbury operation time, batch size and total production volume data are summarized in Table 1. According to the assumptions mentioned above, we calculated machine utilization to define current capacity. The results of each machine utilization and the production time were shown in Table 2.

The initial model, which only the properties of current production capacity were entered, provided the information about the behaviour of the current system. Processing time, Size change time (Set-up time) and Time between batch (Recovery time) were set as dEmp as illustrated in Fig. 7. After a model was run for 31 days of the simulation time, the machine utilization results were obtained as shown in Table 3.

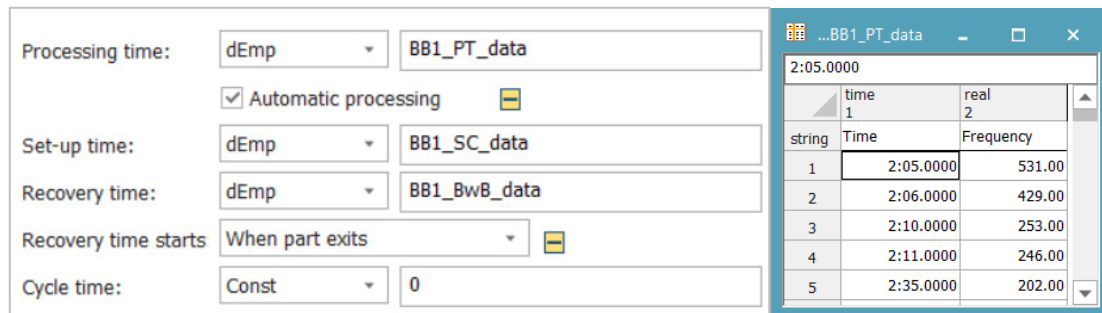


Fig. 7 Simulation setting window

Model validation was performed to validate data and information. The model output for an existing system was compared with the corresponding output for the system itself. Hypothesis testing given in Table 3 illustrates the difference values of machine utilization in the real system and the simulation model. Number of machines (n) is 6 and degree of freedom ($n-1$) is 5. Significant level at 0.05. After testing, the t-value is greater than -2.101 and less than 2.101 with 95 percent of confident interval. Therefore, H_0 is accepted. It can be concluded that there is no statistically significant difference between the real system and the simulation model.

After the model was validated, the production time was changed to be dynamic. This model was ended up after all production volumes were produced. The production volumes were separated into each Banbury mixing process including non-pro, pro and special. The machine utilizations were also separated including Non-pro BB, Pro BB and Special BB. The simulation results of this situation were obtained as shown in Fig. 8(b). Machine utilization was averaged for each BB type as shown in Fig. 8(a). The summary of the current performance is presented in Table 4.

Table 3 Hypothesis testing, real and simulation machine utilization (%)

Machine	Utilization (%)		$d_i = x_r - x_s$	Hypothesis
	Real (x_r)	Sim (x_s)		
BB1	63.62	63.34	0.28	Null hypothesis (H_0): $\bar{X}_r - \bar{X}_s = 0$ Alternative (H_1): $\bar{X}_r - \bar{X}_s \neq 0$ <hr/> The test statistic t <hr/> 0.1547 <hr/> $-2.101 \leq t \leq 2.101$
BB2	81.00	81.64	-0.64	
BB3	86.77	88.45	-1.67	
BB4	73.96	74.34	-0.38	
BB5	78.38	77.61	0.77	
BB6	69.52	69.08	0.43	
		\bar{d}	-0.20	
		S.D.	0.81	

Table 4 The summary results of the current performance

Production volume (batch)			Time (days)	Machine utilization (%)			
Non-pro	Pro	Special		Non-pro BB	Pro BB	Special BB	Avg
20,190	17,404	6,800	25.11	91.50	89.85	100	93.69

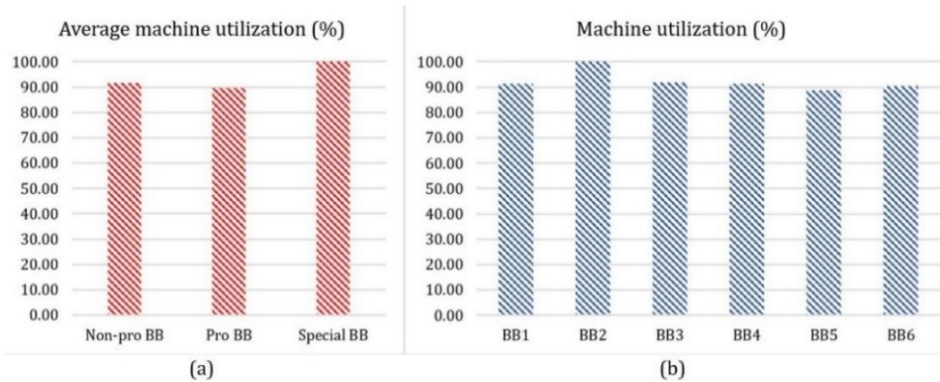


Fig. 8 (a) Average machine utilization of each BB type, (b) Machine utilization of each BB

3. Results and discussion

3.1 Simulation scenarios and experiments

Since the result of the current capacity was found that the average machine utilization of Special BB was full (100 %), the proposed idea to increase capacity was to change BB1 to Special BB in order to reduce the Special BB workload as presented in Fig. 9(a). After this idea was created and run in the Plant simulation, it was found that the workload of Special BB was reduced to 35.30 % but the machine utilization of Non-pro BB was increased to 100 % as illustrated Fig. 9(b). After changing BB1 to Special BB, the production time increased from 25.11 days to 36.20 days and the total average machine utilization reduced from 93.69 % to 65.84 % as presented in Table 5. Therefore, it was implied that this concept was not valid. The reason would probably be because of the unsuitable amount of the production volume for Non-pro BB.

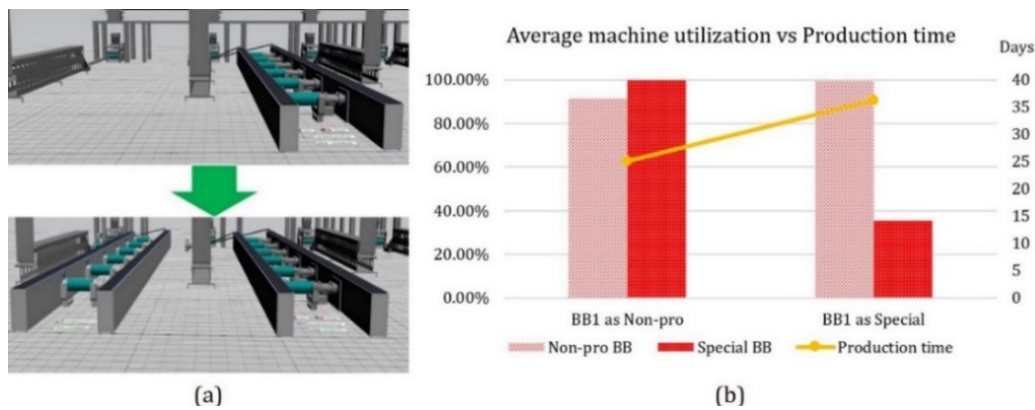


Fig. 9 (a) Changing BB1 from normal BB to Special BB, (b) The result that BB1 changing

Table 5 The summary results of Changing BB1

Production volume (batch)			Time (days)	Machine BB1	Machine utilization (%)			
Non-pro	Pro	Special			Non-pro BB	Pro BB	Special BB	Avg
20,190	17,404	6,800	36.20	Special BB	99.40	62.82	35.30	65.84

Due to the invalid scenario above, we decided to reduce the workload from Non-pro BB by reducing numbers of steps. The numbers of steps were reduced by combining the normal process with the second special process called the fourth special Banbury mixing process (4th) as shown in Fig. 10(a). The fourth special Banbury mixing process is to assign Non-pro BB to pro-

duce 1 step, Special BB to produce 1 step and Pro BB to produce 1 step as illustrated in Fig. 10(b). However, all compounds were also not applied to the fourth special process. There were only 7 compounds which could be produced by the normal process or the fourth special process. Therefore, the amount of the normal type had been changed from 20 compounds to 13 compounds and the amount of the special type had been changed from 11 compounds to 18 compounds. The summary of compound sets and the numbers of compound in each type are shown in Table 7.

The experiments were the grouping in all compound sets. For instance, as shown in Table 6, experiment 24 means that compound set 1 is assigned to be produced by normal process (N), compound set 3 and 5 are assigned to be produced by second special process (2nd), compound set 2 is assigned to be produced by first special process (1st) and compound set 4 is assigned to be produced by third special process (3rd). As presented in Table 7, the numbers of groups were calculated by multiplying all possible processes in each condition. The number of groups in the current condition is 24 groups. The number of groups in the combined process condition is 48 groups.

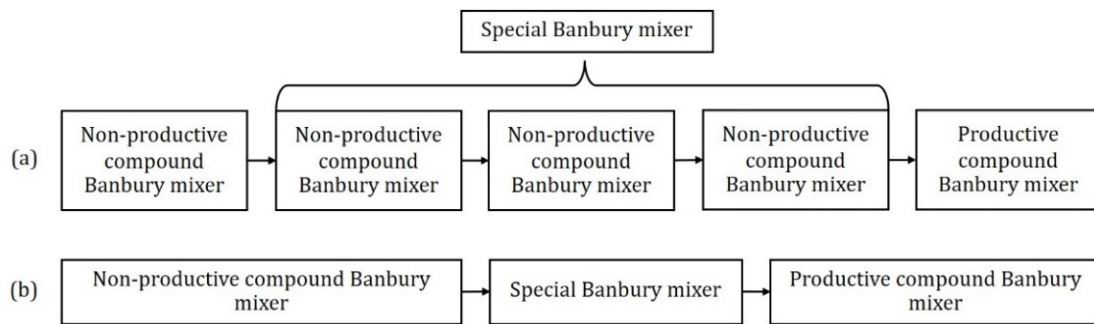


Fig. 10 (a) Mixing the normal and the second special process, (b) The fourth special Banbury mixing process

Table 6 All experiments from grouping the compound sets

Ex.	Compound set					Ex.	Compound set						
	1	2	3	4	5		1	2	3	4	5		
1	N	N	N	N	N	13	N	1st	N	N	N		
2	N	N	N	N	1st	14	N	1st	N	N	1st		
3	N	N	N	N	2nd	15	N	1st	N	N	2nd		
4	N	N	N	3rd	N	16	N	1st	N	3rd	N		
5	N	N	N	3rd	1st	17	N	1st	N	3rd	1st		
6	N	N	N	3rd	2nd	18	N	1st	N	3rd	2nd		
7	N	N	2nd	N	N	19	N	1st	2nd	N	N		
8	N	N	2nd	N	1st	20	N	1st	2nd	N	1st		
9	N	N	2nd	N	2nd	21	N	1st	2nd	N	2nd		
10	N	N	2nd	3rd	N	22	N	1st	2nd	3rd	N		
11	N	N	2nd	3rd	1st	23	N	1st	2nd	3rd	1st		
12	N	N	2nd	3rd	2nd	24	N	1st	2nd	3rd	2nd		
Ex.	Compound set						Ex.	Compound set					
	1	2	3	4	5	6		1	2	3	4	5	6
25	N	N	N	N	N	4th	37	N	1st	N	N	N	4th
26	N	N	N	N	1st	4th	38	N	1st	N	N	1st	4th
27	N	N	N	N	2nd	4th	39	N	1st	N	N	2nd	4th
28	N	N	N	3rd	N	4th	40	N	1st	N	3rd	N	4th
29	N	N	N	3rd	1st	4th	41	N	1st	N	3rd	1st	4th
30	N	N	N	3rd	2nd	4th	42	N	1st	N	3rd	2nd	4th
31	N	N	2nd	N	N	4th	43	N	1st	2nd	N	N	4th
32	N	N	2nd	N	1st	4th	44	N	1st	2nd	N	1st	4th
33	N	N	2nd	N	2nd	4th	45	N	1st	2nd	N	2nd	4th
34	N	N	2nd	3rd	N	4th	46	N	1st	2nd	3rd	N	4th
35	N	N	2nd	3rd	1st	4th	47	N	1st	2nd	3rd	1st	4th
36	N	N	2nd	3rd	2nd	4th	48	N	1st	2nd	3rd	2nd	4th

Table 7 The summary of Banbury process and compound groups

No.	Compound sets	Current condition		Combined process condition	
		No. of comps.	Possible process	No. of comps.	Possible process
1	Only Normal	20	1	13	1
2	Normal/1st special	5	2	5	2
3	Normal/2nd special	4	2	4	2
4	Normal/3rd special	1	2	1	2
5	Normal/1st special/2nd special	1	3	1	3
6	Normal/4th special	0	0	7	2
	Total	31	24	31	48

Each experiment contained 3 types of batch amount for each compound including non-pro, pro and special. For Banbury production planning, production volumes of each compound can be calculated by Eq. 1.

$$\text{Production volume(batch)} = \text{Productive compound demand(batch)} \times \text{Process step} \tag{1}$$

For example, considering a productive compound in the set 5, with 1 batch of demand, if the compound is produced by normal process, production volumes will be 4 batches of non-pro and 1 batch of pro. If it is produced by first special process, production volume will be 2 batches of special. If it is produced by second special process, production volumes will be 1 batch of special and 1 batch of pro. After the production volume were calculated, the batch amount for each compound was summarized for each experiment as shown in Table 8.

Table 8 The production volumes of the experiments

Current condition				Combined process condition							
Ex.	Non-pro	Pro	Special	Ex.	Non-pro	Pro	Special	Ex.	Non-pro	Pro	Special
1	29,665	20,175	0	1	29,665	20,175	0	25	25,625	20,175	2,746
2	29,356	20,175	150	2	29,356	20,175	150	26	25,316	20,175	2,896
3	29,356	20,014	293	3	29,356	20,014	293	27	25,316	20,014	3,039
4	27,376	18,994	1,956	4	27,376	18,994	1,956	28	23,027	18,994	4,702
5	27,067	18,994	2,106	5	27,067	18,994	2,106	29	23,027	18,994	4,852
6	27,067	18,833	2,249	6	27,067	18,833	2,249	30	23,027	18,833	4,995
7	25,593	20,175	2,300	7	25,296	20,175	2,480	31	21,256	20,175	5,226
8	25,284	20,175	2,450	8	24,987	20,175	2,630	32	20,947	20,175	5,376
9	25,284	20,014	2,593	9	24,987	20,014	2,773	33	20,947	20,014	5,519
10	23,304	18,994	4,256	10	23,007	18,994	4,436	34	18,967	18,994	7,182
11	22,995	18,994	4,406	11	22,698	18,994	4,586	35	18,658	18,994	7,332
12	22,995	18,833	4,549	12	22,698	18,833	4,729	36	18,658	18,833	7,475
13	23,276	15,011	4,639	13	21,302	13,538	5,946	37	17,262	13,538	8,692
14	22,967	15,011	4,789	14	20,993	13,538	6,096	38	16,953	13,538	8,842
15	22,967	14,850	4,932	15	20,993	13,377	6,239	39	16,953	13,377	8,985
16	20,987	13,830	6,595	16	19,013	12,357	7,902	40	14,973	12,357	10,648
17	20,678	13,830	6,745	17	18,704	12,357	8,052	41	14,664	12,357	10,798
18	20,678	13,669	6,888	18	18,704	12,196	8,195	42	14,664	12,196	10,941
19	19,204	15,011	6,939	19	16,933	13,538	8,426	43	12,893	13,538	11,172
20	18,895	15,011	7,089	20	16,624	13,538	8,576	44	12,584	13,538	11,322
21	18,895	14,850	7,232	21	16,624	13,377	8,719	45	12,584	13,377	11,465
22	16,915	13,830	8,895	22	14,644	12,357	10,382	46	10,604	12,357	13,128
23	16,606	13,830	9,045	23	14,335	12,357	10,532	47	10,295	12,357	13,278
24	16,606	13,669	9,188	24	14,335	12,196	10,675	48	10,295	12,196	13,421

All resource allocation plans were set up in 4 simulation scenarios illustrated in Table 9. Scenario I is the current capacity which has 5 compound sets, 20 normal compounds and 11 special compounds. BB1 is set as Non-pro BB, and there are 24 experiments. Scenarios II is the changing BB1 which has 5 compound sets, 20 normal compounds and 11 special compounds. BB1 is set as Special BB, and there are 24 experiments. Scenario III is applying fourth special process which has 6 compound sets, 13 normal compounds and 18 special compounds. BB1 is set as Non-pro BB, and there are 48 experiments. Scenarios IV is changing BB1 and applying fourth special process which has 6 compound sets, 13 normal compounds and 18 special compounds. BB1 is set as

Special BB, and there are 48 experiments. All scenarios are set to run 5 replications per experiment.

Simulation scenarios were created in the Plant simulation and the simulation tool named “Experiment Manager” was used to set experiments and replication as presented in Fig. 11(a). The output values were defined including working proportion, setting-up proportion, recovery proportion, total proportion, and production time of each experiment in Fig. 11(b). The input values were defined as the production volume in each type and experiments were defined as the current input or the adjusted input in Table 6. In addition, all experiments were designed to have 5 observations per experiment as shown in Fig. 11(c).

The graphs of results from experiments were plotted to find the lowest point which represented the best production time. Fig. 12(a-d) illustrates the experiment results of scenario I, II, III and IV. These graphs provide the lowest point at experiment 16, 24, 15 and 45, respectively. Most of the production times were varied according to Special BB and Non-pro BB. At this lowest point, either Special BB or Non-pro BB would be the maximum utilization.

Table 9 The simulation scenarios

Scenarios	Compound sets	Types		Machine BB1	No. of exp. (based on grouping)	No. of replications per experiment
		Normal	Special			
I	5	20	11	Non-pro BB	24	5
II		Special BB				
III	6	13	18	Non-pro BB		
IV		Special BB				

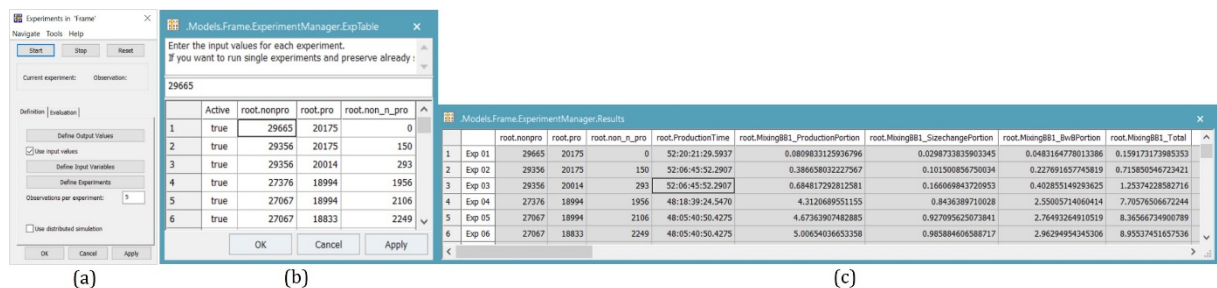


Fig. 11 Plant simulation tool named “Experiment Manager”, (a) setting window, (b) experiment table, (c) result table

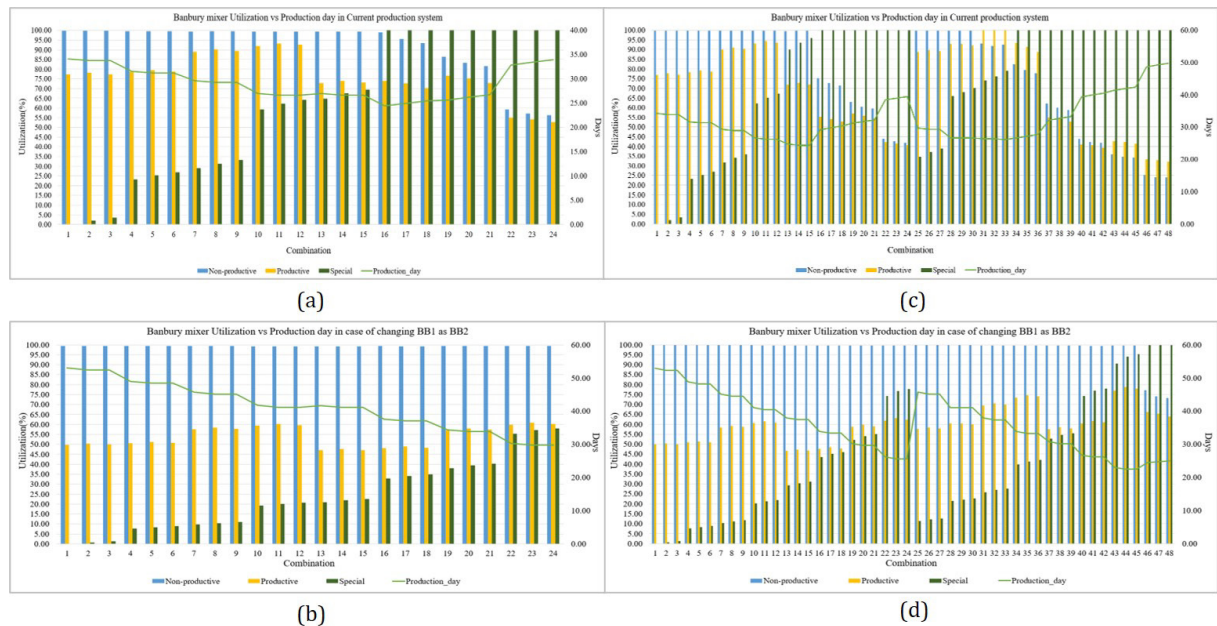


Fig. 12 The simulation results in each experiment, (a) Scenario I, (b) Scenario II, (c) Scenario III, (d) Scenario IV

3.2 Scenario results comparisons

Five scenarios were proposed to compare various capacity levels. The best experiment result of each scenario presented Banbury mixer machine utilization and production time. The graph in Fig. 13 represents the best experiment results of Scenario C, I, II, III and IV. As Scenario I results, the shortest production time was 24.43 days at experiment 16 which decreased by 0.68 days from current capacity (-2.71 %). Machine utilization of Non-pro BB, Pro BB and Special BB were 98.94 %, 74 % and 100 %, respectively. As Scenario II results, the shortest production time was 29.76 days at experiment 24 which increased by 4.65 days from production time (+18.52 %). Machine utilization of Non-pro BB, Pro BB and Special BB were 99.34 %, 60.16 % and 58.01 %, respectively. As Scenario III results, the shortest production time was 24.31 days at experiment 15 which decreased by 0.8 days from production time (-3.19%). Machine utilization of Non-pro BB, Pro BB and Special BB were 99.63 %, 71.95 % and 95.81 %, respectively. As Scenario IV results, the shortest production time was 22.46 days at experiment 45 which decreased by 2.65 days from current capacity (-10.55 %). Machine utilization of Non-pro BB, Pro BB and Special BB were 99.58 %, 77.95 % and 95.27 %, respectively. The summary results are shown in Table 10.

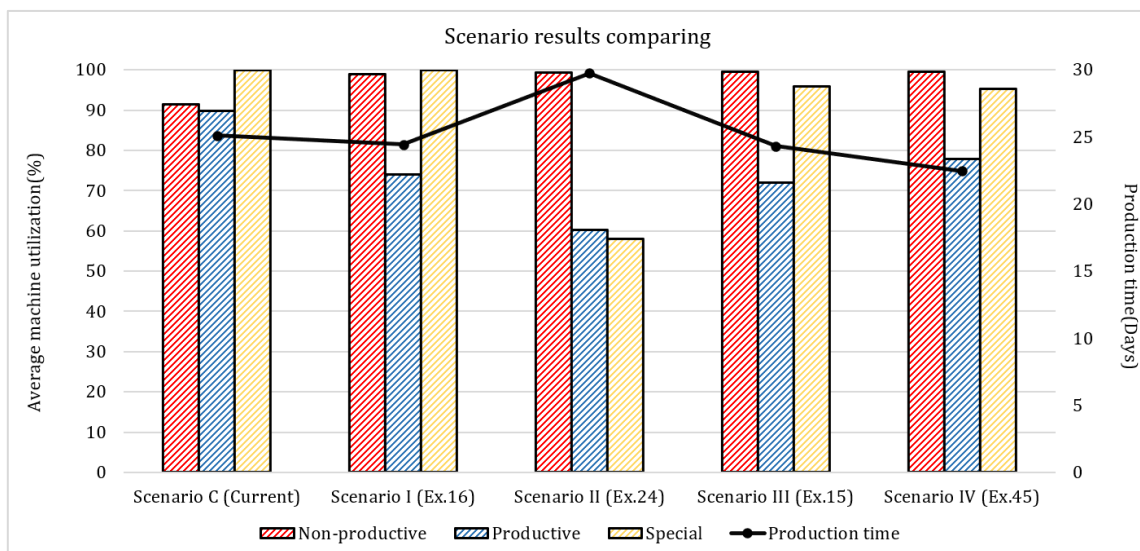


Fig. 13 The best result of each scenario comparison

Table 10 The summary results of each scenario at the best experiment

Sce.	Exp.	Production volume (batch)			Sets	BB1	Time (days)	Diff (%)	Machine utilization (%)			Avg
		Non-pro	Pro	Special					Non-pro BB	Pro BB	Special BB	
C	-	20,190	17,404	6,800	5	Non-pro	25.11	-	91.50	89.85	100	93.69
I	16	20,987	13,830	6,595	5	Non-pro	24.43	-2.71	98.94	74.00	100	90.98
II	24	16,606	13,669	9,188	5	Pro	29.76	18.52	99.34	60.16	58.01	72.50
III	15	20,993	13,377	6,239	6	Non-pro	24.31	-3.19	99.63	71.95	95.81	89.13
IV	45	12,584	13,377	11,465	6	Pro	22.46	-10.55	99.58	77.95	95.27	90.93

3.3 Estimation of production cost saving

As mentioned earlier, it recommended that BB1 should be changed to Special BB and fourth special process should be applied in order to reduce production time and utilize machine capacity. If the case study company implement this solution, the labor cost can be saved by production time reduction. In the current situation, BB1 required 4 workers to run the process but BB2 required 5 workers. To implement the solution, an additional worker of BB1 was recommended. Therefore, the total worker in the Banbury mixing process would be increased from 33 to 34 workers per shift. The wage per person was 1.22 USD per hours. As a result, the production time was reduced from 25.11 to 22.46 days per month. The yearly production saving was 22,834.90 USD per year as shown in Table 11.

Table 11 The summary of production cost saving after implement the solution

Cases	No. of workers	Production time per month		Wage	Month	Labor cost Year	Diff
		Days	Hours				
Current	33	25.11	602.64	1.22	12	291,147.44	-22,834.90
Solution	34	22.46	539.04				

4. Conclusion

In this study, a Plant Simulation approach for optimal resource utilization was proposed. Plant simulation was applied to create Banbury mixing process 3D models and simulate the production data. Those models applied discrete empirical distribution (dEmp) to population data. Experiment manager tool set up the scenarios with the experiments and provided results. Experiment results displayed the production time and machine utilization. The shortest production time of an experiment represented the best result of a scenario. Four scenarios were compared to determine the optimal group of compound sets and number of machines. The results showed that scenario IV at experiment 45, which BB1 was changed from non-productive Banbury mixer to special Banbury mixer along with the normal process were combined with the second special process to be fourth special process, provided the shortest production time. This scenario required investment in changing Banbury mixer machine BB1. This solution could save production cost by reducing the production time by 22,834.90 USD per year.

This study provides the resource utilization for Banbury mixing process to solve the capacity limitation. The adjustment in numbers of machines and the grouping in the compound sets are the solutions to reduce the production time. Discrete empirical distribution is demonstrated to deal with population data. The suitable method for verifying and optimizing various scenarios using Plant simulation are illustrated. Software configuration for setting operation times and experiments is explained. The simulation results found the shortest production time in each experiment and used to compare the shortest production time in each scenario. Our work also estimates the production cost saving for the best scenario from simulations.

Future research can be conducted to more production situation input and output, such as worker and area. Moreover, this simulation model concept can be applied to other tire production lines or the entire tire production systems to optimize the total resource as well.

References

- [1] Krajewski, L.J., Ritzman, L.P., Malhotra, M.K. (2013). *Operations management: Processes and supply chains*, 10th Edition, Pearson Education, London, United Kingdom.
- [2] Wolniak, R., Skotnicka- Zasadzień, B., Gębalska-Kwiecień, A. (2018). Identification of bottlenecks and analysis of the state before applying lean management, In: *Proceedings of 12th International Conference Quality Production Improvement - QPI 2018*, Zaborze near Myszków, Poland, Article No. 01001, [doi: 10.1051/mateconf/201818301001](https://doi.org/10.1051/mateconf/201818301001).
- [3] Kokareva, V.V., Malyhin, A.N., Smelov, V.G. (2015). Production processes management by simulation in tecnomatix plant simulation, *Applied Mechanics and Materials*, Vol. 756, 604-609, [doi: 10.4028/www.scientific.net/AMM.756.604](https://doi.org/10.4028/www.scientific.net/AMM.756.604).
- [4] Fil'o, M., Markovič, J., Kliment, M., Trebuňa, P. (2013). PLM systems and Tecnomatix plant simulation, a description of the environment, control elements, creation simulations and models, *American Journal of Mechanical Engineering*, Vol. 1, No. 7, 165-168.
- [5] Zupan, H., Herakovic, N. (2015). Production line balancing with discrete event simulation: A case study, *IFAC-PapersOnLine*, Vol. 48, No. 3, 2305-2311, [doi: 10.1016/j.ifacol.2015.06.431](https://doi.org/10.1016/j.ifacol.2015.06.431).
- [6] Borojevic, S., Jovisevic, V., Jokanovic, S. (2011). Modelling, simulation and optimization of process planning, *Journal of Production Engineering*, Vol. 12, No. 1, 87-90.
- [7] Zupan, H., Herakovic, N. (2015). Production line balancing with discrete event simulation: A case study, *IFAC-PapersOnLine*, Vol. 48, No. 3, 2305-2311, [doi: 10.1016/j.ifacol.2015.06.431](https://doi.org/10.1016/j.ifacol.2015.06.431).
- [8] Kurkin, O., Šimon, M. (2011). Optimization of layout using discrete event simulation, *IBIMA Business Review*, Vol. 2011, Article ID 180343, [doi: 10.5171/2011.180343](https://doi.org/10.5171/2011.180343).
- [9] Bangsow, S. (2010). Plant simulation, In: *Manufacturing simulation with plant simulation and SimTalk*, Springer, Berlin, Germany, 7-15, [doi: 10.1007/978-3-642-05074-9_2](https://doi.org/10.1007/978-3-642-05074-9_2).
- [10] Ištoković, D., Perinić, M., Doboviček, S., Bazina, T. (2019). Simulation framework for determining the order and size of the product batches in the flow shop: A case study, *Advances in Production Engineering & Management*, Vol. 14, No. 2, 166-176, [doi: 10.14743/apem2019.2.319](https://doi.org/10.14743/apem2019.2.319).

- [11] Arunkumar, Y., Patil, R., Mohankumar, S. (2012). Discrete event simulation for increasing productivity in digital manufacturing, *International Journal of Engineering Research and Development*, Vol. 1, No. 10, 36-40.
- [12] Yang, S.L., Xu, Z.G., Li, G.Z., Wang, J.Y. (2020). Assembly transport optimization for a reconfigurable flow shop based on a discrete event simulation, *Advances in Production Engineering & Management*, Vol. 15, No. 1, 69-80, [doi: 10.14743/apem2020.1.350](https://doi.org/10.14743/apem2020.1.350).
- [13] Li, G.Z., Xu, Z.G., Yang, S.L., Wang, H.Y., Bai, X.L., Ren, Z.H. (2020). Bottleneck identification and alleviation in a blocked serial production line with discrete event simulation: A case study, *Advances in Production Engineering & Management*, Vol. 15, No. 2, 125-136, [doi: 10.14743/apem2020.2.353](https://doi.org/10.14743/apem2020.2.353).
- [14] Żywicki, K., Rewers, P. (2020). A simulation-based approach to study the influence of different production flows on manufacturing of customized products, *Advances in Production Engineering & Management*, Vol. 15, No. 4, 467-480, [doi: 10.14743/apem2020.4.379](https://doi.org/10.14743/apem2020.4.379).
- [15] Ištoković, D., Perinić, M., Borić, A. (2021). Determining the minimum waiting times in a hybrid flow shop using simulation-optimization approach, *Tehnički Vjesnik – Technical Gazette*, Vol. 28, No. 2, 568-575, [doi: 10.17559/TV-20210216132702](https://doi.org/10.17559/TV-20210216132702).
- [16] Rupnik, B., Kragelj, D., Šinko, S., Kramberger, T. (2020). Distributed energy resource operation analysis using discrete event-simulation, *Tehnički Vjesnik – Technical Gazette*, Vol. 27, No. 3, 860-867, [doi: 10.17559/TV-20190626184415](https://doi.org/10.17559/TV-20190626184415).
- [17] Law, A.M. (2012). A tutorial on how to select simulation input probability distributions, In: *Proceedings of the 2012 Winter Simulation Conference (WSC)*, Berlin, Germany, 1-15, [doi: 10.1109/WSC.2012.6465281](https://doi.org/10.1109/WSC.2012.6465281).
- [18] Fishman, G.S., Kiviat, P.J. (1968). The statistics of discrete-event simulation, *Simulation*, Vol. 10, No. 4, 185-195, [doi: 10.1177/003754976801000406](https://doi.org/10.1177/003754976801000406).

Calendar of events

- 16th International Conference on Micromachining Technology, October 17-18, 2022, Dubai, United Arab Emirates.
- 36th Annual European Simulation and Modelling Conference, October 26-28, 2022, Porto, Portugal.
- 33rd DAAAM International Symposium, Virtual Online Edition, hosted by Vienna University of Technology, October 27-28, 2022, Vienna, Austria.
- 7th International Conference of Computational Methods in Engineering Science, November 24-26, 2022, Zamosc, Poland.
- 14th International Conference on Mechatronics and Manufacturing, February 10-12, 2023, Royal Princess Larn Luang, Bangkok, Thailand.
- 7th International Conference on Material Engineering and Manufacturing, April 7-10, 2023, Chiba University, Japan.
- 51th North American Manufacturing Research Conference, June 12-16, 2023, Rutgers University, New Brunswick, New Jersey, USA.

Notes for contributors

General

Articles submitted to the *APEM journal* should be original and unpublished contributions and should not be under consideration for any other publication at the same time. Manuscript should be written in English. Responsibility for the contents of the paper rests upon the authors and not upon the editors or the publisher. The content from published paper in the *APEM journal* may be used under the terms of the Creative Commons Attribution 4.0 International Licence (CC BY 4.0). For most up-to-date information please see the APEM journal homepage apem-journal.org.

Submission of papers

A submission must include the corresponding author's complete name, affiliation, address, phone and fax numbers, and e-mail address. All papers for consideration by *Advances in Production Engineering & Management* should be submitted by e-mail to the journal Editor-in-Chief:

Miran Brezocnik, Editor-in-Chief
UNIVERSITY OF MARIBOR
Faculty of Mechanical Engineering
Chair of Production Engineering
Smetanova ulica 17, SI – 2000 Maribor
Slovenia, European Union
E-mail: editor@apem-journal.org

Manuscript preparation

Manuscript should be prepared in *Microsoft Word 2010* (or higher version) word processor. *Word .docx* format is required. Papers on A4 format, single-spaced, typed in one column, using body text font size of 11 pt, should not exceed 12 pages, including abstract, keywords, body text, figures, tables, acknowledgements (if any), references, and appendices (if any). The title of the paper, authors' names, affiliations and headings of the body text should be in *Calibri* font. Body text, figures and tables captions have to be written in *Cambria* font. Mathematical equations and expressions must be set in *Microsoft Word Equation Editor* and written in *Cambria Math* font. For detail instructions on manuscript preparation please see instruction for authors in the *APEM journal* homepage apem-journal.org.

The review process

Every manuscript submitted for possible publication in the *APEM journal* is first briefly reviewed by the editor for general suitability for the journal. Notification of successful submission is sent. After initial screening, and checking by a special plagiarism detection tool, the manuscript is passed on to at least two referees. A double-blind peer review process ensures the content's validity and relevance. Optionally, authors are invited to suggest up to three well-respected experts in the field discussed in the article who might act as reviewers. The review process can take up to eight weeks on average. Based on the comments of the referees, the editor will take a decision about the paper. The following decisions can be made: accepting the paper, reconsidering the paper after changes, or rejecting the paper. Accepted papers may not be offered elsewhere for publication. The editor may, in some circumstances, vary this process at his discretion.

Proofs

Proofs will be sent to the corresponding author and should be returned within 3 days of receipt. Corrections should be restricted to typesetting errors and minor changes.

Offprints

An e-offprint, i.e., a PDF version of the published article, will be sent by e-mail to the corresponding author. Additionally, one complete copy of the journal will be sent free of charge to the corresponding author of the published article.

APEM

journal

Advances in Production Engineering & Management

Chair of Production Engineering (CPE)
University of Maribor
APEM homepage: apem-journal.org

Volume 17 | Number 2 | June 2022 | pp 137-258

Contents

Scope and topics	140
A method for prediction of S-N curve of spot-welded joints based on numerical simulation Yang, L.; Yang, B.; Yang, G.W.; Xiao, S.N.; Zhu, T.; Wang, F.	141
Sustainability and digitalisation: Using Means-End Chain Theory to determine the key elements of the digital maturity model for research and development organisations with the aspect of sustainability Kupilas, K.J.; Rodriguez Montequín, V.; Díaz Piloñeta, M.; Alonso Álvarez, C.	152
Supply chain coordination based on the probability optimization of target profit Jian, M.; Liu, T.; Hayrutdinov, S.; Fu, H.	169
A bi-objective optimization of airport ferry vehicle scheduling based on heuristic algorithm: A real data case study Han, X.; Zhao, P.X.; Kong, D.X.	183
Ultrasonic abrasive polishing of additive manufactured parts: An experimental study on the effects of process parameters on polishing performance Liu, X.; Wang, J.; Zhu, J.; Liew, P.J.; Li, C.; Huang, C.	193
Machinability analysis and multi-response optimization using NGS-II algorithm for particle reinforced aluminum based metal matrix composites Umer, U.; Mohammed, M.K.; Abidi, M.H.; Alkhalefah, H.; Kishawy, H.A.	205
Supply chain coordination contract design: The case of farmer with capital constraints and behavioral preferences Wang, Y.L.; Yin, X.M.; Zheng, X.Y.; Cai, J.R.; Fang, X.	219
Numerical study of racking resistance of timber-made double-skin façade elements Kozem Šilih, E.; Premrov, M.	231
A Plant Simulation approach for optimal resource utilization: A case study in the tire manufacturing industry Butrat, A.; Supsomboon, S.	243
Calendar of events	256
Notes for contributors	257

Published by CPE, University of Maribor



apem-journal.org